ON THE MECHANICS OF CONTACT AND REATTACHMENT IN LAYERED AEROSPACE AND OCULAR STRUCTURES

by

PEINAN GE

A dissertation submitted to the

Graduate School-New Brunswick

Rutgers, The State University of New Jersey

In partial fulfillment of the requirements

For the degree of

Doctor of Philosophy

Graduate Program in Mechanical and Aerospace Engineering

Written under the direction of

William J. Bottega

And approved by

_____

_____

_____

_____

New Brunswick, New Jersey

October, 2014

ABSTRACT OF THE DISSERTATION

ON THE MECHANICS OF CONTACT AND REATTACHMENT IN LAYERED AEROSPACE AND OCULAR STRUCTURES

by PEINAN GE

Dissertation Director:

William J. Bottega

Contact and reattachment of two types of layered structures are examined. In the first part of the dissertation, a constrained patched structure subjected to uniform temperature change with edge damage is studied. Geometric nonlinearities and shear deformation are included in the mathematical model, and the effects of shear deformation are examined. The formulation is based on the calculus of variations with propagating boundaries, and yields the governing equations, boundary conditions, matching conditions and transversality condition. Results are compared with previously published results with transverse shear deformation neglected. The effects of shear deformation on the recently discovered instabilities referred to as 'sling-shot buckling' and 'buckle trapping' are demonstrated and discussed. The influence of the relative size of the detached region and of the difference between the material properties of the base plate and of the patch (in particular, the shear moduli) on the afforementioned thermo-mechanical instabilities are elucidated.

In the second part, a representative mathematical model of the eye encircled by a scleral buckle in the vicinity of the equator is developed. The effects of the buckle on the

mechanical behavior of the eye, and then on closing posterior retinal detachment are both studied. Both problems are formulated using variational methods. Closed form analytical solutions of the coupled differential equations are obtained. Results of numerical simulations are presented and critical phenomena are unveiled. The effects of material and geometric parameters (radius, width, thickness and Young's modulus) of the scleral buckle, as well as of the ocular pressure, on the deformation of the eye are studied. Volume changes for each case are evaluated as well. It is seen that the radius of the buckle is the dominant parameter with regard to mechanical behavior of the eye. In the final major chapter, the effect of the scleral buckle on closure and reattachment of posterior retinal detachment is studied. It is seen that as the radius of the scleral buckle reduces, the distance between the detached segment of retina and the retinal pigment epithelium decreases, thus encouraging reattachment between the two surfaces. This, evidently, has ramifications with regard to treatment of posterior retinal detachment.

Acknowledgements

I came to Rutgers University five years ago for my Ph.D study as an international student. Throughout this portion of my life, I received so much help from so many people and learned a great deal from them. Here I would like to recognize them.

The first person I want to thank is my advisor, Dr. William J. Bottega. When I came here, I was in the control and design field, and I found myself more interested in solid mechanics after I took the Mechanics of Materials course with Dr. Bottega in 2010. We discussed research in this area. Then I switched majors and became his graduate student. I had gone through a lot of pressure during this time period (2009 - 2010), but luckily, doing research with Dr. Bottega was the right decision for me. As a newbie in this area, I always ask very simple questions. Dr. Bottega was and is very patient, encouraging. He isn't only just a brilliant individual, but also an honest and caring instructor. His sense of humor is greatly appreciated by all the group members. However, he is very strict and careful, which is very helpful from not only a research perspective, but a life perspective as well. As I got my fellowship from the Chinese government for only four years, he tried his best to apply for funding to support my fifth-year research. Here I really appreciate his effort.

I would also like to thank Dr. Haim Baruh and Dr. Haym Benaroya, for serving on my dissertation committee. Dr. Baruh and Dr. Benaroya are both quite easygoing, and I really appreciate all they have done for me during my graduate study. In addition, I want to thank Dr. Howard F. Fine who specializes in Ophthalmology and has been doing research on retinal detachment with our groups since 2012. I am very grateful for his willingness to serve on my committee.

Our research group members (Joseph M. Lakawicz, Michael J. Pavlou, Joseph Hunt and Michelle E. Chernick) are amazing, and they are always willing to help me with my research and English. Thanks to my friends also, Feruza Amirkulova, Andrew Dmitrzak, Wing Fi Lam, Fei Liu and Han Sun.

Finally, I'd like to give thanks to all my family members. They have always taken care of me whenever I needed, unconditionally. Although they are back in China, they have encouraged me each time we had talked online or on the phone.

Table of Contents

List of Tables

List of Figures

Chapter 1 Introduction

1.1 Motivation

Patched Plates

Patched structures are widely used in a variety of engineering systems. Such a structure consists of a secondary component adhered to a primary structure. Engineers have been using patches on aircraft in recent years to alleviate the stress intensity in the vicinity of cracks in the primary structures. It is necessary to predict and characterize the functionality of a patched structure during its servicing period. In the structures of this class, the mechanical properties of the composite structure change with respect to the properties of the patch and base components. With varying the temperature environments, with ensuing increased stress and buckling, transverse shear deformation may affect the system greatly. Therefore the characterization of the shear effect is of critical importance.

Scleral Buckle

Retinal detachment is one of the major causes of vision loss world-wide. It occurs when the retina separates from the choroid (the cellular layer between the retina and the sclera). Typically, the retina detaches from the nine layers of the sensory retina along the interface with the retinal pigment epithelium. In clinical practice, one of the common methods for retinal reattachment is the application of a closed elastic band (circlage) along the equator. This piece of silicone sponge, rubber, or semi-hard plastic is placed by the ophthalmologist on the outside of the eye, known as the sclera (the white of the eye)

and is referred to as a "scleral buckle". The buckle is typically sutured to the eye to keep it in place. The understanding of how and why the sutured scleral buckle could cause the retina to come back into contact with the eye is of great practical importance.

In the following section, we review some of the literature discussing the characteristics of patched plate and retinal detachment and reattachment.

1.2 A Survey of Related Literature

Patched Plates

It is well known that a composite structure will eventually buckle when it is subjected to temperature change. The classic papers on thermal buckling include Timoshenko (1925); Wittrick, et al. (1953); and Wahl (1944). Karlsson and Bottega (1999) studied the presence of edge contact in patched cylindrical panels, and found that edge contact often occurs, and that it can influence the debonding behavior of the structure. Karlsson and Bottega (2000a; 2000b) and Rutgerson and Bottega (2002), subsequently studied the behavior of patched plates and layered shells, respectively, subjected to uniform temperature change. Their results showed that the structure will dynamically sling to an equilibrium configuration associated with deflections in the opposite sense of the original. The phenomenon is referred to as “sling-shot buckling” by the authors. Recently, Bottega and Carabetta (2009) studied the detachment and separation failure of layered structures under thermal loading. The behaviors of several representative structures and loadings were studied. Carabetta and Bottega (2012; 2014) studied the instability of patched structures with edge damage where a new phenomenon referred to as 'buckle trapping′ was unveiled. A detailed review of the pertinent literature is presented therein. In addition,

Carabetta (2011) studied the interaction of thermal buckling and detachment of patched structures. Carabetta and Bottega (2012) studied the existence of intermediate propogating contact for different bond zone sizes and edge supports. These representative results significantly help to understand engineering structural problems. However, a more sophisticated elastic theory containing shear deformation, will further elucidate the phenomena of interest.

Timoshenko (1921) was the first to introduce shear deformation as well as rotatory inertia into beam theory. Shen (1998) presented a post-buckling analysis for laminated composite plates subjected to uniform or non-uniform temperature loading . Reddy (1984) adopted higher order shear deformation in the formulation to show that the characteristics of thermal post-buckling are significantly influenced by transverse shear deformation. Aydogdu (2007) applied the Ritz method and performed an analysis of thermal buckling behavior on cross-ply laminated beams. In that work, a shear deformable theory was used in conjunction with a shape function to fulfill geometric and material constraints. Zenkour and Sobhy (2010) used a sinusoidal shear deformation plate theory to model thermal buckling phenomena of sandwich plates. Different thermal loads were applied under various configurations of the plates.

Scleral Buckle

A lot of studies have been conducted on the ocular structure mechanics in the past decades. Bauer, et al. (1995a) studied the local behavior of the eye under an encircling band with negligible band width. The normal displacement and the buckling of the axisymmetric state were derived. Keeling, et al. (2009) presented a mathematical model for the mechanics of the combined eye/band structure, and an algorithm was developed

to predict the maximal intraocular pressure as well as the final indentation of the eye in three phases of cerclage operation. Thompson and Michels (1985) derived the formula using solid geometry to determine the volume displacement of the eye based on several important assumptions, and compared the results with measured volume displaecments. Some researchers also studied the axial length changes after retinal detachment surgery. Seo, et al. (2002) investigated the postoperative changes and the mechanism of retinal reattachment after an encircling scleral buckle was applied and showed that the encircling scleral buckle changes the anxial length and decreases the volume and internal surface area of the eye. Foster, et al. (2010) found it is necessary to couple fluid mechanics with structural mechanics, laminar fluid flow and the Bernoulli effect for consistent explanation of retinal reattachment because rapid eye movements and associated fluid flow facilitate more rapid retinal reattachment. The critical buckling characteristics of hydrostatically pressurized complete spherical shells filled with an elastic medium are demonstrated by Sato, et al. (2012), and simplified approximations based on the Rayleigh-Ritz approach are also introduced with a considerable degree of accuracy. Bottega, et al. (2012) studied the fundmental mechanics of detachment propagation of the retina, and analytical solutions were derived while assuming the meridian displacements of the retina are negligible. Recently, Lakawicz, et al. (2014) considered the meridian displacements to be small but not necessarily negligible. More accurate analytical solutions for the model of retinal detachment is obtained and the importance of retaining the meridian displacements was presented.

1.3 Current Objective

Patched Plates

The present work first focuses on the response of patched plates subjected to a uniform temperature field for a variety of support conditions and material properties. We extend the model and analysis of Carabetta and Bottega (2012; 2014); Carabetta (2011); Carabetta (2007) to include transverse shear deformation. The formulations are based on Mindlin (1951), Timoshenko (1921), and the calculus of variations. Numerical simulations are performed to elucidate representative behavior of the composite structure. Of particular interest is how the inclusion of transverse shear deformation in the overall formulation affects the response of the composite structure. In addition, the effects that the length of the patch, the proportion of Poisson's ratio and Young's modulus between the patch and the base plate have on the behavior of the structure are also examined.

Scleral Buckle

In the second part of the dissertation, a representative mathematical model of the eye encircled by a scleral buckle/band is developed, where the buckle is applied in the vicinity of the equator of the eye. The problem is formulated using variational methods. This yields the self-consistent governing equations, boundary conditions and matching conditions of the spherical ocular structure. Closed form analytical solutions of the coupled set of differential equations are obtained, and results of numerical simulations based on the analytical solutions are presented and critical phenomena are unveiled. We intend to study the effects of material and geometric parameters (radius, width, thickness

and Young's modulus) of the scleral buckle, as well as of the ocular pressure, on the deformation of the eye. Volume changes for each case are evaluated as well.

In addition, we advance the study and include the retina layer with posterior detachment in the evolving structure to study the influence of the scleral buckle on the detachment occurs far away from the equator. Total potential energy of the ocular structure is formulated and the governing equations, boundary conditions and matching conditions are obtained by applying the calculus of variation. The results of simulations reveal critical characteristic behavior of the evolving structure. The effect of the buckle radius on the behavior of the retina and the deformation of the eye membrane are evaluated.

1.4 Outline of the Dissertation

The dissertation is presented in five chapters. Chapter 2 details the problem of the effect of transverse shear deformation on the instability of layered patched beam-plate. Chapter 3 describes the mechanical behavior of the eye encircled by the scleral buckle. In Chapter 4, we advance the study presented in Chapter 3 and include the retina in the evolving structure. The influence of the scleral buckle to a posterior detachment (away from the equator) is presented in detail. Chapter 5 offers a thorough discussion on the findings of this work and future considerations.

Chapter 2 *Effect of transverse shear deformation on patched beam-plate with edge damage under uniform thermal loading*

2.1 Introduction

In this chapter, we formulate the problem for the patched structure with a preexisting detached region emanating from each edge of the patch. The structure is subject to a uniform temperature differences. We advance the work of Carabetta (2011); Carabetta and Bottega (2012; 2014) and include the effect of transverse shear deformation to examine its influence on critical phenomena under two different edge support conditions. The formulation is based on the calculus of variations with propagating boundaries, and yields the governing equations, boundary conditions, matching conditions and transversality condition.

2.2 Formulation

2.2.1 Geometry

The thin patched plate is comprised of two substructures: a base plate of half-span length L, and a patch of half-span L_p centrally and partially adhered to the base structure (Figure 2.1).

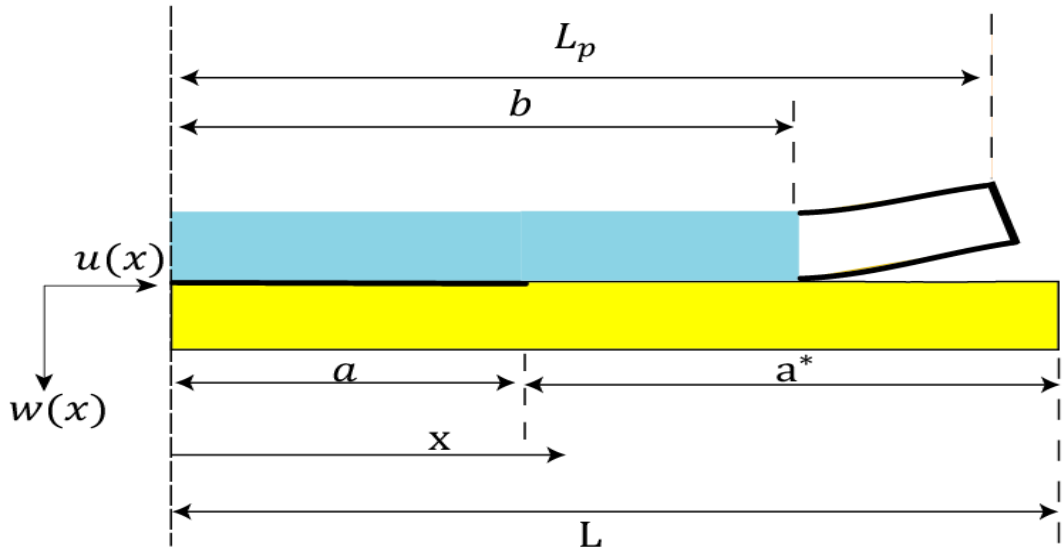

Figure 2.1 Half-span of structure

The thicknesses of the base plate and the patch are h_b and h_p, respectively. The coordinate x originates at the centerspan and runs along the reference surface-the upper surface of the base plate. All the length scales are normalized with respect to the half-length of the base plate, and other pertinent parameters are normalized in accordance with Bottega and Carabetta (2009). Thus, for the structure of interest, the half-span length of the base plate is $L = 1$. The structure is mathematically partitioned into three domains: $S_1 : x \in [0, a]$, $S_2 : x \in [a, b]$ and $S_3 : x \in [b, 1]$, which are denoted as the bond zone, contact zone and lift zone, respectively. The functions $w(x)$ and $w_p(x)$ (positive downward) represent the normalized transverse displacements of the base plate and of the patch, respectively. The functions $u(x)$ and $u_p(x)$ (positive outward from centerspan) denote the corresponding normalized in-plane displacements of material particles located at the centroid of the base plate and of the patch, respectively. Correspondingly, the

functions $\phi(x)$ and $\phi_p(x)$ represent the angle of rotation of the cross section due to bending for the base plate and of the patch, respectively. In addition, the functions $\gamma(x)$ and $\gamma_p(x)$ represent the shear angles of the base plate and of the patch, respectively. Paralleling the developments inCarabetta and Bottega (2014), the membrane strain of the baseplate and of the patch, $e_i(x)$ and $e_p(x)$, respectively, are given by

$$e_i = u_{bi}' + \frac{1}{2} w_{bi}'^2 - \alpha_b \Theta \qquad (i = 1,2,3) \tag{2.1}$$

$$e_p = u_{p_2}'^2 + \frac{1}{2} w_{p_2}'^2 - \alpha_p \Theta \tag{2.2}$$

where $(\ )' = \dfrac{d(\ )}{dx}$ and α_b, α_p are described in what follows.

In the formulation we allow for three configurations: (1) no contact of the debonded segments of the substructures; (2) the "free" edge of the debonded segment of the patch maintains sliding contact with the base plate ("edge contact"); (3) a full contact zone. (the entire debonded segment contacts the base plate.) Each of these configurations are shown in Figure 2.2.

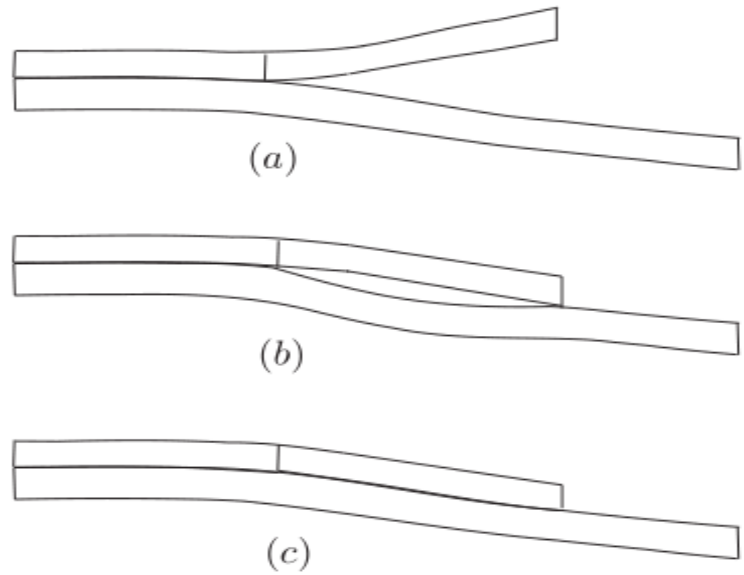

Figure 2.2 Deformed plate showing various configurations. (a) panel with 'no contact' of debonded segments. (b) plate with 'edge contact' of debonded segments. (c) plate with 'full contact' of debonded segments of patch plate and base.

2.2.2 Potential Energy Functional

Paralleling the developments in Karlsson and Bottega (2000b; 2000c); Rutgerson and Bottega (2002), but now incorporating transverse shear deformation, we next formulate an energy functional in terms of the membrane energies, bending energies and shear energies of each substructure for each segment of the base panel and of the patch, and we also include constraint functionals which match the transverse displacements in the contact zone and the transverse and in-plane displacements and the angle of rotation due to bending in the bond zone. We thus formulate the energy functional, Π , as follows:

$$\Pi = \sum_{1}^{3}(U_B^{(i)} + U_{Bp}^{(i)} + U_M^{(i)} + U_{Mp}^{(i)} + U_S^{(i)} + U_{Sp}^{(i)}) - \Lambda \tag{2.3}$$

where

$$U_B^{(i)} = \int_{S_i} \frac{1}{2} D\kappa_i^2 dx, \qquad U_{Bp}^{(i)} = \int_{S_i} \frac{1}{2} D_p \kappa_{pi}^2 dx, (i = 1,2,3) \tag{2.4}$$

are the bending energies in the base plate and patch in Region S_i,

$$U_M^{(i)} = \int_{S_i} \frac{1}{2} C e_i^2 dx, \qquad U_{Mp}^{(i)} = \int_{S_i} \frac{1}{2} C_p e_{pi}^2 dx, (i = 1,2,3) \tag{2.5}$$

are the membrane energies in the base plate and patch in Region S_i. Further

$$U_{Sr}^{(i)} = \int_{S_i} \frac{1}{2} G_b \gamma_i^{\,2} dx, \qquad U_{Srp}^{(i)} = \int_{S_i} \frac{1}{2} G_p \gamma_{pi}^{\,2} dx, \ (i = 1,2,3) \tag{2.6}$$

are the shear energies in the base plate and in the patch in Region S_i. The constraint functional Λ in Eq. (2.3) is given by

$$\Lambda = \sum_1^2 \int_{S_i} \sigma_i (w_{pi} - w_i) dx + \int_{S_1} \tau (u_{p1}^{\ *} - u_1^*) dx + \int_{S_1} \lambda (\phi_{p1}^* - \phi_1^*) dx \tag{2.7}$$

In Eqs. (2.4) – (2.7) D and D_p are the nondimensional bending stiffness of the base plate and the patch, respectively. C and C_p are the corresponding nondimensional membrane stiffness, and G_b and G_p are the nondimensional shear stiffness, respectively. In addition, σ_i represents the interfacial normal stress, τ is the interfacial shear stress, and λ is the interfacial moment couple. According to Mindlin Plate Theory (1951), Timoshenko Beam Theory (1921) and Bottega (2006) where a shear correction and rotatory inertia are considered, the strain-displacement relation is given by

$$\frac{dw}{dx} = \phi + \gamma \tag{2.8}$$

$$\gamma = \frac{V}{kGh} \tag{2.9}$$

where w is the transverse displacement, ϕ is the angle of rotation due to bending and γ is the transverse shear angle of the cross section. In Eq. (2.9), the parameter G is the shear modulus and V is the transverse shear force. In addition, k is the 'shape factor' or 'shear coefficient' of the structure, which depends on the shape of the cross section. In the past decades, the shear coefficients for various cross sections of beams were derived. Examples of related work may be found in the papers by Cowper (1966); Hutchinson (1981); Ritchie, et al. (1973) etc. Incorporating Eq. (2.8) into the development through Eqs. (2.3) – (2.7), the problem is expressed in terms of the in-plane displacement, $u(x)$, the transverse displacement, $w(x)$, and the angle of rotation due to bending, $\phi(x)$.

2.2.3 Parameters Normalization

The parameters shown in the above formulation of the total potential energy of the system are defined in terms of their dimensional forms as follows:

$$
\begin{aligned}
x &= \bar{x} / \bar{L} \qquad D = 1 \\
u(x) &= \bar{u}(\bar{x}) / \bar{L} \quad C = \bar{C} / \bar{D} = 12 / h_b^2 \\
w(x) &= \bar{w}(\bar{x}) / \bar{L} \quad D_p = \bar{D}_p / \bar{D} = E_p h_0^3 \\
\phi(x) &= \bar{\phi}(\bar{x}) \quad C_p = \bar{C}_p / \bar{D} = C E_p h_0^3 \\
G_b &= k_b \bar{G}_b \bar{h}_b \bar{L}^2 / \bar{D} \quad G_p = k_p \bar{G}_p \bar{h}_p \bar{L}^2 / \bar{D} \\
\sigma_i &= \bar{\sigma}_i \bar{L}^3 / \bar{D} \quad \tau = \bar{\tau} \bar{L}^3 / \bar{D} \\
h_b &= \bar{h}_b / \bar{L} \quad E_p = \bar{E}_p / \bar{E}_b \quad h_p = \bar{h}_p / \bar{L} \\
h_0 &= h_p / h_b \quad L = 1 \quad \lambda = \bar{\lambda} \bar{L}^2 / \bar{D}
\end{aligned}
\tag{2.10}
$$

where length scales have been normalized with respect to the dimensional half-span $\bar{L}$ of the base plate. Invoking the principle of stationary potential energy, which is described in the present context as $\delta\Pi = 0$, we take the appropriate variations and allow the boundary b to vary along with the displacements. This results in the corresponding

governing equations, boundary and matching conditions, and transversality condition. After eliminating the Lagrange multipliers, we arrive at the self-consistent equations and conditions for the composite structure. These are presented next.

2.3 Governing Equations and Boundary Conditions

Adopting the method presented in Rutgerson and Bottega (2002), integrating the differential equations for membrane force in each domain (defined in Appendix B) and applying the appropriate boundary/matching conditions, it is seen that

$$N_1^* = N_2 = N_3 = -N_0 = constant, \qquad N_{p2} = N_{p3} = 0, \tag{2.11}$$

where N_0 is yet to be determined. With this important result, the problem is recast into a mixed formulation, expressed in terms of the transverse displacement, $w(x)$, the angle of rotation due to bending, $\phi(x)$, and the uniform membrane force, N_0.

The equations of transverse motion and rotation then take the form

$$\begin{aligned} D^*\phi_{b1}'' + (G_b + G_p)(w_{b1}' - \phi_{b1}) &= 0 \\ -N_0 w_{b1}'' + (G_b + G_p)(w_{b1}' - \phi_{b1})' &= 0 \qquad x \in [0, a] \end{aligned} \tag{2.12}$$

We next rearrange the above equations, eliminate w_{b1} and decouple the governing equations in terms of the angle of rotation due to bending, ϕ_{b1}, and the uniform membrane force, N_0. Applying the same procedure for other regions gives the following governing equations. Hence,

$$g^*\phi_{b1}''' + N_0\phi_{b1}' = 0, \qquad (0 \le x \le a) \tag{2.13}$$

$$g_3\phi_{b2}'''' + N_0\phi_{b2}' + D_p\phi_{p2}'''' = 0, \qquad (a \le x \le b) \tag{2.14}$$

$$g_3\phi_{b3}'''' + N_0\phi_{b3}' = 0, \qquad (b \le x \le 1) \tag{2.15}$$

$$g_4\phi_{p3}'''' = 0, \qquad (b \le x \le L_p) \tag{2.16}$$

where

$$\begin{aligned} g^* &= g^*(N_0) = D^*(1 - \frac{N_0}{G_b + G_p}) \\ g_3 &= g_3(N_0) = D_b(1 - \frac{N_0}{G_b}) \\ g_4 &= g_4(N_0) = D_p(1 - \frac{N_0}{G_p}) \end{aligned} \tag{2.17}$$

$$\begin{aligned} &w_{b1}''(x) = -\frac{D^*}{G_b + G_p}\phi_b'' + \phi_b, \quad w_{b2}'(x) = -\frac{D_b}{G_b}\phi_{b2}'' + \phi_{b2}, \\ &w_{b3}'(x) = -\frac{D_b}{G_b}\phi_{b3}'' + \phi_{b3} \end{aligned} \tag{2.18}$$

$$w_{p2}'(x) = -\frac{D_p}{G_p}\phi_{p2}'' + \phi_{p2}, \qquad w_{p3}'(x) = -\frac{D_p}{G_p}\phi_{p3}'' + \phi_{p3} \tag{2.19}$$

The associated boundary and matching conditions are obtained from the variational operation as

$$\begin{aligned} \phi_{b1}(0) &= 0, \qquad \phi_{b1}''(0) = 0 \\ \phi_{b3}(1) &= 0, \qquad w_{b3}(1) = 0 \\ \phi_{p3}'(L_p) &= 0, \qquad \phi_{p3}''(L_p) = 0 \end{aligned} \tag{2.20}$$

$$\begin{aligned} M_\lambda(a) &= \left[D^*\phi_b' - D_b\phi_{b2}' - D_p\phi_{p2}'\right]_{x=a} \\ \left[g^*\phi_{b1}'' + N_0\phi_{b1}\right]_{x=a} &= \left[g_3\phi_{b2}'' + N_0\phi_{b2} + D_p\phi_{p2}''\right]_{x=a} \\ \phi_{b1}(a) &= \phi_{b2}(a) = \phi_{p2}(a) \\ w_{b1}(a) &= w_{b2}(a) = w_{p2}(a) \end{aligned} \tag{2.21}$$

$$
\begin{aligned}
\phi_{b2}'(b) &= \phi_{b3}'(b) \\
\phi_{p2}'(b) &= \phi_{p3}'(b) \\
\left[g_3\phi_{b2}''+N_0\phi_{b2}+D_p\phi_{p2}''\right]_{x=b} &= \left[g_3\phi_{b3}''+N_0\phi_{b3}+D_p\phi_{p3}''\right]_{x=b} \\
\phi_{b2}(b) &= \phi_{b3}(b) \\
\phi_{p2}(b) &= \phi_{p3}(b) \\
w_{b2}(b) &= w_{b3}(b)=w_{p3}(b)=w_{p2}(b)
\end{aligned}
\tag{2.22}
$$

where

$$
M_\lambda = m^*\Theta + (\rho^* + \frac{1}{2}h_b)N_0 \tag{2.23}
$$

The parameter M_λ in the matching condition is denoted as the transverse loading parameter, which was first introduced by Karlsson and Bottega (2000a), from which the external thermal loading enters the problem for the composite structure. The two components of the loading parameter compete with each other when they have opposite sign, which is central to the 'sling-shot buckling' phenomenon and other related issues presented by Bottega (2006). The parameters m^* and ρ^* are given in Appendix A.

2.4 Conditions

2.4.1 Integrability Condition and Transversality Condition

The use of a mixed formulation offers mathematically convenient governing equations describing the system, yet omits related information regarding in-plane deflections. We must enforce continuity among the in-plane deflections in each domain and the membrane force N_0. By integrating the strain-displacement relations and imposing the boundary and matching conditions for the in-plane displacements, we derive the integrability condition as

$$
\begin{aligned}
u_{b2}(1)-u_b(0) &= -N_0\left(\frac{1-a}{C_b}+\frac{a^*}{C}\right)+\left(1-a+a\frac{n^*}{C^*}\right)\Theta \\
&- \left(\frac{1}{2}h_b+\rho^*\right)\phi_b(a)-\frac{1}{2}\int_0^a (w_b'^2)dx-\frac{1}{2}\int_a^b (w_{b2}'^2)dx-\frac{1}{2}\int_b^1 (w_{b3}'^2)dx
\end{aligned}
\tag{2.24}
$$

The partially debonded structure discussed in the previous section (Figure 2.1) is divided into three segments - bond zone, contact zone and lift zone. The location of the boundary between the contact zone and the lift zone is determined by the corresponding transversality condition that is derived by taking the appropriate variations and allowing the boundary b to vary along with the displacements. This condition reduces to the equality of the total angular displacement of the patch and the base plate at the contact zone boundary. Therefore, a propagating contact boundary may occur only if the following condition is satisfied

$$w_{b3}'(b) = w_{p3}'(b) \tag{2.25}$$

$$w_{b3}'(b) > 0 \tag{2.26}$$

where Eq. (2.26) is added to prohibit penetration of the patch plate to the base. If Eqs. (2.25) and (2.26) are not satisfied, the system will possess either a full contact zone ($b = L_p$), no contact zone ($b = a$), or edge point contact, whichever possesses the lowest system energy.

2.4.2 Condition for (Full) Contact or Lift

To establish whether full contact between, or lift off of, the detached segment of the patch and the base plate occurs for clamped-fixed support conditions, we establish a kinematic criterion based on physical arguments. For lift off to occur, a pseudo inflection point must occur at the bond zone boundary, $x = a$. This can be characterized by the

product of the total rotations of the composite plate in the bond zone and in the contact zone, evaluated at the bond zone boundary. That is,

$$J_a \equiv w_1''(a) \cdot w_2''(a) \tag{2.27}$$

If

$$J_a < 0 \tag{2.28}$$

a full contact zone is possible. If

$$J_a > 0 \tag{2.29}$$

lift is possible. The above is coupled with the sense of the deflections when making an assessment.

On physical grounds, for hinged fixed support conditions, the flaps are in full contact with the baseplate when deflected down and are lifted off the baseplate when deflected up. Thus, a partially debonded hinged structure possesses a *dual nature*, depending on whether the flaps have fully lifted or are in full contact.

2.4.3 Stability Criterion

For a given value of the applied thermal loading, if multiple equilibrium configurations exist, it is necessary to determine which of the configurations are stable and which are unstable. In this regard, we utilize the second variation of the potential energy functional to assess the stability of each equilibrium configuration [the approach implemented in Karlsson and Bottega (2000a)]. The configuration is considered stable if the second variation of the total potential is positive definite ($\delta^2\Pi > 0$). We adopt the approach discussed in Karlsson and Bottega (2000b), in which the transverse displacements and the axial strains are perturbed via their coefficients. Doing this, we obtain the second variation of the total potential energy in the following form,

$$\delta^2\Pi = \hat{F}(\delta M_\lambda)^2 + \zeta(\delta N_0)^2 \tag{2.30}$$

where Π is the total potential energy, δ is the variational operator,

$$\zeta = \frac{1}{2}\left(\frac{a}{C^*} + \frac{a^*}{C_b}\right) \quad \text{and} \quad \hat{F} = \hat{F}(N_0, a, b) \tag{2.31}$$

As discussed in Carabetta (2011), the form of the function $\hat{F}$ depends on the particular support conditions for the specific structure. Since $\zeta > 0$, the requirement of positive definiteness of the second variation reduces to the stability criterion

$$\hat{F} > 0 \tag{2.32}$$

In this regard, a configuration is stable when Eq. (2.32) is satisfied. The function $\hat{F}$ is therefore referred to as the stability function.

2.5 Analysis

Solving Eqs. (2.13)–(2.16), subject to the boundary and matching conditions of Eqs. (2.20)–(2.22), yields the solutions for the angle of rotation due to bending in each region. The solutions are presented for two extreme support conditions: hinged-fixed and clamped-fixed ends. The general solutions to the governing equations, Eqs. (2.13) – (2.16), are found to be

$$\phi_{b1}(x) = C_1 + C_2\cos(K_b x) + C_3\sin(K_b x) \tag{2.33}$$

$$\phi_{b2}(x) = A_1\cosh(\mu_1 x) + A_2\sinh(\mu_1 x) + A_3\sin(\beta_1 x) + A_4\cos(\beta_1 x) + A_5 \tag{2.34}$$

$$\phi_{p2}(x) = P_1\left[A_1\cosh(\mu_1 x) + A_2\sinh(\mu_1 x)\right] + P_2\left[A_3\sin(\beta_1 x) + A_4\cos(\beta_1 x)\right] + A_5 \tag{2.35}$$

$$\phi_{b3}(x) = C_4 + C_5\cos(K_{b3} x) + C_6\sin(K_{b3} x) \tag{2.36}$$

The parameters $\mu_1, K_b, K_{b3}, \beta_1, P_1$, and P_2 are given in Appendix C. Note that, for both support conditions, the rotations for the base plate and patch within the contact zone are not identical ($P_1 \neq 1$, and $P_2 \neq 1$) when the shear deformation is included. The relations between transverse deflection and the angle of rotation due to bending are described by Eqs. (2.18) – (2.19). The expressions for the constants $C_1 - C_6$ and $A_1 - A_5$, which depend on the specific support conditions imposed at $x = 1$, are cumbersome, and are omitted for brevity. It is noted that the equations presented above reduce to the solutions for a perfectly intact structure in the limiting scenario when $G_b, G_P \to \infty$.

2.6 Simulation results

The purpose of this study is to demonstrate the influence of transverse shear deformation on the behavior of the structure under thermal loading. This is done by comparing results of the present model with those found by Carabetta and Bottega (2014) using the corresponding model that neglects transverse shear deformation. In this section, numerical results are presented for structures with hinged-fixed edges and for structures with clamped-fixed ends, under uniform temperature change. The effect of changing the shear modulus of the patch and base plate will be analyzed to reveal characteristic behavior. The corresponding thickness ratio is taken as $h_0 = 1$ and the ratio of coefficient of thermal expansion of the patch to the base is $\alpha_p^0 = .5$, which are consistent with those used in Karlsson and Bottega (2000a; 2000b); Rutgerson and Bottega (2002); Bottega and Carabetta (2009) and Bottega (2006).

2.6.1 Hinged Ends

We first consider the structure with hinged-fixed supports, presented in Figure 2.3(a). That is, the edges of the base plate are hinged with respect to rotation and fixed with respect to in-plane translation.

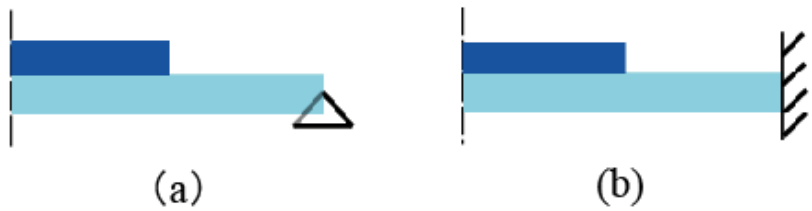

Figure 2.3 (a) Half span depiction of patched structure showing hinged-fixed edges (b) Half span depiction of patched structure showing clamped-fixed edges

For such support conditions, no contact zone exists when the partially detached structure deflects upward, due to the lack of an inflection point or pseudo-inflection point. When in this configuration, the partially detached structure is equivalent to the intact structure having the same bond zone size in terms of global stiffness and energy. This is consistent with previous studies; Bottega and Carabetta (2009), Carabetta and Bottega (2012) and Carabetta (2011). In contrast, the structure possesses a full contact zone when it deflects downwards. Thus, as discussed in Carabetta and Bottega (2014), a 'dual nature' exists for a partially debonded structure with hinged-fixed supports. In order to appropriately capture the overall behavior of the structure under thermal loading, results of simulations for a structure with no contact zone ($b = a$) and a structure having a full contact zone ($b = L_p$) are presented together. To show the effect of transverse shear on the behavior of the structure, two cases are presented: (1) equal shear stiffness for the two layers; (2) unequal shear stiffness for the base plate and patch.

Case 1: Equal shear stiffness $(G_b = G_p)$

The shear stiffnesses of the base plate and of the patch are identical, for equal thickness, if both the Young's modulus and Poisson's ratio are equal (see Eq. (2.37)).

$$G = \frac{E}{(1+\nu)} \tag{2.37}$$

The results for a structure possessing a bond zone of length $a = 0.6$ and a patch length $L_p = 0.9$ are displayed in Figures 2.4–2.7. Carabetta and Bottega (2012; 2014) and Carabetta (2011) studied the behavior of the same structure with the transverse shear deformation neglected. The results displayed in Figure 2.4 are regenerated according to Carabetta and Bottega (2014).

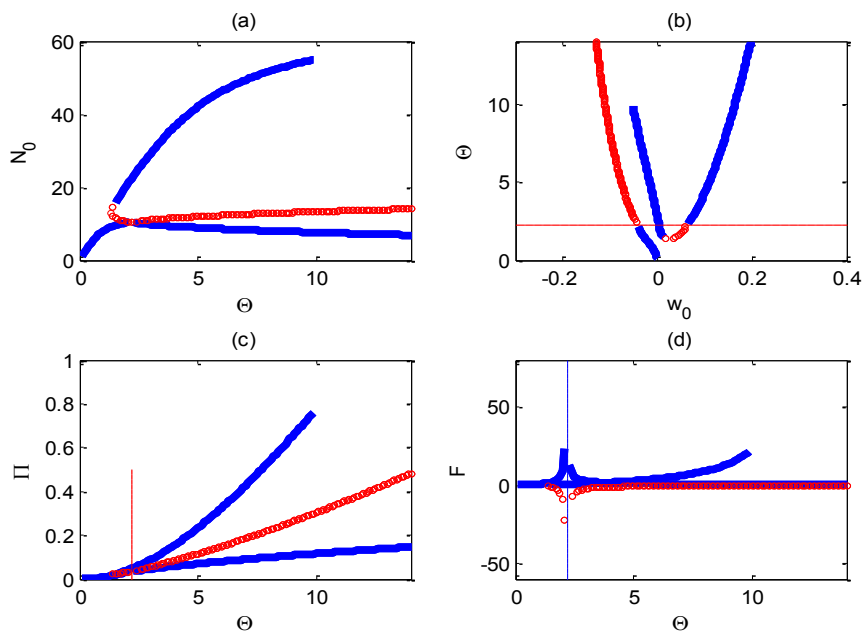

Figure 2.4 Behavior of hinged-fixed structure with shear deformation neglected; fully lifted flap, ($a = 0.6, L_p = 0.9$) (a) membrane force vs. temperature difference; (b) temperature difference vs. center-span transverse deflection, (c) total potential energy vs. temperature difference, (d) stability function vs. temperature difference. (red circles represent stable configurations and blue lines indicate the unstable configurations)

The load-deflection path is shown in Figure 2.4b as the applied temperature change as a function of the center point deflection. The membrane force, total energy and stability function are shown as a function of the appliedtemperature change in Figures. 2.4a, 2.4c and 2.4d, respectively, with the shear deformation neglected. The corresponding results , with shear deformation accounted for, are displayed in Figure 2.5.

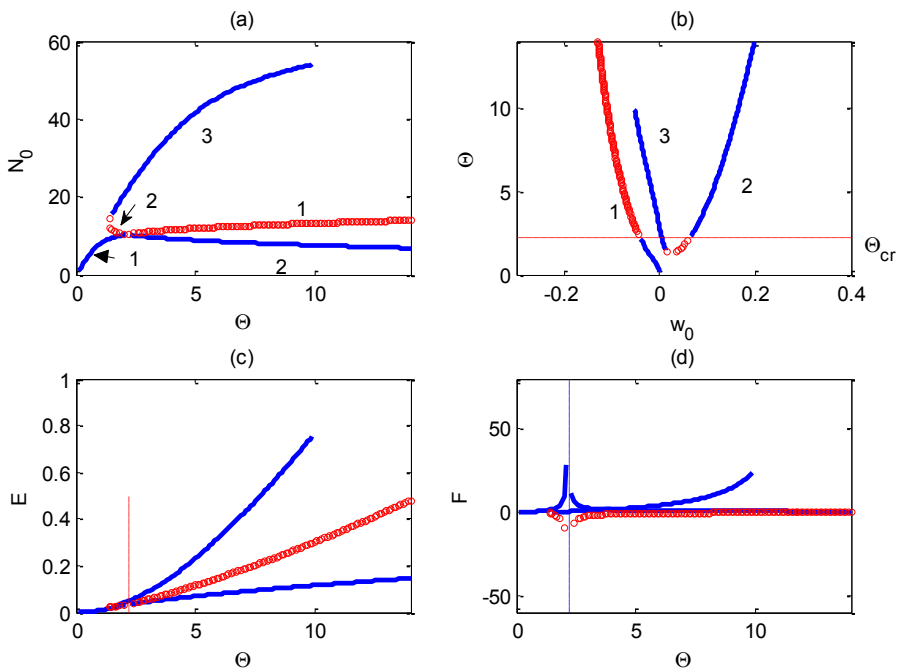

Figure 2.5 Behavior of hinged-fixed structure with $G_b = G_p$; fully lifted flap ($a = 0.6, L_p = 0.9$) (a) membrane force vs. temperature difference, (b) temperature difference vs. center-span transverse deflection, (c) total potential energy vs. temperature difference; (d) stability function vs. temperature difference.(red circles represent stable configurations and blue lines indicate the unstable configurations)

Comparison of Figures 2.4 and 2.5 shows virtually no difference in the response of the structure, indicating that the transverse shear has little effect for the case when $G_b = G_p$. In these figures, red color indicates the stable equilibrium configurations and

blue color indicates the unstable equilibrium configurations. It is seen from Figure 2.5b that, as the temperature change is increased from zero, the structure initially deflects upward and continues to do so until the critical temperature temperature is achieved, $\Theta_{cr} = 2.2$. At this point, the configuration associated with Branch 1 becomes unstable and the structure sling-shots to an alternate stable configuration on Branch 2. As the structure deflects downward, the detached 'flap' of the patch comes into contact with the base plate when $w(0) \geq 0$ and a full contact configuration appears. Thus the right most path shown in Figure 2.5b is dismissed on physical grounds.

Figures 2.6 and 2.7 display profiles of the temperature difference vs. centerspan displacement and the total energy vs. temperature difference, respectively for the structure. In these figures, red color corresponds to the full contact configuration and blue color to the fully lifted configuration. The squares indicate the stable equilibrium positions and the dots indicate the unstable positions. In these figures, the gap between the critical temperatures of the two configurations is shown. When the structure switches from the fully lifted configuration to the full contact configuration, there is no stable equilibrium position in either configuration. Thus, the structure is trapped between the two. This phenomenon is referred as 'Buckle-Trapping' as established by Bottega and Carabetta (2009) and Carabetta (2011) who proposed the exsitence of an energy casp, and hence a stable equilbrium configuration, when $w = 0$ $\left(\Theta_{cr1} \leq \Theta \leq \Theta_{cr2}\right)$.

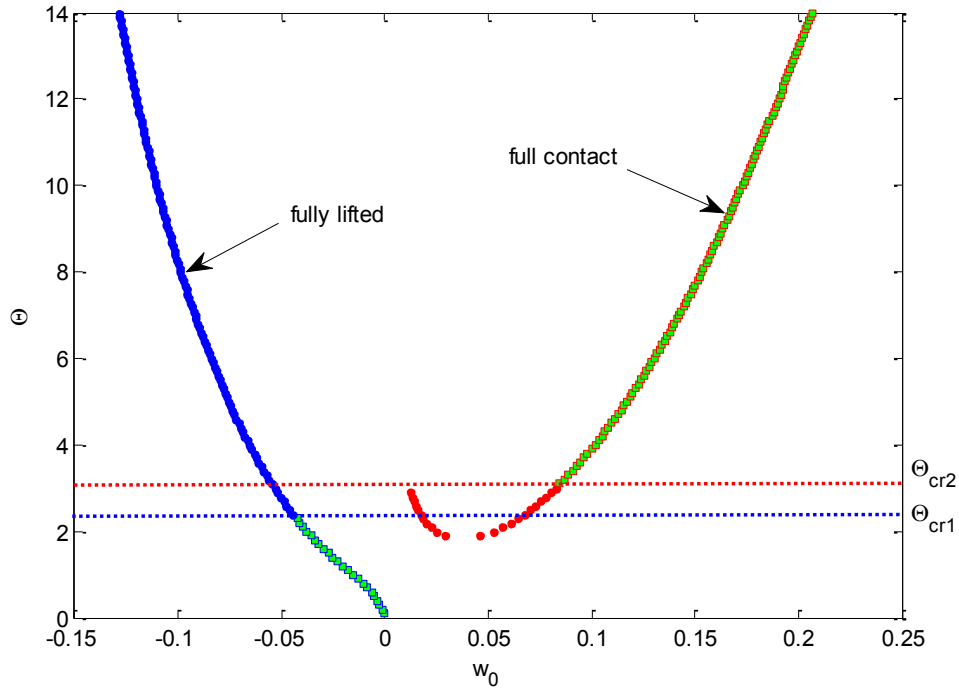

Figure 2.6 Thermal load-deflection paths for hinged-fixed total structure with $G_b = G_p$, $a = 0.6, L_p = 0.9$

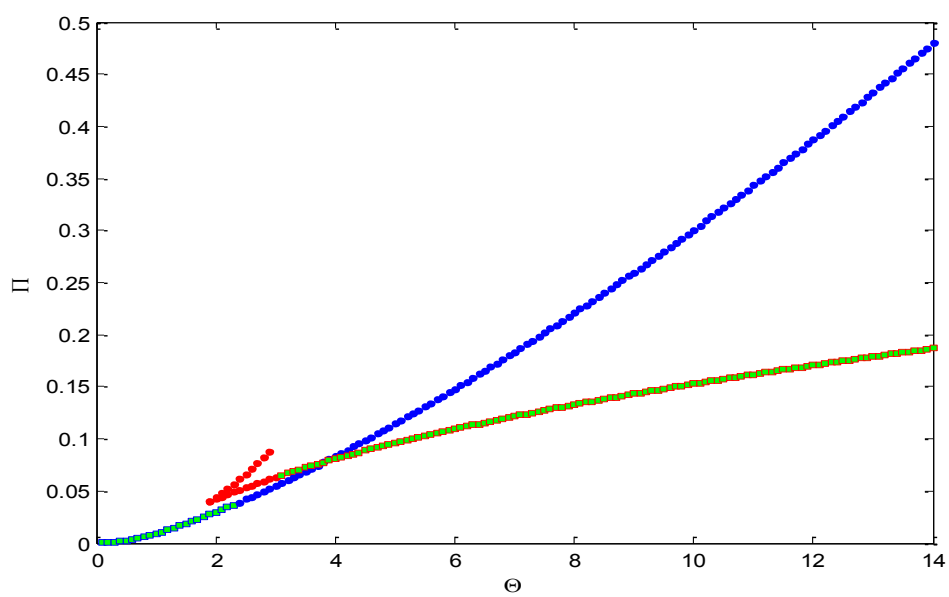

Figure 2.7 Total energy as function of temperature change for hinged-fixed total structure with $G_b = G_p$, $a = 0.6, L_p = 0.9$

Simulations for a bond zone of length $a = 0.8$ with the same patch length are also studied, but the results are omitted for brevity. However, It is observed that the 'buckle trapping' phenomenon exists even with the shear correction for this case. It is thus seen that, in this regard, the effects of transverse shear deformation are not apparent when the base plate and the patch possess equal shear stiffness.

Case 2: Unequal shear stiffness $(G_b \neq G_p)$

We next consider the case when the base plate and the patch possess unequal shear stiffness $(G_b \neq G_p)$. Selected results of simulations based on the solutions discussed in Section 3 are presented in what follows.

Results for a structure possessing a bond zone of length $a = 0.6$ and a patch length $L_p = 0.9$ are displayed in Figures 2.8-2.10. A comparison of the thermal load-deflection paths is displayed in Figure 2.8 for both cases: (1) equal shear stiffness ($G_b/G_p = 1$) and (2) unequal shear stiffness ($G_b/G_p = 2.2/2.6$), between the base plate and the patch. The profile for equal shear stiffness was already discussed under Case 1. In Figure 2.8, the black curves correspond to $G_b \neq G_p$ case and the colored curves correspond to $G_b = G_p$ case. The dashed lines indicate stable equilibrium configurations and the circles indicate the unstable states. Although the critical temperature for both cases is the same ($\Theta_{cr} = 2.2$), the deflection corresponding to the structure with unequal shear stiffnesses is seen to be much larger than that of the structure with equal shear stiffnesses, as Θ increases. Thus, the effect of shear deformation on the behavior of the structure is apparent in this case.

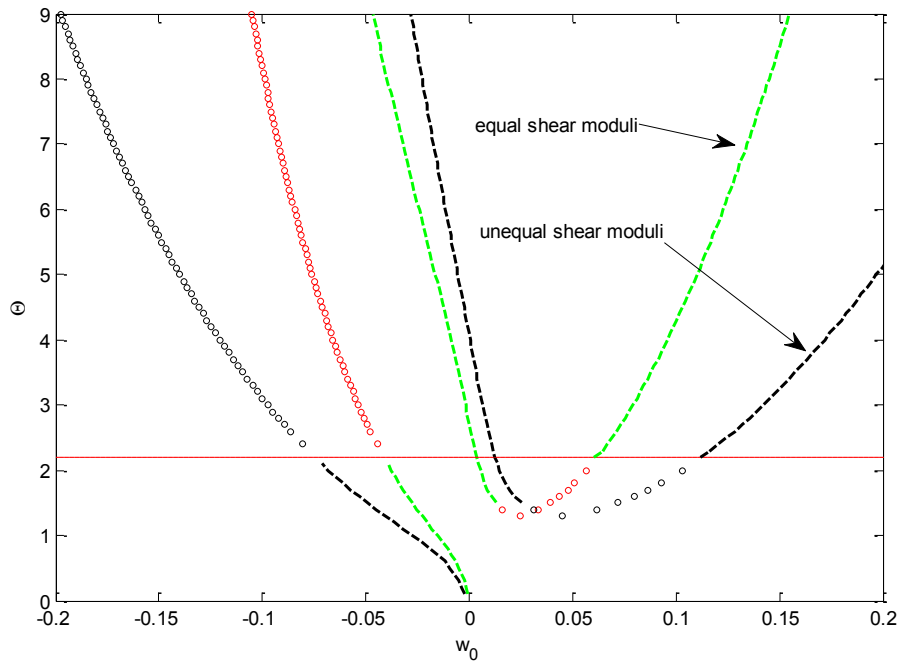

Figure 2.8 Comparison of thermal load-deflection paths for hinged-fixed structures with with $G_p \neq G_b$ ($\nu_b / \nu_p = 0.3/0.2$) with those for $G_p = G_b$, $a = 0.6, L_p = 0.9$ (dashed lines represent stable configurations and circles indicate the unstable configurations)

Figures 2.9 and 2.10 show the dual load-deflection curve and the total energy profile as a function of the temperature change (both the full contact and fully lifted configurations are presented). It was shown previously for Case 1 where, at the critical temperature, the structure buckles from the fully lifted configuration, and Buckle-Trapping occurs before the structure reaches the full contact configuration. However, from Figures 2.9 and 2.10, it is seen that the partially detached structure buckles from a fully lifted configuration to a full contact configuration at the critical temperature $\Theta_{cr} = 2.2$, where it is stable for the full contact configuration. Thus, the Buckle-Trapping phenomenon disappears for this case.

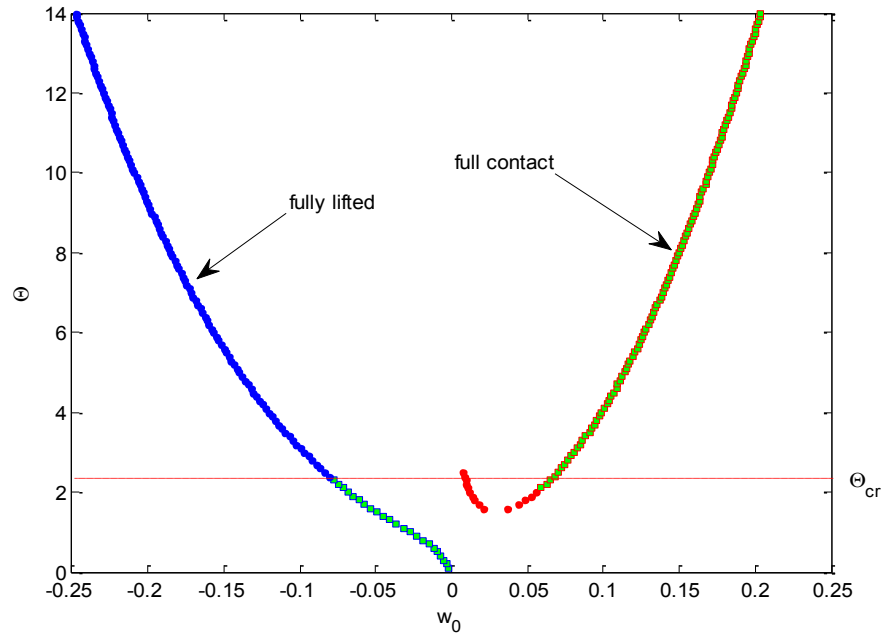

Figure 2.9 Thermal load-deflection paths for hinged-fixed structure with $\nu_b / \nu_p = 0.3/0.2$ **,** $a = 0.6, L_p = 0.9$

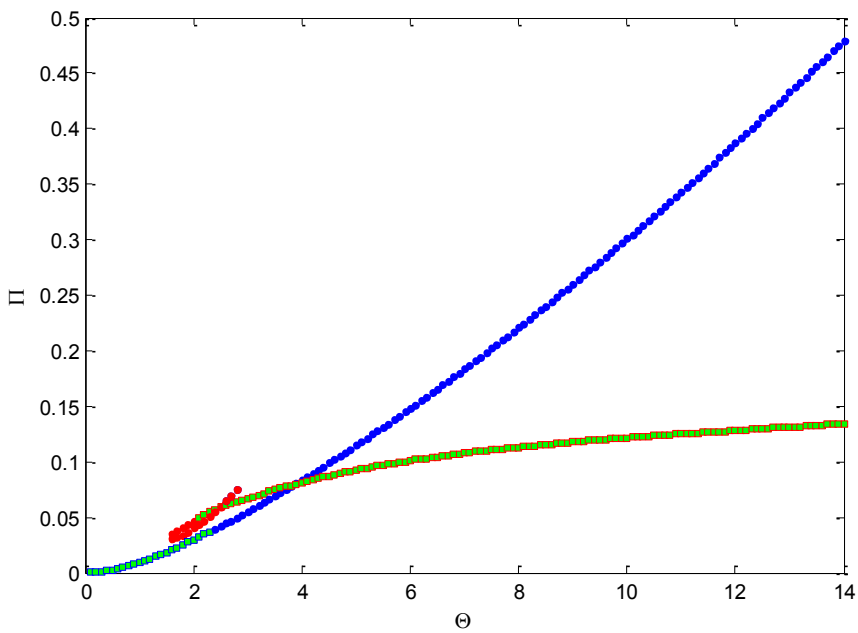

Figure 2.10 Total energy of hinged-fixed structure as function of temperature change; $\nu_b / \nu_p = 0.3/0.2$ **,** $a = 0.6, L_p = 0.9$

We also examined the partially debonded structure with differing shear stiffnesses for a bond zone size $a = 0.8$ and observed similar behavior. The results are omitted for brevity. Comparing these results to those for the case of a structure with equal shear stiffnesses, we observe that the 'buckle trapping' phenomenon does not occur when the base plate and the patch posses unequal shear stiffnesses for the case considered. This is in contrast to what was predicted by Carabetta and Bottega (2014), with the transverse shear neglected. We next proceed to the case of structures with clamped-fixed edges under uniform temperature change.

2.6.2 Clamped Ends

We next consider the situation when the edges of the base-plate are clamped-fixed. That is, when the edges of the structure are clamped with respect to rotation and fixed with respect to both transverse and in-plane translation. The general behavior of the whole structure will be seen to be notablely different from that of the structure with hinged-fixed supports described earlier. It was established by Bottega and Carabetta (2009), Carabetta and Bottega (2014) and Carabetta (2011) that a propagating intermediate contact zone is possible for certain bond zone sizes. For the present case, we demonstrate the existence of fully lifted, full contact, intermediate contact and edge contact configurations, with transverse shear effect included. As the structure flips upward, edge contact may occur as discussed by Karlsson and Bottega (1999) for patched cylindrical panels. It is observed for the present case that, in contrast to what was observed for hinged supports, contact occurs in prebuckling and lift occurs in postbuckling. When intermediate contact occurs, the transversality conditions (Eqs. (2.25) – (2.26)) are used to determine the location of the contact zone/lift zone boundary under a certain

temperature change. In this section, some representative examples will be presented to demonstrate the variety of behaviors. The first example is for the case when the shear stiffnesses of the base plate and the patch are equal.

Case 1: Equal shear stiffness $(G_b = G_p)$

Results for a structure possessing a bond zone of length $a = 0.6$ and a patch length $L_p = 0.9$ are presented in Figures 2.11 – 2.14. For a structure with clamped ends, edge contact as well as full contact configurations are possible when the structure deflects upward. Unlike the situation when shear deformation is neglected, it is found presently that, when shear deformation is accounted for, an edge contact configuration may occur when the structure deflects upward. In situations when the patched structure has more than one admissible configuration for a given bond zone size, the one with the lowest total potential energy will be considered as the 'preferred' configuration for a particular patch and base structure [Karlsson and Bottega (1999)]. The total energies for three different configurations (full contact, no contact and edge contact) are presented in Figure 2.11.

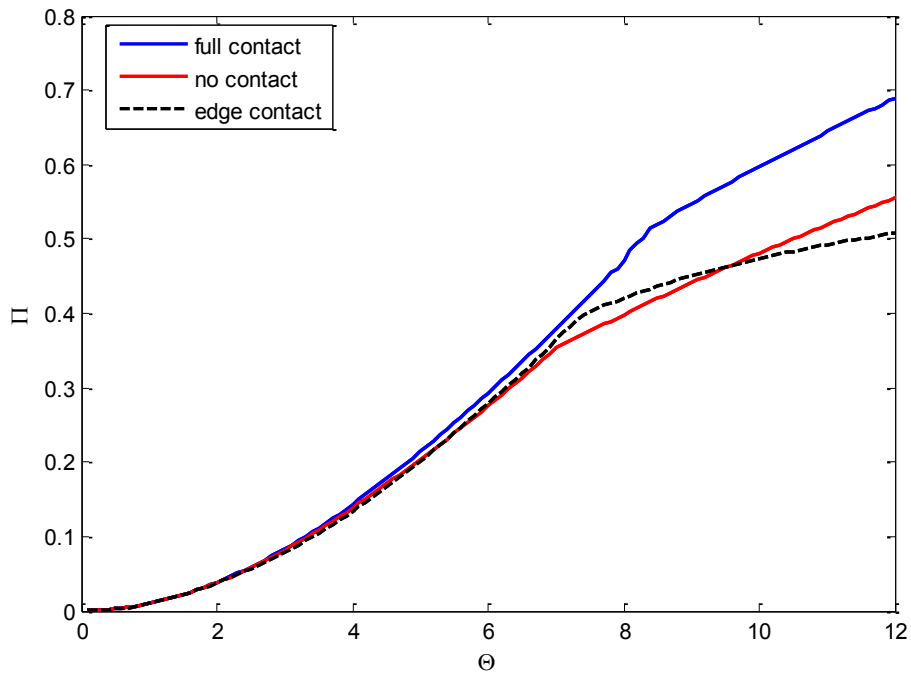

Figure 2.11 Comparison of total energy (three cases: full contact, fully lifted and edge contact), vs. temperature difference for clamped-fixed structure with $G_b = G_p$**,** $a = 0.6, L_p = 0.9$

Based on the results of the junction rotation product, J_a, presented in Figure 2.12, it is observed that at $\Theta = 2.4$, the full contact configuration is no longer valid as the sign of J_a becomes positive. The structure, thus, has two possible configurations for Θ >2.4 – no contact or edge contact. However, it is seen from Figure 2.11 that the edge contact configuration has a lower potential energy at this temperature. Thus, we take the edge contact configuration as the 'preferred' configuration for the system. As the temperature increases, the total energy of the edge contact case exceeds that of the no contact configuration, and the patched structure switches to no contact configuration at $\Theta = 5.5$, with the patch lifting away from the base plate.

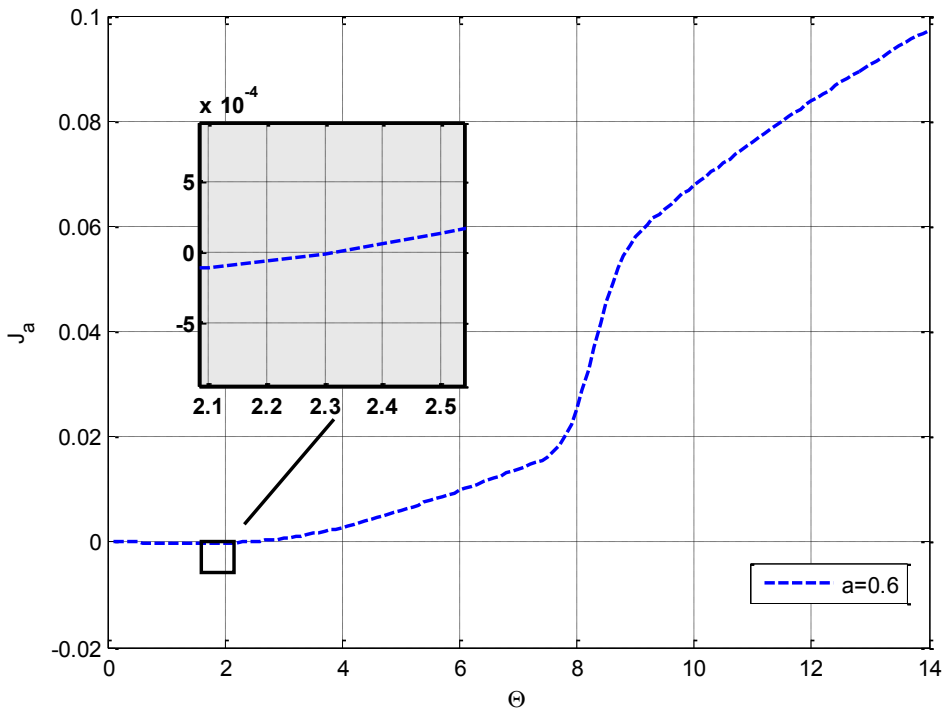

Figure 2.12 Junction rotation parameter, J_a, as function of temperature difference for clamped-fixed structure with $G_b = G_p$, $a = 0.6, L_p = 0.9$

The final load-deflection profile and the total energy of the structure (only stable configurations) are presented in Figure 2.13 and Figure 2.14, respectively. It is noticed that the structure first possesses a full contact zone and then, at $\Theta = 2.4$ it 'jumps' to edge contact, and then to no contact configuration when $\Theta \geq 5.5$.

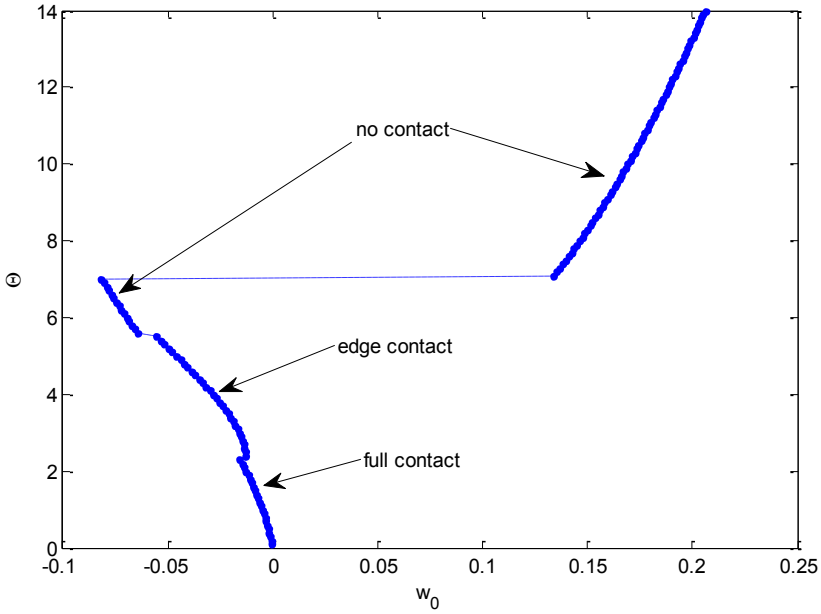

Figure 2.13 Thermal load-deflection paths for camped-fixed structure with $G_b = G_p$**,** $a = 0.6, L_p = 0.9$

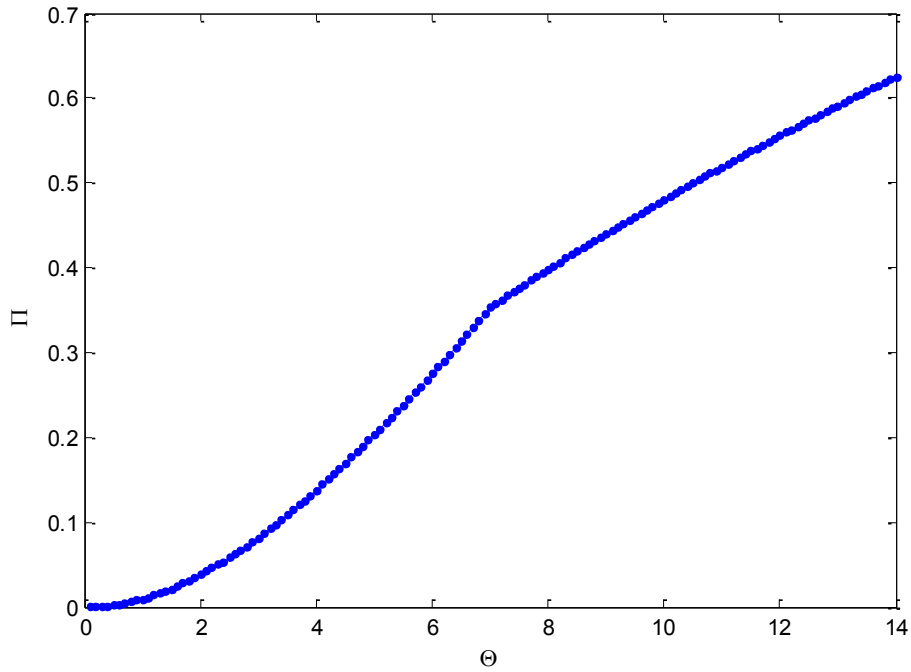

Figure 2.14 Clamped-fixed structure, $G_b = G_p$**, total energy vs. temperature difference;** $a = 0.6, L_p = 0.9$

Table 2.1: Summary of the simulation results for clamped-fixed edge

	$E_b = E_p$			$\nu_b = \nu_p$		$E_b = E_p$ $\nu_b = \nu_p$
	$\frac{\nu_b}{\nu_p} = \frac{0.3}{0.25}$	$\frac{\nu_b}{\nu_p} = \frac{0.25}{0.3}$	$\frac{\nu_b}{\nu_p} = \frac{0.1}{0.3}$	$\frac{E_b}{E_p} = 0.1$	$\frac{E_b}{E_p} = 10$	$G_b = G_p$
$a = 0.8$	Full $\Downarrow \theta = 4.3$ No	Full $\Downarrow \theta = 4.2$ No	Full $\Downarrow \theta = 4.2$ No	Full $\Downarrow \theta = 3.3$ No	Full $\Downarrow \theta = 2.5$ No	Full $\Downarrow \theta = 4$ No
$a = 0.6$	Full $\Downarrow \theta = 1.8$ Edge $\Downarrow \theta = 5.6$ No	Full $\Downarrow \theta = 2$ Edge $\Downarrow \theta = 5.5$ No	Full $\Downarrow \theta = 2.6$ Edge $\Downarrow \theta = 5.5$ No	Full $\Downarrow \theta = 3.2$ No	Full $\Downarrow \theta = 2.5$ No	Full $\Downarrow \theta = 2.4$ Edge $\Downarrow \theta = 5.5$ No
Full represents 'Full contact'; Edge represents 'Edge contact'; No represents 'No contact'.						

The simulation results for a bond zone length of $a = 0.8$ are summarized in Table 2.1. At this point, it is concluded that for the case with equal shear stiffness, the patched plate possesses three configurations during the temperature increases: full contact, edge contact

and no contact configuration. Intermediate contact does not occur. Next, let us consider the case when the base plate and the patch have different shear stiffness.

Case 2: Unequal shear stiffness $(G_b \neq G_p)$

In this section, we consider the case when the shear stiffnesses of the patch and of the base plate are unequal. We remark that this is equivalent to the substructures possessing different Poisson's ratios and/or different Young's moduli per the well known relation (Eq. (2.37)) .

As discussed in the previous section, the analytical solution for this situation differs substantially from that of the case with equal shear stiffness. It is anticipated that some interesting behaviors of the patched structure will be unveiled.

(1) Unequal Poisson's Ratio and Equal Young's Moduli

Results for a structure possessing a bond zone size of $a = 0.6$ and a patch length $L_p = 0.9$ are presented in Figures 2.15 – 2.18. To identify the existence of the contact zone and edge contact configurations, we combine the results of the junction rotation product, J_a, in Figure 2.16 with those for the total potential energy of the three configurations presented in Figure 2.15.

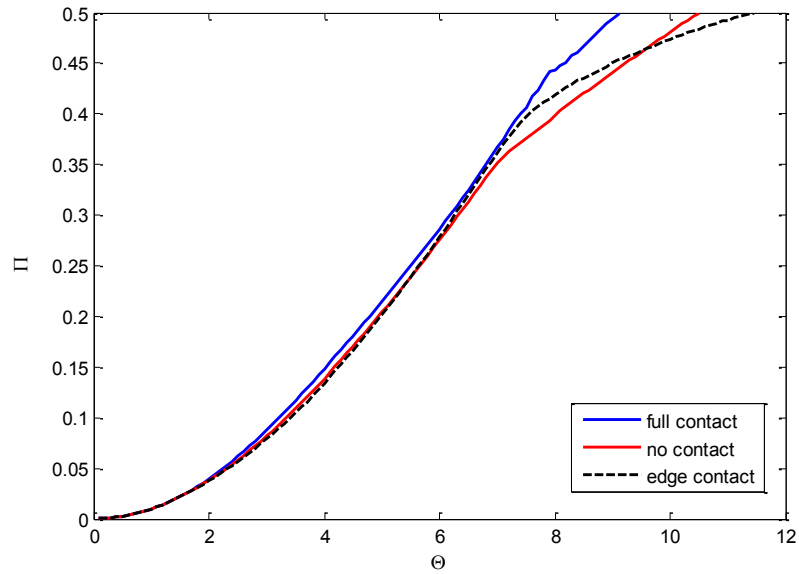

Figure 2.15 Comparison of total energy (full contact, fully lifted and edge contact) as function of temperature difference for clamped-fixed structure with $\nu_b / \nu_p = 0.3/0.2$, $a = 0.6, L_p = 0.9$

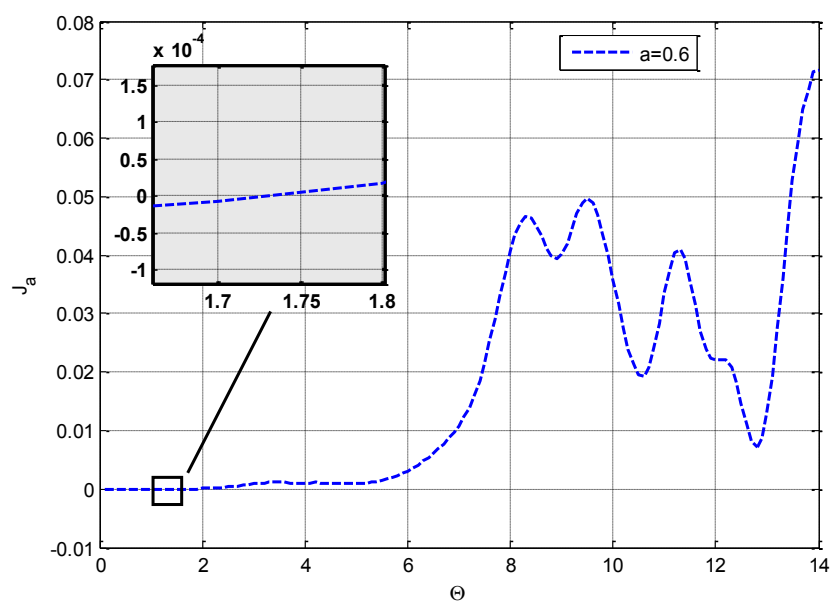

Figure 2.16 Junction rotation parameter, J_a, as function of temperature difference for clamped-fixed structure with $\nu_b / \nu_p = 0.3/0.2$, $a = 0.6, L_p = 0.9$.

The full contact configuration is no longer valid when the sign of $J_a \equiv$ $J_a \equiv w_1''(\mathrm{a}) \cdot w_2''(\mathrm{a})$ changes in Figure 2.16. Thus, the structure 'jumps' to a configuration with edge contact when the temperature achieves the value $\Theta = 1.7$. At this point, the system assumes a configuration with edge contact which has a lower total potential energy. The structure then switches to a configuration with no contact, when $\Theta = 5.3$. The trend is similar to that for the case of equal shear stiffness, however the critical 'jump' temperature changes substantially.

The results displayed in Figure 2.17 and Figure 2.18 show the 'actual' load-deflection paths and the total energy, respectively. It is noticed that the structure initially possesses a full contact zone, but at $\Theta = 1.7$, it 'jumps' to a configuration with edge contact, and then to a configuration with no contact when $\Theta = 5.3$.

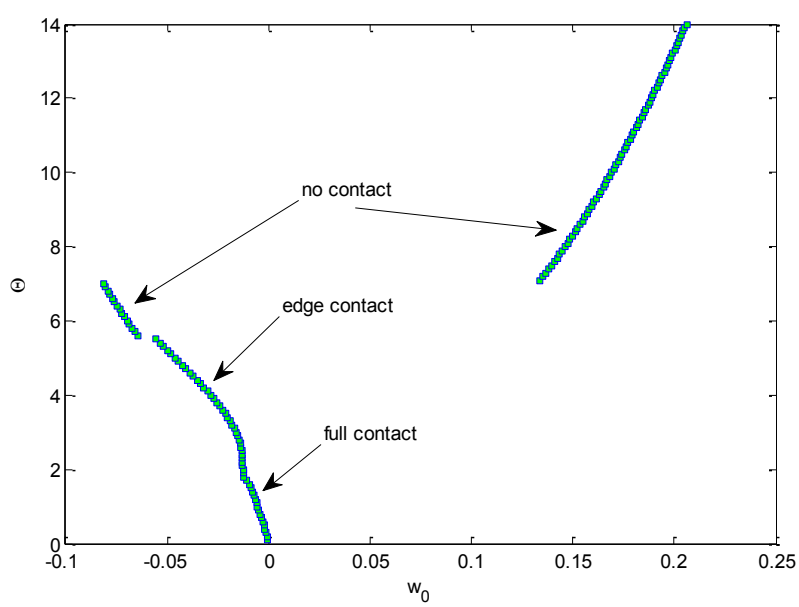

Figure 2.17 Thermal load-deflection paths for clamped-fixed structure with $\nu_b / \nu_p = 0.3/0.2$, $a = 0.6, L_p = 0.9$

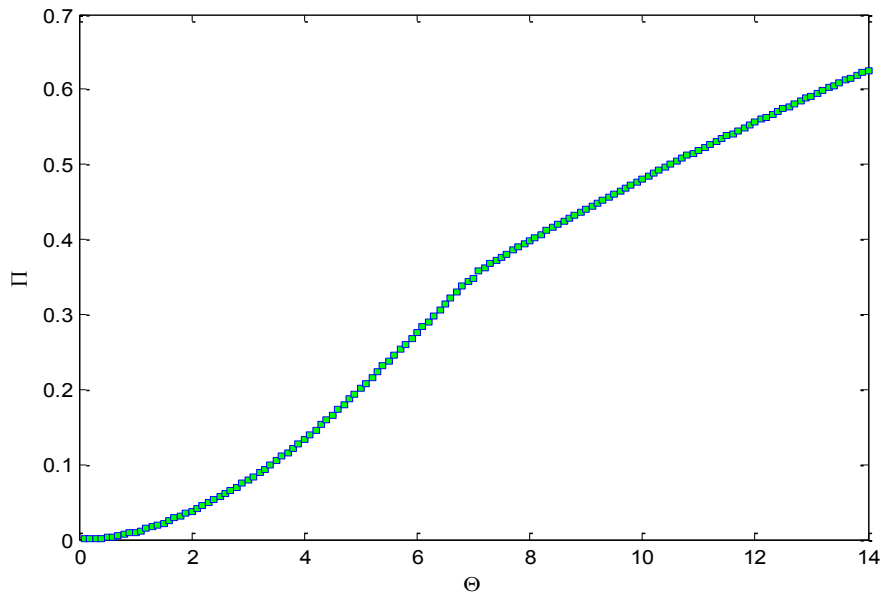

Figure 2.18 Clamped-fixed structure, $\nu_b / \nu_p = 0.3/0.2$, total energy vs. temperature difference; $a = 0.6, L_p = 0.9$

Results are also obtained for the case of a bond zone length of $a = 0.8$ and for different Poisson's ratio of the two layers. Characteristic behavior for this case is summarized in Table 2.1 along with those for a structure with a bond zone length of $a = 0.6$. Based on these results, we see that for different Poisson's ratios, the structure follows a similar trend as for $a = 0.8$. We next consider the effect of Young's modulus on the behavior of the structure.

(2) Unequal Young's Moduli and Equal Poisson's Ratio

Different Young's moduli will result in different shear stiffnesses between the patch and the base plate, per Eq. (2.37). However, unlike for Poisson's ratio, Young's modulus will also affect the membrane energy and bending energy of the system.

It is therefore essential to study the behavior of the patched structure when Young's modulus for the patch and that of the base plate differ. Results for the case when the ratio

of Young's modulus of the base plate to that of the patch is $E_b / E_p = 0.1$ are displayed in Figures 2.19 – 2.21 for a structure that possesses a bond zone size of $a = 0.6$.

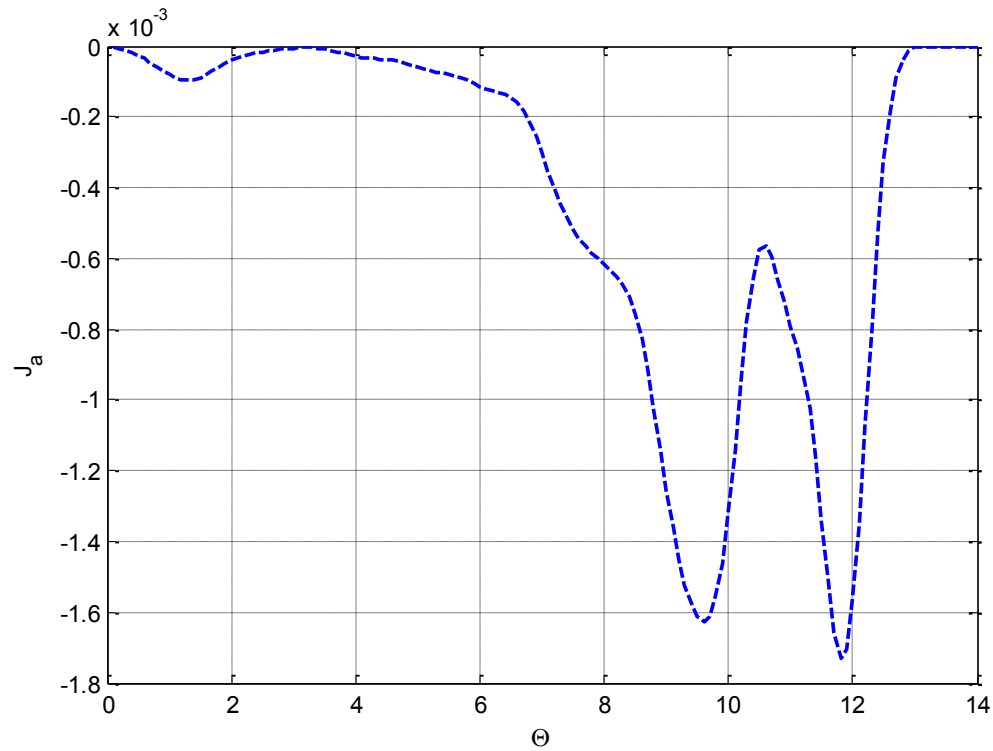

Figure 2.19 Junction rotation parameter, J_a, as function of temperature difference for clamped-fixed structure with $E_b / E_p = 0.1$**,** $a = 0.6, L_p = 0.9$

The transversality condition is then examined to check the existence of an intermediate contact zone and to determine the location of the contact zone boundary. It is seen from Figure 2.19 that when the structure deflects upward it will initially possess a full contact zone until the critical temperature is reached. At this temperature, the structure buckles downward. We note that, for this range of temperatures, the sign of J_a is negative, which indicates that the structure will not possess a contact zone when it deflects downward. For this case, we also find that there is no edge contact configuration during the temperature increase. Therefore, at the critical temperature, the structure sling-

shots from a configuration with full contact to a configuration with no contact. The 'actual' load-deflection curve and the total energy profile (stable configurations) of the system are shown in Figure 2.20 and Figure 2.21, respectively.

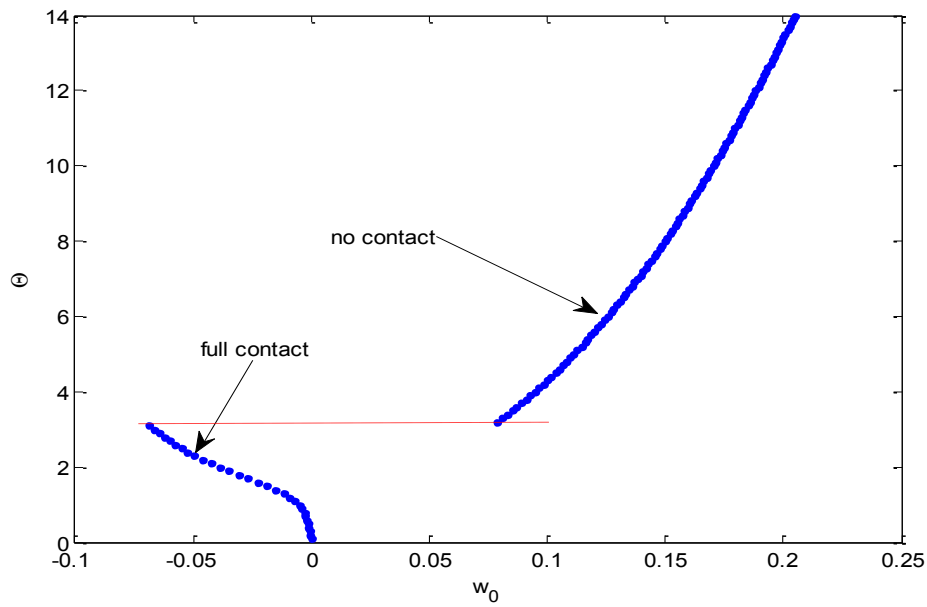

Figure 2.20 Clamped-fixed structure, $E_b / E_p = 0.1$, center-span displacement vs. temperature difference; $a = 0.6, L_p = 0.9$

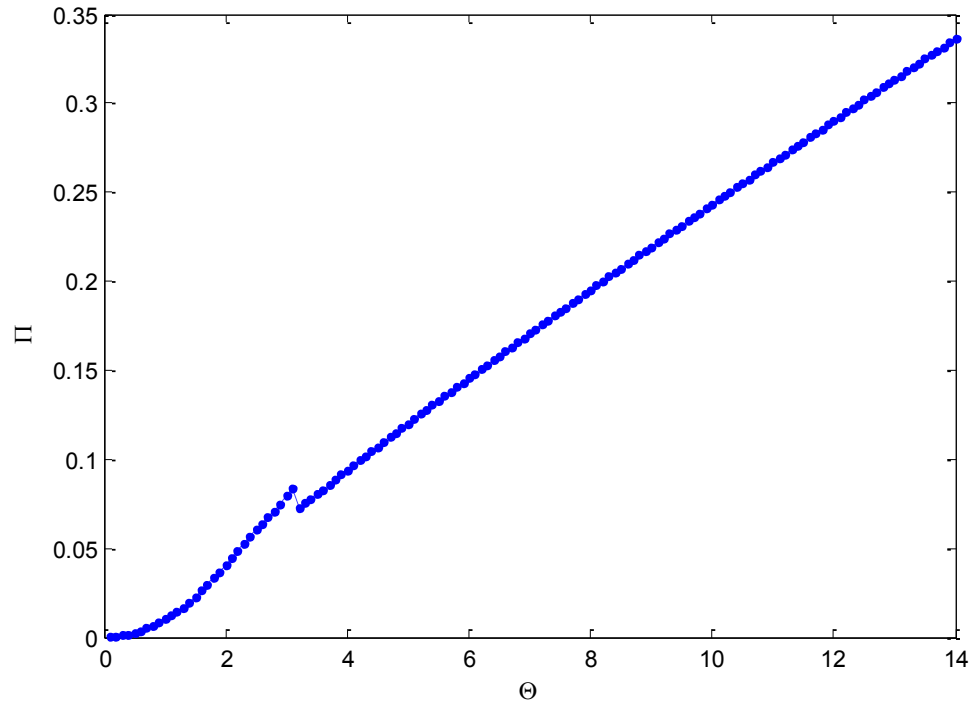

Figure 2.21 Clamped-fixed structure, $E_b / E_p = 0.1$, total energy vs. temperature difference; $a = 0.6, L_p = 0.9$

It is seen that, as the temperature is increased, the structure first possesses a full contact zone and then 'jumps' to a no contact configuration at $\Theta = 3.2$. Compared Fig 2.21 with Fig 2.18, it is noticed that there is a jump in the total potential energy function. This is due to the structure switches to a new configuration which is shown in Fig. 2.20.

A summary of characteristic behavior, and its relation to bond zone size, Young's modulus and Poisson's ratio of the layers is presented in Table 2.1. The morphological 'transition' temperatures, at which the structure will switch from one type of configuration to another type of configuration (e.g., full contact, edge contact, no contact) are shown separately for each case. It is seen that edge contact will not occur, for the larger bond zone size considered, $a = 0.8$. In contrast, it seen that edge contact often occurs for the

other bond zone size considered, $a = 0.6$, except for the case when the two layers have the same Young's modulus, but different Poisson's ratio. Thus, the morphology of the partially detached patched structure is very sensitive to the material properties (the bond zone size, Poisson's ratio and Young's modulus) of the constituent structures.

2.7 Conclusions

In this chapter, we advance prior studies concerning thermal instabilities in patched beam-plates with partial edge detachment by including trasverse shear deformation into consideration. The resulting governing equations, internal and external boundary conditions, trasnversality condition and stability criterion are derived using a variational formulation. Closed form analytical solutions to the governing equations are determined and simulations based on these solutions are performed. The associated analysis and numerical simulations reveal representative and critical behavior of the partially detached structure under uniform temperature change for both hinged-fixed and clamped-fixed edges. It is seen that transverse shear deformation plays a very important role in some cases.

Chapter 3 ***Behavior of the eye encircled by a scleral buckle***

3.1 Introduction

In clinical practice, one of the commom methods for closure of a retinal tear is the application of a closed elastic band (cerclage) along the equator. This elastic band is called the scleral buckle. The buckle usually is sutured to the eye to keep it in place and left there permanently. In this chapter, we study the mechanical behavior of the eye resulting from the application of a scleral buckle. The problem is formulated using variational methods in conjunction with the Theorem of Stationary Potential Energy. Closed form analytical solutions of the coupled set of differential equations that govern the curved ocular system are obtained, and results of numerical simulations based on those solutions are presented and critical phenomena of the ocular structure are unveiled. The effects of material and geometric parameters (radius, width, thickness and Young's modulus) of the scleral buckle, as well as of the ocular pressure, on the deformation and volume change of the eye are studied.

3.2 Formulation

We formulate the problem of quasi-static mechanical behavior of the eyeball due to application of an encircling elastic buckle. The thickness to radius ratio of the wall of the eye comprised of the sclera and choiroid is typically $h/R \sim O(10^{-2})$ (see Wilkinson and Rice (1997), Uchio, et al. (1999), and Sigal, et al. (2014)). This suggests that the

composite structure comprised of these layers can be modeled as a thin shell. Likewise, the thickness to radius ratio of a typical scleral buckle is $h_b/R_b \sim O(10^{-1})$ (See Chou and Siegel (2013), Jones, et al. (1992), and Wollensak and Spoerl (2004)), which suggests that the buckle can be modeled as a thin ring structure. In light of this, the eye is modeled as a spherical elastic shell, and the scleral buckle is modeled as a uniform elastic ring of smaller initial radius that is sutured to the equator of the sphere. As we are interested in the deformation of the eye due to the presence of the buckle, the problem reduces to one of axisymmetric deformation about the equator. In addition, as discussed in Bottega, et al. (2013), the thickness to radius ratio for the retina is very small, and the associated bending and membrane stiffnesses are much smaller than those of the sclera-choroid composite, and therefore can be neglected in this regard when considering the overall stiffness of the eye.

3.2.1 Geometry

The mathematical model for the eye with scleral buckle is depicted in Figure 3.1. Spherical coordinates, (r, θ, φ), are used to describe the deforming eye-buckle structure, where r is the radial coordinate, θ is the polar angle, and φ is the azimuth angle, as indicated. The scleral buckle is situated at $\varphi = \pi/2$.

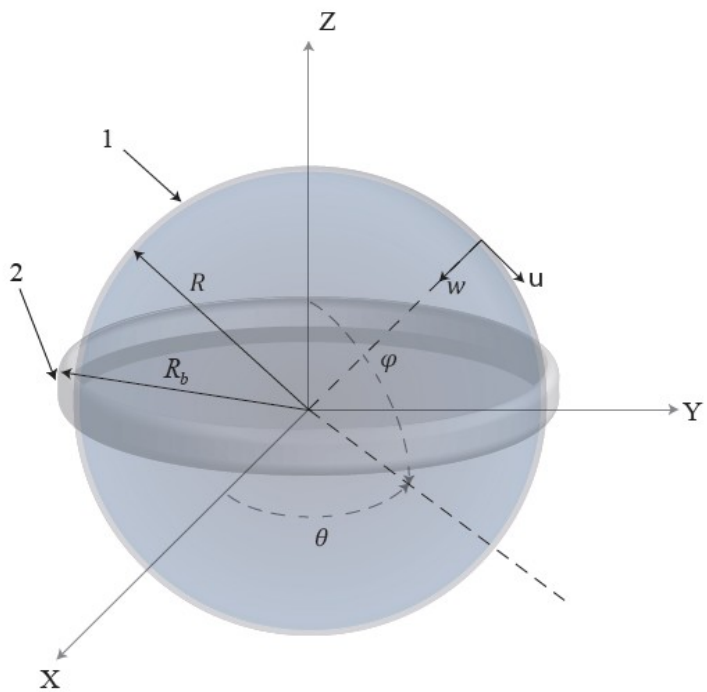

Figure 3.1 3-D Human eyeball with scleral buckle. (r, θ, φ) **Coordinates** φ **and** θ **are shown. The parameters** w **and** u **are the radial and meridian displacements, respectively. The number 1 indicates the eye membrane and 2 indicates the scleral buckle.**

As a result of the inherent geometry and "loading" of the idealized system, symmetry is assumed about $\varphi = 0$ (the *z*-axis), over the domain $0 \le \theta \le 2\pi$. Therefore, the analysis of the axisymmetric structure is a function of the meridian angle alone, and need only be performed over the segment shown in Figure 3.2. In this regard, the structure is partitioned into two domains; $S_1 : \varphi \in [0, \varphi_1]$ – the region comprised of the eye alone, and $S_2 : \varphi \in [\varphi_1, \pi/2]$ – the region comprised of both the eye and the scleral buckle. In the ensuing analysis, we shall denote the radial deflection of the eye wall in region *j* as $w_j(\varphi)$ (*j* = 1,2) taken as positive inward, and denote the corresponding meridian deflection as

$u_j(\varphi)\,(j = 1,2)$ taken as positive in the direction of increasing φ. The undeformed radius of the eye is taken as R and that of the buckle is taken as R_b.

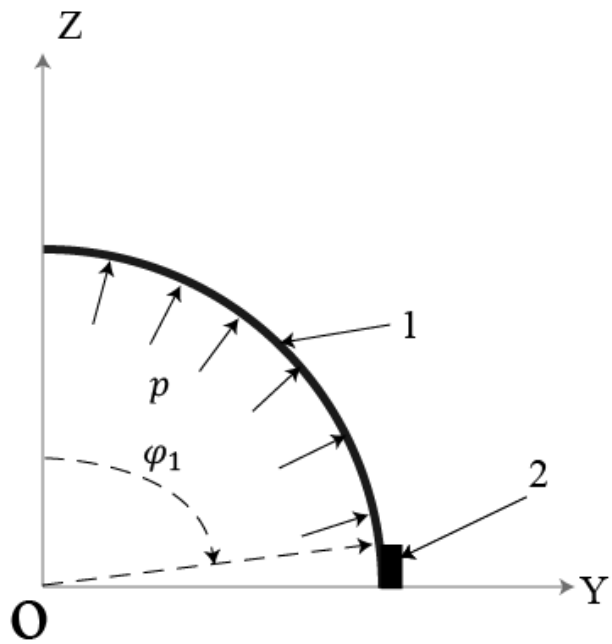

Figure 3.2 Schematic of the eye with scleral buckle. The number 1 indicates the eye wall and 2 indicates the scleral buckle. The symbol φ_1 indicates the contact boundary.

3.2.3 Potential Energy Functional

To derive the governing equations and boundary conditions for the eye and buckle system, we first formulate the associated energy functional in terms of the corresponding membrane energy, $\bar{U}_M$, and bending energy, $\bar{U}_B$, of the ocular system comprised of the eye and the buckle, and the work, $\bar{W}$, done by the normalized ocular pressure, $\bar{p}$. In addition, the scleral buckle is sutured to the outside surface of the eye. As a result of this, the deflections of the outer surface of the sclera and the inner surface of the buckle are effectively constrained to deflect together in Region S_2. We therefore include a

constraint functional, $\bar{\Lambda}$, to account for this. We thus formulate the energy functional, $\bar{\Pi}$, as follows,

$$\bar{\Pi} = \bar{U}_B + \bar{U}_M - \bar{\Lambda} - \bar{W} \tag{3.1}$$

where

$$\begin{aligned}\bar{U}_M &= 2\pi\bar{R}^2\int_0^{\varphi_1}\left[\frac{1}{2}\bar{N}_{\varphi\varphi}^{(1)}\varepsilon_{\varphi\varphi}^{(1)} + \frac{1}{2}\bar{N}_{\theta\theta}^{(1)}\varepsilon_{\theta\theta}^{(1)}\right]\sin(\varphi)d\varphi \\ &+2\pi\bar{R}^2\int_{\varphi_1}^{\pi/2}\left[\frac{1}{2}\bar{N}_{\varphi\varphi}^{(2)}\varepsilon_{\varphi\varphi}^{(2)} + \frac{1}{2}\bar{N}_{\theta\theta}^{(2)}\varepsilon_{\theta\theta}^{(2)}\right]\sin(\varphi)d\varphi + \bar{R}_b\int_{\varphi_1}^{\pi/2}\frac{1}{2}\bar{N}_{b\theta\theta}^{(2)}\varepsilon_{b\theta\theta}^{(2)}d\theta\end{aligned} \tag{3.2}$$

$$\begin{aligned}U_B &= 2\pi\bar{R}^2\int_0^{\varphi_1}\left[\frac{1}{2}\bar{M}_{\varphi\varphi}^{(1)}\chi_{\varphi\varphi}^{(1)} + \frac{1}{2}\bar{M}_{\theta\theta}^{(1)}\chi_{\theta\theta}^{(1)}\right]\sin(\varphi)d\varphi \\ &+2\pi\bar{R}^2\int_{\varphi_1}^{\pi/2}\left[\frac{1}{2}\bar{M}_{\varphi\varphi}^{(2)}\chi_{\varphi\varphi}^{(2)} + \frac{1}{2}\bar{M}_{\theta\theta}^{(2)}\chi_{\theta\theta}^{(2)}\right]\sin(\varphi)d\varphi + \bar{R}_b\int_{\varphi_1}^{\pi/2}\frac{1}{2}\bar{M}_{b\theta\theta}^{(2)}\chi_{b\theta\theta}^{(2)}d\theta\end{aligned} \tag{3.3}$$

$$\bar{W} = 2\pi\bar{R}^2\int_0^{\varphi_1}\bar{p}\bar{w}_1(\varphi)\sin(\phi)\,\mathrm{d}\phi + 2\pi\bar{R}^2\int_{\varphi_1}^{\pi/2}\bar{p}\bar{w}_2(\varphi)\sin(\phi)\,\mathrm{d}\phi \tag{3.4}$$

$$\bar{\Lambda} = 2\pi\bar{R}_b^{\,2}\int_{\phi_1}^{\pi/2}\bar{\sigma}(\bar{w}_2 - \bar{w}_{b2} + \bar{R} - \bar{R}_b)\,d\phi + 2\pi\bar{R}_b^{\,2}\int_{\phi_1}^{\pi/2}\bar{\tau}(\bar{u}_2 - \bar{u}_{b2})\,d\phi \tag{3.5}$$

In Eqs. (3.2) and (3.3),

$$\bar{N}_{\varphi\varphi}^{(j)} = \bar{C}\left[\varepsilon_{\varphi\varphi}^{(j)}(\varphi) + \nu\,\varepsilon_{\theta\theta}^{(j)}(\varphi)\right],\quad \bar{N}_{\theta\theta}^{(j)} = \bar{C}\left[\varepsilon_{\theta\theta}^{(j)}(\varphi) + \nu\,\varepsilon_{\varphi\varphi}^{(j)}(\varphi)\right]\ (j = 1,2) \tag{3.6}$$

correspond to the normalized membrane force per unit length of the sclera in Region S_j (j = 1,2), in the direction indicated by the subscripts, and $\bar{C}$ is the normalized membrane stiffness of the eye wall. Likewise,

$$\bar{M}_{\varphi\varphi}^{(j)} = \bar{D}\left[\bar{\chi}_{\varphi\varphi}^{(j)}(\varphi) + \nu\,\bar{\chi}_{\theta\theta}^{(j)}(\varphi)\right],\quad \bar{M}_{\theta\theta}^{(j)} = \bar{D}\left[\bar{\chi}_{\theta\theta}^{(j)}(\varphi) + \nu\,\bar{\chi}_{\varphi\varphi}^{(j)}(\varphi)\right]\ (j = 1,2) \tag{3.7}$$

are the associated normalized bending moments in the globe, $\bar{D}$ is the corresponding bending stiffness and ν is Poisson's ratio. In addition,

$$\varepsilon_{\varphi\varphi}^{(j)}(\varphi)=\frac{1}{\bar{R}}\left\{\bar{u}_j{}'(\varphi)-\bar{w}_j(\varphi)\right\},\quad \varepsilon_{\theta\theta}^{(j)}(\varphi)=\frac{\cot\varphi}{\bar{R}}\left\{\bar{u}_j(\varphi)-\bar{w}_j(\varphi)\tan\varphi\right\}\ (j=1,2) \tag{3.8}$$

are the corresponding membrane strains, $\bar{R}$ is the non-dimensional radius of the undeformed eye, and

$$\bar{\chi}_{\varphi\varphi}^{(j)}(\varphi)=\frac{1}{\bar{R}^2}\left\{\bar{u}_j{}'(\varphi)+\bar{w}_j{}''(\varphi)\right\},\quad \bar{\chi}_{\theta\theta}^{(j)}(\varphi)=\frac{\cot\varphi}{\bar{R}^2}\left\{\bar{u}_j(\varphi)+\bar{w}_j{}'(\varphi)\right\}\ (j=1,2) \tag{3.9}$$

are the associated changes in non-dimensional curvature of the surface of the eye wall. In the above expressions, superposed primes indicate differentiation with respect to φ. Similarly,

$$\bar{N}_{b\theta\theta}^{(2)}=\bar{C}_b\varepsilon_{b\theta\theta}^{(2)}(\varphi),\quad \bar{M}_{b\theta\theta}^{(2)}=\bar{D}_b\bar{\chi}_{b\theta\theta}^{(2)}(\varphi) \tag{3.10}$$

$$\varepsilon_{b\theta\theta}^{(2)}(\varphi)=-\frac{1}{\bar{R}_b}\bar{w}_{b2}(\varphi),\quad \bar{\chi}_{b\theta\theta}^{(2)}(\varphi)=\frac{1}{\bar{R}_b{}^2}\left\{\bar{w}_{b2}(\varphi)+\bar{w}_{b2}^{''}(\varphi)\right\} \tag{3.11}$$

represent the normalized membrane forces, bending moments, membrane strains and curvature changes of the scleral buckle, where $\bar{R}_b$ is the non-dimensional radius of the undeformed buckle. Finally, the parameters $\bar{\sigma}$ and $\bar{\tau}$ appearing in Eq. (3.5) are Lagrange multipliers and physically correspond to the non-dimensional radial normal stress and meridian shear stress at the interface between the eye and the buckle. The non-dimensional parameters appearing in the above relations are related to their dimensional counterparts as follows,

$$\begin{aligned}
&\bar{R}=R/R=1,\quad \bar{R}_b=R_b/R,\quad \bar{h}=h/R,\quad \bar{h}_b=h_b/R,\quad \bar{t}_b=t_b/R,\\
&\bar{u}=u/R,\quad \bar{w}=w/R,\quad \bar{M}_{\varphi\varphi}^{(j)}=\frac{R}{D}M_{\varphi\varphi}^{(j)},\quad \bar{M}_{\theta\theta}^{(j)}=\frac{R}{D}M_{\theta\theta}^{(j)},\quad \bar{p}=\frac{R^3}{D}p,\\
&\bar{C}=\frac{R^2}{D}C=\frac{12}{\bar{h}^2},\quad \bar{C}_b=\frac{C_b}{D}\frac{R^2}{R_b}=12\frac{E_b}{E}\frac{\bar{h}_b}{\bar{h}^3}\frac{\bar{t}_b}{\bar{R}_b},\quad \bar{D}_b=\frac{D_b}{D}\frac{R^2}{R_b{}^3}=\frac{E_b}{E}\frac{\bar{h}_b{}^3}{\bar{h}^3}\frac{\bar{t}_b}{\bar{R}_b}\frac{1}{\bar{R}_b{}^2}
\end{aligned} \tag{3.12}$$

where unbarred quantities are the dimensional quantities, all length scales are normalized with respect to the dimensional radius R of the undeformed globe, E and E_b are the dimensional Young's modulus of the sclera and of the scleral buckle, respectively, $\bar{h}$ and $\bar{h}_b$ are the corresponding non-dimensional thicknesses, and $\bar{t}_b$ is the non-dimensional half-width of the scleral buckle.

3.3 Governing Equations and Boundary Conditions

We next invoke the Theorem of Stationary Potential Energy. Hence,

$$\delta \bar{\Pi} = 0 \tag{3.13}$$

where δ represents the variational operator and $\bar{\Pi}$ is the energy functional defined by Eq. (3.1).

Region S_2: The elastic ring model of the scleral buckle implicitly assumes that the deviance of the deflection through the width is negligible. As the width of the scleral buckle is relatively small compared with the surface area of the eye, the assumption that its meridian displacement (i.e., the displacement of the buckle along the φ - direction) is negligible, as well as the variance of the radial deflection, is a reasonable one. As a result of this, as well as due to the symmetry of the problem, the transverse displacement of the buckle will be uniform around its periphery. It then follows from Eq. (3.1) that the equation governing the radial displacement of both the buckle and the sclera in Region S_2 is reduced to the simple form

$$\bar{w}_{b2} = \frac{-\bar{p}\cos(\varphi_1)}{2\bar{C}(1+\nu)\cos(\varphi_1) + \bar{C}_b + \bar{D}_b} \tag{3.14}$$

(The meridian displacement in each vanishes identically.)

Region S_1: To solve the problem in Region S_1, we follow the procedure described in Timoshenko, et al. (1959), Flugge (1960), and Lakawicz, Bottega, Prenner and Fine (2014). After eliminating the Lagrange multipliers, we express the equilibrium equations for the globe found from the variational principle, in terms of the resultant non-dimensional transverse shear force per unit arc length, $\bar{Q}^{(1)}(\varphi)$, and the rotation of the cross section in the meridian direction, $\bar{\Psi}(\varphi)$. This gives the corresponding set of *governing equations* in Region S_1,

$$\bar{\Psi}'' + \bar{\Psi}' \cot\varphi - \bar{\Psi}\left[\nu + \cot^2\varphi\right] = \bar{Q}^{(1)} \tag{3.15}$$

$$\bar{Q}^{(1)''} + \bar{Q}^{(1)'} \cot\varphi + \bar{Q}^{(1)}\left[\nu - \cot^2\varphi\right] = -\bar{C}(1-\nu^2)\bar{\Psi} \tag{3.16}$$

$$\bar{Q}^{(1)} = \left(\bar{M}^{(1)}_{\varphi\varphi}\sin\varphi\right)' - \cos\varphi \bar{M}^{(1)}_{\theta\theta}, \quad \bar{\Psi} = \bar{u}_1 + \bar{w}_1' \tag{3.17}$$

where $(\ )' = d(\ )/d\varphi$. In addition, the boundary conditions follow directly from implementation of the variational principle as

$$\bar{u}_1(0) = 0, \quad w_1'(0) = 0, \quad \bar{Q}^{(1)}(0) = 0, \tag{3.18}$$

$$\bar{u}_1(\varphi_1) = 0, \quad \bar{w}_1(\varphi_1) = w_{b2}, \quad \bar{w}_1'(\varphi_1) = 0 \tag{3.19}$$

The system of coupled equations given by Eqs. (3.14) – (3.17) are readily solved, in conjunction with the boundary conditions given by Eqs.(3.18) and (3.19). The solution is presented in the next section.

3.3 Analysis

Adopting the method presented in Timoshenko, Woinowsky-Krieger and Woinowsky (1959), Flugge (1960) and Lakawicz, Bottega, Prenner and Fine (2014), we obtain the analytical solutions for the eye wall in Region S_1. Hence,

$$\begin{aligned}\bar{Q}^{(1)}(\varphi) &= A_1 \sin\varphi \, {}_2F_1\left(\alpha_1, \beta_1; 2; \sin^2\varphi\right) + A_2 \sin\varphi \, {}_2F_1\left(\hat{\alpha}_1, \hat{\beta}_1; 2; \sin^2\varphi\right) \\ &+ A_3 \sin\varphi G_{2\ 2}^{2\ 0}\left(\sin^2\varphi \left| \begin{matrix} \alpha_1 - \frac{1}{2} & \beta_1 - \frac{1}{2} \\ -1 & 0 \end{matrix} \right.\right) + A_4 \sin\varphi G_{2\ 2}^{2\ 0}\left(\sin^2\varphi \left| \begin{matrix} \hat{\alpha}_1 - \frac{1}{2} & \hat{\beta}_1 - \frac{1}{2} \\ -1 & 0 \end{matrix} \right.\right)\end{aligned} \tag{3.20}$$

$$\bar{u}_1(\varphi) = A_6 \sin\varphi - \frac{1}{\bar{C}(1-\nu)}\left\{\bar{Q} + (\frac{1}{2}\bar{p} + A_5)(\cot\varphi + g(\varphi)\sin\varphi)\right\} \tag{3.21}$$

$$\begin{aligned}\bar{w}_1(\varphi) &= A_6 \cos\varphi - \frac{1}{\bar{C}(1-\nu^2)}(\bar{Q}' + \bar{Q}\cot\varphi) \\ &+ \frac{1}{\bar{C}(1-\nu^2)}\bar{p}(1 - \frac{1}{2}(1+\nu)g(\varphi)\cos\varphi) + \frac{1}{\bar{C}(1-\nu)}A_5(1 - g(\varphi)\cos\varphi)\end{aligned} \tag{3.22}$$

where

$$g(\varphi) = \ln\left(\cos\varphi/2\right) - \ln\left(\sin\varphi/2\right) \tag{3.23}$$

$$\alpha_1 = \frac{3+\sqrt{5+iZ}}{4}, \quad \beta_1 = \frac{3-\sqrt{5+iZ}}{4}, \quad \hat{\alpha}_1 = \frac{1+\sqrt{5-iZ}}{4}, \quad \hat{\beta}_1 = \frac{1-\sqrt{5-iZ}}{4}, \tag{3.24}$$

$$Z = 4\sqrt{(1-\nu^2)\bar{C} - \nu^2} \tag{3.25}$$

In addition, ${}_2F_1$ represents a Hypergeometric function, $G_{2\ 2}^{2\ 0}$ represents a Meijer G function, and $A_1 - A_6$ are constants of integration. With the expressions for the meridian and radial displacements established in Eqs. (3.21) and (3.22), respectively, we proceed to solve for the constants $A_1 - A_6$ by applying the boundary conditions. It is required, on physical grounds, that the deflections at $\varphi = 0$, and throughout the domain of definition,

should be finite. However, the Meijer G function and natural logarithm function are singular at the origin. Thus, to render the shear force and displacement finite, the coefficients of these terms in Eqs. (3.20) – (3.22) must vanish. Hence,

$$A_3 = 0, \quad A_4 = 0, \quad A_5 = -\frac{\bar{p}}{2} \tag{3.26}$$

Imposing the boundary conditions at $\varphi = \varphi_1$, as specified in Eq. (3.16), the remaining constants must satisfy the system given by

$$\begin{Bmatrix} A_1 \\ A_2 \\ A_6 \end{Bmatrix} = \begin{bmatrix} l_1 X_{11} & l_1 X_{12} & -\sin\varphi_1 \\ l_3(X_{21} + X_{11}\cot\varphi_1) & l_3(X_{22} + X_{12}\cot\varphi_1) & -\cos\varphi_1 \\ l_3(X_{31} + X_{21}\cot\varphi_1 - X_{11}\csc^2\varphi) & l_3(X_{32} + X_{22}\cot\varphi_1 - X_{12}\csc^2\varphi) & \sin\varphi_1 \end{bmatrix}^{-1} \begin{bmatrix} 0 \\ \frac{1}{2} l_2 \bar{p} - \bar{w}_0 \\ 0 \end{bmatrix} \tag{3.27}$$

where

$$\begin{aligned}
&l_1 = \frac{1}{\bar{C}(1-\nu)}, \quad l_2 = \frac{1}{\bar{C}(1+\nu)}, \quad l_3 = \frac{1}{\bar{C}(1-\nu^2)} \\
&X_{11} = \sin\varphi_1 F_{11}, \quad X_{12} = \sin\varphi_1 F_{12} \\
&X_{21} = \cos\varphi_1 F_{11} + \alpha_1\beta_1 \sin^2\varphi_1 \cos\varphi_1 F_{21}, \quad X_{22} = \cos\varphi_1 F_{12} + \hat{\alpha}_1\hat{\beta}_1 \sin^2\varphi_1 \cos\varphi_1 F_{22} \\
&X_{31} = -\sin\varphi_1 F_{11} + \alpha_1\beta_1(3\sin\varphi_1\cos^2\varphi_1 - \sin^3\varphi_1)F_{21} + \frac{2}{3}\sin^3\varphi_1\cos^2\varphi_1\alpha_1(\alpha_1+1)\beta_1(\beta_1+1) \\
&X_{32} = -\sin\varphi_1 F_{12} + \hat{\alpha}_1\hat{\beta}_1(3\sin\varphi_1\cos^2\varphi_1 - \sin^3\varphi_1)F_{22} + \frac{2}{3}\sin^3\varphi_1\cos^2\varphi_1\hat{\alpha}_1(\hat{\alpha}_1+1)\hat{\beta}_1(\hat{\beta}_1+1) \\
&F_{11} = {}_2F_1\left(\alpha_1, \beta_1; 2; \sin^2\varphi_1\right), \quad F_{12} = {}_2F_1\left(\hat{\alpha}_1, \hat{\beta}_1; 2; \sin^2\varphi\right) \\
&F_{21} = {}_2F_1\left(\alpha_1+1, \beta_1+1; 3; \sin^2\varphi_1\right), \quad F_{22} = {}_2F_1\left(\hat{\alpha}_1+1, \hat{\beta}_1+1; 3; \sin^2\varphi_1\right) \\
&F_{31} = {}_2F_1\left(\alpha_1+2, \beta_1+2; 4; \sin^2\varphi_1\right), \quad F_{32} = {}_2F_1\left(\hat{\alpha}_1+2, \hat{\beta}_1+2; 4; \sin^2\varphi_1\right)
\end{aligned} \tag{3.28}$$

After the integration coefficients are obtained, the solutions for the displacements are explicitly described in Eqs. (3.20) – (3.22). Finally, the total non-dimensional volume change, $\Delta\bar{V}$, is given by

$$\Delta\bar{V} = \bar{V} - \bar{V}_0 = 4\pi \int_0^{\pi/2} \bar{x}^2 \sqrt{\bar{x}^2 + \bar{y}^2}\, d\varphi - \frac{4}{3}\pi\bar{R}^3 \tag{3.29}$$

where $\bar{x}$ and $\bar{y}$ are the Cartesian components of displacements of a material particle of the eye wall obtained by coordinate transformation of the analytical solutions delineated by Eqs. (3.20)–(3.22).

3.4 Simulation results

In this section, the behavior of the ocular system is studied for various configurations of the scleral buckle. The results presented are based on the analytical solutions described earlier in this section. We study the influence of various parameters of the band on the behavior of the eye. Specifically, we examine the effect of the radius of the band, the width of the band, thickness (height) of the band, and Young's mdulus. We also consider the effect of the band, in conjunction with changes in ocular pressure. Specifically, we consider pressure differences of 20, 23, 40 and 76 mmHg for all cases of band parameters (As discussed by Keeling, Propst, Stadler and Wackernagel (2009) the ocular pressure of a normal eye is typically of the order of 23 mmHg, but could reach a maximum of about 76 mmHg during scleral buckle surgery. They also point out that after the buckle is attached, the autoregulation mechanism of the eye will reduce the volume of fluid in the eye and thereby reduce the pressure to around 20 mmHg).

3.4.1 Influence of buckle radius

Results for various (initial) buckle radii, R_b = 10.5, 11, and 11.5 mm, as well as increasing pressure, p, are presented in Figures 3.3–3.6. (The undeformed radius of the eye is taken as R =12 mm.) The corresponding deflection profiles, per unit applied stress, are presented in Figures 3.3 and 3.4. In each case, the buckle is attached at $\varphi = \varphi_1 \approx 1.4$.

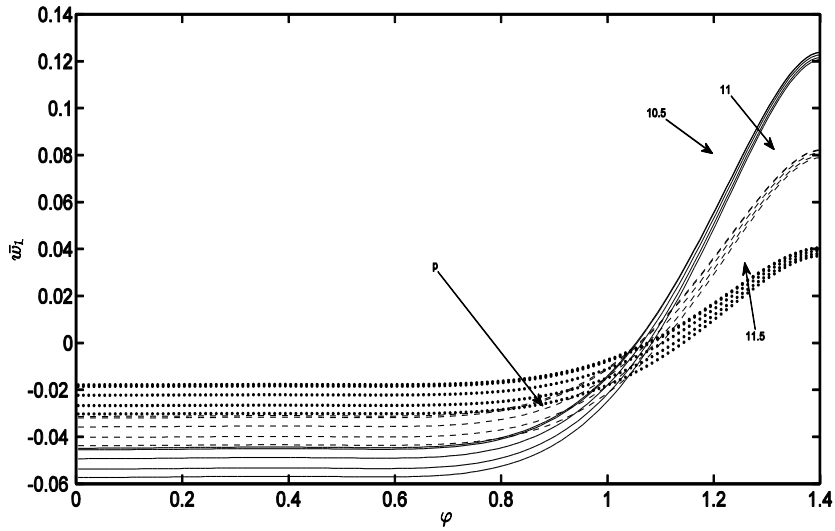

Figure 3.3 Radial displacement of the eye with applying buckles with different radius, as a function of φ , under changing pressure. The arrow indicates the increasing direction of the pressure.

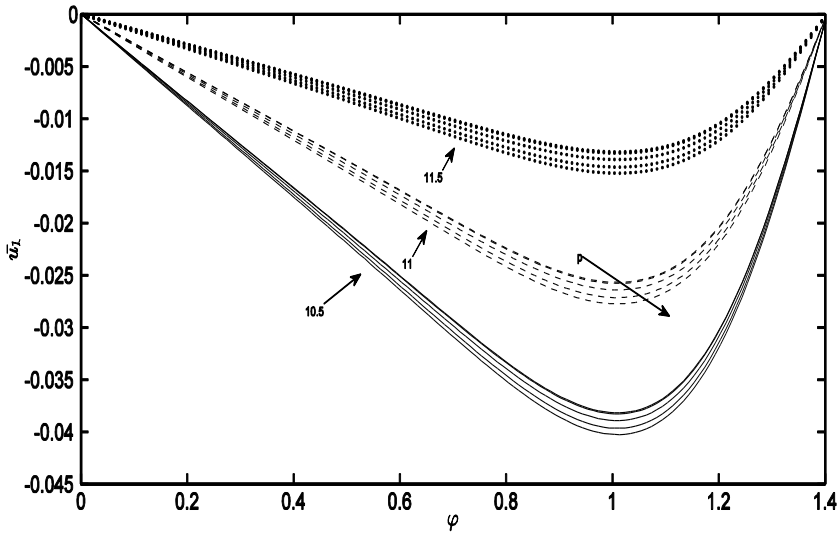

Figure 3.4 Meridian displacement of the eye with applying buckles with different radius, as a function of φ , under changing pressure. The arrow indicates the increasing direction of the pressure.

It is seen in Figure 3.3 that the radial displacement of the buckle ($\varphi = \varphi_1 \approx 1.4$) decreases as the pressure increases for each value of the (initial) buckle radius. It is also seen that as the meridian angle, φ , decreases (that is, as we proceed away from the buckle), the sign of the radial displacement switches from positive to negative. This indicates that the eye wall deflects outwards at locations sufficiently far from the buckle. It is also seen that, for each value of the pressure, there is one point where the radial displacement vanishes. This is an inflection point, where the curvature of the deflected eye wall changes from concave to convex. It is also observed for this figure that the deflections are larger for smaller buckles, as one might expect. Finally, it is seen that the location of the inflection point along the globe varies with the radius of the undeformed buckle. The corresponding deflection profiles of the meridian displacement are shown in Figure 3.4. It is seen that the meridian displacement is negative for all cases considered. Moreover, the gradient of the displacement is negative for smaller angles and then turns positive. This suggests that the eye wall stretches in the vicinity of the buckle, and contracts at locations away from the buckle (when the meridan angle is less than $\varphi \approx 1$ for each case).

Profiles of a deformed eye with a buckle of (initial) radius $R_b = 11$ mm are displayed in Figure 3.5 for various values of the ocular pressure. Similarly, profiles of a deformed eye with ocular pressure $p = 23$ mmHg are displayed in Figure 3.6 for various values of (initial) buckle radii. In each figure, the stars describe the profile of the eye before deformation by the buckle $(\bar{w}(\varphi) = 0, \forall \varphi)$.

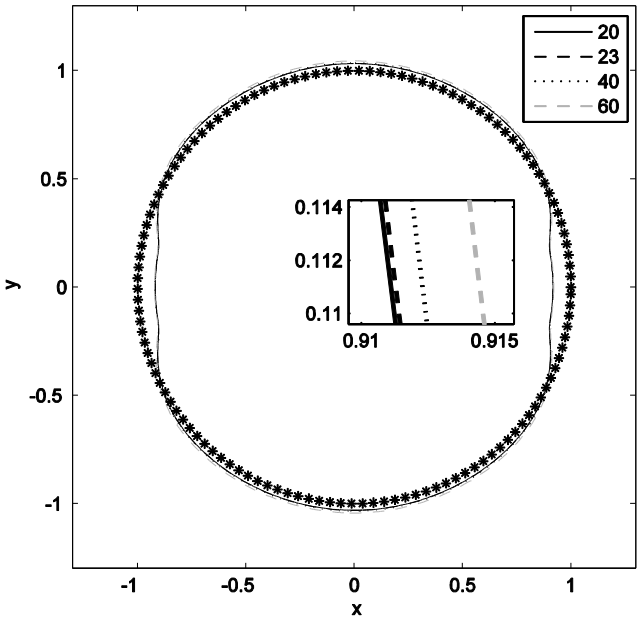

Figure 3.5 Deformation of the eyeball under different pressure in Cartesian coordinates. The radius of the buckle is kept as a constant (11 mm).

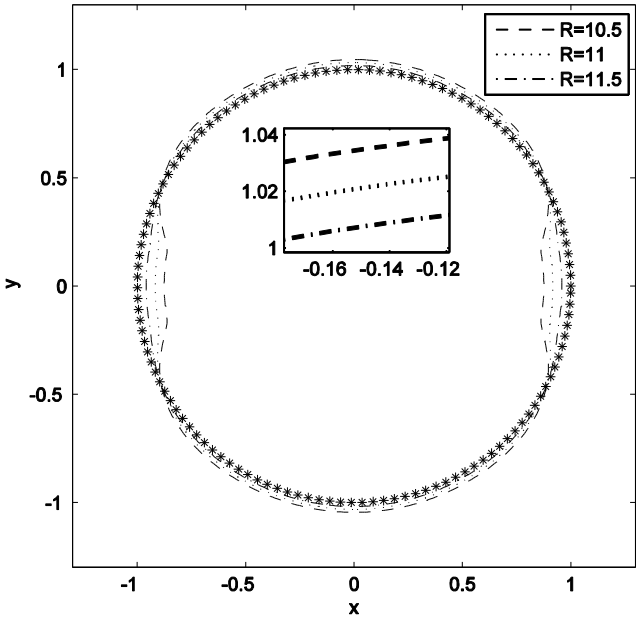

Figure 3.6 Deformation of the eyeball with different scleral buckle radius in Cartesian coordinates. The pressure is kept as a constant (20 mmHg).

It is seen from Figure 3.5 that, within the range of values considered, the pressure change has only a minute influence on the deformation induced by the scleral buckle. The inset in the figure shows a magnified view of the deformations under various values of the pressure. The effect of initial buckle radius is shown in Figure 3.6. It is seen from that figure that the deformation of the eye wall increases substantially as the initial radius of the scleral buckle decreases. Finally, it is seen in both Figures 3.5 and 3.6 that, for each case considered, the diameter of the equator of the eye (the horizontal diameter) is substantially compressed by the presence of the buckle, while the diameter of the axis of the eye (the vertical) is expanded. It is also seen that the most severe deformation of the eye occurs in a region that is relatively local to the buckle.

3.4.2 Influence of buckle width

Results for various values of the buckle width are displayed in Figures 3.7–3.10 for initial buckle radius R_b = 11mm, where the width is characterized by the boundary angle for the buckle, $\varphi = \varphi_1$. The corresponding deflection profiles, per unit applied stress, are presented in Figures 3.7 and 3.8, for buckle half-widths of 2, 3 and 4 mm, as well as for increasing pressure.

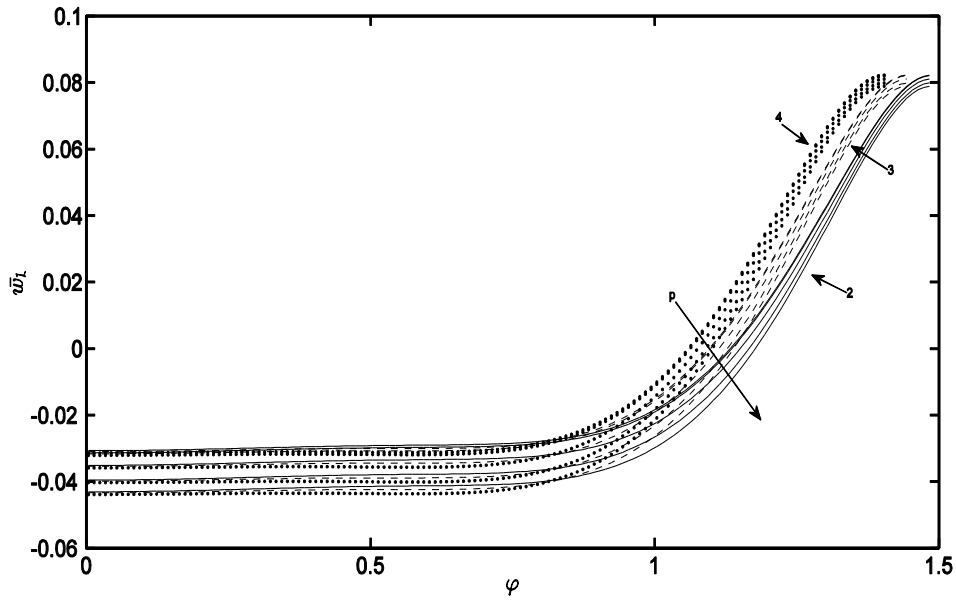

Figure 3.7 Radial displacement of the eye with applying different width of buckles, as a function of φ , under changing pressure. The arrow indicates the increasing direction of the pressure.

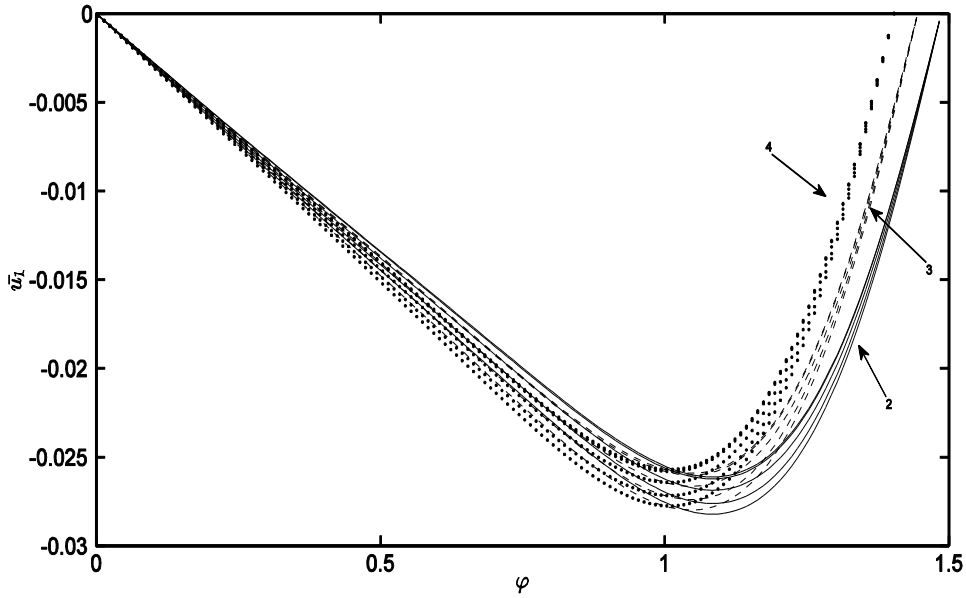

Figure 3.8 Meridian displacement of the eye with applying buckles with different widths, as a function of φ , under changing pressure. The arrow indicates the increasing direction of the pressure.

Upon consideration of Figure 3.7 it is seen that, for a given buckle (half) width, the radial displacement of the eye wall decreases with increasing pressure in the vicinity of the buckle, while the displacement increases at points relatively far from from the buckle. Moreover, the displacements of the eye wall at points far from the buckle appear to be almost independent of the width of the buckle. The corresponding deflection profiles of the meridian displacement are shown in Figure 3.8.

Profiles of a deformed eye with a buckle of (initial) radius $R_b = 11$ mm are displayed in Figure 3.9 for various values of the ocular pressure. Similarly, profiles of a deformed eye with ocular pressure $p = 23$mmHg are displayed in Figure 3.10 for various values of the buckle half-width, t. In each figure, the stars describe the profile of the eye before deformation by the buckle $(\bar{w}(\varphi) = 0, \forall \varphi)$. It is seen from Figure 3.9 that the pressure change has little influence on the deformation for a given value of the buckle width. The effect of buckle width is shown in Figure 3.10. It is seen from the figure that the width of the buckle has little effect on the deformation of the eye wall away from the vicinity of the scleral buckle. Thus, the corresponding diameter appears to be independent of the buckle width in that figure.

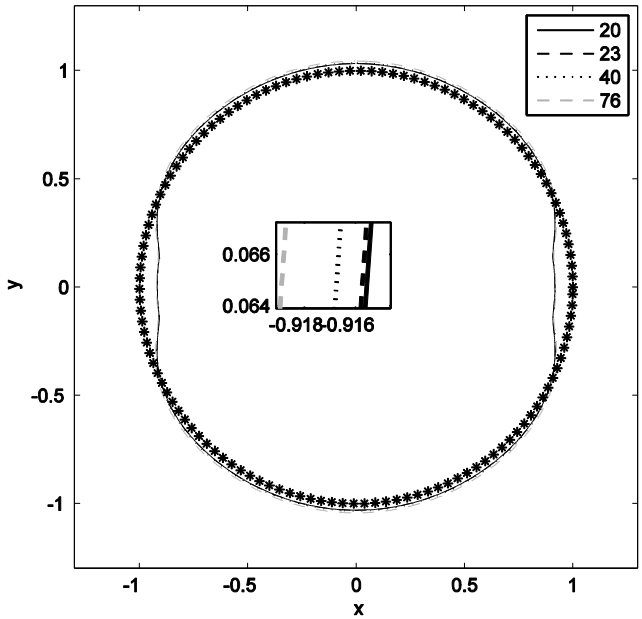

Figure 3.9 Deformation of the eyeball under different pressure in Cartesian coordinates. The width of the buckle is kept as a constant (4 mm).

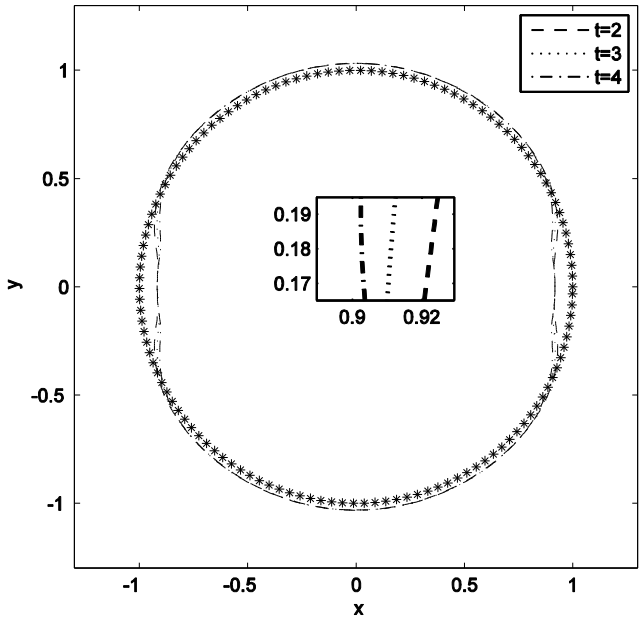

Figure 3.10 Deformation of the eyeball with different scleral buckle width in Cartesian coordinates. The pressure is kept as a constant (20 mmHg).

3.4.3 Influence of buckle height (thickness)

Results for various values of the buckle "height" (thickness) are presented in Figures 3.11–3.14 for initial buckle radius R_b = 11 mm. The deflection profiles corresponding to buckle heights of 2, 3 and 4 mm are presented in Figures 3.11 and 3.12. Specifically, the radial displacements are displayed as a function of meridian angle in Figure 3.11, and the meridian displacements are displayed Figure 3.12.

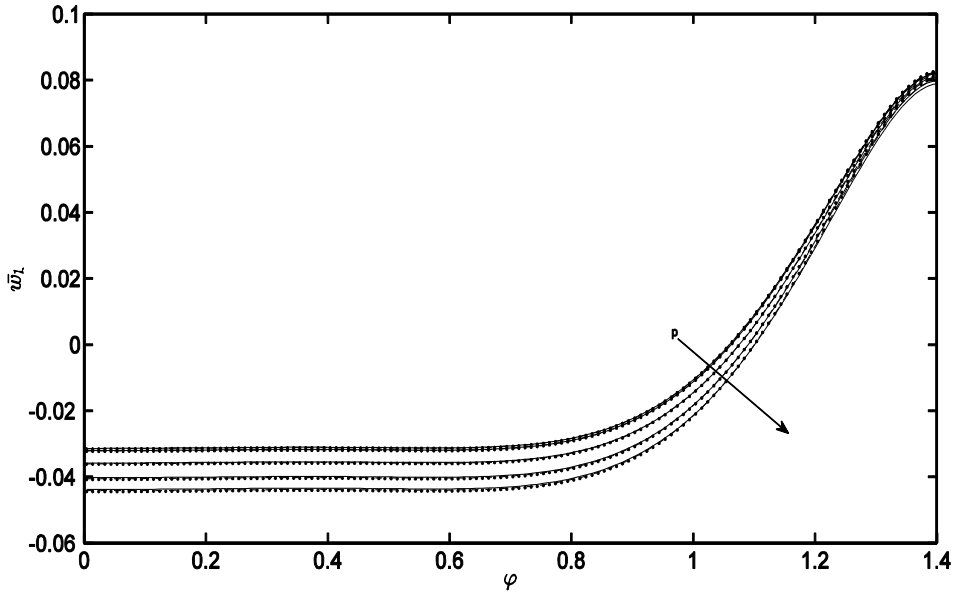

Figure 3.11 Radial displacement of the eye with applying buckles with different heights, as a function of φ , under changing pressure. The arrow indicates the increasing direction of the pressure.

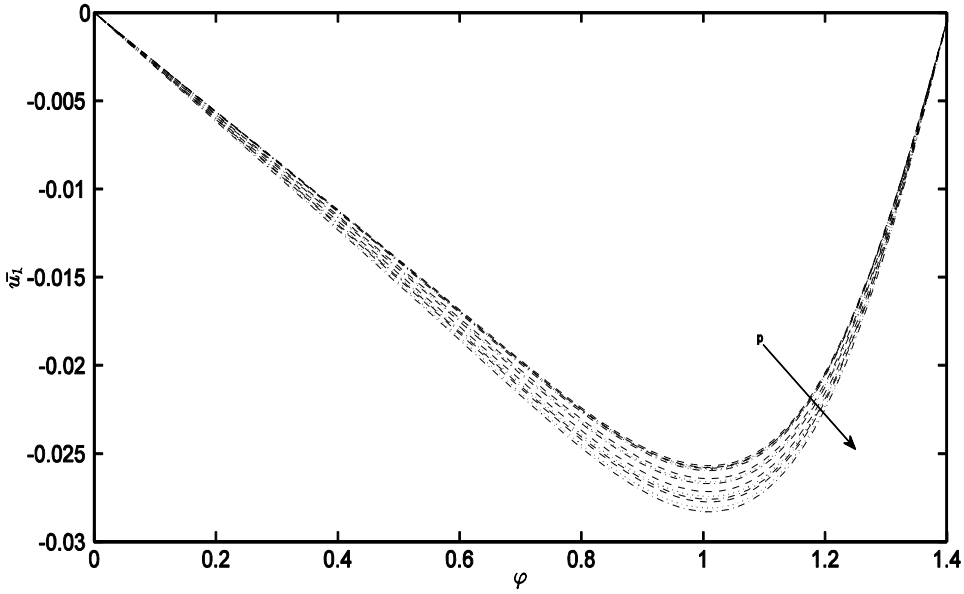

Figure 3.12 Meridian displacement of the eye with applying buckles with different heights, as a function of φ , under changing pressure. The arrow indicates the increasing direction of the pressure.

It is seen from the figures that, for each buckle height, the magnitudes of both the radial and meridian displacements increase with increasing pressure. It is also seen that the displacements vary little with buckle height for a given value of the pressure. It is therefore concluded that the buckle thickness has little effect on the deformation of the eye. To further illustrate these results, we present the deformation profile of the surface of the eye with respect to the pressure and with respect to the buckle height in Figures 3.13 and 3.14, respectively.

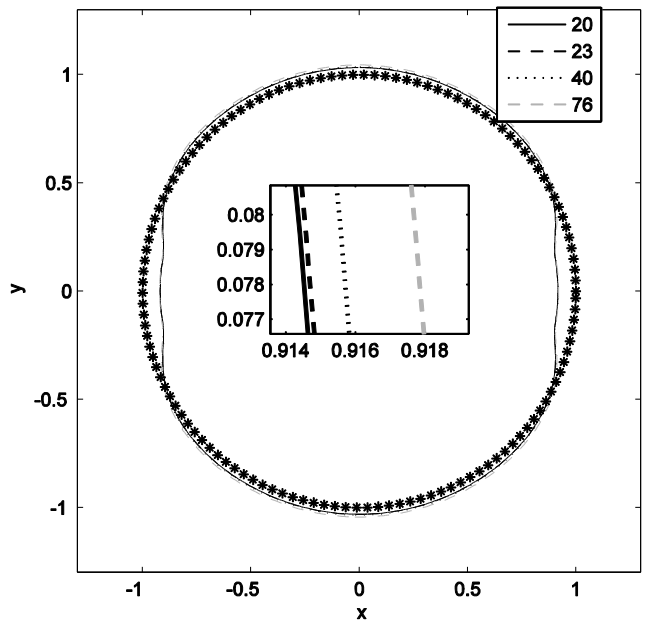

Figure 3.13 Deformation of the eyeball under different pressure in Cartesian coordinates. The height of the buckle is kept as a constant (4 mm).

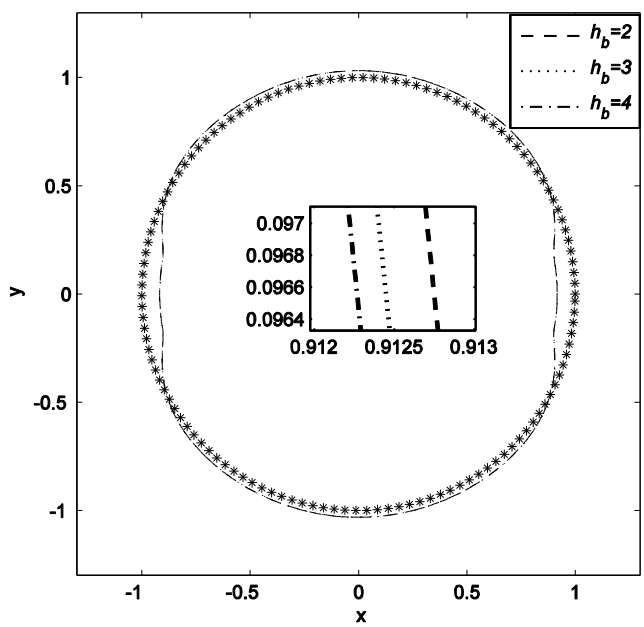

Figure 3.14 Deformation of the eyeball with different scleral buckle height in Cartesian coordinates. The pressure is kept as a constant (20 mmHg).

3.4.4 Influence of Buckle Modulus

We next study the influence of Young's modulus of the buckle on the behavior of the banded eye. The Young's modulus for a typical scleral buckle is around 1.5 – 5.0 Mpa (Bauer, et al. (1995b), Keeling, Propst, Stadler and Wackernagel (2009)). The corresponding results are displayed in Figures 3.15 – 3.18 for a buckle with an undeformed radius of $R_b = 11$ mm.

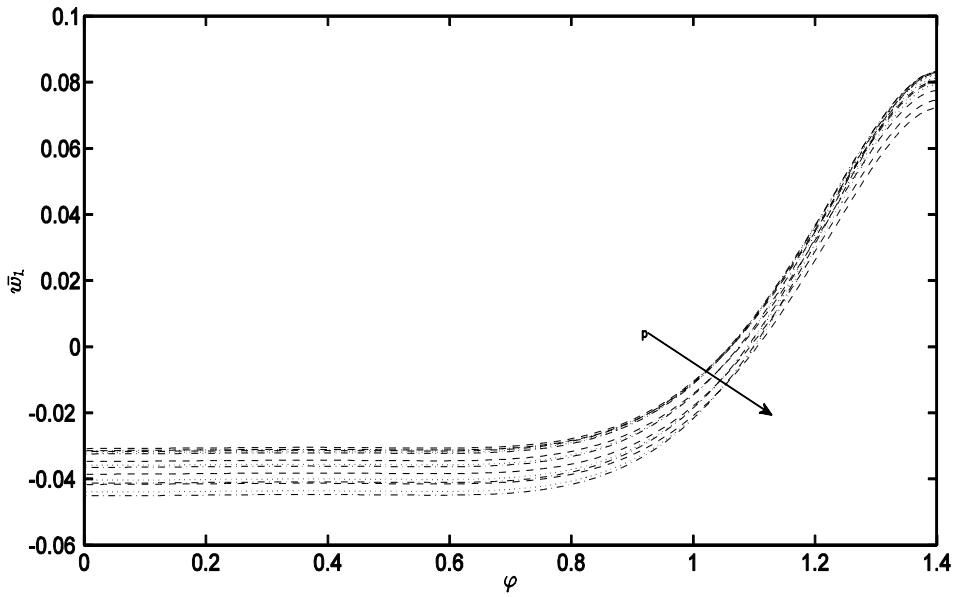

Figure 3.15 Radial displacement of the eye with applying buckles with different Young's moduli, as a function of φ, under changing pressure. The arrow indicates the increasing direction of the pressure.

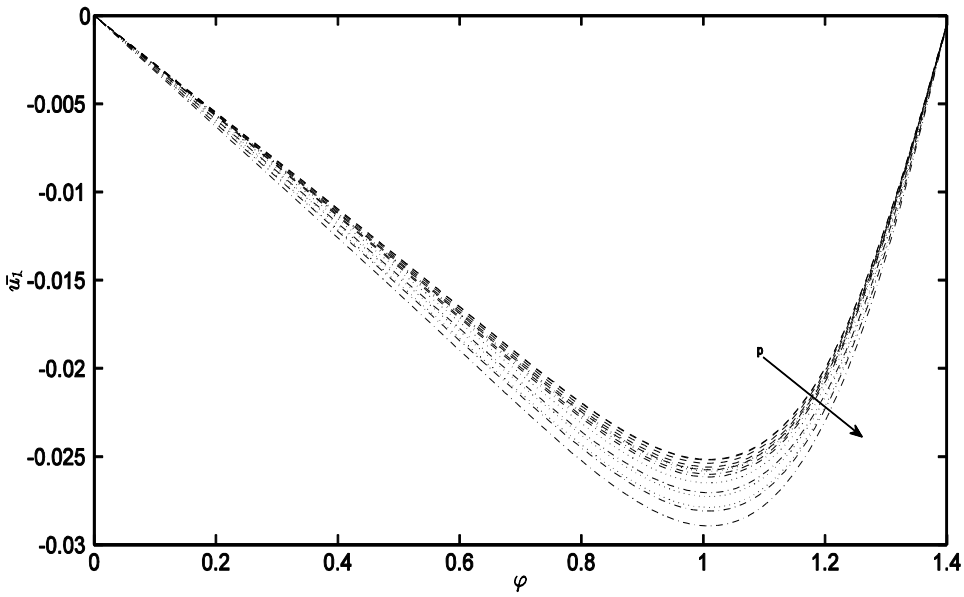

Figure 3.16 Meridian displacement of the eye with applying buckles with different Young's moduli, as a function of φ , under changing pressure. The arrow indicates the increasing direction of the pressure.

The profiles corrsponding to the radial and meridian deflections are shown in Figures 3.15 and 3.16, respectively. It is seen that Young's modulus has little effect on the deformation of the eye wall. Cross sections of the deformed eye for various values of the ocular pressure are shown in Figure 3.17 for E_b = 2.8 Mpa. Similarly, profiles of the deformed eye for various values of Young's modulus of the band are shown in Figure 3.18 for p = 20 mmHg.

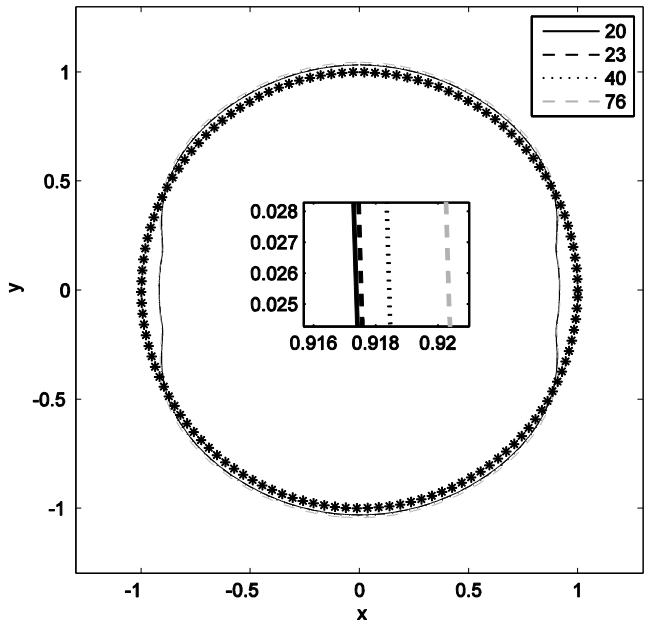

Figure 3.17 Deformation of the eyeball under different pressure in Cartesian coordinates. The Young's modulus of the buckle is kept as a constant (4 mm).

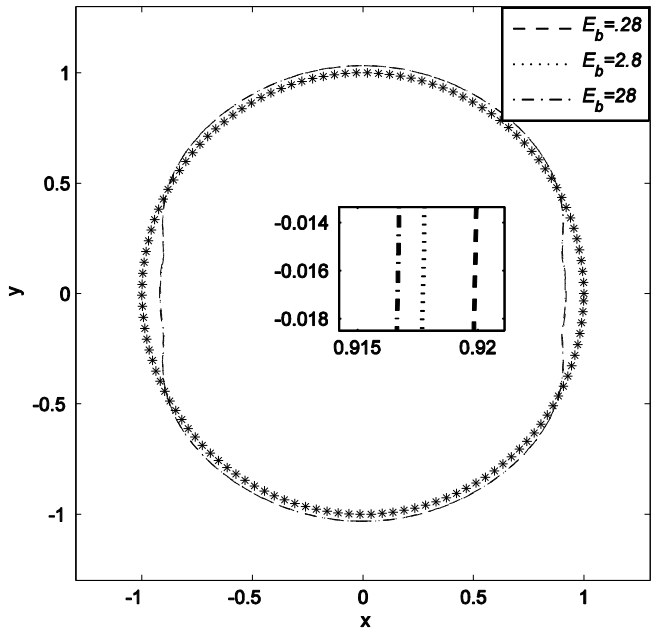

Figure 3.18 Deformation of the eyeball with applying buckles with different Young's moduli in Cartesian coordinates. The pressure is kept as a constant (20 mmHg).

3.5 Volume change

After the scleral buckle is applied to the eye during the retinal detachment surgery, the volume of the eye will change, which might result in discomfort for the patient. In this section, we study the volume displacement for the various cases studied in the previous sections.

The simulation results are listed in Table 3.1. It is seen that the volume increases less as the pressure increases for the same buckle radius and also for increasing buckle radius under the same pressure. For some configurations, the volume change becomes negative, which indicates that the volume is smaller than its intial value after applying the scleral buckle. For a given buckle width, the volume increases less as the pressure increases, while it increases more for increasing buckle width under the same pressure. For some configurations, the volume change is negative, indicating that the volume decreases from that of the unbanded eye for these cases. Finally, upon consideration of the results presented in Table 3.1, it is seen that, for the cases considered, the volume change is essentially unaltered by changes in Young's modulus as well as the buckle height.

Table 3.1: Influence of buckle properties on volume change of the eye

Pressure (mmHg)		20	23	40	60	76
Radius (mm)	10.5	0.1200	0.1170	0.1001	0.0801	0.0640
	11	0.0810	0.0780	0.0612	0.0412	0.0252
	11.5	0.0345	0.0316	0.0148	-0.0052	-0.0212
Half width (mm)	2	0.0403	0.0371	0.0191	-0.0022	-0.0194
	3	0.0607	0.0576	0.0402	0.0195	0.0029
	4	0.0810	0.0780	0.0612	0.0412	0.0252
Height(Thickness) (mm)	2	0.0810	0.0780	0.0612	0.0412	0.0252
	3	0.0813	0.0784	0.0618	0.0421	0.0263
	4	0.0815	0.0786	0.0622	0.0427	0.0270
Young's Modulus (Mpa)	.28	0.0792	0.0759	0.0576	0.0358	0.0183
	2.8	0.0811	0.0782	0.0614	0.0416	0.0256
	28	0.0820	0.0792	0.0633	0.0444	0.0292

3.6 Conclusion

The model for the deformation of an eyeball after applying a scleral buckle was presented and the total energy of the system was formulated in this chapter. The analytical solutions for the transverse and meridian displacements, as well as the corresponding boundary conditions and matching conditions, were obtained for the eyeball and the buckle, respectively. Simulation results based on the analytical solutions were performed and revealed the characteristic behavior of the deformation of the structure. The results demonstrate the effect of different material properties of the scleral buckle (radius, width, thickness, Young's modulus), and are of interest for planning the surgery. The volume changes for all the cases considered were presented as well.

Chapter 4 *The effect of an equatorially sutured scleral buckle on posterior retinal detachment*

4.1 Introduction

In the previous chapter, we studied the mechanical behavior of the eye under the action of a buckle. The scleral buckle is usually placed in the vicinity of a retinal tear, typically at the equator of the eye. Simulation results based on the present analyses demonstrate the effect of different material properties of the scleral buckle on the deformation of the eye wall. In this chapter, we will advance the study of the previous chapter to include the retina layer in the mathematical model. In particular, we will focus our attention on the influence of a slceral buckle applied at the equator of the eye on a distant retinal detachment at the posterior of the eye. The mathematical model of the layered ocular structure is presented and analytical solutions of the evolving ocular structure are determined. Numerical simulations based on the analytical solutions are presented, and unveil some interesting behavior.

4.2 Formulation

4.2.1 Geometry

The schematic for the ocular structure is shown in Figure 4.1, and the notations 1, 2, 3 indicate the region of retinal detachment, the intact region of the eye, and the scleral buckle, respectively. Spherical coordinates, (r, θ, φ), are used to describe the evolving structure, where r is the radial coordinate, θ is the polar angle and φ is the azimuth

angle. The human eyeball is modeled as a spherical shell and the scleral band is considered to be sutured to the eye at its equator. Symmetry is assumed about the $\varphi = 0$ axis and over the domain $0 \le \theta \le 2\pi$, with the scleral band applied at $\varphi = \frac{\pi}{2}$.

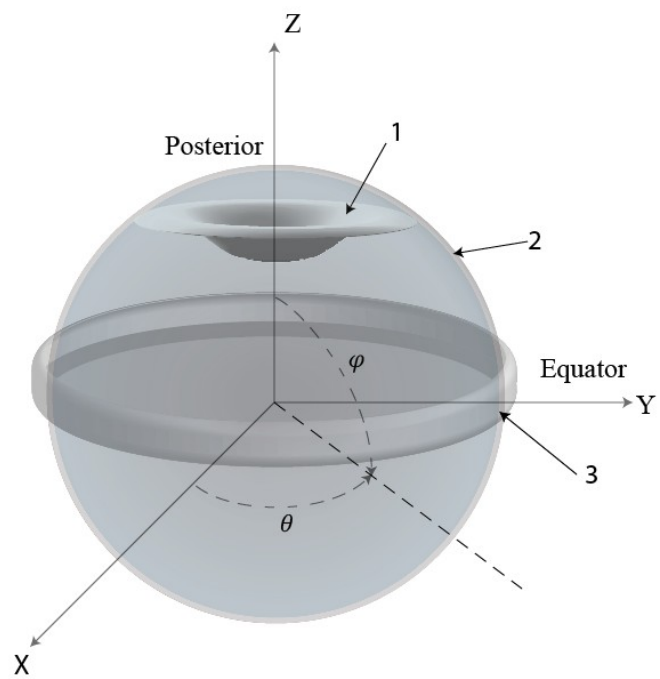

Figure 4.1 3-D Human eyeball with scleral band. (r, θ, φ) **coordinates** φ **and** θ **are shown. The parameters** w **and** u **are the radial and meridian displacements, respectively. The number 1 indicates the eye membrane, 2 indicates the retina and 3 indicates the scleral buckle.**

As a result of these assumptions, the model for the evolving structure is represented as shown in Figure 4.2. The notations R , R_b and R_r stand for the initial radius of the eye, the scleral buckle and the retina respectively, which are measured from the origin to the centerline of each layer. We denote $w_j(\varphi)$, positive inward, as the radial deflections, and $u_j(\varphi)$ (positive in the direction of increasing φ) as the cooresponding meridian deflections. The portion of the retina defined on $S_1 : \varphi \in [0, \varphi_1]$ is lifted / detached from the

base structure, while the the band is sutured to the eye over the Region $S_2 : \varphi \in [\varphi_1, \varphi_2]$.

Let us consider scleral buckle to be sutured to the eye in the Region $S_3 : \varphi \in [\varphi_2, \frac{\pi}{2}]$.

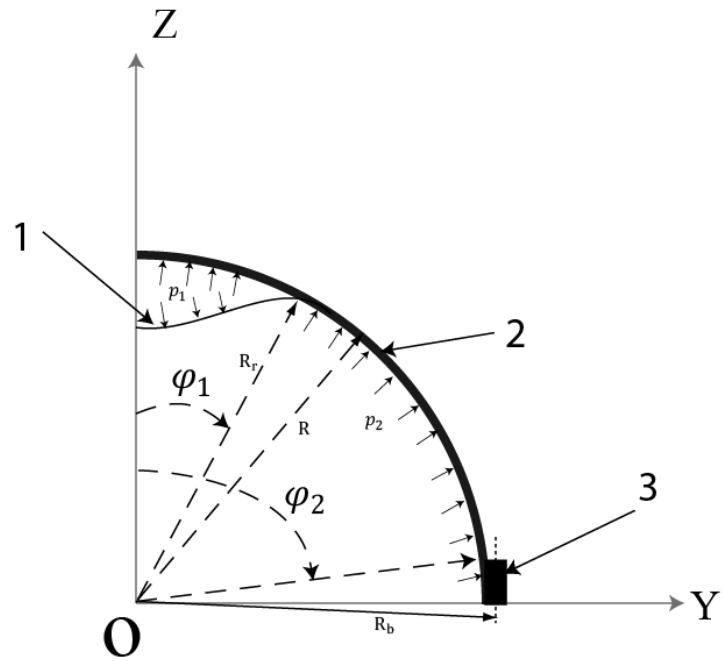

Figure 4.2 Schematic of the eye with scleral band. R , R_b and R_r are the radius of the eye, the scleral buckle and the retina, respectively. The symbols φ_1 and φ_2 are the boundaries where the retina is lifted and the buckle is sewed to the eye membrane.

4.2.2 Potential Energy Functional

Most retinal detachments occur as a result of a retinal break, hole, or tear. Vitreous fluid then passes through the tear and accumulates behind the retina in Region S_1. The pressure due to the fluid will separate the retina from the back of the eye, leading to a retinal detachment. In this study, we examine the effect of different pressures on the deformation of the eye with a scleral buckle. In a manner similar to that of the previous

chapter, based on their geometry the eye and the retina are each modeled as thin shells, while the scleral buckle is modeled as a thin elastic ring structure.

We next formulate an energy functional in terms of the membrane energies (U_M), bending energies (U_B) of each substructure, and we also include a constraint functional (Λ) which matches the radial and meridian displacement of the eye and the scleral band. In addition, we include the work (W) done by the pressure difference across the entire eye wall and the detached segment of the retina. The total potential energy, Π, of the ocular system modeled as described above is then

$$\Pi = U_B + U_M - \Lambda - W \tag{4.1}$$

where

$$\begin{aligned} U_M &= 2\pi R^2 \int \left[\frac{1}{2} N_{\varphi\varphi}^{(j)} \varepsilon_{\varphi\varphi}^{(j)} + \frac{1}{2} N_{\theta\theta}^{(j)} \varepsilon_{\theta\theta}^{(j)} \right] \sin(\varphi) d\varphi \\ &+ 2\pi R_r^{\,2} \int \left[\frac{1}{2} N_{\varphi\varphi r}^{(j)} \varepsilon_{\varphi\varphi r}^{(j)} + \frac{1}{2} N_{\theta\theta r}^{(j)} \varepsilon_{\theta\theta}^{(j)} \right] \sin(\varphi) d\varphi \\ &+ R_b \int_{\varphi_1}^{\frac{\pi}{2}} \frac{1}{2} N_{b\theta\theta}^{(2)} \varepsilon_{b\theta\theta}^{(2)} d\theta \end{aligned} \tag{4.2}$$

$$\begin{aligned} U_B &= 2\pi R^2 \int \left[\frac{1}{2} M_{\varphi\varphi}^{(j)} \chi_{\varphi\varphi}^{(j)} + \frac{1}{2} M_{\theta\theta}^{(j)} \chi_{\theta\theta}^{(j)} \right] \sin(\varphi) d\varphi \\ &+ 2\pi R_r^{\,2} \int \left[\frac{1}{2} M_{\varphi\varphi r}^{(j)} \chi_{\varphi\varphi r}^{(j)} + \frac{1}{2} M_{\theta\theta r}^{(j)} \chi_{\theta\theta r}^{(j)} \right] \sin(\varphi) d\varphi \\ &+ R_b \int_{\varphi_1}^{\frac{\pi}{2}} \frac{1}{2} M_{b\theta\theta}^{(2)} \chi_{b\theta\theta}^{(2)} d\theta; \\ j &= 1, 2, 3 \end{aligned} \tag{4.3}$$

In Eqs. (4.1) – (4.3),

$$\begin{aligned} N_{\varphi\varphi}^{(j)} &= C\left[\varepsilon_{\varphi\varphi}^{(j)}(\varphi) + \nu\, \varepsilon_{\theta\theta}^{(j)}(\varphi) \right], \quad N_{\theta\theta}^{(j)} = C\left[\varepsilon_{\theta\theta}^{(j)}(\varphi) + \nu\, \varepsilon_{\varphi\varphi}^{(j)}(\varphi) \right] \\ N_{\varphi\varphi r} &= C_r\left[\varepsilon_{\varphi\varphi r}(\varphi) + \nu_r\, \varepsilon_{\theta\theta r}(\varphi) \right], \quad N_{\theta\theta r} = C_r\left[\varepsilon_{\theta\theta r}(\varphi) + \nu_r\, \varepsilon_{\varphi\varphi r}(\varphi) \right] \end{aligned} \tag{4.4}$$

are the membrane forces in the directions indicated by the subscripts,

$$M_{\varphi\varphi}^{(j)} = D\left[\chi_{\varphi\varphi}^{(j)}(\varphi) + \nu\,\chi_{\theta\theta}^{(j)}(\varphi)\right],\quad M_{\theta\theta}^{(j)} = D\left[\chi_{\theta\theta}^{(j)}(\varphi) + \nu\,\chi_{\varphi\varphi}^{(j)}(\varphi)\right]$$
$$M_{\varphi\varphi r} = D_r\left[\chi_{\varphi\varphi r}(\varphi) + \nu_r\,\chi_{\theta\theta r}(\varphi)\right],\quad M_{\theta\theta r} = D_r\left[\chi_{\theta\theta r}(\varphi) + \nu_r\,\chi_{\varphi\varphi r}(\varphi)\right] \tag{4.5}$$

are the corresponding bending moments,

$$\varepsilon_{\varphi\varphi}^{(j)}(\varphi) = \frac{1}{R}\left\{u_j{}'(\varphi) - w_j(\varphi)\right\},\quad \varepsilon_{\theta\theta}^{(j)}(\varphi) = \frac{\cot\varphi}{R}\left\{u_j(\varphi) - w_j(\varphi)\tan\varphi\right\}$$
$$\varepsilon_{\varphi\varphi r}(\varphi) = \frac{1}{R_r}\left\{u_r{}'(\varphi) - w_r(\varphi)\right\},\quad \varepsilon_{\theta\theta r}(\varphi) = \frac{\cot\varphi}{R_r}\left\{u_r(\varphi) - w_r(\varphi)\tan\varphi\right\} \tag{4.6}$$

are the associated membrane strains, and

$$\chi_{\varphi\varphi}^{(j)}(\varphi) = \frac{1}{R^2}\left\{u_j{}'(\varphi) + w_j{}''(\varphi)\right\},\quad \chi_{\theta\theta}^{(j)}(\varphi) = \frac{\cot\varphi}{R^2}\left\{u_j(\varphi) + w_j{}'(\varphi)\right\};\quad j = 1, 2$$
$$\chi_{\varphi\varphi r}(\varphi) = \frac{1}{R_r{}^2}\left\{u_r{}'(\varphi) + w_r{}''(\varphi)\right\},\quad \chi_{\theta\theta r}(\varphi) = \frac{\cot\varphi}{R_r{}^2}\left\{u_r(\varphi) + w_r{}'(\varphi)\right\} \tag{4.7}$$

are the associated changes in curvature. Similarly,

$$N_{b\theta\theta}^{(2)} = C_b\varepsilon_{b\theta\theta}^{(2)}(\varphi),\qquad M_{b\theta\theta}^{(2)} = D_b\chi_{b\theta\theta}^{(2)}(\varphi) \tag{4.8}$$

$$\varepsilon_{b\theta\theta}^{(2)}(\varphi) = -\frac{1}{R_b}w_{b2}(\varphi),\quad \chi_{b\theta\theta}^{(2)}(\varphi) = \frac{1}{R_b{}^2}\left\{w_{b2}(\varphi) + w_{b2}^{''}(\varphi)\right\} \tag{4.9}$$

are the membrane force, bending moment, membrane strain and curvature change of the scleral buckle.

In the above expressions, C, C_b and C_r are the membrane stiffnesses of the eye, the silicone band and the retina, respectively. D, D_b and D_r are the corresponding bending stiffnesses. ν and ν_r correspond to the associated Poisson's ratios.

The work, W, done by the pressure difference across the entire eye wall and the detached segment of the retina is given by

$$W = 2\pi R^2 \int_0^{\varphi_1} p_1 w_1(\varphi)\sin(\phi)\,\mathrm{d}\phi + 2\pi R^2 \int_{\varphi_1}^{\varphi_2} p_2 w_2(\varphi)\sin(\phi)\,\mathrm{d}\phi$$
$$+2\pi R^2 \int_{\varphi_2}^{\frac{\pi}{2}} p_2 w_3(\varphi)\sin(\phi)\,\mathrm{d}\phi + 2\pi R_r^{\,2} \int_0^{\varphi_1} (p_2 - p_1) w_r(\varphi)\sin(\phi)\,\mathrm{d}\phi \tag{4.10}$$

As the scleral buckle will be permanently stitched to the outside surface of the eye wall in the treatment for retinal detachment, the radial and meridian deflections at the interface of the two layers should be nearly identical. To enforce this, we, thus, introduce the constraint functional, Λ , as

$$\Lambda = 2\pi R_b^{\,2} \int_{\phi_2}^{\frac{\pi}{2}} \sigma(w_2 - w_{b2} + R - R_b) d\phi + 2\pi R_b^{\,2} \int_{\phi_2}^{\frac{\pi}{2}} \tau(u_2 - u_{b2}) d\phi \tag{4.11}$$

where the parameters σ and τ are Lagrange multipliers and physically correspond to the interfacial radial normal stress and interfacial meridian shear stress in the bonded region.

4.2.3 Governing Equations and Boundary Conditions

Following the procedure described in Timoshenko, Woinowsky-Krieger and Woinowsky (1959), Flugge (1960), and Lakawicz, Bottega, Prenner and Fine (2014), we next rewrite Eqs. (4.1) – (4.11) in non-dimensional form and invoke the Principle of Stationary Potential Energy, which is described in the present context as $\delta\Pi = 0$. Taking the appropriate variations yields the corresponding governing equations and boundary conditions. As the size of the scleral buckle is relatively small and, per the results of Chapter 3, its effect to the entire structure is localized, we assume that its transverse displacement is uniform and that the meridian displacement is negligible in φ direction. Thus, the equation governing the radial displacement of the band is derived as

$$\bar{w}_{b3} = \frac{-\bar{p}_2 \cos(\varphi_2)}{2\bar{C}(1+\nu)\cos(\varphi_2) + \bar{C}_b + \bar{D}_b} \tag{4.12}$$

After eliminating the Lagrange multipliers, we arrive at the self-consistent equations and conditions for the eye wall in Regions S_1 and S_2. Hence,

Governing Equations:

$$\begin{aligned}&\bar{\Psi}^{''(j)} + \bar{\Psi}^{'(j)} \cdot \cot(\varphi) - \bar{\Psi}^{(j)} \cdot (\nu + \cot^2(\varphi)) = \bar{Q}^{(j)} \\ &\bar{Q}^{(j)''} + \bar{Q}^{(j)'} \cot(\varphi) + \bar{Q}^{(j)} \cdot (\nu - \cot^2(\varphi)) = -\bar{C} \cdot (1-\nu^2) \cdot \bar{\Psi}^{(j)};\end{aligned} \tag{4.13}$$

where

$$\bar{Q}^{(j)} = \left(\bar{M}^{(j)}_{\varphi\varphi} \sin\varphi\right)' - \cos\varphi \bar{M}^{(j)}_{\theta\theta}, \quad \bar{\Psi}^{(j)} = \bar{u}_1 + \bar{w}_1 \tag{4.14}$$

Boundary conditions:

$$\bar{u}_1(0) = 0, \quad w_1^{'}(0) = 0, \quad \bar{Q}^{(1)}(0) = 0 \tag{4.15}$$

$$\begin{aligned}&\bar{u}_1(\varphi_1) = \bar{u}_2(\varphi_1), \quad \bar{u}_1^{'}(\varphi_1) = \bar{u}_2^{'}(\varphi_1), \quad \bar{Q}^{(1)}(\varphi_1) = \bar{Q}^{(2)}(\varphi_1) \\ &\bar{w}_1(\varphi_1) = \bar{w}_2(\varphi_1), \quad \bar{w}_1^{'}(\varphi_1) = \bar{w}_2^{'}(\varphi_1), \quad \bar{w}_1^{''}(\varphi_1) = \bar{w}_2^{''}(\varphi_1)\end{aligned} \tag{4.16}$$

$$\bar{u}_2(\varphi_2) = 0, \quad \bar{w}_2(\varphi_2) = \bar{w}_{b3}, \quad \bar{w}_2^{'}(\varphi_2) = 0 \tag{4.17}$$

where the normalized parameters are related to their dimensional counterparts as follows:

$$\begin{aligned}&\bar{M}_{\varphi\varphi} = \frac{R}{D} M_{\varphi\varphi}, \quad \bar{M}_{\theta\theta} = \frac{R}{D} M_{\theta\theta}, \quad \bar{u} = u/R, \quad \bar{w} = w/R \\ &\bar{p}_1 = \frac{R^3}{D} p_1, \quad \bar{p}_2 = \frac{R^3}{D} p_2, \quad \bar{C} = \frac{R^2}{D} C = \frac{12}{\bar{h}^2} \\ &\bar{C}_b = \frac{C_b}{D}\frac{R^2}{R_b} = 12\frac{E_b}{E}\frac{\bar{h}_b}{\bar{h}^3}\frac{\bar{t}_b}{\bar{R}_b}, \quad \bar{D}_b = \frac{D_b}{D}\frac{R^2}{R_b^{\,3}} = \frac{E_b}{E}\frac{\bar{h}_b^{\,3}}{\bar{h}^3}\frac{\bar{t}_b}{\bar{R}_b}\frac{1}{\bar{R}_b^{\,2}} \\ &\bar{h} = \frac{h}{R}, \quad \bar{h}_b = \frac{h_b}{R}, \quad \bar{t}_b = \frac{t_b}{R}, \quad \bar{R}_b = \frac{R_b}{R}\end{aligned} \tag{4.18}$$

In all, length scales have been normalized with respect to the dimensional radius, R, of the eye wall. E and E_b corresponding to the the Young's modulus of the eye and the sclera buckle, respectively, $\bar{h}$ and $\bar{h}_b$ are the corresponding nondimensional thicknesses.

$\overline{t_b}$ is the nondimensional half width of the scleral buckle and $\overline{R}_b$ is the nondimensional radius of the buckle. The system of coupled differential equations described by Eqs. (4.13) – (4.14) are solved in conjunction with the boundary conditions presented in Eqs. (4.15) – (4.17). The solutions are presented next.

4.3 Analysis

Adopting the method presented in Timoshenko, Woinowsky-Krieger and Woinowsky (1959), Flugge (1960) and Lakawicz, Bottega, Prenner and Fine (2014), we obtain the analytical solutions for the deflections of the eye wall in Regions S_1 and S_2 as

$$\begin{aligned}
\overline{u}_1 &= A_6 \sin\varphi - \frac{1}{\overline{C}(1-\nu)}\left\{\overline{Q}^{(1)} + (\frac{1}{2}\overline{p}_1 + A_5)(\cot\varphi + g(\phi)\sin\varphi)\right\} \\
\overline{w}_1 &= A_6 \cos\varphi - \frac{1}{\overline{C}(1-\nu^2)}(\overline{Q}^{(1)'} + \overline{Q}^{(1)}\cot\varphi) \\
&\quad + \frac{1}{\overline{C}(1-\nu^2)}\overline{p}_1(1-\frac{1}{2}(1+\nu)g(\varphi)\cos\varphi) + \frac{1}{\overline{C}(1-\nu)}A_5(1-g(\phi)\cos\varphi)
\end{aligned} \tag{4.19}$$

$$\begin{aligned}
\overline{u}_2 &= B_6 \sin\varphi - \frac{1}{\overline{C}(1-\nu)}\left\{\overline{Q}^{(2)} + (\frac{1}{2}\overline{p}_2 + B_5)(\cot\varphi + g(\phi)\sin\varphi)\right\} \\
\overline{w}_2 &= B_6 \cos\varphi - \frac{1}{\overline{C}(1-\nu^2)}(\overline{Q}^{(2)'} + \overline{Q}^{(2)}\cot\varphi) \\
&\quad + \frac{1}{\overline{C}(1-\nu^2)}\overline{p}_2(1-\frac{1}{2}(1+\nu)g(\varphi)\cos\varphi) + \frac{1}{\overline{C}(1-\nu)}B_5(1-g(\phi)\cos\varphi)
\end{aligned} \tag{4.20}$$

where

$$
\begin{aligned}
\bar{Q}^{(1)}(\varphi) &= A_1 \sin\varphi \, {}_2F_1\left(\alpha_1, \beta_1; 2; \sin^2\varphi\right) + A_2 \sin\varphi \, {}_2F_1\left(\hat{\alpha}_1, \hat{\beta}_1; 2; \sin^2\varphi\right) \\
&\quad + A_3 \sin\varphi G_{2\ 2}^{2\ 0}\left(\sin^2\varphi \left| \begin{matrix} \alpha_1 - \frac{1}{2} & \beta_1 - \frac{1}{2} \\ -1 & 0 \end{matrix} \right.\right) + A_4 \sin\varphi G_{2\ 2}^{2\ 0}\left(\sin^2\varphi \left| \begin{matrix} \hat{\alpha}_1 - \frac{1}{2} & \hat{\beta}_1 - \frac{1}{2} \\ -1 & 0 \end{matrix} \right.\right) \\
\bar{Q}^{(2)}(\varphi) &= B_1 \sin\varphi \, {}_2F_1\left(\alpha_1, \beta_1; 2; \sin^2\varphi\right) + B_2 \sin\varphi \, {}_2F_1\left(\hat{\alpha}_1, \hat{\beta}_1; 2; \sin^2\varphi\right) \\
&\quad + B_3 \sin\varphi G_{2\ 2}^{2\ 0}\left(\sin^2\varphi \left| \begin{matrix} \alpha_1 - \frac{1}{2} & \beta_1 - \frac{1}{2} \\ -1 & 0 \end{matrix} \right.\right) + B_4 \sin\varphi G_{2\ 2}^{2\ 0}\left(\sin^2\varphi \left| \begin{matrix} \hat{\alpha}_1 - \frac{1}{2} & \hat{\beta}_1 - \frac{1}{2} \\ -1 & 0 \end{matrix} \right.\right) \\
\alpha_1 &= \frac{3 + \sqrt{5 + iZ}}{4}, \quad \beta_1 = \frac{3 - \sqrt{5 + iZ}}{4}, \quad \hat{\alpha}_1 = \frac{3 + \sqrt{5 - iZ}}{4}, \quad \hat{\beta}_1 = \frac{3 - \sqrt{5 - iZ}}{4} \\
Z &= 4\sqrt{\bar{C}(1 - \nu^2) - \nu^2}, \quad g(\varphi) = \ln\cos\frac{\varphi}{2} - \ln\sin\frac{\varphi}{2}
\end{aligned}
\tag{4.21}
$$

i is the imaginary unit ($\sqrt{-1}$), ${}_2F_1$ represents a Hypergeometric function, $G_{2\ 2}^{2\ 0}$ represents a Meijer G function, and A_1 through A_6 and B_1 through B_6 are constants of integration. Based on the explicit solutions described in Eqs. (4.19) – (4.20) for the eye in Regions S_1 and S_2, all the integration constants can be solved by applying the boundary conditions presented in Eqs. (4.15) – (4.17). In addition, it is required on physical grounds that the deflections at $\varphi = 0$ and throughout the domain of definition should be finite. However, the Meijer G function and natural logarithm function are singular at the origin. Thus, the pertinent coefficients in Eq. (4.21) are required to be

$$
A_3 = 0, \quad A_4 = 0, \quad A_5 = -\frac{\bar{p}_1}{2} \tag{4.22}
$$

Upon imposing the boundary conditions at $\varphi = \varphi_1$, as specified in Eqs. (4.16) – (4.17), the remaining constants satisfy the following matrix equation:

$$
\tilde{C}_{cst} \quad \tilde{\ } \quad \tilde{\ } \tag{4.23}
$$

where

$$\tilde{C}_{cst} \quad [\cdots \quad A_2 \quad A_6 \quad B_1 \quad B_2 \quad B_3 \quad B_4 \quad B_5 \quad B_6]'$$
$$\tilde{I} \quad [\cdots \quad p_{12} \quad p_{13} \quad p_{14} \quad p_{15} \quad p_{16} \quad p_{17} \quad p_{18} \quad p_{19}]' \tag{4.24}$$
$$\tilde{I} \quad \begin{bmatrix} I_{11} & \cdots & \cdots \\ \vdots & \ddots & \vdots \\ I_{91} & \cdots & \cdots \end{bmatrix}$$

The components of $\tilde{I}$ are comprised of the Hypergeometric functions and their derivatives and we will neglect the tedious equations for brevity. The components of the pressure loading $\tilde{I}$ are described as

$$\begin{aligned}
&p_{11} = \frac{1}{2}\bar{p}_2\left(\mathrm{g}(\varphi_1)\sin(\varphi_1) + \cot(\varphi_1)\right), \quad p_{12} = \frac{1}{2}\bar{p}_2\left(\mathrm{g}(\varphi_1)\cos(\varphi_1) - 1 - \csc^2(\varphi_1)\right) \\
&p_{13} = \frac{1}{2}\bar{p}_1(1-\nu) - \bar{p}_2\left(\frac{1}{2}(1-\nu)\,\mathrm{g}(\varphi_1)\cos(\varphi_1)\right), \\
&p_{14} = -\frac{1}{2}\bar{p}_2(1+\nu)\left(\mathrm{g}(\varphi_1)\sin(\varphi_1) + \cot(\varphi_1)\right) \\
&p_{15} = -\frac{1}{2}\bar{p}_2(1+\nu)\left(\mathrm{g}(\varphi_1)\cos(\varphi_1) - 1 - \csc^2(\varphi_1)\right), \quad p_{16} = 0 \\
&p_{17} = -\frac{1}{2}\bar{p}_2\left(\mathrm{g}(\varphi_2)\sin(\varphi_2) + \cot(\varphi_2)\right), \\
&p_{18} = \bar{p}_2\left(\frac{1}{2}(1-\nu)\,\mathrm{g}(\varphi_2)\cos(\varphi_2)\right) - \bar{C}(1-\nu^2)\bar{w}_{b3}(\varphi_2) \\
&p_{19} = \frac{1}{2}\bar{p}_2(1+\nu)\left(\mathrm{g}(\varphi_2)\sin(\varphi_2) + \cot(\varphi_2)\right)
\end{aligned} \tag{4.25}$$

After the integration constants A_1 through A_6 and B_1 through B_6 are solved, the deflection profiles for the eye wall in Regions S_1 and S_2 can be expressed explicitly. We next include the retina in the ocular system by matching the deflections at the boundaries $\varphi = \varphi_1$ to the eye membrane. Following the procedure presented by Lakawicz, Bottega, Prenner and Fine (2014), the analytical solutions for the retina itself are given as

$$
\begin{aligned}
\bar{u}_r &= A_{6r}\sin\varphi - \frac{1}{\bar{C}_r(1-\nu_r)}\left\{\bar{Q}^{(r)} + (\frac{1}{2}\Delta\bar{p} + A_{5r})(\cot\varphi + g(\varphi)\sin\varphi)\right\} \\
\bar{w}_r &= A_{6r}\cos\varphi - \frac{1}{\bar{C}_r(1-\nu_r^{\,2})}(\bar{Q}^{(r)'} + \bar{Q}^{(1)}\cot\varphi) \\
&\quad + \frac{1}{\bar{C}_r(1-\nu_r^{\,2})}\Delta\bar{p}(1-\frac{1}{2}(1+\nu_r)g(\varphi)\cos\varphi) + \frac{1}{\bar{C}_r(1-\nu_r)}A_{5r}(1-g(\varphi)\cos\varphi)
\end{aligned}
\tag{4.26}
$$

where

$$
\begin{aligned}
\bar{Q}^{(r)}(\varphi) &= A_{1r}\sin\varphi\,{}_2F_1\left(\alpha_1,\beta_1;2;\sin^2\varphi\right) + A_{2r}\sin\varphi\,{}_2F_1\left(\hat{\alpha}_1,\hat{\beta}_1;2;\sin^2\varphi\right) \\
&\quad + A_{3r}\sin\varphi G_{2\;\;2}^{2\;\;0}(\sin^2\varphi\left|\begin{matrix}\alpha_1-\frac{1}{2} & \beta_1-\frac{1}{2} \\ -1 & 0\end{matrix}\right.) + A_{4r}\sin\varphi G_{2\;\;2}^{2\;\;0}(\sin^2\varphi\left|\begin{matrix}\hat{\alpha}_1-\frac{1}{2} & \hat{\beta}_1-\frac{1}{2} \\ -1 & 0\end{matrix}\right.) \\
\bar{h}_r &= \frac{h_r}{h}, \quad \bar{R}_r = \frac{R_r}{R} \\
\bar{C}_r &= \frac{C_r R^2}{D}, \quad \bar{D}_r = \frac{D_r \bar{R}_r^{\,2}}{D}, \quad \Delta\bar{p} = \frac{(p_1-p_2)R_r^{\,3}}{D}
\end{aligned}
\tag{4.27}
$$

Similar to the normalization presented in Eq. (4.18), all length scales have been normalized with respect to the dimensional radius R of the eye wall. In addition, $\bar{R}_r$ is the nondimensional radius of the retina and $\bar{h}_r$ is the corresponding nondimensional thickness. Further, $\bar{C}_r$ and $\bar{D}_r$ are the normalized membrane and bending stiffness, and $\Delta\bar{p}$ is the nondimensional pressure loading on the retina. Based on physical grounds, the integration constants are $A_{3r}=0,\quad A_{4r}=0,\quad A_{5r}=-\frac{\bar{p}_1}{2}$. The other constants are solved by matching the deflections and its slope of the eye and the retina at $\varphi=\varphi_1$. This gives the relation

$$
\begin{bmatrix} A_{1r} \\ A_{2r} \\ A_{6r} \end{bmatrix} = \begin{bmatrix} l_1 X_{11} & l_1 X_{12} & -\sin\varphi_1 \\ l_3(X_{21}+X_{11}\cot\varphi_1) & l_3(X_{22}+X_{12}\cot\varphi_1) & -\cos\varphi_1 \\ l_3(X_{31}+X_{21}\cot\varphi_1 - X_{11}\csc^2\varphi) & l_3(X_{32}+X_{22}\cot\varphi_1 - X_{12}\csc^2\varphi) & \sin\varphi_1 \end{bmatrix}^{-1} \begin{bmatrix} -\bar{u}_1(\varphi_1) + \frac{1}{2}(\bar{h}_r+\bar{h})\bar{w}_1(\varphi_1) \\ \frac{1}{2}l_2\Delta\bar{p} - \bar{w}_1(\varphi_1) + 1 - \bar{R}_r \\ -\bar{w}_1^{\,'}(\varphi_1) \end{bmatrix}
\tag{4.28}
$$

where

$$l_1 = \frac{\bar{D}_r}{\bar{C}_r(1-\nu_r)}, \quad l_2 = \frac{1}{\bar{C}_r(1+\nu_r)}, \quad l_3 = \frac{\bar{D}_r}{\bar{C}_r(1-\nu_r^{\,2})} \tag{4.29}$$

$$\begin{aligned}
&X_{11} = \sin\varphi_1 F_{11}, \quad X_{12} = \sin\varphi_1 F_{12} \\
&X_{21} = \cos\varphi_1 F_{11} + \alpha_2\beta_2 \sin^2\varphi_1 \cos\varphi_1 F_{21}, \quad X_{22} = \cos\varphi_1 F_{12} + \hat{\alpha}_2\hat{\beta}_2 \sin^2\varphi_1 \cos\varphi_1 F_{22} \\
&X_{31} = -\sin\varphi_1 F_{11} + \alpha_2\beta_2(3\sin\varphi_1\cos^2\varphi_1 - \sin^3\varphi_1)F_{21} + \frac{2}{3}\sin^3\varphi_1\cos^2\varphi_1\alpha_2(\alpha_2+1)\beta_2(\beta_2+1) \\
&X_{32} = -\sin\varphi_1 F_{12} + \hat{\alpha}_2\hat{\beta}_2(3\sin\varphi_1\cos^2\varphi_1 - \sin^3\varphi_1)F_{22} + \frac{2}{3}\sin^3\varphi_1\cos^2\varphi_1\hat{\alpha}_2(\hat{\alpha}_2+1)\hat{\beta}_2(\hat{\beta}_2+1) \\
&F_{11} = {}_2F_1\left(\alpha_2, \beta_2; 2; \sin^2\varphi_1\right), \quad F_{12} = {}_2F_1\left(\hat{\alpha}_2, \hat{\beta}_2; 2; \sin^2\varphi\right) \\
&F_{21} = {}_2F_1\left(\alpha_2+1, \beta_2+1; 3; \sin^2\varphi_1\right), \quad F_{22} = {}_2F_1\left(\hat{\alpha}_2+1, \hat{\beta}_2+1; 3; \sin^2\varphi_1\right) \\
&F_{31} = {}_2F_1\left(\alpha_2+2, \beta_2+2; 4; \sin^2\varphi_1\right), \quad F_{32} = {}_2F_1\left(\hat{\alpha}_2+2, \hat{\beta}_2+2; 4; \sin^2\varphi_1\right) \\
&\alpha_2 = \frac{3+\sqrt{5+iZ_2}}{4}, \quad \beta_2 = \frac{3-\sqrt{5+iZ_2}}{4}, \quad \hat{\alpha}_2 = \frac{3+\sqrt{5-iZ_2}}{4}, \quad \hat{\beta}_2 = \frac{3-\sqrt{5-iZ_2}}{4} \\
&Z_2 = 4\sqrt{\frac{\bar{C}_r}{\bar{D}_r}(1-\nu_r^{\,2}) - \nu_r^{\,2}}
\end{aligned} \tag{4.30}$$

The radial and meridian displacements in each segment of the ocular structure are expressed explicitly after all the integration constants are evaluated in Eqs. (4.19) – (4.20) and Eq. (4.26). Numerical simulations are performed based on these solutions and are presented in the next section.

4.4 Simulation Results

In this section, the results of simulations based on the analytical solutions presented in the previous section are presented for different scleral buckle radii and pressure differences. As shown in the study presented in the previous chapter, the buckle radius has the most important influence on the deformation of the eye membrane, compared with other factors (buckle width, buckle height and buckle Young's modulus). The purpose of this

study is to demonstrate the behavior of the detached retina distant from the sutured scleral buckle and also the deformation of the eye under pressure difference changes under different configurations.

Most retinal detachments are a result of a retinal break, hole, or tear. In this scenario, the tear appears and the fluid comes between the retina and the RPE. The buildup of fluid behind the retina is what separates (detaches) the retina from the back of the eye. Before scleral buckle surgery, the surgeon will drain some of the fluid that has passed through and behind the retina. The removal of this fluid allows the retina to flatten in place against the back wall of the eye. According to this, we study the behavior of the retina while decreasing the pressure difference, Δp, in the present study. Based on the study by Keeling, Propst, Stadler and Wackernagel (2009) , experiments show that the normal inner pressure of the eye is 23 mmHg, and that it could reach a maximum of about 76 mmHg during the surgery. After encircling the band, the autoregulation mechanism will reduce the volume of fluid in the eye and thereby bring the pressure down to around 20 mmHg. So the pressure inside of the eye is taken to be 20 mmHg for the cases considered here in the present study.

In what follows, we take the radius of the eye wall and of the retina to be $R = 12$ mm and $R_r = 11.5$ mm, respectively. The thicknesses of the eye, the retina and the scleral buckle are taken as $h = 0.8$ mm, $h_b = 2$ mm and $h_r = 0.2$ mm, respectively, and the width of the scleral buckle is taken to be $t = 4$ mm. Finally, Young's modulus of the eye, of the retina and of the scleral buckle are taken to be E =2.4 Mpa, $E_r = 0.3$ Mpa and E_b =2.8 Mpa, respectively (See Sigal, et al. (2014), Chou and Siegel (2013), Jones, et al.

(1992), and Wollensak and Spoerl (2004)). We first examine the influence of the radius of the scleral buckle.

4.4.1 The influence of buckle radius

In this case, the pressure difference between the retina and the RPE is set to be $\Delta p = 100$ Pa and we study the behavior of the ocular system, including the detached retina, for various values of the radius of the scleral buckle. The displacement profiles of the ocular system are shown in Figure 4.3 and Figure 4.4 for the buckle radius $R_b = 11.5$ mm.

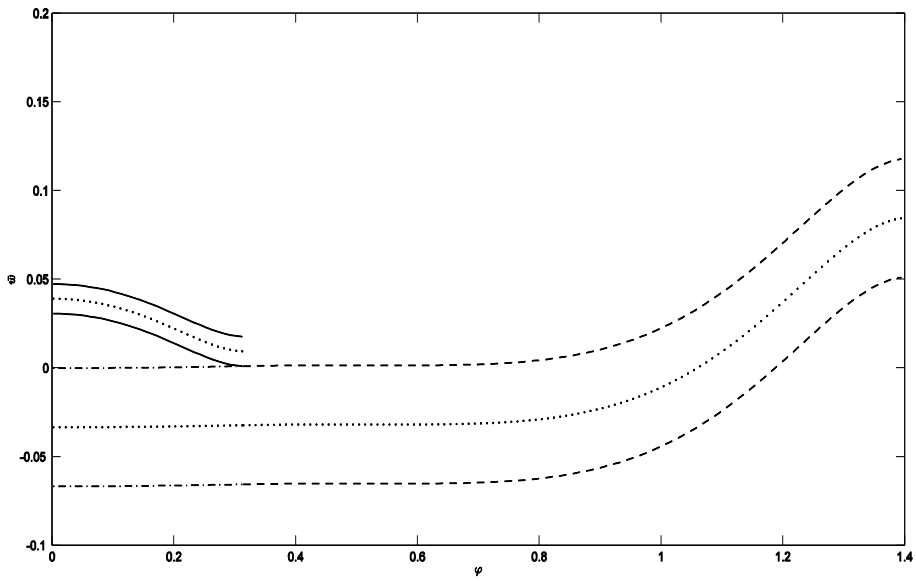

Figure 4.3 Radial displacement of the eye and the retina as a function of φ . R_b =11.5 mm, Δp =100 Pa.

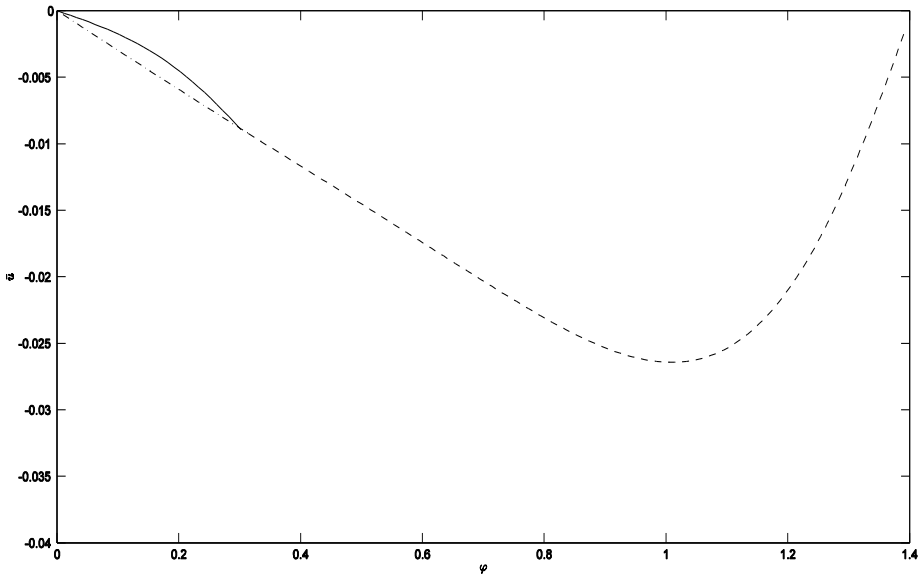

Figure 4.4 Meridian displacements of the eye and the retina as a function of φ . R_b =11.5 mm, Δp =100 Pa.

The nondimensional radial displacements, $\overline{w}$, of the retina and of the eye wall are shown in Figure 4.3 as a function of the angle φ . The corresponding nondimensional meridian displacement, $\overline{u}$, of the contact surface of the retina and the eye wall is displayed in Figure 4.4 as a function of the angle φ . In Figure 4.3, the lower plot is the deflection of the eye wall and the upper plot is that of the detached retina. The dotted line of each plot stands for the centerline of the retina and the eye wall as indicated, and the dashed lines show the inner and outter surfaces of the eye wall in Region S_2. The solid lines correspond to the inner and outer surfaces of the detached segment of the retina, and the dashed dotted lines are the correponding surfaces of the eye wall in Region S_1. It is seen from Figure 4.3 that the retina is detached from the eye wall in Region S_1.

The nondimensional displacement profiles are shown in Figure 4.4 and Figure 4.5 for the buckle radius $R_b = 10.5$ mm.

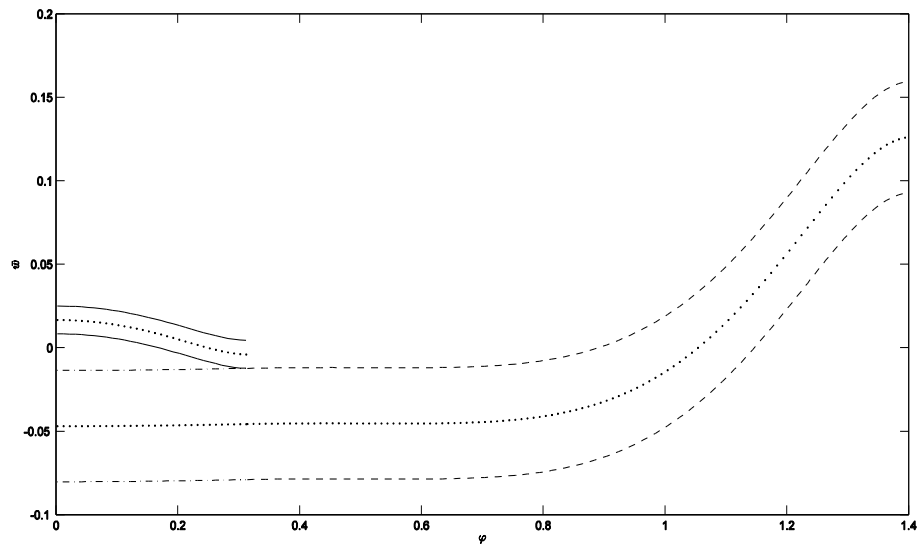

Figure 4.5 Radial displacements of the eye and the retina as a function of φ . R_b =10.5 mm, Δp =100 Pa.

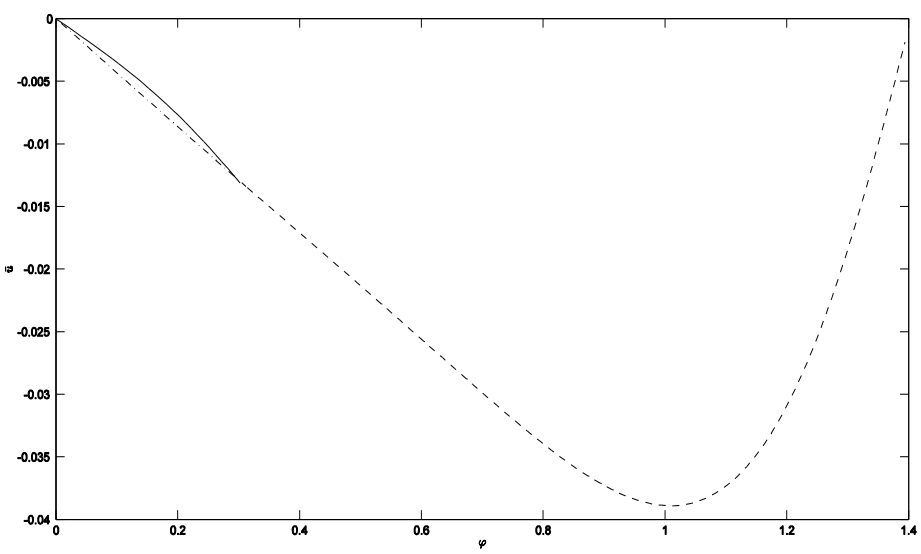

Figure 4.6 Meridian displacements of the eye and the retina as a function of φ .R_b =10.5 mm, Δp =100 Pa.

Comparing Figure 4.3 and Figure 4.5, it is seen that the distance between the retina and the eye membrane (in the radial direction) is reduced as the radius of the buckle decreases. To better illustrate these results, we transform the displacement profiles to Cartesian coordinates for various buckle radii under the pressure difference $\Delta p = 100$ Pa. The corresponding results are shown in Figures 4.7 – 4.11.

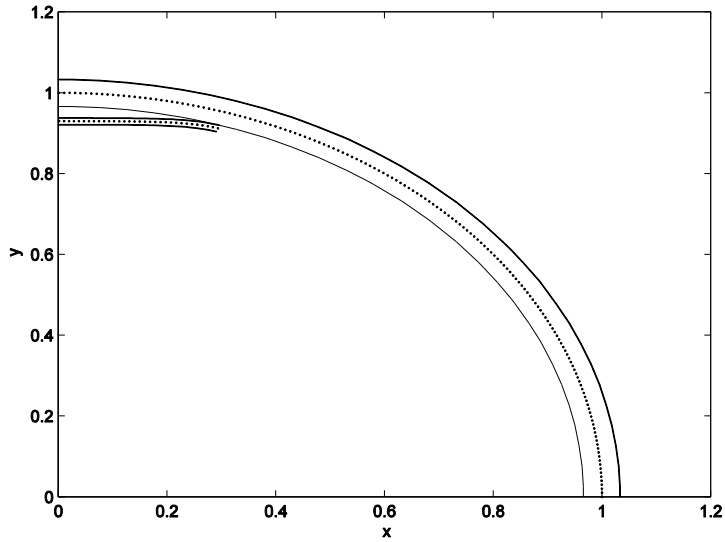

Figure 4.7 The deformation profile of the ocular structure with no scleral buckle applied in Cartesian coordinates. Δp =100 Pa.

The profile displayed in Figure 4.6 is the original distance between the eye and the retina when there is no scleral buckle (i.e., before the surgery). The deformations presented in Figures 4.7 – 4.10 are for buckle radius sizes $R_b = 11.5$, 11, 10.5, and 10 mm, respectively.

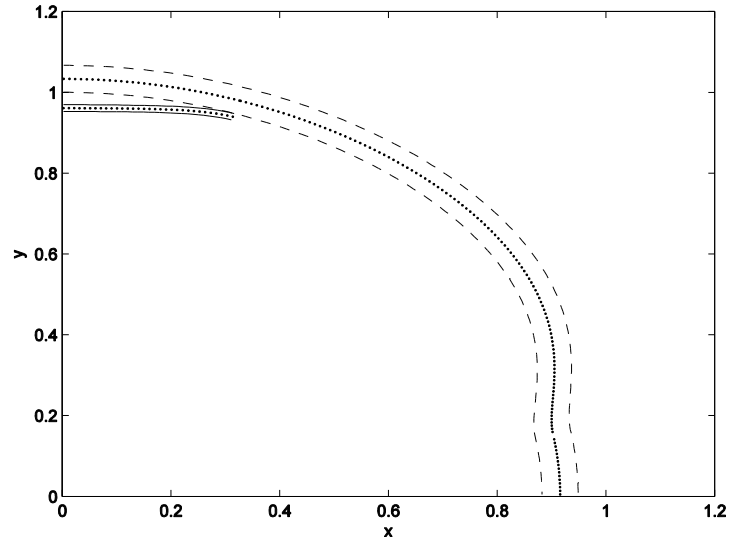

Figure 4.8 The deformation profile of the ocular structure with buckle radius R_b =11.5 mm in Cartesian coordinates. Δp =100 Pa.

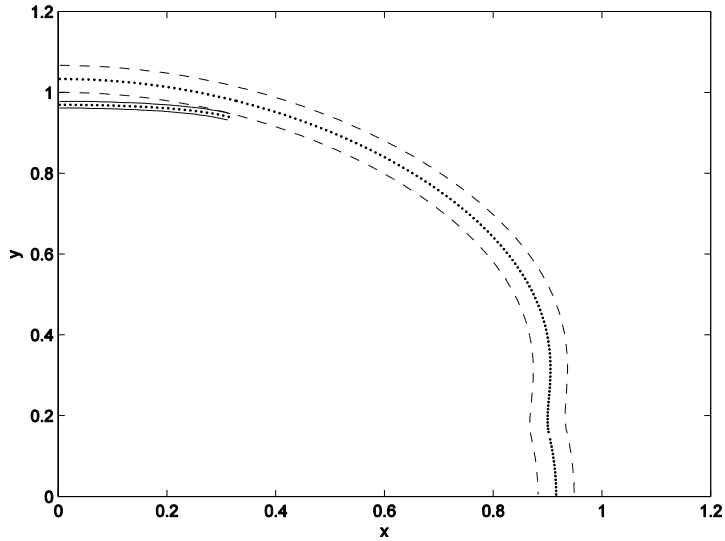

Figure 4.9 The deformation profile of the ocular structure with buckle radius R_b =11mm in Cartesian coordinates. Δp =100 Pa.

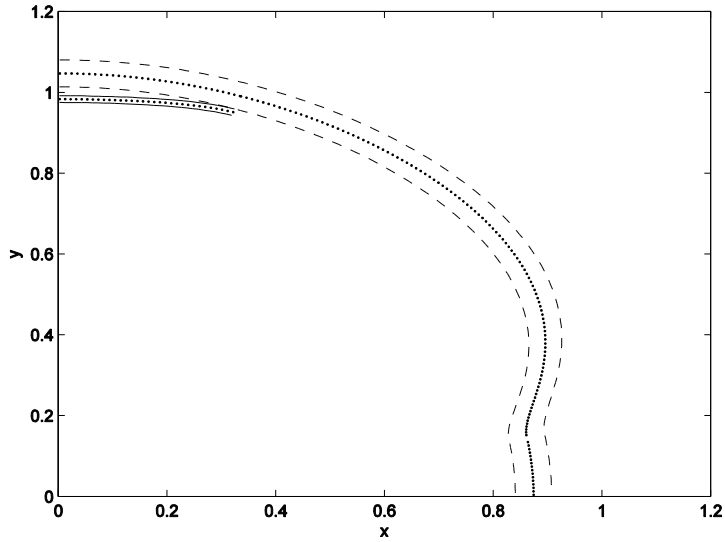

Figure 4.10 The deformation profile of the ocular structure with buckle radius R_b =10.5 mm in Cartesian coordinates. Δp =100 Pa.

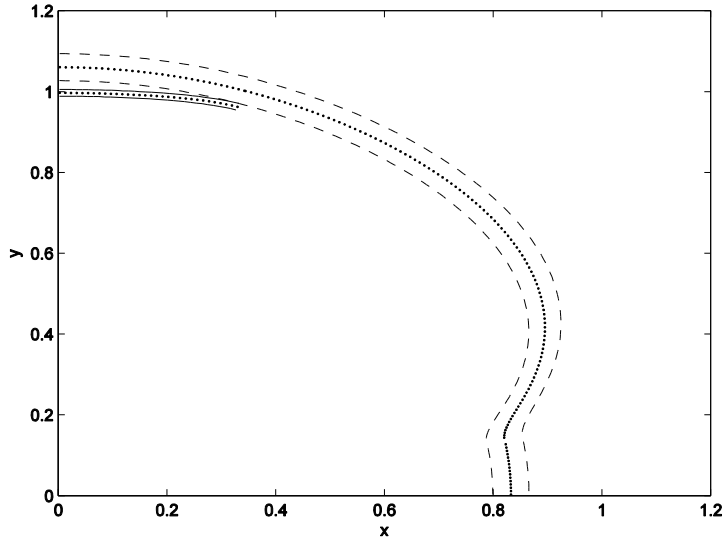

Figure 4.11 The deformation profile of the ocular structure with buckle radius R_b =10 mm in Cartesian coordinates. Δp =100 Pa.

Table 4.1: Center-span distance w.r.t. pressure change and buckle radius change

R_b (mm) \ Δp	500	200	100	0
0 (no buckle)	0.1412	0.0562	0.0279	0
11.5	0.1034	0.0426	0.024	0.0022
11	0.1032	0.0424	0.0225	0.002
10.5	0.103	0.0423	0.0221	0.0018
10	0.1028	0.0421	0.0219	0.0016
Displacement change percentage w.r.t. no buckle case	26.7% – 27%	24.2% – 25%	14% – 21.5%	

According to Figures 4.7 – 4.11, it is noticed that the deformation of the eye wall is larger as the the buckle radius is increased, while the detachment distance between the detached segment of the retina and the eye reduces. Based on the details listed in Table 4.1, it is seen that the separation distance at $\varphi = 0$ decreases from 0.024 to 0.0219 with a pressure difference $\Delta p = 100$ Pa. Comparing these results with the original distance (no buckle applied), it is seen that the maximum separation reduces by about 14% – 21.5%, which is significant for retinal reattachment. It is concluded that after applying the scleral

buckle to the eye, the retina is closer to the eye wall as the buckle radius decreases, although the deformation of the eye is larger. Thus, the smaller the buckle radius, the greater inducement for achieving contact and reattachment of the retina with the RPE.

4.4.2 The Influence of the pressure differences Δp

In this case, we study the influence of the pressure difference Δp on the deformation of the eye and the reattachment of the retina. Simulation results are shown in Figures 4.12 – 4.16 for the pressure difference $\Delta p = 200$ Pa. The original distance between the eye and the retina is presented in Figure 4.12 when no scleral buckle is applied.

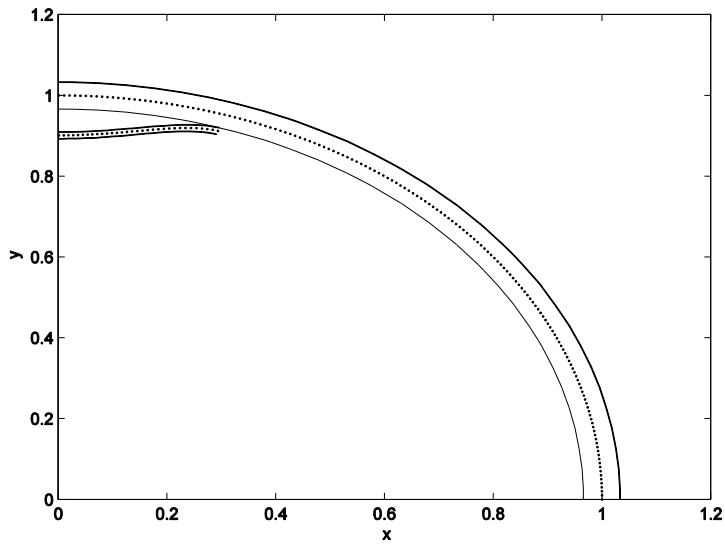

Figure 4.12 The deformation profile of the ocular structure when no scleral buckle is applied (Cartesian coordinates). Δp =200 Pa.

The deformation profile for various buckle radii (R_b = 11.5, 11, 10.5, 10 mm) are displayed in Figures 4.13 – 4.16, respectively.

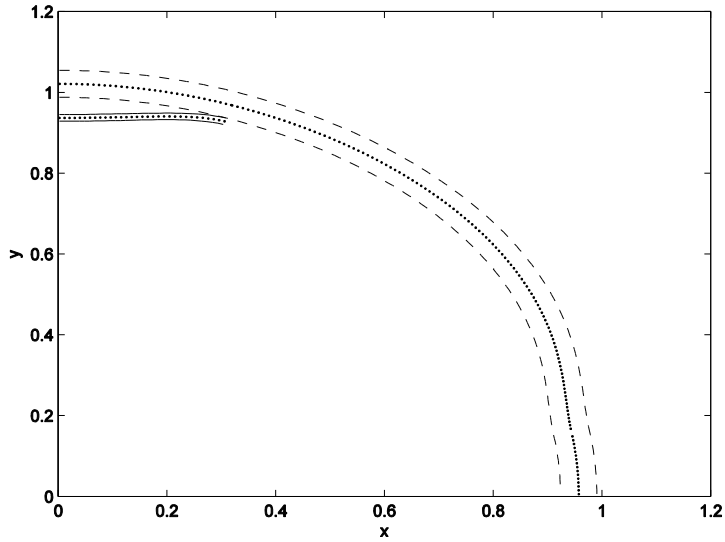

Figure 4.13 The deformation profile of the ocular structure with buckle radius R_b =11.5 mm in Cartesian coordinates. Δp =200 Pa.

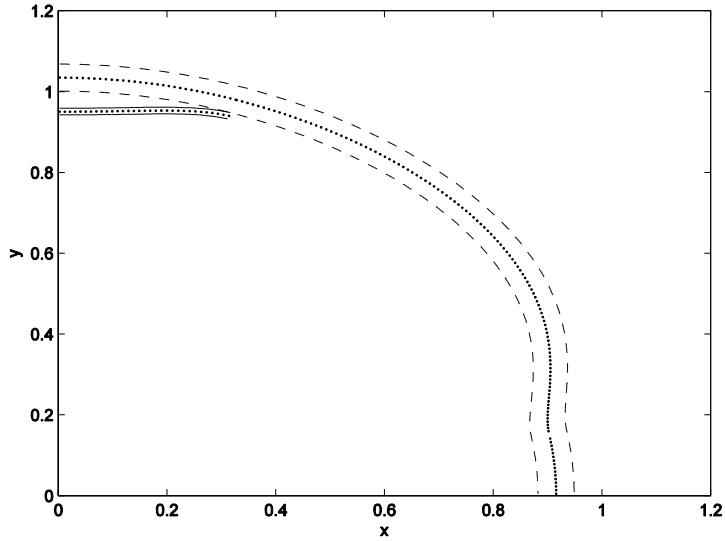

Figure 4.14 The deformation profile of the ocular structure with buckle radius R_b =11 mm in Cartesian coordinates. Δp =200 Pa.

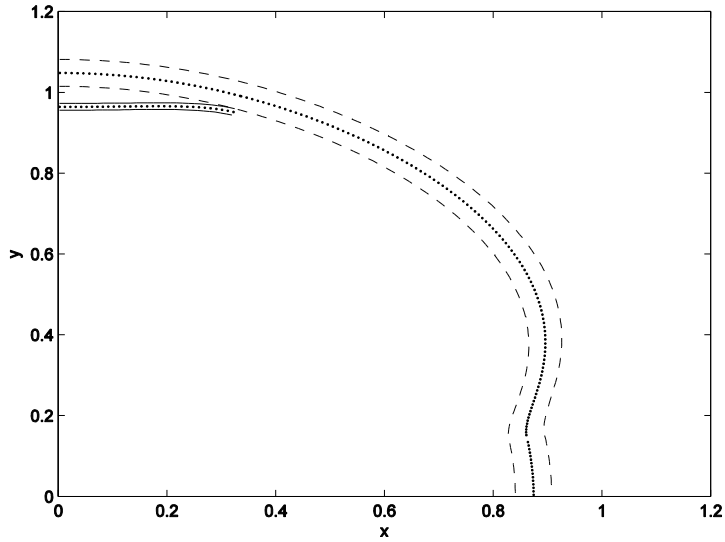

Figure 4.15 The deformation profile of the ocular structure with buckle radius R_b =10.5 mm in Cartesian coordinates. Δp =200 Pa.

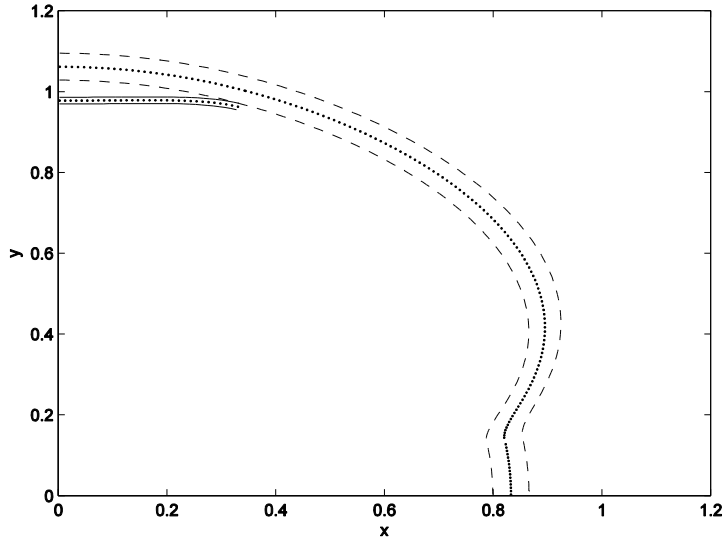

Figure 4.16 The deformation profile of the ocular structure with buckle radius R_b =10 mm in Cartesian coordinates. Δp =200 Pa.

Similarly to the previous case, it is seen that for fixed pressure difference $\Delta p = 200$ Pa, the distance decreases from 0.0426 to 0.0421 as the buckle radius decreases. In order to study the effect of the pressure difference, we compare the results for $\Delta p = 100$ Pa of the previous case with those presented here. Specifically, we compare the result of Figure 4.7 with Figure 4.12, of Figure 4.8 with Figure 4.13, and of Figure 4.9 with Figure 4.14 etc. Upon consideration of these figures, it is found that for the configurations without buckle or with the same buckle, the distance between the retina and the eye wall increases as the pressure difference, Δp , increases. Simulations for a pressure difference $\Delta p =$ 500 and no pressure difference ($\Delta p = 0$) Pa are also studied, but the results are omitted for brevity. The distances between the retina and the eye wall at $\varphi = 0$ are listed in detail in Table 4.1. The results imply that the reduction of the pressure difference between the detached segment of the retina and the sclera (drained of fluid by the surgeon) will also greatly help the reattachment of the retina far away from the equator.

4.5 Conclusion

In this chapter, the effect of the equatorially sutured scleral buckle on the distant retinal detachment. The total potential energy of the evolved structure is fomulated. By applying the principle of stationary potential energy, the analytical solutions for the radial and meridian displacements, as well as the corresponding boundary conditions and matching conditions, are obtained for the eyeball and for the buckle, respectively. Then, we match the radial and meridian displacements at the contact surface of the retina and the eye wall at $\varphi = \varphi_1$ and determine the analytical solutions for the retina. Simulation results based on the analytical solutions are performed and reveal the characteristic behavior of the

deformation of the detached segment of the retina and of the eye. Results are presented for various buckle radii, which were shown in Chapter 3 to have the most effect on the deformation of the system compared to other factors (buckle width, thickness and Young's modulus). It is seen that as the radius of the scleral buckle decreases, the vertical axial length increases. However, the distance between the detached segment of the retina and the eye wall decreases. The study of the influence of the pressure difference Δp shows that the detached retina moves closer to the eye as Δp decreases for the configuration with the same buckle radius, and that when Δp approaches zero, the distance between the detached segment of the retina and the eye becomes very small and can be assumed to be negligible. This study shows that the buckle placed on the equator of the eye will also help with reattachment of the detached segment of the retina that is far away from the equator.

Chapter 5 *Concluding remarks*

5.1 Transverse shear effect on patched plates with edge damage

The current work includes transverse shear deformation and, in this regard, advances on specific prior studies concerning thermal instabilities in patched beam-plates with partial edge detachment. The resulting governing equations, internal and external boundary conditions, trasnversality condition and stability criterion are derived using a variational formulation. Closed form analytical solutions to the governing equations are determined and simulations based on these solutions are performed. The associated analysis and numerical simulations reveal representative and critical behavior of the partially detached structure under uniform temperature changes for both hinged-fixed and clamped-fixed edges. The influence of transverse shear on critical behavior is assessed through examination of these results. For structures with hinged-fixed supports, when the shear moduli of the patch and of the base plate are equal, it is observed that transverse shear deformation has minimal influence on the representative cases considered. It is also seen that the phenomonon of 'buckle-trapping' still exists (first revealed in a prior study using a classical model - no transverse shear deformation). However, behavior is altered and 'buckle trapping' is not observed to occur when the shear moduli of the substructures are unequal. This is in contrast to prior results predicted using the simpler (no transverse shear) model. One concludes from this that the simpler model for the structure, that neglects transverse shear deformation, is inadequate in this case. Structures with clamped-fixed supports allow for several possible local configurations of the detached

segment of patch and base plate: full contact, no contact and edge contact. Those that are not physically realizable are disqualified, based on local kinematic conditions and the relative maginitudes of the total potential energies for each case. For these structures, we also consider the situation where the patch and base plate possess the same shear stiffnesses but have different Poisson's ratios and different Young's moduli. Results for structures with clamped-fixed supports are seen to differ significantly from those of previous studies using the simpler (no transverse shear) model. For the cases considered here, propagating intermediate contact zone configurations (predicted by the model without shear deformation) are not observed. However, edge contact configurations not observed with the simpler model are often seen to occur for structures with relatively small bond zone sizes in the results of the present analysis. To conclude, based on the results of the present study, it is found that transverse shear deformation generally has substantial influence on the critical behavior of the structures of interest.

5.2 Effects of the scleral buckle on retinal reattachment

In this work, we study the mechanical behavior of the ocular structure. The scleral buckle is sutured on the equator of the eye, for cases where the retinal detachment occurs in the vicinity of, and far away from, the buckle are studied. A mathematical model and total potential energy of the ocular structure are formulated for both cases. The radial displacement of the buckle is assumed to be uniform and the meridian displacement is assumed to be negligible for the elastic scleral buckle. Based on these assumptions and applying the Principle of Stationary Potential Energy, the governing equations for the transverse and meridian displacements, as well as the corresponding boundary conditions

and matching conditions. Closed form analytical solutions are obtained for the coupled set of equations and results of simulations based on the analytical solutions were performed and revealed the characteristic behavior of the deformation of the structure. For the case when the scleral buckle is placed in the vicinity of the detachment, the results demonstrate the effect of different material properties of the scleral buckle (radius, width, thickness, Young's modulus), and are of interest for planning surgery. The volume displacements for all the cases considered are presented as well. For all the cases, the transverse axial length is enlarged while the horizontal axial length is compressed. Of the parameters considered (buckle radius, width, thickness and Young's modulus), it is seen that the buckle radius and width have more influence on the deformation of the human eyeball.

When the detachment occurs far away from the equator, the influence of the scleral buckle placed on the equator of the eye is also presented. Results are presented for various buckle radii, which has the most effect to the deformation of the system when compared with other factors (buckle width, thickness and Young's modulus). It is seen that as the radius of the scleral buckle reduces, the vertical axial length increases, while the distance between the retina and the eye wall decreases. The study of the influence of the pressure difference, Δp, shows that the retinal moves closer to the eye as Δp decreases for the same buckle radius, and when Δp reaches close to zero, the distance between the retina and the eye becomes very small and is effectively negligible. We consider this is the situation when the reattachment of the retina to the RPE is possible.

5.3 Future considerations

It is of great importance to study the mechanics of layered structure from a design and analysis standpoint. In the work, we present two types of composite structures (patched plates with edge damage, and eye with retinal detachment and scleral buckle). The effect of transverse shear deformation is included for the layered plates and it is seen that for some cases the 'buckle trapping' phenomenon will not occur while the edge contact configuration may come to play. However, the propagation of the bonded zone boundary may further expand on this work. In addition, the mechanical and thermal properties of the two layers may also have impact on the buckling and debonding behavior.

As to the other type of composite structure studied in this dissertation (the eye with scleral buckle), our formulation begins with use of a thin-shell theory for the eye and for the retina, and ring theory for the scleral buckle, which are suitable for the needs of the work of the dissertation. However, using a more sophisticated nonlinear model may expand the results shown here. In addition, the mechanics of the fluid inside and outside of the eye during suturing the scleral buckle is also of great interest. Moreover, the relation between the pressure difference of the eye and the volume of the eye may be included during the formulation of the problem.

This overall work serves as a significant step toward the better fundamental understanding of layered aerospace and ocular structures.

References

Aydogdu, M. (2007), "Thermal buckling analysis of cross-ply laminated composite beams with general boundary conditions," *Composites science and technology*, **67**:6. 1096-1104.

Bauer, S. M., Tovstik, P. E., and Katchanov, A. B. (1995b), "On the Stability of the Eye Shell under an Encircling Band," **15**. 183-190.

Bottega, W. J. (2006), "Sling-shot buckling of composite structures under thermo-mechanical loading," *International Journal of Mechanical Sciences*, **48**:5. 568-578.

Bottega, W. J., and Carabetta, P. M. (2009), "On the detachment of patched panels under thermomechanical loading," *Journal of Mechanics of Materials and Structures*, **4**:7. 1227-1250.

Bottega, W. J., Bishay, P. L., Prenner, J. L., and Fine, H. F. (2013), "On the mechanics of a detaching retina," *Mathematical Medicine and Biology*, **30**:4. 287-310.

Carabetta, P. M., 2007, "Effects of geometric nonlinearities and uniform temperature fields on the detachment of patched beam-plates under pressure loading," Rutgers University-Graduate School-New Brunswick.

Carabetta, P. M., 2011, "On the interaction of thermal buckling and debonding of patched structures," Rutgers University-Graduate School-New Brunswick.

Carabetta, P. M., and Bottega, W. J. (2012), "On the Interaction of Thermally Induced Buckling and Debonding of Patched Structures," *J. Appl. Mech*, **79**.

Carabetta, P. M., and Bottega, W. J. (2014), "Thermo-Mechanical Instabilities in Patched Structures with Edge Damage," *International journal of non-linear mechanics*, **58**. 89-98.

Chou, T., and Siegel, M. (2013), "The mechanics of retinal detachment," *Bulletin of the American Physical Society*, **58**.

Cowper, G. R. (1966), "The shear coefficient in Timoshenko's beam theory," *Journal of Applied Mechanics*, **33**. 335-340.

Flugge, W. (1960), "Stresses in shells," *Julius Springer, Berlin*.

Foster, W. J., Dowla, N., Joshi, S. Y., and Nikolaou, M. (2010), "The fluid mechanics of scleral buckling surgery for the repair of retinal detachment," *Graefe's Archive for Clinical and Experimental Ophthalmology*, **248**:1. 31-36.

Hutchinson, J. R. (1981), "Transverse vibrations of beams, exact versus approximate solutions," *ASME, Transactions, Journal of Applied Mechanics*, **48**. 923-928.

Jones, I., Warner, M., and Stevens, J. (1992), "Mathematical modelling of the elastic properties of retina: a determination of Young's modulus," *Eye*, **6**:6. 556-559.

Karlsson, A. M., and Bottega, W. J. (1999), "The presence of edge contact and its influence on the debonding of patched panels," *International Journal of Fracture*, **96**:4. 383-406.

Karlsson, A. M., and Bottega, W. J. (2000a), "On thermal buckling of patched beam-plates," *International Journal of Solids and Structures*, **37**:34. 4655-4690.

Karlsson, A. M., and Bottega, W. J. (2000b), "Thermo-mechanical response of patched plates," *AIAA Journal*, **38**:6. 1055-1062.

Karlsson, A. M., and Bottega, W. J. (2000c), "On the behavior of a class of patched plates during cooling," *International Journal of Non-linear Mechanics*, **35**:3. 543-566.

Keeling, S. L., Propst, G., Stadler, G., and Wackernagel, W. (2009), "A mathematical model for the deformation of the eyeball by an elastic band," *Mathematical Medicine and Biology*, **26**:2. 165-185.

Lakawicz, J. M., Bottega, W. J., Prenner, J. L., and Fine, H. F. (2014), "An analysis of the mechanical behaviour of a detaching retina," *Mathematical Medicine and Biology*. DOI: 10.1093/imammb/dqt023.

Mindlin, R. D. (1951), " Influence of rotary inertia and shear on flexural motions of isotropic elastic plates," *ASME Journal of Applied Mechanics*, **18**. 31-38.

Reddy, J. N. (1984), "A Simple Higher-Order Theory for Laminated Composite Plates," *Journal of Applied Mechanics*, **51**:4. 745-752.

Ritchie, R. O., Knott, J. F., and Rice, J. R. (1973), "On the relationship between critical tensile stress and fracture toughness in mild steel," *Journal of the Mechanics and Physics of Solids*, **21**:6. 395-410.

Rutgerson, S. E., and Bottega, W. J. (2002), "Thermo-elastic buckling of layered shell segments," *International Journal of Solids and Structures*, **39**:19. 4867-4887.

Sato, M., Wadee, M. A., Iiboshi, K., Sekizawa, T., and Shima, H. (2012), "Buckling patterns of complete spherical shells filled with an elastic medium under external pressure," *International Journal of Mechanical Sciences*, **59**:1. 22-30.

Seo, J. M., Park, K. S., Yu, H. G., and Chung, H. (2002), "Geometric changes of the eye with an encircling scleral buckle," *Journal of the Korean Ophthalmological Society*, **43**:6. 1072-1080.

Shen, H. S. (1998), "Thermomechanical post-buckling analysis of imperfect laminated plates using a higher-order shear-deformation theory," *Computers and Structures*, **66**:4. 395-409.

Sigal, I., Grimm, J., Schuman, J., Kagemann, L., Ishikawa, H., and Wollstein, G. (2014), "A Method to Estimate Biomechanics and Mechanical Properties of Optic Nerve Head Tissues From Parameters Measurable Using Optical Coherence Tomography," *IEEE transactions on medical imaging*, **33**:6. 1381-1389.

Thompson, J. T., and Michels, R. G. (1985), "Volume displacement of scleral buckles," *Archives of ophthalmology*, **103**:12. 1822-1824.

Timoshenko, S. P. (1921), "On the correction for shear of the differential equation for transverse vibrations of prismatic bars," *The London, Edinburgh, and Dublin Philosophical Magazine and Journal of Science*, **41**:245. 744-746.

Timoshenko, S. P. (1925), "Analysis of bi-metal thermostats," *J. Opt. Soc. Am*, **11**:3. 233-255.

Timoshenko, S., Woinowsky-Krieger, S., and Woinowsky, S., (1959), Theory of plates and shells, McGraw-hill New York.

Uchio, E., Ohno, S., Kudoh, J., Aoki, K., and Kisielewicz, L. T. (1999), "Simulation model of an eyeball based on finite element analysis on a supercomputer," *British Journal of Ophthalmology*, **83**:10. 1106-1111.

Wahl, A. M. (1944), "Analysis of Valverde thermostat," *J. Appl. Mech*, **11**. A183-A189.

Wittrick, W. H., Myers, D. M., and Blunden, W. R. (1953), "Stability of a bimetallic disk," *The Quarterly Journal of Mechanics and Applied Mathematics*, **6**:1. 15-31.

Wilkinson, C. P., and Rice, T. A., (1997), Michels's Retinal Detachment, Mosby, Incorporated.

Wollensak, G., and Spoerl, E. (2004), "Biomechanical characteristics of retina," *Retina*, **24**:6. 967-970.

Zenkour, A. M., and Sobhy, M. (2010), "Thermal buckling of various types of FGM sandwich plates," *Composite Structures*, **93**:1. 93-102.

Appendix

A – Stiffnesses of Composite Structure (patched plate) in Bond Zone

$$A^* = D_b + D_p + (h_b/2)^2 C_b + (h_p/2)^2 C_p \tag{A-1}$$

$$B^* = (h_p/2)C_p - (h_b/2)C_b \tag{A-2}$$

$$C^* = C_p + C_b; \quad D^* = A^* - \rho^* B^* \tag{A-3}$$

$$\rho^* = \frac{B^*}{C^*} \tag{A-4}$$

$$n^* = C_b\alpha_b + C_p\alpha_p \tag{A-5}$$

$$\mu^* = \frac{1}{2}h_p C_p \alpha_p - \frac{1}{2}h_b C_b \alpha_b \tag{A-6}$$

$$m^* = \mu^* - \rho^* n^* \tag{A-7}$$

The quantity ρ^* is seen to give the transverse location of the centroid of the composite structure with respect to the reference surface.

B – Constitutive Relations (patched plate)

$$N_1^* = C^* e_1^* + B^* \kappa_1^* - n^* \Theta; \quad M_1^* = D^* (\kappa_1^* - \beta^* \Theta) + \rho^* N_1^* \tag{B-1}$$

$$N_i = C\left[e_i - \alpha\Theta\right]; \quad N_{pi} = C_p\left[e_{pi} - \alpha_p \Theta\right] \tag{B-2}$$

$$M_i = D\kappa_i - \frac{h}{2} N_i; \quad M_{pi} = D_p \kappa_{pi} - \frac{h_p}{2} N_{pi} \tag{B-3}$$

$$e_i = u_i^{'} + \frac{1}{2}\phi_i^2 \quad e_{pi} = u_{pi}^{'} + \frac{1}{2}\phi_{pi}^2; \quad i = 1, 2 \tag{B-4}$$

M^* and N^* are the normalized bending moment and membrane force of the composite structure within the bonded region, respectively. The membrane forces in the base plate and the patch within Region S_i are

N_i and M_i , respectively. e_i and e_{pi} are the corresponding membrane strains at the centroid of the individual primitive structures. The stiffnesses are listed in Appendix A.

C – Solution Parameters (patched plate)

$$\mu_1 = \frac{(\hat{b}-\sqrt{R})}{-2\hat{a}} \quad \beta_1 = \frac{(\hat{b}+\sqrt{R})}{-2\hat{a}} \quad P_1 = \frac{1-\frac{D_b}{G_b}\alpha_1^2}{1-\frac{D_p}{G_p}\alpha_1^2} \quad P_2 = \frac{1-\frac{D_b}{G_b}\beta_1^2}{1-\frac{D_p}{G_p}\beta_1^2} \; (General\ case) \qquad \text{(C-1)}$$

$$\mu_1 = \sqrt{\frac{G_b}{D_b}} \quad \beta_1 = \sqrt{\frac{N_0}{D_b(2-\frac{N_0}{G_b})}} \quad P_1 = -1 \quad P_2 = 1\,(Special\ case: G_p = G_b) \qquad \text{(C-2)}$$

$$\hat{b} = -(D_b + D_p - N_0(\frac{D_b}{G_b} + \frac{D_p}{G_p})) \quad \hat{c} = -N_0 \quad K_b = \sqrt{\frac{N_0}{g^*}} \qquad \text{(C-3)}$$

$$\hat{a} = \frac{D_b * D_p}{G_b * G_p}(G_b + G_p - N_0) \quad R = \hat{b}^2 - 4\hat{a}\hat{c} \quad K_{b3} = \sqrt{\frac{N_0}{g_3}} \qquad \text{(C-4)}$$

D – MATLAB code (patched plate)

For hinged fixed edge support

```
%Generate the transverse displacements and total energy profile for the
intact case with no shear deformation is included
clear
% use noshear5 is much faster
HB=0.05;HP=0.05; a=0.6;  alpha1=.002; alpha2=.5;
%HB HP are the thickness of the base and the patch, a is the bond zone
size
thermal=.1:0.1:14;
syms x
N0=sym('N0');
Ninput=[0:.05:160];
yy=[];
MemN0=[];
Dis1=[];
Dis2=[];
Dis=[];
W0=[];
Energy=[];
k=1;
 for i=1:size(thermal,2)
    tic

[yy(i,:),f,W1,W2,Eng,hh,phi1,phi2]=noshear(HB,HP,alpha1,alpha2,a,therma
l(i),Ninput);
   num=1;
     for j=1:size(yy,2)-1
         if yy(i,j)*yy(i,j+1)<0
             MemN0(i,num)=fminsearch(f,Ninput(j),optimset('TolX',1e-4));
             Dis1=subs(W1,{N0,x},{MemN0(i,num),0:.01:a});
             Dis2=subs(W2,{N0,x},{MemN0(i,num),a+.01:0.01:1});
             W0(i,num)=Dis1(1);
             Dis(i,num,:)=[Dis1,Dis2];
             Phi1=subs(phi1,{N0,x},{MemN0(i,num),0:.01:a});
             Phi2=subs(phi2,{N0,x},{MemN0(i,num),a+.01:0.01:1});
             Phi(i,num,:)=[Phi1,Phi2];
             Energy(i,num)=subs(Eng,MemN0(i,num));
             num=num+1;
         end
     end
     i
     toc
 end
totalF=stable(thermal, MemN0);
%
%% plot the memebrane force WRT the thermal loading.
hh=fzero(hh,[4,40]);%%%% find the critical membrane force.
index=find(abs(MemN0-hh)<.0448);
criticaltemp=thermal(index);
criticalMemN0=MemN0(index);
for i=1:size(thermal,2)
    for j=1:size(MemN0,2)
```

```
        if totalF(i,j)>0
            figure(1)
            plot(thermal(i),MemN0(i,j),'ro')
            hold on
        elseif totalF(i,j)<0
            plot(thermal(i),MemN0(i,j),'.')
            hold on
        end
    end
end
plot(criticaltemp,criticalMemN0,'ro')
text(criticaltemp-
1,criticalMemN0+8,['(',num2str(criticaltemp),',',num2str(criticalMemN0)
,')'],'FontSize',15)
ylabel('Membrane force')
xlabel('Thermal Loading')
axis([0 14 0 160])
h=gcf;
saveas(h,'membrane.fig')

for i=1:size(thermal,2)
    for j=1:size(MemN0,2)
        if totalF(i,j)>0
            figure(2)
            plot(W0(i,j),thermal(i),'ro')
            hold on
        elseif totalF(i,j)<0
            plot(W0(i,j),thermal(i),'.')
            hold on
        end
    end
end
plot([-3,0.4],[criticaltemp,criticaltemp],'r--')
xlabel('centerspan displacement')
ylabel('Thermal Loading')
axis([-0.3 0.4 0 14])
h=gcf;
saveas(h,'centerspandisplacement.fig')

for i=1:size(thermal,2)
    for j=1:size(MemN0,2)
        if totalF(i,j)>0
            figure(3)
            plot(thermal(i),Energy(i,j),'ro')
            hold on
        elseif totalF(i,j)<0
            plot(thermal(i),Energy(i,j),'.')
            hold on
        end
    end
end
plot([criticaltemp,criticaltemp],[0,0.5],'r--')
ylabel('total energy')
xlabel('Thermal Loading')
axis([0 14 0 2.5])
h=gcf;
```

```
saveas(h,'totalenergy.fig')
for i=1:size(thermal,2)
    for j=1:size(MemN0,2)
        if totalF(i,j)>0
            figure(4)
            plot(thermal(i),totalF(i,j),'ro')
            hold on
        elseif totalF(i,j)<0
            plot(thermal(i),totalF(i,j),'.')
            hold on
        end
    end
end
plot([criticaltemp,criticaltemp],[-400,500],'p--')
ylabel('stability analysis')
xlabel('Thermal Loading')
axis([0 14 -60 80])
h=gcf;
saveas(h,'stability.fig')
savefile = 'pqfile06.mat';
save(savefile)

function [y1,f,W1,W2,Eng,hh,phi1,phi2]
=noshear(HB,HP,alpha1,alpha2,a,thermal,Ninput)
%%%% Ninput is to get the plot with N0=Ninput and draw the relation be-
tween
%%%% N0 and transversality equation. y is the coreesponding value of
the
%%%% trans-equation
format long
syms x  C1  C3 C4 C5  C7 C8 C2 C6
N0=sym('N0'); % DEFINE IT THIS WAY&&&&&&&&
Thermal=thermal*alpha1;
Cb=12/HB^2;
Cp=12*(HP/HB)/(HB^2);
Ct=Cb+Cp;
Bt=(1/2)*HP*Cp-(1/2)*HB*Cb;
roh=Bt/Ct;
DB=1;
DP=(HP/HB)^3;
D1=DB+DP+Cb*((1/2)*HB)^2+Cp*(HP/2)^2-roh*Bt;
K1=sqrt(N0/DB);
K2=sqrt(N0/D1);
miu=-(HB/2)*Cb+alpha2*(HP/2)*Cp;
n=Cb+alpha2*Cp;
m=miu-roh*n;
aa=1-a;

%% equations for displacement of base and patch
H=-sin(K2*a)*sin(K1*aa)+sqrt(D1/DB)*cos(K2*a)*cos(K1*aa);
hh=matlabFunction(H);
Mlamda=m*Thermal+(roh+.5*HB)*N0;
W1=(Mlamda/(N0*H))*(H-sqrt(D1/DB)*cos(K1*aa)*cos(K2*x));
W2=-(Mlamda/(N0*H))*sin(K2*a)*sin(K1*(1-x));
phi1=diff(W1,x);
phi2=diff(W2,x);
a1=-N0/Ct; a2=roh+.5*HB; a3=(n/Ct-1)*Thermal;a4=DB+DP;
```

```
b2=roh-.5*HP; b3=(n/Ct-alpha2)*Thermal;
mm1=Cb*a2^2+Cp*b2^2+a4; mm2=-2*Cb*a2*(a1+a3)-2*Cp*b2*(a1+b3);
mm3=Cb*(a1+a3)^2+Cp*(a1+b3)^2;

ff=-N0*(aa/Cb+a/Ct)-(1/2)*(int(diff(W1, x)^2,x,0, a))-
(1/2)*(int(diff(W2, x)^2,x,a, 1))-(.5*HB+roh)*(subs(diff(W1, x),
a))+(aa+a*n/Ct)*Thermal;
Energy=(1/2)*mm1*(int(diff(W1,x,2)^2,x,0,
a))+(1/2)*mm2*(int(diff(W1,x,2),x,0,
a))+(1/2)*a*mm3+(1/2)*DB*(int(diff(W2,  x,2)^2,x,a,  1))+(1/2)*N0^2*aa/Cb;

y1=subs(ff,N0,Ninput);
ff=ff^2;
f=matlabFunction(ff);
W1=matlabFunction(W1);
W2=matlabFunction(W2);
phi1=matlabFunction(phi1);
phi2=matlabFunction(phi2);
Eng=matlabFunction(Energy);

function stableF=stable(thermal,MemN0)
%%Caculate F for stability analysis
format long
HB=0.05;HP=0.05; a=0.6; alpha1=.002; alpha2=.5;
syms x
N0=MemN0;
Cb=12/HB^2;
Cp=12*(HP/HB)/(HB^2);
Ct=Cb+Cp;  Bt=(1/2)*HP*Cp-(1/2)*HB*Cb;  roh=Bt/Ct;
DB=1;
DP=(HP/HB)^3;
D1=DB+DP+Cb*((1/2)*HB)^2+Cp*(HP/2)^2-roh*Bt; K1=sqrt(N0/DB);
K2=sqrt(N0/D1);
miu=-(HB/2)*Cb+alpha2*(HP/2)*Cp;
n=Cb+alpha2*Cp;
m=miu-roh*n;
aa=1-a;
H=-sin(K2*a).*sin(K1*aa)+sqrt(D1/DB).*cos(K2*a).*cos(K1*aa);
A1=-sqrt(D1/DB).*cos(K1*aa);
B0=sin(K2*a);
stableF=.25*((A1./H).*(A1./H).*sin(2*K2*a).*K2-
(B0./H).*(B0./H).*sin(2*K1*aa).*K1);
```

Case 1. Equal shear stiffness

```
%%Intact structure with shear deformation included
%%Same Poisson's ratio for the base and the patch,
%%and in this file, we use 0.2. For other cases, just need to change
the
%%value in the simulation.
clear
%%% FOR G=E/2(1+nu), where nu is Poisson's ratio and E is Young's modu-
lus
HB=0.05;HP=0.05; a=0.8;  alpha1=.002; alpha2=.5;
thermal=.1:0.1:14;
syms x
N0=sym('N0');
```

```
Ninput=[0:.05:160];
yy=[];MemN0=[];Dis1=[];Dis2=[];Dis=[];
W0=[];Gama1=[];Gama2=[];Gama=[];
Phi1=[];Phi2=[];Phi=[];Energy=[];
k=1;
for i=1:size(thermal,2)

[yy(i,:),f,W1,W2,phi1,phi2,gama1,gama2,Eng,hh]=withshear5(HB,HP,alpha1,
alpha2,a,thermal(i),Ninput);
   yy ;
   num=1;
     for j=1:size(yy,2)-1
         if yy(i,j)*yy(i,j+1)<0
             MemN0(i,num)=fminsearch(f,Ninput(j),optimset('TolX',1e-5))
             Dis1=subs(W1,{N0,x},{MemN0(i,num),0:.01:a});
             Dis2=subs(W2,{N0,x},{MemN0(i,num),a+.01:0.01:1});
             Gama1=subs(gama1,{N0,x},{MemN0(i,num),0:.01:a});
             Gama2=subs(gama2,{N0,x},{MemN0(i,num),a+.01:0.01:1});
             Phi1=subs(phi1,{N0,x},{MemN0(i,num),0:.01:a});
             Phi2=subs(phi2,{N0,x},{MemN0(i,num),a+.01:0.01:1});
             W0(i,num)=Dis1(1);
             Dis(i,num,:)=[Dis1,Dis2];
             Gama(i,num,:)=[Gama1,Gama2];
             Phi(i,num,:)=[Phi1,Phi2];
             Energy(i,num)=subs(Eng,MemN0(i,num));
             num=num+1;
         end
     end
     i
end
totalF=stable(thermal, MemN0);
hh=fzero(hh,[4,40]);%%%% find the critical membrane force.
%% plot the memebrane force WRT the thermal loading.
index=find(abs(MemN0-hh)<6e-2);
criticaltemp=thermal(index);
criticalMemN0=MemN0(index);
for i=1:size(thermal,2)
    for j=1:size(MemN0,2)
        if totalF(i,j)>0
            figure(1)
            plot(thermal(i),MemN0(i,j),'ro')
            hold on
        elseif totalF(i,j)<0
            plot(thermal(i),MemN0(i,j),'.')
            hold on
        end
    end
end
 plot(criticaltemp,criticalMemN0,'ro')
 text(criticaltemp-
1,criticalMemN0+8,['(',num2str(criticaltemp),',',num2str(criticalMemN0)
,')'],'FontSize',15)
ylabel('Membrane force')
xlabel('Thermal Loading')
axis([0 14 0 160])
h=gcf;
saveas(h,'membrane.fig')
```

```
for i=1:size(thermal,2)
    for j=1:size(MemN0,2)
        if totalF(i,j)>0
            figure(2)
            plot(W0(i,j),thermal(i),'ro')
            hold on
        elseif totalF(i,j)<0
            plot(W0(i,j),thermal(i),'.')
            hold on
        end
    end
end
plot([-0.15,0.25],[criticaltemp,criticaltemp],'r--')
xlabel('centerspan displacement')
ylabel('Thermal Loading')
axis([-0.15 0.25 0 14])
h=gcf;
saveas(h,'centerspandisplacement.fig')

for i=1:size(thermal,2)
    for j=1:size(MemN0,2)
        if totalF(i,j)>0
            figure(3)
            plot(thermal(i),Energy(i,j),'ro')
            hold on
        elseif totalF(i,j)<0
            plot(thermal(i),Energy(i,j),'.')
            hold on
        end
    end
end
plot([criticaltemp,criticaltemp],[0,0.5],'r--')
ylabel('total energy')
xlabel('Thermal Loading')
axis([0 14 0 2.5])
h=gcf;
saveas(h,'totalenergy.fig')
for i=1:size(thermal,2)
    for j=1:size(MemN0,2)
        if totalF(i,j)>0
            figure(4)
            plot(thermal(i),totalF(i,j),'ro')
            hold on
        elseif totalF(i,j)<0
            plot(thermal(i),totalF(i,j),'.')
            hold on
        end
    end
end
plot([criticaltemp,criticaltemp],[-400,500],'p--')
ylabel('stability analysis')
xlabel('Thermal Loading')
axis([0 14 -60 80])
h=gcf;
saveas(h,'stability.fig')
```

```
savefile = 'pqfile.mat';
save(savefile)

function
[y1,f,W1,W2,phi1,phi2,gama1,gama2,PE,hh]=withshear5(HB,HP,alpha1,alpha2
,a,thermal,Ninput)
%%%% Ninput is to get the plot with N0=Ninput and draw the relation be-
tween
%%%% N0 and transversality equation. y is the coreesponding value of
the
%%%% transversality equation
%%%% y1 is the value of intergrability equation;
format long
 syms x
N0=sym('N0'); %%% DEFINE IT THIS WAY&&&&&&&&
Thermal=thermal*alpha1;
Cb=12/HB^2;
Cp=12*(HP/HB)/(HB^2);
Ct=Cb+Cp;  %%%C*
Bt=(1/2)*HP*Cp-(1/2)*HB*Cb;  %B*
roh=Bt/Ct;
DB=1;
DP=(HP/HB)^3;
D1=DB+DP+Cb*((1/2)*HB)^2+Cp*(HP/2)^2-roh*Bt; %D*
miu=-(HB/2)*Cb+alpha2*(HP/2)*Cp;
nstar=Cb+alpha2*Cp;
mstar=miu-roh*nstar;
kb= .9;
ratio=1/2.4;
LamdaB= kb*ratio*Cb;
LamdaP= kb*ratio*Cp; %%%Here we take shear modulus/youngs modulus==0.1
aa=1-a;
%% define some parameters
m=D1*(1-N0/(LamdaB+LamdaP));
m2=DB*(1-N0/LamdaB);
Kb=sqrt(N0/m);
Kb2=sqrt(N0/m2);
b1=cos(Kb*a)*cos(Kb2*aa);
b2=sin(Kb*a)*sin(Kb2*aa);

LAMDA=sqrt(1+LamdaP/LamdaB)*sqrt(1-LamdaP/(LamdaB+LamdaP-N0));

%% equations for displacement of base and patch
Mlamda=mstar*Thermal+(roh+.5*HB)*N0;
H=D1*Kb2*m2*b1/(DB*Kb*m)-b2;
hh=matlabFunction(H);

BB=sqrt(D1/DB)*LAMDA;
phi1=((Mlamda*(1-N0/LamdaB)*Kb2)/(N0*H))*cos(Kb2*aa)*sin(Kb*x);
phi2=((Mlamda*(1-N0/LamdaB)*Kb2)/(N0*H))*sin(Kb*a)*cos(Kb2*(1-x));
W1=(Mlamda/(N0*H))*(H-BB*cos(Kb2*aa)*cos(Kb*x));
W2=-(Mlamda/(N0*H))*sin(Kb*a)*sin(Kb2*(1-x));
gama1=diff(W1,x)-phi1;
gama2=diff(W2,x)-phi2;
a1=0.5*(DB+DP)+Cb*Cp*(HB+HP)^2/Ct/8-D1;
a2=0.5*Cb*Cp*(HB+HP)*(1-alpha2)*Thermal/Ct;
```

```
phi1prime=diff(phi1,x);
phi2prime=diff(phi2,x);
intW1square=int(diff(W1,x)^2,x,0, a);
intW2square=int(diff(W2,x)^2,x,a, 1);

Energy=a1*(int(phi1prime^2,x,0,
a))+0.5*(LamdaB+LamdaP)*intW1square+D1*(subs(phi1*phi1prime,x,a))-
.5*(LamdaB+LamdaP)*(int(phi1^2,x,0, a))...
    +a2*(int(phi1prime,x,0, a))+0.5*int((N0^2+Cb*Cp*(1-
alpha2)^2*Thermal^2)/Ct,x,0,a)...
    -0.5*DB*(int(phi2prime^2,x,a,1))+0.5*LamdaB*intW2square-
.5*LamdaB*(int(phi2^2,x,a, 1))+0.5*(int(N0^2/Cb,x,a,1))-
DB*(subs(phi2*phi2prime,x,a));
%%
PE=matlabFunction(Energy);

ff=-N0*(aa/Cb+a/Ct)-(1/2)*intW1square-(1/2)*intW2square-
(.5*HB+roh)*(subs(phi1, a))+(aa+a*nstar/Ct)*Thermal;% subs(C1,N0,1)
y1=subs(ff,N0,Ninput);
ff=ff^2;
f=matlabFunction(ff);
W1=matlabFunction(W1);
W2=matlabFunction(W2);
gama1=matlabFunction(gama1);
gama2=matlabFunction(gama2);
phi1=matlabFunction(phi1);
phi2=matlabFunction(phi2);

function stableF=stable(thermal,N0)
%%Caculate F for stability analysis
format long
HB=0.05;HP=0.05; a=0.8;  alpha1=.002; alpha2=.5;
syms x
Cb=12/HB^2;
Cp=12*(HP/HB)/(HB^2);
Ct=Cb+Cp;
Bt=(1/2)*HP*Cp-(1/2)*HB*Cb;
roh=Bt/Ct;
DB=1;
DP=(HP/HB)^3;
D1=DB+DP+Cb*((1/2)*HB)^2+Cp*(HP/2)^2-roh*Bt;
miu=-(HB/2)*Cb+alpha2*(HP/2)*Cp;
nstar=Cb+alpha2*Cp;
mstar=miu-roh*nstar;
kb= .9;
ratio=1/2.4;
LamdaB= kb*ratio*Cb;
LamdaP= kb*ratio*Cp;
aa=1-a;
m=D1*(1-N0./(LamdaB+LamdaP));
m2=DB*(1-N0./LamdaB);
Kb=sqrt(N0./m);
Kb2=sqrt(N0./m2);
A2=-sqrt(D1/DB)*cos(Kb2*aa);
B0=sin(Kb*a);
b1=cos(Kb2*aa).*cos(Kb*a);
```

```
b2=sin(Kb2*aa).*sin(Kb*a);
H=D1.*Kb2.*m2.*b1./(DB.*Kb.*m)-b2;
stableF=.25*(1-N0./LamdaB).*((A2./H).*(A2./H).*sin(2*Kb*a).*Kb-
(B0./H).*(B0./H).*sin(2*Kb2*aa).*Kb2);
```

Case 2. Unequal shear stiffness

```
%%Intact structure with shear deformation included
%%Different Poisson's ratio, and in this file, we use 0.3 and 0.1 for
the base and the patch separately.
clear
HB=0.05;HP=0.05; a=0.6;  alpha1=.002; alpha2=.5;
thermal=.1:0.1:14;
syms x
N0=sym('N0');
Ninput=[0:.05:80];
yy=[];MemN0=[];Dis1=[];Dis2=[];Dis=[];
W0=[];Gama1=[];Gama2=[];Gama=[];Phi1=[];
Phi2=[];Phi=[];Energy=[];
 k=1;
 for i=1:size(thermal,2)

[yy(i,:),f,W1,W2,phi1,phi2,gama1,gama2,Eng,hh]=withshear5(HB,HP,alpha1,
alpha2,a,thermal(i),Ninput);
    yy ;
    num=1;
     for j=1:size(yy,2)-1
         if yy(i,j)*yy(i,j+1)<0
             MemN0(i,num)=fminsearch(f,Ninput(j),optimset('TolX',1e-5))
             Dis1=subs(W1,{N0,x},{MemN0(i,num),0:.01:a});
             Dis2=subs(W2,{N0,x},{MemN0(i,num),a+.01:0.01:1});
             Gama1=subs(gama1,{N0,x},{MemN0(i,num),0:.01:a});
             Gama2=subs(gama2,{N0,x},{MemN0(i,num),a+.01:0.01:1});
             Phi1=subs(phi1,{N0,x},{MemN0(i,num),0:.01:a});
             Phi2=subs(phi2,{N0,x},{MemN0(i,num),a+.01:0.01:1});
             W0(i,num)=Dis1(1);
             Dis(i,num,:)=[Dis1,Dis2];
             Gama(i,num,:)=[Gama1,Gama2];
             Phi(i,num,:)=[Phi1,Phi2];
             Energy(i,num)=subs(Eng,MemN0(i,num));
             num=num+1;
         end
     end
     i
 end
totalF=stable(thermal, MemN0);
hh=fzero(hh,[4,40]);%%%% find the critical membrane force.
%% plot the memebrane force WRT the thermal loading.
index=find(abs(MemN0-hh)<5e-2);
criticaltemp=thermal(index);
criticalMemN0=MemN0(index);
for i=1:size(thermal,2)
    for j=1:size(MemN0,2)
        if totalF(i,j)>0
            figure(1)
            plot(thermal(i),MemN0(i,j),'o')
            hold on
```

```
        elseif totalF(i,j)<0
            plot(thermal(i),MemN0(i,j),'.')
            hold on
        end
    end
end
plot(criticaltemp,criticalMemN0,'ro')
text(criticaltemp,criticalMemN0+2,['(',num2str(criticaltemp),',',num2st
r(criticalMemN0),')'],'FontSize',20)
ylabel('Membrane force')
xlabel('Thermal Loading')
h=gcf;
saveas(h,'membrane.fig')

for i=1:size(thermal,2)
    for j=1:size(MemN0,2)
        if totalF(i,j)>0
            figure(2)
            plot(W0(i,j),thermal(i),'o')
            hold on
        elseif totalF(i,j)<0
            plot(W0(i,j),thermal(i),'.')
            hold on
        end
    end
end
plot([-0.15,0.25],[criticaltemp,criticaltemp],'r--')
xlabel('centerspan displacement')
ylabel('Thermal Loading')
h=gcf;
saveas(h,'centerspandisplacement.fig')

for i=1:size(thermal,2)
    for j=1:size(MemN0,2)
        if totalF(i,j)>0
            figure(3)
            plot(thermal(i),Energy(i,j),'o')
            hold on
        elseif totalF(i,j)<0
            plot(thermal(i),Energy(i,j),'.')
            hold on
        end
    end
end
plot([criticaltemp,criticaltemp],[0,0.5],'r--')
ylabel('total energy')
xlabel('Thermal Loading')
h=gcf;
saveas(h,'totalenergy.fig')

for i=1:size(thermal,2)
    for j=1:size(MemN0,2)
        if totalF(i,j)>0
            figure(4)
            plot(thermal(i),totalF(i,j),'o')
            hold on
```

```
        elseif totalF(i,j)<0
            plot(thermal(i),totalF(i,j),'.')
            hold on
        end
    end
end
plot([criticaltemp,criticaltemp],[-400,500],'r--')
ylabel('stability analysis')
xlabel('Thermal Loading')
h=gcf;
saveas(h,'stability.fig')
savefile = 'pqfile06diffshear.mat';
save(savefile)

function
[y1,f,W1,W2,phi1,phi2,gama1,gama2,PE,hh]=withshear6(HB,HP,alpha1,alpha2
,a,thermal,Ninput)
%%%% Ninput is to get the plot with N0=Ninput and draw the relation be-
tween
%%%% N0 and transversality equation. y is the coreesponding value of
the
%%%% transversality condition
%%%% y1 is the value of intergrability equation;
format long
syms x
N0=sym('N0'); %%% DEFINE IT THIS WAY&&&&&&&&
Thermal=thermal*alpha1;
Cb=12/HB^2;
Cp=12*(HP/HB)/(HB^2);
Ct=Cb+Cp;  %%%C*
Bt=(1/2)*HP*Cp-(1/2)*HB*Cb;  %B*
roh=Bt/Ct;
DB=1;
DP=(HP/HB)^3;
D1=DB+DP+Cb*((1/2)*HB)^2+Cp*(HP/2)^2-roh*Bt; %D*
miu=-(HB/2)*Cb+alpha2*(HP/2)*Cp;
nstar=Cb+alpha2*Cp;
mstar=miu-roh*nstar;
kb= .9;
ratio1=1/2.6;
ratio2=1/2.5;
LamdaB= kb*ratio1*Cb;
LamdaP= kb*ratio2*Cp; %%%Here we take shear modulus/youngs modulus==0.1
aa=1-a;
%% define some parameters
m=D1*(1-N0/(LamdaB+LamdaP));
m2=DB*(1-N0/LamdaB);
Kb=sqrt(N0/m);
Kb2=sqrt(N0/m2);
b1=cos(Kb2*aa)*cos(Kb*a);
b2=sin(Kb2*aa)*sin(Kb*a);
LAMDA=sqrt(1+LamdaP/LamdaB)*sqrt(1-LamdaP/(LamdaB+LamdaP-N0));
%% equations for displacement of base and patch
Mlamda=mstar*Thermal+(roh+.5*HB)*N0;
H=D1*Kb2*m2*b1/(DB*Kb*m)-b2;
hh=matlabFunction(H);
```

```
BB=sqrt(D1/DB)*LAMDA;
phi1=((Mlamda*(1-N0/LamdaB)*Kb2)/(N0*H))*cos(Kb2*aa)*sin(Kb*x);
phi2=((Mlamda*(1-N0/LamdaB)*Kb2)/(N0*H))*sin(Kb*a)*cos(Kb2*(1-x));
W1=(Mlamda/(N0*H))*(H-sin(Kb*a)-BB*cos(Kb2*aa)*cos(Kb*x));
W2=-(Mlamda/(N0*H))*sin(Kb*a)*sin(Kb2*(1-x));
gama1=diff(W1,x)-phi1;
gama2=diff(W2,x)-phi2;
a1=0.5*(DB+DP)+Cb*Cp*(HB+HP)^2/Ct/8-D1;
a2=0.5*Cb*Cp*(HB+HP)*(1-alpha2)*Thermal/Ct;
phi1prime=diff(phi1,x);
phi2prime=diff(phi2,x);
intW1square=int(diff(W1,x)^2,x,0, a);
intW2square=int(diff(W2,x)^2,x,a, 1);
Energy=a1*(int(phi1prime^2,x,0,
a))+0.5*(LamdaB+LamdaP)*intW1square+D1*(subs(phi1*phi1prime,x,a))-
.5*(LamdaB+LamdaP)*(int(phi1^2,x,0, a))...
    +a2*(int(phi1prime,x,0, a))+0.5*int((N0^2+Cb*Cp*(1-
alpha2)^2*Thermal^2)/Ct,x,0,a)...
    -0.5*DB*(int(phi2prime^2,x,a,1))+0.5*LamdaB*intW2square-
.5*LamdaB*(int(phi2^2,x,a, 1))+0.5*(int(N0^2/Cb,x,a,1))-
DB*(subs(phi2*phi2prime,x,a));
PE=matlabFunction(Energy);
ff=-N0*(aa/Cb+a/Ct)-(1/2)*intW1square-(1/2)*intW2square-
(.5*HB+roh)*(subs(phi1, a))+(aa+a*nstar/Ct)*Thermal
y1=subs(ff,N0,Ninput);
ff=ff^2;
f=matlabFunction(ff);
W1=matlabFunction(W1);
W2=matlabFunction(W2);
gama1=matlabFunction(gama1);
gama2=matlabFunction(gama2);
phi1=matlabFunction(phi1);
phi2=matlabFunction(phi2);

function stableF=stable(thermal,N0)
%%Caculate F for stability analysis
format long
HB=0.05;HP=0.05; a=0.6;  alpha1=.002; alpha2=.5;
syms x
Cb=12/HB^2;
Cp=12*(HP/HB)/(HB^2);
Ct=Cb+Cp;
Bt=(1/2)*HP*Cp-(1/2)*HB*Cb;
roh=Bt/Ct;
DB=1;
DP=(HP/HB)^3;
D1=DB+DP+Cb*((1/2)*HB)^2+Cp*(HP/2)^2-roh*Bt;
miu=-(HB/2)*Cb+alpha2*(HP/2)*Cp;
nstar=Cb+alpha2*Cp;
mstar=miu-roh*nstar;
kb= .9;
ratio1=1/2.6;
ratio2=1/2.5;
LamdaB= kb*ratio1*Cb;
LamdaP= kb*ratio2*Cp;
```

```
aa=1-a;

m=D1*(1-N0./(LamdaB+LamdaP));
m2=DB*(1-N0./LamdaB);
Kb=sqrt(N0./m);
Kb2=sqrt(N0./m2);
A2=-sqrt(D1/DB)*cos(Kb2*aa);
B0=sin(Kb*a);
b1=cos(Kb2*aa).*cos(Kb*a);
b2=sin(Kb2*aa).*sin(Kb*a);
H=D1.*Kb2.*m2.*b1./(DB.*Kb.*m)-b2;
stableF=.25*(1-N0./LamdaB).*((A2./H).*(A2./H).*sin(2*Kb*a).*Kb-
(B0./H).*(B0./H).*sin(2*Kb2*aa).*Kb2);
clear
Ninput=.1:.01:50;
thermal=.1:.1:14;
syms x
W0=[];
MemN0=[];
Energy=[];
matlabpool(2)
s=size(Ninput,2);
tic
y=[];
parfor i=1:size(thermal,2)
  for j=1:s
    y(i,j)=abc3(thermal(i),Ninput(j));
%     y2=[thermal(i),y(i,j)];
  end
   i
end
toc
for i=1:size(y,1)
   plot(y(i,:))
   axis([0 320 -0.1 0.1])
   grid on
   pause(0.2)
end
 N0=Ninput;
 for i=1:size(thermal,2)
  num=1;
    for j=1:size(y,2)-1
         if y(i,j)*y(i,j+1)<0
             MemN0(i,num)=(N0(j)+N0(j+1))/2;
             num=num+1;
         end
   end
 end

  for i=1:size(thermal,2)
  for j=1:size(MemN0,2)
      if MemN0(i,j)~=0
       [Ener-
gy(i,j),W0(i,j),totalF(i,j),P1(i,j),P2(i,j)]=WB03(thermal(i),MemN0(i,j)
);
        i
```

```
      end
  end
  end
matlabpool close

totalF=double(totalF);
for i=1:size(thermal,2)
    for j=1:size(MemN0,2)
        if totalF(i,j)>0
            figure(1)
            plot(thermal(i),MemN0(i,j),'o')
            hold on
        elseif totalF(i,j)<0
            plot(thermal(i),MemN0(i,j),'.')
            hold on
        end
    end
end
ylabel('Membrane force')
xlabel('Thermal Loading')
h=gcf;
saveas(h,'membrane.fig')

for i=1:size(thermal,2)
    for j=1:size(MemN0,2)
        if totalF(i,j)>0
            figure(2)
            plot(W0(i,j),thermal(i),'o')
            hold on
        elseif totalF(i,j)<0
            plot(W0(i,j),thermal(i),'.')
            hold on
        end
    end
end
xlabel('centerspan displacement')
ylabel('Thermal Loading')
h=gcf;
saveas(h,'centerspandisplacement.fig')
for i=1:size(thermal,2)
    for j=1:size(MemN0,2)
        if totalF(i,j)>0
            figure(3)
            plot(thermal(i),Energy(i,j),'o')
            hold on
        elseif totalF(i,j)<0
            plot(thermal(i),Energy(i,j),'.')
            hold on
        end
    end
end
ylabel('total energy')
xlabel('Thermal Loading')
h=gcf;
saveas(h,'totalenergy.fig')
```

```
for i=1:size(thermal,2)
    for j=1:size(MemN0,2)
        if totalF(i,j)>0
            figure(4)
            plot(thermal(i),totalF(i,j),'o')
            hold on
        elseif totalF(i,j)<0
            plot(thermal(i),totalF(i,j),'.')
            hold on
        end
    end
end
ylabel('stability analysis')
xlabel('Thermal Loading')
h=gcf;
saveas(h,'stability.fig')

savefile = 'pqfile06.mat';
save(savefile)



function y1=abc3(thermal,N0)
%Full contact case for hinged fixed support condition
%Different shear modulus included
format long
 HB=0.05;HP=0.05; a=0.6;  alpha11=.002; alpha22=.5; b=0.9; Lp=b;
syms x
Thermal=thermal*alpha11;
Cb=12/HB^2;
Cp=12*(HP/HB)/(HB^2);
Ct=Cb+Cp;
Bt=(1/2)*HP*Cp-(1/2)*HB*Cb;
roh=Bt/Ct;
DB=1;
DP=(HP/HB)^3;
D1=DB+DP+Cb*((1/2)*HB)^2+Cp*(HP/2)^2-roh*Bt;
DC=DB+DP;
miu=-(HB/2)*Cb+alpha22*(HP/2)*Cp;
nstar=Cb+alpha22*Cp;
mstar=miu-roh*nstar;
kb= .9;
ratio=1/2.6;
ratio1=1/2.5;
LamdaB= kb*ratio*Cb;
LamdaP= kb*ratio1*Cp;
aa=1-a;
bb=1-b;
%% define some parameters
m1=D1*(1-N0/(LamdaB+LamdaP));
m2=DC*(1-N0/(LamdaB+LamdaP));
m3=DB*(1-N0/LamdaB);
Kb=sqrt(N0/m1);
Kb3=sqrt(N0/m3);
bb1=-(DB+DP-N0*(DB/LamdaB+DP/LamdaP));
aa1=DB*DP/LamdaB/LamdaP*(LamdaB+LamdaP-N0);
```

```
delta=bb1^2+4*aa1*N0;
alpha1=sqrt((-bb1+sqrt(delta))/aa1/2);
beta1=sqrt((+bb1+sqrt(delta))/aa1/2);
P1=(1-DB*alpha1^2/LamdaB)/(1-DP*alpha1^2/LamdaP);
P2=(1+DB*beta1^2/LamdaB)/(1+DP*beta1^2/LamdaP);
%% equations for displacement of base and patch
Mlamda=mstar*Thermal+(roh+.5*HB)*N0;
Com1=cosh(alpha1*(b-a));
H_11=((1-P2)*(sin(beta1*a)*cosh(alpha1*b))/(P1-
1)+P2*beta1*(sinh(alpha1*a)*cos(beta1*b))/P1/alpha1)/Com1;
H_12=((1-P2)*(cos(beta1*a)*cosh(alpha1*b))/(P1-1)-
P2*beta1*(sinh(alpha1*a)*sin(beta1*b))/P1/alpha1)/Com1;
H_21=-((1-P2)*(sinh(alpha1*b)*sin(beta1*a))/(P1-
1)+P2*beta1*(cosh(alpha1*a)*cos(beta1*b))/P1/alpha1)/Com1;
H_22=-((1-P2)*(sinh(alpha1*b)*cos(beta1*a))/(P1-1)-
P2*beta1*(cosh(alpha1*a)*sin(beta1*b))/P1/alpha1)/Com1;
JJ1=(m3+DP*P1)*alpha1^2;
JJ2=(m3+DP*P2)*beta1^2;

PR1=(1-P2/P1)*beta1*cos(Kb3*bb);
PR2=Kb3*sin(Kb3*bb);
PR3=P2*beta1/P1/alpha1*sinh(alpha1*(b-a));

H1=(N0*PR1*cos(beta1*b)-JJ2*PR2*sin(beta1*b))*Com1-JJ1*PR2*((1-
P2)*sin(beta1*a)/(P1-1)-PR3*cos(beta1*b));
H2=-(N0*PR1*sin(beta1*b)+JJ2*PR2*cos(beta1*b))*Com1-JJ1*PR2*((1-
P2)*cos(beta1*a)/(P1-1)+PR3*sin(beta1*b));
PR0=H2/H1;

C21=H_22-PR0*H_21;
C20=H_12-PR0*H_11;
PR6=sin(beta1*a)+cos(beta1*a)*PR0;
PR7=cosh(alpha1*a)*C21+sinh(alpha1*a)*C20;
PR8=C20*cosh(alpha1*b)+C21*sinh(alpha1*b);
PR9=cos(beta1*b)-PR0*sin(beta1*b);
PR10=sin(beta1*b)+PR0*cos(beta1*b);
PR11=cos(beta1*a)-PR0*sin(beta1*a);
H3=-(JJ1*(1-P2)/(P1-1)-JJ2+(P1-P2)*N0/(P1-1))*PR11/N0;
H4=(P2/P1-
1)*beta1*(PR0*cos(beta1*b)+sin(beta1*b))*cos(Kb3)/Kb3/sin(Kb3*bb);
H5=-((1-P2)/(P1-1)*JJ1-JJ2)*PR11/N0/sin(Kb*a);
H6=D1*Kb*cos(Kb*a)*H5-(DB+DP*P1)*alpha1*PR7+(DB+DP*P2)*beta1*PR6;
H8=PR8+PR9+H3-H4*cos(Kb3*bb)/cos(Kb3);
MM=Mlamda/H6;
jj1=(1-DB*alpha1^2/LamdaB);
jj2=(1+DB*beta1^2/LamdaB);
phi1=H5*sin(Kb*x)*MM;
%% define the energy equation
wb2prime=MM*((1-
DB*alpha1^2/LamdaB)*(cosh(alpha1*x)*C20+sinh(alpha1*x)*C21)+(1+DB*beta1
^2/LamdaB)*(-sin(beta1*x)*PR0+cos(beta1*x))+H3);
wb2primesquare=(H3 + jj2*(cos(beta1*x) - PR0*sin(beta1*x)) +
jj1*(C20*cosh(alpha1*x) + C21*sinh(alpha1*x)))^2;

intW1square=MM^2*((LamdaB+LamdaP)*H5/(LamdaB+LamdaP-N0))^2*(0.5*a-
sin(2*Kb*a)/4/Kb);
```

```
intW2square=MM^2*(.5*(b-a)*(jj1^2*(C20^2-
C21^2)+jj2^2*(1+PR0^2)+2*H3^2)+jj1^2*(1/4/alpha1)*((C20^2+C21^2)*(sinh(
2*alpha1*b)-sinh(2*alpha1*a))+2*C20*C21*(cosh(2*alpha1*b)-
cosh(2*alpha1*a)))...
                   +jj2^2*(1/4/beta1)*((1-PR0^2)*(sin(2*beta1*b)-
sin(2*beta1*a))+2*PR0*(cos(2*beta1*b)-cos(2*beta1*a)))...

+2*jj1*jj2/(alpha1^2+beta1^2)*(alpha1*(C20*sinh(alpha1*b)+C21*cosh(alph
a1*b))*(cos(beta1*b)-PR0*sin(beta1*b))...
                   -
alpha1*(C20*sinh(alpha1*a)+C21*cosh(alpha1*a))*(cos(beta1*a)-
PR0*sin(beta1*a))...

+beta1*(C20*cosh(alpha1*b)+C21*sinh(alpha1*b))*(sin(beta1*b)+PR0*cos(be
ta1*b))...
                   -
be-
ta1*(C20*cosh(alpha1*a)+C21*sinh(alpha1*a))*(sin(beta1*a)+PR0*cos(beta1
*a)))...
                   +2*H3*jj1/alpha1*(C20*(sinh(alpha1*b)-
sinh(alpha1*a))+C21*(cosh(alpha1*b)-cosh(alpha1*a)))...
                   +2*H3*jj2/beta1*(PR0*(cos(beta1*b)-
cos(beta1*a))+sin(beta1*b)-sin(beta1*a)));

intW3square=MM^2*(H8^2*(1-Lp)+((LamdaB/(LamdaB-N0))*H4/cos(Kb3))^2*((1-
Lp)/2+sin(2*Kb3*(1-Lp))/4/Kb3)+2*(LamdaB/(LamdaB-N0))*H4*H8*sin(Kb3*(1-
Lp))/cos(Kb3)/Kb3);

ff=-N0*(aa/Cb+a/Ct)-(1/2)*intW1square-(1/2)*intW2square-
(1/2)*intW3square-(.5*HB+roh)*(subs(phi1, a))+(aa+a*nstar/Ct)*Thermal;
y1=ff;

function [Eng,W0,totalF,P1,P2]=WB03(thermal,N0)
format long
HB=0.05;HP=0.05; a=0.6;  alpha11=.002; alpha22=.5; b=0.9; Lp=b;
syms x
Thermal=thermal*alpha11;
Cb=12/HB^2;
Cp=12*(HP/HB)/(HB^2);
Ct=Cb+Cp;
Bt=(1/2)*HP*Cp-(1/2)*HB*Cb;
roh=Bt/Ct;
DB=1;
DP=(HP/HB)^3;
D1=DB+DP+Cb*((1/2)*HB)^2+Cp*(HP/2)^2-roh*Bt;
DC=DB+DP;
miu=-(HB/2)*Cb+alpha22*(HP/2)*Cp;
nstar=Cb+alpha22*Cp;
mstar=miu-roh*nstar;
kb= .9;
ratio=1/2.6;
ratio1=1/2.5;
LamdaB= kb*ratio*Cb;
LamdaP= kb*ratio1*Cp;

aa=1-a;
```

```
bb=1-b;

m1=D1*(1-N0/(LamdaB+LamdaP));
m2=DC*(1-N0/(LamdaB+LamdaP));
m3=DB*(1-N0/LamdaB);
Kb=sqrt(N0/m1);
Kb3=sqrt(N0/m3);
bb1=-(DB+DP-N0*(DB/LamdaB+DP/LamdaP));
aa1=DB*DP/LamdaB/LamdaP*(LamdaB+LamdaP-N0);
delta=bb1^2+4*aa1*N0;
alpha1=sqrt((-bb1+sqrt(delta))/aa1/2);
beta1=sqrt((+bb1+sqrt(delta))/aa1/2);

P1=-.999998;%(1-DB*alpha1^2/LamdaB)/(1-DP*alpha1^2/LamdaP);
P2=1.00002;%(1+DB*beta1^2/LamdaB)/(1+DP*beta1^2/LamdaP);
Mlamda=mstar*Thermal+(roh+.5*HB)*N0;
Com1=cosh(alpha1*(b-a));

H_11=((1-P2)*(sin(beta1*a)*cosh(alpha1*b))/(P1-
1)+P2*beta1*(sinh(alpha1*a)*cos(beta1*b))/P1/alpha1)/Com1;
H_12=((1-P2)*(cos(beta1*a)*cosh(alpha1*b))/(P1-1)-
P2*beta1*(sinh(alpha1*a)*sin(beta1*b))/P1/alpha1)/Com1;
H_21=-((1-P2)*(sinh(alpha1*b)*sin(beta1*a))/(P1-
1)+P2*beta1*(cosh(alpha1*a)*cos(beta1*b))/P1/alpha1)/Com1;
H_22=-((1-P2)*(sinh(alpha1*b)*cos(beta1*a))/(P1-1)-
P2*beta1*(cosh(alpha1*a)*sin(beta1*b))/P1/alpha1)/Com1;
JJ1=(m3+DP*P1)*alpha1^2;
JJ2=(m3+DP*P2)*beta1^2;

PR1=(1-P2/P1)*beta1*cos(Kb3*bb);
PR2=Kb3*sin(Kb3*bb);
PR3=P2*beta1/P1/alpha1*sinh(alpha1*(b-a));

H1=(N0*PR1*cos(beta1*b)-JJ2*PR2*sin(beta1*b))*Com1-JJ1*PR2*((1-
P2)*sin(beta1*a)/(P1-1)-PR3*cos(beta1*b));
H2=-(N0*PR1*sin(beta1*b)+JJ2*PR2*cos(beta1*b))*Com1-JJ1*PR2*((1-
P2)*cos(beta1*a)/(P1-1)+PR3*sin(beta1*b));
PR0=H2/H1;

C21=H_22-PR0*H_21;
C20=H_12-PR0*H_11;
PR6=sin(beta1*a)+cos(beta1*a)*PR0;
PR7=cosh(alpha1*a)*C21+sinh(alpha1*a)*C20;
PR8=C20*cosh(alpha1*b)+C21*sinh(alpha1*b);
PR9=cos(beta1*b)-PR0*sin(beta1*b);
PR10=sin(beta1*b)+PR0*cos(beta1*b);
PR11=cos(beta1*a)-PR0*sin(beta1*a);
H3=-(JJ1*(1-P2)/(P1-1)-JJ2+(P1-P2)*N0/(P1-1))*PR11/N0;
H4=(P2/P1-
1)*beta1*(PR0*cos(beta1*b)+sin(beta1*b))*cos(Kb3)/Kb3/sin(Kb3*bb);
H5=-((1-P2)/(P1-1)*JJ1-JJ2)*PR11/N0/sin(Kb*a);
H6=D1*Kb*cos(Kb*a)*H5-(DB+DP*P1)*alpha1*PR7+(DB+DP*P2)*beta1*PR6;
H8=PR8+PR9+H3-H4*cos(Kb3*bb)/cos(Kb3);
PR12=sinh(alpha1*b)*H_12+cosh(alpha1*b)*H_22-
PR0*(sinh(alpha1*b)*H_11+cosh(alpha1*b)*H_21);
PR13=sin(beta1*b)+cos(beta1*b)*PR0;
```

```
C13=(Mlamda*H5/H6)*((1-DB*alpha1^2/LamdaB)*(PR7-
PR12)/alpha1/H5+(1+DB*beta1^2/LamdaB)*(PR6-PR13)/beta1/H5+H3*(a-
b)/H5+...
    (LamdaB+LamdaP)*cos(Kb*a)/Kb/(LamdaB+LamdaP-N0)-
LamdaB*H4*sin(Kb3*bb)/cos(Kb3)/Kb3/(LamdaB-N0)/H5-H8*bb/H5);

phi1=H5*sin(Kb*x)*(Mlamda/H6);
phib2=(cosh(alpha1*x)*H_12+sinh(alpha1*x)*H_22-
PR0*(cosh(alpha1*x)*H_11+sinh(alpha1*x)*H_21)+cos(beta1*x)-
PR0*sin(beta1*x)+H3)*(Mlamda/H6);
phip2=(P1*(cosh(alpha1*x)*H_12+sinh(alpha1*x)*H_22-
PR0*(cosh(alpha1*x)*H_11+sinh(alpha1*x)*H_21))+P2*(cos(beta1*x)-
PR0*sin(beta1*x))+H3)*(Mlamda/H6);
phib3=(H8+H4*cos(Kb3*bb)/cos(Kb3))*(Mlamda/H6);
phi1prime=diff(phi1,x);
phib2prime=diff(phib2,x);
phip2prime=diff(phip2,x);
phib3prime=diff(phib3,x);

phi1doubleprime=diff(phi1,x,2);
phib2doubleprime=diff(phib2,x,2);
phip2doubleprime=diff(phip2,x,2);
phib3doubleprime=diff(phib3,x,2);
MM=Mlamda/H6;
intphib1primesquare=(MM*H5*Kb)^2*(0.5*a+sin(2*Kb*a)/4/Kb);
intphib3primesquare=(MM*H4*Kb3/cos(Kb3))^2*(0.5*bb-sin(2*Kb3*bb)/4/Kb3);
intphib1doubleprimesquare=(MM*H5*Kb^2)^2*(0.5*a-sin(2*Kb*a)/4/Kb);
intphib3doubleprimesquare=(MM*H4*Kb3^2/cos(Kb3))^2*(0.5*bb+sin(2*Kb3*bb
)/4/Kb3);
C21=H_22-PR0*H_21;
C20=H_12-PR0*H_11;
jj1=alpha1^2;
jj2=-beta1^2;
H3=0;
intphib2doubleprimesquare=MM^2*(.5*(b-a)*(jj1^2*(C20^2-
C21^2)+jj2^2*(1+PR0^2)+2*H3^2)+jj1^2*(1/4/alpha1)*((C20^2+C21^2)*(sinh(
2*alpha1*b)-sinh(2*alpha1*a))+2*C20*C21*(cosh(2*alpha1*b)-
cosh(2*alpha1*a)))...
                   +jj2^2*(1/4/beta1)*((1-PR0^2)*(sin(2*beta1*b)-
sin(2*beta1*a))+2*PR0*(cos(2*beta1*b)-cos(2*beta1*a)))...

+2*jj1*jj2/(alpha1^2+beta1^2)*(alpha1*(C20*sinh(alpha1*b)+C21*cosh(alph
a1*b))*(cos(beta1*b)-PR0*sin(beta1*b))...
                   -
alpha1*(C20*sinh(alpha1*a)+C21*cosh(alpha1*a))*(cos(beta1*a)-
PR0*sin(beta1*a))...

+beta1*(C20*cosh(alpha1*b)+C21*sinh(alpha1*b))*(sin(beta1*b)+PR0*cos(be
ta1*b))...
                   -
be-
ta1*(C20*cosh(alpha1*a)+C21*sinh(alpha1*a))*(sin(beta1*a)+PR0*cos(beta1
*a)))...
                   +2*H3*jj1/alpha1*(C20*(sinh(alpha1*b)-
sinh(alpha1*a))+C21*(cosh(alpha1*b)-cosh(alpha1*a)))...
```

```
                    +2*H3*jj2/beta1*(PR0*(cos(beta1*b)-
cos(beta1*a))+sin(beta1*b)-sin(beta1*a)));
jj1=P1*alpha1^2;
jj2=-P2*beta1^2;
H3=0;
intphip2doubleprimesquare=MM^2*(.5*(b-a)*(jj1^2*(C20^2-
C21^2)+jj2^2*(1+PR0^2)+2*H3^2)+jj1^2*(1/4/alpha1)*((C20^2+C21^2)*(sinh(
2*alpha1*b)-sinh(2*alpha1*a))+2*C20*C21*(cosh(2*alpha1*b)-
cosh(2*alpha1*a)))...
                    +jj2^2*(1/4/beta1)*((1-PR0^2)*(sin(2*beta1*b)-
sin(2*beta1*a))+2*PR0*(cos(2*beta1*b)-cos(2*beta1*a)))...

+2*jj1*jj2/(alpha1^2+beta1^2)*(alpha1*(C20*sinh(alpha1*b)+C21*cosh(alph
a1*b))*(cos(beta1*b)-PR0*sin(beta1*b))...
                    -
alpha1*(C20*sinh(alpha1*a)+C21*cosh(alpha1*a))*(cos(beta1*a)-
PR0*sin(beta1*a))...

+beta1*(C20*cosh(alpha1*b)+C21*sinh(alpha1*b))*(sin(beta1*b)+PR0*cos(be
ta1*b))...
                    -
be-
ta1*(C20*cosh(alpha1*a)+C21*sinh(alpha1*a))*(sin(beta1*a)+PR0*cos(beta1
*a)))...
                    +2*H3*jj1/alpha1*(C20*(sinh(alpha1*b)-
sinh(alpha1*a))+C21*(cosh(alpha1*b)-cosh(alpha1*a)))...
                    +2*H3*jj2/beta1*(PR0*(cos(beta1*b)-
cos(beta1*a))+sin(beta1*b)-sin(beta1*a)));
jj1=alpha1;
jj2=beta1;
intphib2primesquare=MM^2*(jj1^2*(.5*(b-a)*(C21^2-
C20^2)+(1/4/alpha1)*((C20^2+C21^2)*(sinh(2*alpha1*b)-
sinh(2*alpha1*a))+2*C20*C21*(cosh(2*alpha1*b)-cosh(2*alpha1*a))))...
                       +jj2^2*(1/4/beta1)*((PR0^2-1)*(sin(2*beta1*b)-
sin(2*beta1*a))+2*PR0*(cos(2*beta1*b)-cos(2*beta1*a)))+jj2^2*.5*(b-
a)*(1+PR0^2)...
                      -
2*jj1*jj2/(alpha1^2+beta1^2)*(beta1*(C20*sinh(alpha1*b)+C21*cosh(alpha1
*b))*(cos(beta1*b)-PR0*sin(beta1*b))...

+beta1*(C20*sinh(alpha1*a)+C21*cosh(alpha1*a))*(cos(beta1*a)-
PR0*sin(beta1*a))...

+alpha1*(C20*cosh(alpha1*b)+C21*sinh(alpha1*b))*(sin(beta1*b)+PR0*cos(b
eta1*b))...
                    -
al-
pha1*(C20*cosh(alpha1*a)+C21*sinh(alpha1*a))*(sin(beta1*a)+PR0*cos(beta
1*a))));

jj1=P1*alpha1;
jj2=P2*beta1;
intphip2primesquare=MM^2*(jj1^2*(.5*(b-a)*(C21^2-
C20^2)+(1/4/alpha1)*((C20^2+C21^2)*(sinh(2*alpha1*b)-
sinh(2*alpha1*a))+2*C20*C21*(cosh(2*alpha1*b)-cosh(2*alpha1*a))))...
```

```
                      +jj2^2*(1/4/beta1)*((PR0^2-1)*(sin(2*beta1*b)-
sin(2*beta1*a))+2*PR0*(cos(2*beta1*b)-cos(2*beta1*a)))+jj2^2*.5*(b-
a)*(1+PR0^2)...
                    -
2*jj1*jj2/(alpha1^2+beta1^2)*(beta1*(C20*sinh(alpha1*b)+C21*cosh(alpha1
*b))*(cos(beta1*b)-PR0*sin(beta1*b))...

+beta1*(C20*sinh(alpha1*a)+C21*cosh(alpha1*a))*(cos(beta1*a)-
PR0*sin(beta1*a))...

+alpha1*(C20*cosh(alpha1*b)+C21*sinh(alpha1*b))*(sin(beta1*b)+PR0*cos(b
eta1*b))...
                   -
al-
pha1*(C20*cosh(alpha1*a)+C21*sinh(alpha1*a))*(sin(beta1*a)+PR0*cos(beta
1*a))));

a1=0.5*(DB+DP)+Cb*Cp*(HB+HP)^2/Ct/8;
a2=0.5*Cb*Cp*(HB+HP)*(1-alpha22)*Thermal/Ct;
%  Eng=1;
Eng=a1*intphib1primesquare+.5*D1^2/(LamdaB+LamdaP)*intphib1doubleprimes
quare...
    +a2*(subs(phi1,a))+0.5*((N0^2+Cb*Cp*(1-
alpha22)^2*Thermal^2)/Ct)*a...

+0.5*DB*intphib2primesquare+.5*DB^2/(LamdaB)*intphib2doubleprimesquare.
..

+0.5*DP*intphip2primesquare+.5*DP^2/(LamdaP)*intphip2doubleprimesquare.
..

+0.5*DB*intphib3primesquare+.5*DB^2/(LamdaB)*intphib3doubleprimesquare+
0.5*(N0^2/Cb)*aa;
jj1=(1-DB*alpha1^2/LamdaB);
jj2=(1+DB*beta1^2/LamdaB);
intW2square=MM^2*(.5*(b-a)*(jj1^2*(C20^2-
C21^2)+jj2^2*(1+PR0^2)+2*H3^2)+jj1^2*(1/4/alpha1)*((C20^2+C21^2)*(sinh(
2*alpha1*b)-sinh(2*alpha1*a))+2*C20*C21*(cosh(2*alpha1*b)-
cosh(2*alpha1*a)))...
                   +jj2^2*(1/4/beta1)*((1-PR0^2)*(sin(2*beta1*b)-
sin(2*beta1*a))+2*PR0*(cos(2*beta1*b)-cos(2*beta1*a)))...

+2*jj1*jj2/(alpha1^2+beta1^2)*(alpha1*(C20*sinh(alpha1*b)+C21*cosh(alph
a1*b))*(cos(beta1*b)-PR0*sin(beta1*b))...
                   -
alpha1*(C20*sinh(alpha1*a)+C21*cosh(alpha1*a))*(cos(beta1*a)-
PR0*sin(beta1*a))...

+beta1*(C20*cosh(alpha1*b)+C21*sinh(alpha1*b))*(sin(beta1*b)+PR0*cos(be
ta1*b))...
                   -
be-
ta1*(C20*cosh(alpha1*a)+C21*sinh(alpha1*a))*(sin(beta1*a)+PR0*cos(beta1
*a)))...
                   +2*H3*jj1/alpha1*(C20*(sinh(alpha1*b)-
sinh(alpha1*a))+C21*(cosh(alpha1*b)-cosh(alpha1*a)))...
```

```
                   +2*H3*jj2/beta1*(PR0*(cos(beta1*b)-
cos(beta1*a))+sin(beta1*b)-sin(beta1*a)));
wb2prime=MM*((1-
DB*alpha1^2/LamdaB)*(cosh(alpha1*x)*C20+sinh(alpha1*x)*C21)+(1+DB*beta1
^2/LamdaB)*(-sin(beta1*x)*PR0+cos(beta1*x))+H3);
H3=-(jj1*(1-P2)/(P1-1)-jj2+(P1-P2)*N0/(P1-1))*PR11/N0;

F1=(H5/H6)^2*D1*Kb/2*sin(2*Kb*a);
F2=(LamdaB+LamdaP-N0)*(DB/LamdaB)^2*intphip2doubleprimesquare-
2*(DB/LamdaB)*(LamdaP-
N0)*int(phib2*phib2doubleprime,a,b)+2*DP*int(phip2*phip2doubleprime,a,b
)+(LamdaP-N0)*int(phib2^2,a,b)-
LamdaP*int(phip2^2,a,b)+DB*intphib2primesquare+DP*intphip2primesquare;
F3=-N0*LamdaB/(LamdaB-N0)*(H4/H6)^2*sin(2*Kb3*bb)/cos(Kb3)^2/Kb3/2-
N0*(H8/H6)^2*bb-
2*N0*(H4*H8/H6^2)*sin(Kb3*bb)/cos(Kb3)/Kb3*(1+LamdaB/(LamdaB-N0));
totalF=F1+F3+F2;
W0=-(Mlamda/H6)*(LamdaB+LamdaP)*H5/Kb/(LamdaB+LamdaP-N0)+C13;
```

For clamped fixed edge support

```
%Generate the transverse displacements and total energy profile for the
intact case with no shear deformation is included
clear
HB=0.05;HP=0.05; a=0.6;  alpha1=.002; alpha2=.5;
%HB HP are the thickness of the base and the patch, a is the bond zone
size
thermal=.1:0.1:14;
syms x
N0=sym('N0');
Ninput=[0:.05:160];
yy=[];MemN0=[];Dis1=[];Dis2=[];Dis=[];W0=[];Energy=[];
 k=1;
 for i=1:size(thermal,2)
     tic

[yy(i,:),f,W1,W2,Eng,hh,phi1,phi2]=noshear2(HB,HP,alpha1,alpha2,a,therm
al(i),Ninput);
     num=1;
     for j=1:size(yy,2)-1
         if yy(i,j)*yy(i,j+1)<0
             MemN0(i,num)=fminsearch(f,Ninput(j),optimset('TolX',1e-4));
             Dis1=subs(W1,{N0,x},{MemN0(i,num),0:.01:a});
             Dis2=subs(W2,{N0,x},{MemN0(i,num),a+.01:0.01:1});
             W0(i,num)=Dis1(1);
             Dis(i,num,:)=[Dis1,Dis2];
             Phi1=subs(phi1,{N0,x},{MemN0(i,num),0:.01:a});
             Phi2=subs(phi2,{N0,x},{MemN0(i,num),a+.01:0.01:1});
             Phi(i,num,:)=[Phi1,Phi2];
              Energy(i,num)=subs(Eng,MemN0(i,num));
             num=num+1;
         end
     end
     i
```

```
     toc
 end
totalF=stable(thermal, MemN0);
%
%% plot the memebrane force WRT the thermal loading.
hh=fzero(hh,[4,40]);%%%% find the critical membrane force.
index=find(abs(MemN0-hh)<3.4452e-2)%3.7e-2);
criticaltemp=thermal(index);
criticalMemN0=MemN0(index);
for i=1:size(thermal,2)
    for j=1:size(MemN0,2)
        if totalF(i,j)>0
            figure(1)
            plot(thermal(i),MemN0(i,j),'ro')
            hold on
        elseif totalF(i,j)<0
            plot(thermal(i),MemN0(i,j),'.')
            hold on
        end
    end
end
 plot(criticaltemp,criticalMemN0,'ro')
 text(criticaltemp-
1,criticalMemN0+8,['(',num2str(criticaltemp),',',num2str(criticalMemN0)
,')'],'FontSize',15)
ylabel('Membrane force')
xlabel('Thermal Loading')
axis([0 14 0 160])
h=gcf;
saveas(h,'membrane.fig')

for i=1:size(thermal,2)
    for j=1:size(MemN0,2)
        if totalF(i,j)>0
            figure(2)
            plot(W0(i,j),thermal(i),'ro')
            hold on
        elseif totalF(i,j)<0
            plot(W0(i,j),thermal(i),'.')
            hold on
        end
    end
end
plot([-0.15,0.25],[criticaltemp,criticaltemp],'r--')
xlabel('centerspan displacement')
ylabel('Thermal Loading')
axis([-0.15 0.25 0 14])
h=gcf;
saveas(h,'centerspandisplacement.fig')

for i=1:size(thermal,2)
    for j=1:size(MemN0,2)
        if totalF(i,j)>0
            figure(3)
            plot(thermal(i),Energy(i,j),'ro')
            hold on
```

```
        elseif totalF(i,j)<0
            plot(thermal(i),Energy(i,j),'.')
            hold on
        end
    end
end
plot([criticaltemp,criticaltemp],[0,0.5],'r--')
ylabel('total energy')
xlabel('Thermal Loading')
axis([0 14 0 2.5])
h=gcf;
saveas(h,'totalenergy.fig')
for i=1:size(thermal,2)
    for j=1:size(MemN0,2)
        if totalF(i,j)>0
            figure(4)
            plot(thermal(i),totalF(i,j),'ro')
            hold on
        elseif totalF(i,j)<0
            plot(thermal(i),totalF(i,j),'.')
            hold on
        end
    end
end
plot([criticaltemp,criticaltemp],[-400,500],'p--')
ylabel('stability analysis')
xlabel('Thermal Loading')
axis([0 14 -60 80])
h=gcf;
saveas(h,'stability.fig')
savefile = 'pqfile06.mat';
save(savefile)

function
[y1,f,W1,W2,Eng,hh,phi1,phi2]=noshear2(HB,HP,alpha1,alpha2,a,thermal,Ni
nput)
%%%% Ninput is to get the plot with N0=Ninput and draw the relation be-
tween
%%%% N0 and transversality equation. y is the coreesponding value of
the
%%%% trans-equation
format long
syms x  C1  C3 C4 C5  C7 C8 C2 C6
N0=sym('N0'); %%% DEFINE IT THIS WAY&&&&&&&&
Thermal=thermal*alpha1;
Cb=12/HB^2;
Cp=12*(HP/HB)/(HB^2);
Ct=Cb+Cp;  Bt=(1/2)*HP*Cp-(1/2)*HB*Cb;  roh=Bt/Ct;
DB=1;
DP=(HP/HB)^3;
D1=DB+DP+Cb*((1/2)*HB)^2+Cp*(HP/2)^2-roh*Bt;
K1=sqrt(N0/DB);
K2=sqrt(N0/D1);
miu=-(HB/2)*Cb+alpha2*(HP/2)*Cp;
n=Cb+alpha2*Cp;
m=miu-roh*n;
aa=1-a;
```

```
% equations for displacement of base and patch
H=sin(K2*a)*cos(K1*aa)+sqrt(D1/DB)*cos(K2*a)*sin(K1*aa);

hh=matlabFunction(H);
Mlamda=m*Thermal+(roh+.5*HB)*N0;
W1=(Mlamda/(N0*H))*(H-sin(K2*a)-sqrt(D1/DB)*sin(K1*aa)*cos(K2*x));
W2=-(Mlamda/(N0*H))*sin(K2*a)*(1-cos(K1*(1-x)));
phi1=diff(W1,x);
phi2=diff(W2,x);
a1=-N0/Ct; a2=roh+.5*HB; a3=(n/Ct-1)*Thermal;a4=DB+DP;
b2=roh-.5*HP; b3=(n/Ct-alpha2)*Thermal;
mm1=Cb*a2^2+Cp*b2^2+a4; mm2=-2*Cb*a2*(a1+a3)-2*Cp*b2*(a1+b3);
mm3=Cb*(a1+a3)^2+Cp*(a1+b3)^2;

ff=-N0*(aa/Cb+a/Ct)-(1/2)*(int(diff(W1, x)^2,x,0, a))-
(1/2)*(int(diff(W2, x)^2,x,a, 1))-(.5*HB+roh)*(subs(phi1,
a))+(aa+a*n/Ct)*Thermal;
Energy=(1/2)*mm1*(int(diff(W1,x,2)^2,x,0,
a))+(1/2)*mm2*(int(diff(W1,x,2),x,0,
a))+(1/2)*a*mm3+(1/2)*DB*(int(diff(W2,  x,2)^2,x,a,  1))+(1/2)*N0^2*aa/Cb;
y1=subs(ff,N0,Ninput);
ff=ff^2;
f=matlabFunction(ff);
W1=matlabFunction(W1);
W2=matlabFunction(W2);
phi1=matlabFunction(phi1);
phi2=matlabFunction(phi2);
Eng=matlabFunction(Energy);

function stableF=stable(thermal,MemN0)
%%Caculate F for stability analysis
format long
HB=0.05;HP=0.05; a=0.6;  alpha1=.002; alpha2=.5;
syms x
N0=MemN0;
Cb=12/HB^2;
Cp=12*(HP/HB)/(HB^2);
Ct=Cb+Cp;  Bt=(1/2)*HP*Cp-(1/2)*HB*Cb;  roh=Bt/Ct;
DB=1;
DP=(HP/HB)^3;
D1=DB+DP+Cb*((1/2)*HB)^2+Cp*(HP/2)^2-roh*Bt; K1=sqrt(N0/DB);
K2=sqrt(N0/D1);  miu=-(HB/2)*Cb+alpha2*(HP/2)*Cp;
n=Cb+alpha2*Cp;
m=miu-roh*n;
aa=1-a;
H=sin(K2*a).*cos(K1*aa)+sqrt(D1/DB)*cos(K2*a).*sin(K1*aa);
A2=-sqrt(D1/DB)*sin(K1*aa);
B0=sin(K2*a);
stableF=.25*((A2./H).*(A2./H).*sin(2*K2*a).*K2+(B0./H).*(B0./H).*sin(2*
K1*aa).*K1);
```

Case 1 Equal shear stiffness

```
%% For same shear stiffnesses for the base and the patch
%% Full contact configuration
clear
Ninput=.1:.01:80;
 thermal=.1:.1:14;%:.5:14;
syms x
W0=[];
MemN0=[];
Energy=[];
yy=[];
 for i=1:size(thermal,2)
    yy(i,:)=abc8(thermal(i),Ninput);
    yy ;
    num=1;
     for j=1:size(yy,2)-1
         if yy(i,j)*yy(i,j+1)<0
             MemN0(i,num)=fminsearch(f,Ninput(j),optimset('TolX',1e-5));
             num=num+1;
         end
     end
     i
 end


for i=1:size(y,1)
   plot(y(i,:))
   axis([0 320 -0.1 0.1])
   grid on
   pause(0.2)
end
s2=size(MemN0,2);
matlabpool(4)
 parfor i=1:size(thermal,2)
  for j=1:s2
        [Energy(i,j),W0(i,j),totalF(i,j)]=WB04(thermal(i),MemN0(i,j));
  end
   i
 end
matlabpool close

 for i=1:size(thermal,2)
  for j=1:s2
     if abs(H6(i,j))<1e-2
        indexi=i;
        indexj=j;
        criticaltemperature=thermal(i);
        criticalmembrane=MemN0(i,j);
     end
  end
 end

totalF=double(totalF);
for i=1:size(thermal,2)
```

```
    for j=1:size(MemN0,2)
        if totalF(i,j)>0
            figure(1)
            plot(thermal(i),MemN0(i,j),'o')
            hold on
        elseif totalF(i,j)<0
            plot(thermal(i),MemN0(i,j),'.')
            hold on
        end
    end
end
ylabel('Membrane force')
xlabel('Thermal Loading')
h=gcf;
saveas(h,'membrane.fig')

for i=1:size(thermal,2)
    for j=1:size(MemN0,2)
        if totalF(i,j)>0
            figure(2)
            plot(W0(i,j),thermal(i),'o')
            hold on
        elseif totalF(i,j)<0
            plot(W0(i,j),thermal(i),'.')
            hold on
        end
    end
end
xlabel('centerspan displacement')
ylabel('Thermal Loading')
h=gcf;
saveas(h,'centerspandisplacement.fig')

for i=1:size(thermal,2)
    for j=1:size(MemN0,2)
        if totalF(i,j)>0
            figure(3)
            plot(thermal(i),Energy(i,j),'o')
            hold on
        elseif totalF(i,j)<0
            plot(thermal(i),Energy(i,j),'.')
            hold on
        end
    end
end
ylabel('total energy')
xlabel('Thermal Loading')
h=gcf;
saveas(h,'totalenergy.fig')

for i=1:size(thermal,2)
    for j=1:size(MemN0,2)
        if totalF(i,j)>0
            figure(4)
            plot(thermal(i),totalF(i,j),'o')
            hold on
```

```
        elseif totalF(i,j)<0
            plot(thermal(i),totalF(i,j),'.')
            hold on
        end
    end
end
ylabel('stability analysis')
xlabel('Thermal Loading')
h=gcf;
saveas(h,'stability.fig')
savefile = 'pqfile.mat';
save(savefile)

function y1=abc8(thermal,N0)
%%%% y1 is the value of intergrability equation;
format long
HB=0.05;HP=0.05; a=0.4;  alpha11=.002; alpha22=.5; b=0.9; Lp=0.9;
syms x
Thermal=thermal*alpha11;
Cb=12/HB^2;
Cp=12*(HP/HB)/(HB^2);
Ct=Cb+Cp;
Bt=(1/2)*HP*Cp-(1/2)*HB*Cb;
roh=Bt/Ct;
DB=1;
DP=(HP/HB)^3;
D1=DB+DP+Cb*((1/2)*HB)^2+Cp*(HP/2)^2-roh*Bt;
DC=DB+DP;
miu=-(HB/2)*Cb+alpha22*(HP/2)*Cp;
nstar=Cb+alpha22*Cp;
mstar=miu-roh*nstar;
kb= .9;
ratio=1/2.6;
ratio1=1/2.5;
LamdaB= kb*ratio*Cb;
LamdaP= kb*ratio1*Cp;
aa=1-a;
bb=1-b;
m1=D1*(1-N0/(LamdaB+LamdaP));
m2=DC*(1-N0/(LamdaB+LamdaP));
m3=DB*(1-N0/LamdaB);
Kb=sqrt(N0/m1);
Kb3=sqrt(N0/m3);
alpha1=sqrt(LamdaB/DB);
beta1=sqrt(N0/DB/(2-N0/LamdaB));
Mlamda=mstar*Thermal+(roh+.5*HB)*N0;
JJ1=(m3-DP)*alpha1^2;
JJ2=(m3+DP)*beta1^2;

PR1=sin(Kb3*bb)*m3*Kb3;
PR2=sinh(alpha1*(b-a))/cosh(alpha1*(b-a));
PR3=JJ1*PR2*sin(beta1*b)*beta1/alpha1+JJ2*sin(beta1*b);
PR4=JJ1*PR2*cos(beta1*b)*beta1/alpha1-JJ2*sin(beta1*b);
PR5=JJ1*PR2*sin(beta1*b)*beta1/alpha1+JJ2*cos(beta1*b);
```

```
H1=(JJ1+N0)*(sinh(alpha1*(b-a))/cosh(alpha1*(b-
a)))*(beta1/alpha1)*cos(beta1*b)-(JJ2-N0)*(sin(beta1*b)-sin(beta1*a))-
(PR4*cosh(Kb3*bb)-2*beta1*PR1*cos(beta1*b));
H2=(JJ1+N0)*(sinh(alpha1*(b-a))/cosh(alpha1*(b-
a)))*(beta1/alpha1)*sin(beta1*b)+(JJ2-N0)*(cos(beta1*b)-cos(beta1*a))-
(PR5*cosh(Kb3*bb)-2*beta1*PR1*sin(beta1*b));
PR0=H2/H1;

PR6=PR0*cos(beta1*b)-sin(beta1*b);
PR7=cos(beta1*a)+PR0*sin(beta1*a);
PR9=PR0*cos(beta1*a)-sin(beta1*a);
PR10=cos(beta1*b)+PR0*sin(beta1*b);
H3=(JJ2/N0-1)*PR7;
H4=-
(1/N0)*(PR0*(2*beta1*m3*Kb3*sin(Kb3*b)*cos(beta1*b)+cos(Kb3*b)*PR4)-
2*beta1*m3*Kb3*sin(Kb3*b)*sin(beta1*b)-cos(Kb3*b)*PR5);
H5=JJ2*PR7/N0/sin(Kb*a);
H6=D1*Kb*cos(Kb*a)*H5-2*DB*beta1*PR9;
H7=-PR2*PR6*beta1/alpha1+PR10;
H9=-(1/N0)*(PR0*(-
2*beta1*m3*Kb3*cos(Kb3*b)*cos(beta1*b)+sin(Kb3*b)*PR4)+2*beta1*m3*Kb3*c
os(Kb3*b)*sin(beta1*b)-sin(Kb3*b)*PR5);
H8=-(H4*cos(Kb3)+H9*sin(Kb3));
MM=Mlamda/H6;
H12=-(sinh(alpha1*a)/cosh(alpha1*(b-a)))*(beta1/alpha1)*PR6;
H22=(cosh(alpha1*a)/cosh(alpha1*(b-a)))*(beta1/alpha1)*PR6;
phi1=H5*sin(Kb*x)*MM;
phib2=(cosh(alpha1*x)*H12+sinh(alpha1*x)*H22+cos(beta1*x)+PR0*sin(beta1
*x)+H3)*MM;
phip2=(-cosh(alpha1*x)*H12-
sinh(alpha1*x)*H22+cos(beta1*x)+PR0*sin(beta1*x)+H3)*MM;

phib3=(H8+H4*cos(Kb3*x)+H9*sin(Kb3*x))*MM;
wb2prime=diff(phib2,x,2);
phib3doubleprime=diff(phib3,x,2);
wb3prime=-DB/LamdaB*phib3doubleprime+phib3;

intW1square=(MM*H5)^2*((LamdaB+LamdaP)/(LamdaB+LamdaP-N0))^2*(0.5*a-
sin(2*Kb*a)/4/Kb);
intW2square=MM^2*(.5*(b-
a)*((1+PR0^2)*(1+DB*beta1^2/LamdaB)^2+2*H3^2)+(1+DB*beta1^2/LamdaB)^2*(
1/2/beta1)*(0.5*(sin(2*beta1*b)-sin(2*beta1*a))*(1-PR0^2)-
PR0*(cos(2*beta1*b)-cos(2*beta1*a)))...

+2*H3*(1+DB*beta1^2/LamdaB)*(1/beta1)*(sin(beta1*b)-sin(beta1*a)-
PR0*(cos(beta1*b)-cos(beta1*a))));
intW3square=MM^2*((H8^2*bb+0.5*(LamdaB/(LamdaB-N0))^2*(H4^2+H9^2))*bb...
    +2*H8*(LamdaB/(LamdaB-N0))*(H4*(sin(Kb3)-sin(Kb3*b))-H9*(cos(Kb3)-
cos(Kb3*b)))/Kb3...
    -(LamdaB/(LamdaB-N0))^2*H4*H9*(cos(2*Kb3)-cos(2*Kb3*b))/Kb3/2+...
    (LamdaB/(LamdaB-N0))^2*(H4^2-H9^2)*(sin(2*Kb3)-sin(2*Kb3*b))/Kb3/4);
ff=-N0*(aa/Cb+a/Ct)-(1/2)*intW1square-(1/2)*intW2square-
(1/2)*intW3square-(.5*HB+roh)*(subs(phi1,  a))+(aa+a*nstar/Ct)*Thermal;  %
subs(C1,N0,1)
y1=subs(ff,N0);
```

```
function [Eng,W0,totalF,H6]=WB04(thermal,N0)
format long
HB=0.05;HP=0.05; a=0.4;  alpha11=.002; alpha22=.5; b=0.9; Lp=0.9;
syms x
Thermal=thermal*alpha11;
Cb=12/HB^2;
Cp=12*(HP/HB)/(HB^2);
Ct=Cb+Cp;  Bt=(1/2)*HP*Cp-(1/2)*HB*Cb;
roh=Bt/Ct;
DB=1;
DP=(HP/HB)^3;
D1=DB+DP+Cb*((1/2)*HB)^2+Cp*(HP/2)^2-roh*Bt;
DC=DB+DP;
miu=-(HB/2)*Cb+alpha22*(HP/2)*Cp;
nstar=Cb+alpha22*Cp;
mstar=miu-roh*nstar;
kb= .9;
ratio=1/2.6;
LamdaB= kb*ratio*Cb;
LamdaP= kb*ratio*Cp
aa=1-a;
bb=1-b;
%% define some parameters
m1=D1*(1-N0/(LamdaB+LamdaP));
m2=DC*(1-N0/(LamdaB+LamdaP));
m3=DB*(1-N0/LamdaB);
m4=DP*(1-N0/LamdaP);
LAMDA=sqrt(1+LamdaP/LamdaB)*sqrt(1-LamdaP/(LamdaB+LamdaP-N0));

Kb=sqrt(N0/m1);
Kb2=sqrt(N0/m2);
Kb3=sqrt(N0/m3);
alpha1=sqrt(LamdaB/DB);
beta1=sqrt(N0/DB/(2-N0/LamdaB));
Mlamda=mstar*Thermal+(roh+.5*HB)*N0;
JJ1=(m3-DP)*alpha1^2;
JJ2=(m3+DP)*beta1^2;

PR1=sin(Kb3*bb)*m3*Kb3;
PR2=sinh(alpha1*(b-a))/cosh(alpha1*(b-a));
PR3=JJ1*PR2*sin(beta1*b)*beta1/alpha1+JJ2*sin(beta1*b);
PR4=JJ1*PR2*cos(beta1*b)*beta1/alpha1-JJ2*sin(beta1*b);
PR5=JJ1*PR2*sin(beta1*b)*beta1/alpha1+JJ2*cos(beta1*b);
H1=(JJ1+N0)*(sinh(alpha1*(b-a))/cosh(alpha1*(b-
a)))*(beta1/alpha1)*cos(beta1*b)-(JJ2-N0)*(sin(beta1*b)-sin(beta1*a))-
(PR4*cosh(Kb3*bb)-2*beta1*PR1*cos(beta1*b));
H2=(JJ1+N0)*(sinh(alpha1*(b-a))/cosh(alpha1*(b-
a)))*(beta1/alpha1)*sin(beta1*b)+(JJ2-N0)*(cos(beta1*b)-cos(beta1*a))-
(PR5*cosh(Kb3*bb)-2*beta1*PR1*sin(beta1*b));
PR0=H2/H1;

PR6=PR0*cos(beta1*b)-sin(beta1*b);
PR7=cos(beta1*a)+PR0*sin(beta1*a);
PR9=PR0*cos(beta1*a)-sin(beta1*a);
PR10=cos(beta1*b)+PR0*sin(beta1*b);
H3=((m3+DP)/DB/(2-N0/LamdaB)-1)*PR7;
```

```
H4=-
(1/N0)*(PR0*(2*beta1*m3*Kb3*sin(Kb3*b)*cos(beta1*b)+cos(Kb3*b)*PR4)-
2*beta1*m3*Kb3*sin(Kb3*b)*sin(beta1*b)-cos(Kb3*b)*PR5);
H5=JJ2*PR7/N0/sin(Kb*a);
H6=D1*Kb*cos(Kb*a)*H5-2*DB*beta1*PR9;
H7=-PR2*PR6*beta1/alpha1+PR10;
H9=-(1/N0)*(PR0*(-
2*beta1*m3*Kb3*cos(Kb3*b)*cos(beta1*b)+sin(Kb3*b)*PR4)+2*beta1*m3*Kb3*c
os(Kb3*b)*sin(beta1*b)-sin(Kb3*b)*PR5);
H8=-(H4*cos(Kb3)+H9*sin(Kb3));
MM=Mlamda/H6;
C13=(Mlamda/H6)*((1+DB*beta1^2/LamdaB)*(PR0*(cos(beta1*b)-
cos(beta1*a))-sin(beta1*b)+sin(beta1*a))/beta1+H3*(a-b)+...
    (LamdaB+LamdaP)*H5*cos(Kb*a)/Kb/(LamdaB+LamdaP-N0)-
LamdaB/Kb3/(LamdaB-N0)*(H4*(sin(Kb3*b)-sin(Kb3))-H9*(cos(Kb3*b)-
cos(Kb3)))-H8*bb);
H12=-(sinh(alpha1*a)/cosh(alpha1*(b-a)))*(beta1/alpha1)*PR6;
H22=(cosh(alpha1*a)/cosh(alpha1*(b-a)))*(beta1/alpha1)*PR6;
phi1=H5*sin(Kb*x)*MM;
phib2=(cosh(alpha1*x)*H12+sinh(alpha1*x)*H22+cos(beta1*x)+PR0*sin(beta1
*x)+H3)*MM;
phip2=(-cosh(alpha1*x)*H12-
sinh(alpha1*x)*H22+cos(beta1*x)+PR0*sin(beta1*x)+H3)*MM;

phib3=(H8+H4*cos(Kb3*x)+H9*sin(Kb3*x))*MM;
phi1prime=H5*cos(Kb*x)*Kb*MM;
phib2prime=diff(phib2,x);
phip2prime=diff(phip2,x);
phib3prime=Kb3*(-H4*sin(Kb3*x)+H9*cos(Kb3*x))*MM;
phi1doubleprime=-H5*Kb^2*sin(Kb*x)*MM;
phib2doubleprime=diff(phib2,x,2);
phip2doubleprime=diff(phip2,x,2);
phib3doubleprime=-Kb3^2*(H4*cos(Kb3*x)+H9*sin(Kb3*x))*MM;
intphib1primesquare=(MM*H5*Kb)^2*(0.5*a+sin(2*Kb*a)/4/Kb);
intphib2andp2primesquare=int(phib2prime^2+phip2prime^2,a,b);%
intphib3primesquare=int(phib3prime^2,x,b,1);
intphib1doubleprimesquare=(MM*H5*Kb^2)^2*(0.5*a-sin(2*Kb*a)/4/Kb);
intphib2andp2doubleprimesquare=int(phib2doubleprime^2+phip2doubleprime^
2,a,b);
intphib3doubleprimesquare=int(phib3doubleprime^2,x,b,1);
wb2prime=-DB/LamdaB*phib2doubleprime+phib2;
a1=0.5*(DB+DP)+Cb*Cp*(HB+HP)^2/Ct/8;
a2=0.5*Cb*Cp*(HB+HP)*(1-alpha22)*Thermal/Ct;
Eng=a1*intphib1primesquare+.5*D1^2/(LamdaB+LamdaP)*intphib1doubleprimes
quare...
    +a2*(subs(phi1,a))+0.5*((N0^2+Cb*Cp*(1-
alpha22)^2*Thermal^2)/Ct)*a...

+0.5*DB*intphib2andp2primesquare+.5*DB^2/(LamdaB)*intphib2andp2doublepr
imesquare...

+0.5*DB*intphib3primesquare+.5*DB^2/(LamdaB)*intphib3doubleprimesquare+
0.5*(N0^2/Cb)*aa;
F1=(LamdaB+LamdaP-N0)*(D1/(LamdaB+LamdaP))^2*phi1doubleprime^2-
N0*phi1^2+D1*phi1prime^2+2*(D1/(LamdaB+LamdaP))*N0*phi1*phi1doubleprime;
F3=(LamdaB-N0)*(DB/LamdaB)^2*phib3doubleprime^2-
N0*phib3^2+DB*phib3prime^2+2*(DB/LamdaB)*N0*phib3*phib3doubleprime;
```

```
F2=(LamdaB+LamdaP-
N0)*wb2prime^2+LamdaB*(phib2^2+phip2^2)+DB*(phib2prime^2+phip2prime^2)-
2*LamdaB*wb2prime*(phib2+phip2);
totalF=(int(F1,x,0,a)+int(F2,a,b)+int(F3,x,b,1))/Mlamda^2;
W0=-(MM)*H5*(LamdaB+LamdaP)/Kb/(LamdaB+LamdaP-N0)+C13;

% For edge contact case, the following profiles provide the displace-
ment, the energy, the stability condition and transversality condition.
clear
N0=.1:.005:40;
thermal=.1:0.1:14;
W0=[];
MemN0=[];
Energy=[];
s=size(N0,2);
matlabpool(2)
tic
y=[];
parfor i=1:size(thermal,2)
  for j=1:s
    y(i,j)=abc4(thermal(i),N0(j));
  end
  i
end
toc
matlabpool close
for i=1:size(y,1)
   plot(y(i,:))
   axis([0 320 -0.1 0.1])
   grid on
   pause(0.2)
end
for i=1:size(thermal,2)
  num=1;
  for j=1:size(y,2)-1
         if y(i,j)*y(i,j+1)<0
             MemN0(i,num)=(N0(j)+N0(j+1))/2;
             num=num+1;
         end
  end
end
s2=size(MemN0,2);

for i=1:size(thermal,2)
  for j=1:s2
      if MemN0(i,j)~=0
    [Ener-
gy(i,j),W0(i,j),totalF(i,j),H6(i,j)]=WB04(thermal(i),MemN0(i,j));
      end
%     y2=[thermal(i),y(i,j)];
  end
   i
end

for i=1:size(thermal,2)
  for j=1:s2
```

```
     if abs(H6(i,j))<1e-2
        indexi=i;
        indexj=j;
        criticaltemperature=thermal(i);
        criticalmembrane=MemN0(i,j);
     end
  end
end

totalF=double(totalF);
for i=1:size(thermal,2)
    for j=1:size(MemN0,2)
        if totalF(i,j)>0
            figure(1)
            plot(thermal(i),MemN0(i,j),'o')
            hold on
        elseif totalF(i,j)<0
            plot(thermal(i),MemN0(i,j),'.')
            hold on
        end
    end
end
ylabel('Membrane force')
xlabel('Thermal Loading')
h=gcf;
saveas(h,'membrane.fig')
% W01=smooth(W0);
for i=1:size(thermal,2)
    for j=1:size(MemN0,2)
        if totalF(i,j)>0
            figure(2)
            plot(W0(i,j),thermal(i),'o')
            hold on
        elseif totalF(i,j)<0
            plot(W0(i,j),thermal(i),'.')
            hold on
        end
    end
end
xlabel('centerspan displacement')
ylabel('Thermal Loading')
h=gcf;
saveas(h,'centerspandisplacement.fig')

for i=1:size(thermal,2)
    for j=1:size(MemN0,2)
        if totalF(i,j)>0
            figure(3)
            plot(thermal(i),Energy(i,j),'o')
            hold on
        elseif totalF(i,j)<0
            plot(thermal(i),Energy(i,j),'.')
            hold on
        end
    end
end
```

```
ylabel('total energy')
xlabel('Thermal Loading')
h=gcf;
saveas(h,'totalenergy.fig')

for i=1:size(thermal,2)
    for j=1:size(MemN0,2)
        if totalF(i,j)>0
            figure(4)
            plot(thermal(i),totalF(i,j),'o')
            hold on
        elseif totalF(i,j)<0
            plot(thermal(i),totalF(i,j),'.')
            hold on
        end
    end
end
ylabel('stability analysis')
xlabel('Thermal Loading')
h=gcf;
saveas(h,'stability.fig')
savefile = 'pqfile06.mat';
save(savefile)

function y1=abc4(thermal,N0)
format long
HB=0.05;HP=0.05; a=0.6;  alpha11=.002; alpha22=.5; b=0.9; Lp=0.9;
syms x
Thermal=thermal*alpha11;
Cb=12/HB^2;
Cp=12*(HP/HB)/(HB^2);
Ct=Cb+Cp;
Bt=(1/2)*HP*Cp-(1/2)*HB*Cb;
roh=Bt/Ct;
DB=1;
DP=(HP/HB)^3;
D1=DB+DP+Cb*((1/2)*HB)^2+Cp*(HP/2)^2-roh*Bt;
DC=DB+DP;
miu=-(HB/2)*Cb+alpha22*(HP/2)*Cp;
nstar=Cb+alpha22*Cp;
mstar=miu-roh*nstar;
kb= .9;
ratio=1/2.6;
ratio1=1/2.5;
LamdaB= kb*ratio*Cb;
LamdaP= kb*ratio*Cp; aa=1-a;
bb=1-b;
%% define some parameters
m1=D1*(1-N0/(LamdaB+LamdaP));
m2=DC*(1-N0/(LamdaB+LamdaP));
m3=DB*(1-N0/LamdaB);
Kb=sqrt(N0/m1);
Kb3=sqrt(N0/m3);
Mlamda=mstar*Thermal+(roh+.5*HB)*N0;
m5=(1+DB/LamdaB*Kb3^2)/Kb3;
m6=(1+D1/(LamdaB+LamdaP)*Kb^2)/Kb;
```

```
f1=N0*(1/3*(Lp^3-a^3)/DP+(Lp-a)/LamdaP-a/DP*(Lp-.5*a)*(Lp-a));
f2=m5*(sin(Kb3*Lp)-sin(Kb3*a))-cos(Kb3*a)*(Lp-a);
f3=m5*(cos(Kb3*Lp)-cos(Kb3*a))-sin(Kb3*a)*(Lp-a);
H1=f1-f3*cos(Kb3*(1-Lp))/sin(Kb3);
H2=f2*cos(Kb3*Lp)-f3*sin(Kb3*Lp)+f1;
H3=-f2*cos(Kb3*(1-Lp))/sin(Kb3)-f1*cos(Kb3)/sin(Kb3);
H4=H2;
H5=(H1*f2-H3*f3)/f1/H2;
H6=(H5+H1*cos(Kb3*a)/H2+H3*sin(Kb3*a)/H4)/sin(Kb*a);
H7=-m5/sin(Kb3);
H8=H7-H5*Lp;
H9=H6*sin(Kb*a)-N0*a*(Lp-0.5*a)*H5/DP;
H11=D1*Kb*cos(Kb*a)*H6+DB*Kb3*(H1*sin(Kb3*a)-H3*cos(Kb3*a))/H2+N0*(a-
Lp)*H5;
MM=Mlamda/H11;
jj1=cos(Kb3)/sin(Kb3);
jj2=LamdaB/(LamdaB-N0);
jj3=sin(2*Kb3*Lp)-sin(2*Kb3*a);
jj4=cos(2*Kb3*Lp)-cos(2*Kb3*a);
jj5=sin(Kb3*Lp)-sin(Kb3*a);
jj6=cos(Kb3*Lp)-cos(Kb3*a);
phi1=H6*sin(Kb*x)*MM;
intW2square=MM^2*(jj2^2/H2^2*(.5*(Lp-a)*(H1^2+H3^2)-(H3^2-
H1^2)/4/Kb3*jj3-H1*H3*jj4/2/Kb3)+H5^2*(Lp-a)+jj2*2*H5/H2*(H1*jj5-
H3*jj6)/Kb3);
intW1square=MM^2*((LamdaB+LamdaP)*H6/(LamdaB+LamdaP-N0))^2*(0.5*a-
sin(2*Kb*a)/4/Kb);
intW3square=MM^2*(.5*(1-Lp)*(1+jj1)-(jj1-1)*jj3/4/Kb3+jj1*jj4/2/Kb3);
ff=-N0*(aa/Cb+a/Ct)-(1/2)*intW1square-(1/2)*intW2square-
(1/2)*intW3square-(.5*HB+roh)*(subs(phi1, a))+(aa+a*nstar/Ct)*Thermal;
y1=ff;

function [Eng,W0,totalF,H6]=WB04(thermal,N0)
format long
 HB=0.05;HP=0.05; a=0.6;  alpha11=.002; alpha22=.5; b=0.9; Lp=0.9;
syms x
Thermal=thermal*alpha11;
Cb=12/HB^2;
Cp=12*(HP/HB)/(HB^2);
Ct=Cb+Cp;  Bt=(1/2)*HP*Cp-(1/2)*HB*Cb;
roh=Bt/Ct;
DB=1;
DP=(HP/HB)^3;
D1=DB+DP+Cb*((1/2)*HB)^2+Cp*(HP/2)^2-roh*Bt;
DC=DB+DP;
miu=-(HB/2)*Cb+alpha22*(HP/2)*Cp;
nstar=Cb+alpha22*Cp;
mstar=miu-roh*nstar;
kb= .9;
ratio=1/2.6;
LamdaB= kb*ratio*Cb;
LamdaP= kb*ratio*Cp;
aa=1-a;
bb=1-b;
m1=D1*(1-N0/(LamdaB+LamdaP));
m2=DC*(1-N0/(LamdaB+LamdaP));
m3=DB*(1-N0/LamdaB);
```

```
m4=DP*(1-N0/LamdaP);
LAMDA=sqrt(1+LamdaP/LamdaB)*sqrt(1-LamdaP/(LamdaB+LamdaP-N0));
Kb=sqrt(N0/m1);
Kb2=sqrt(N0/m2);
Kb3=sqrt(N0/m3);
Mlamda=mstar*Thermal+(roh+.5*HB)*N0;
m5=(1+DB/LamdaB*Kb3^2)/Kb3;
m6=(1+D1/(LamdaB+LamdaP)*Kb^2)/Kb;

f1=N0*(1/3*(Lp^3-a^3)/DP+(Lp-a)/LamdaP-a/DP*(Lp-.5*a)*(Lp-a));
f2=m5*(sin(Kb3*Lp)-sin(Kb3*a))-cos(Kb3*a)*(Lp-a);
f3=m5*(cos(Kb3*Lp)-cos(Kb3*a))-sin(Kb3*a)*(Lp-a);
H1=f1-f3*cos(Kb3*(1-Lp))/sin(Kb3);
H2=f2*cos(Kb3*Lp)-f3*sin(Kb3*Lp)+f1;
H3=-f2*cos(Kb3*(1-Lp))/sin(Kb3)-f1*cos(Kb3)/sin(Kb3);
H4=H2;
H5=(H1*f2-H3*f3)/f1/H2;
H6=(H5+H1*cos(Kb3*a)/H2+H3*sin(Kb3*a)/H4)/sin(Kb*a);
H7=-m5/sin(Kb3);
H8=H7-H5*Lp;
H9=H6*sin(Kb*a)-N0*a*(Lp-0.5*a)*H5/DP;
H10=(m5*(cos(Kb3*(1-Lp)-1))/sin(Kb3)-N0*(Lp^3/DP/3+Lp/LamdaP)*H5-H9*Lp);
H11=D1*Kb*cos(Kb*a)*H6+DB*Kb3*(H1*sin(Kb3*a)-H3*cos(Kb3*a))/H2+N0*(a-
Lp)*H5;
MM=Mlamda/H11;
jj1=cos(Kb3)/sin(Kb3);
C18=(Mlamda/H11)*(m6*cos(Kb*a)*H6+N0*(a^3/DP/3+a/LamdaP)*H5+H9*a+H10);
phi1=H6*sin(Kb*x)*MM;
phib2=(H5+H1/H2*cos(Kb3*x)+H3/H4*sin(Kb3*x))*MM;
phip2=(-.5*N0/DP*H5*x^2+N0/DP*H5*Lp*x+H9)*MM;
phib3=(cos(Kb3*x)-jj1*sin(Kb3*x))*MM;
phi1prime=diff(phi1,x);
phib2prime=diff(phib2,x);
phip2prime=diff(phip2,x);
phib3prime=diff(phib3,x);

phi1doubleprime=diff(phi1,x,2);
phib2doubleprime=diff(phib2,x,2);
phip2doubleprime=diff(phip2,x,2);
phib3doubleprime=diff(phib3,x,2);

a1=0.5*(DB+DP)+Cb*Cp*(HB+HP)^2/Ct/8;
a2=0.5*Cb*Cp*(HB+HP)*(1-alpha22)*Thermal/Ct;
% Eng=1;
Eng=a1*(int(phi1prime^2,x,0,
a))+.5*D1^2/(LamdaB+LamdaP)*(int(phi1doubleprime^2,x,0, a))...
    +a2*(subs(phi1,a))+0.5*((N0^2+Cb*Cp*(1-
alpha22)^2*Thermal^2)/Ct)*a...

+0.5*DB*(int(phib2prime^2,x,a,Lp))+.5*DB^2/(LamdaB)*(int(phib2doublepri
me^2,x,a, Lp))...

+0.5*DP*(int(phip2prime^2,x,a,Lp))+.5*DP^2/(LamdaP)*(int(phip2doublepri
me^2,x,a, Lp))...
```

```
+0.5*DB*(int(phib3prime^2,x,Lp,1))+.5*DB^2/(LamdaB)*(int(phib3doublepri
me^2,x,Lp, 1))+0.5*(N0^2/Cb)*aa;
F1=(LamdaB+LamdaP-N0)*(D1/(LamdaB+LamdaP))^2*phi1doubleprime^2-
N0*phi1^2+D1*phi1prime^2+2*(D1/(LamdaB+LamdaP))*N0*phi1*phi1doubleprime;
F2=(LamdaB-N0)*(DB/LamdaB)^2*phib2doubleprime^2-
N0*phib2^2+DB*phib2prime^2+2*(DB/LamdaB)*N0*phib2*phib2doubleprime;
F3=(LamdaB-N0)*(DB/LamdaB)^2*phib3doubleprime^2-
N0*phib3^2+DB*phib3prime^2+2*(DB/LamdaB)*N0*phib3*phib3doubleprime;
G1=DP*phip2prime+DP^2*phip2doubleprime/LamdaP;
totalF=(int(F1,x,0,a)+int(F2,x,a,Lp)+int(F3,x,Lp,1)+int(G1,x,a,Lp))/Mla
mda^2;
W0=-(Mlamda/H11)*(LamdaB+LamdaP)*H6/Kb/(LamdaB+LamdaP-N0)+C18;
```

Case 2: Unequal shear stiffness

```
%% For different shear stiffnesses for the base and the patch
%% we can change the Poisson's ratio or Young's modulus to change the
shear stiffness
%% Full contact configuration
clear
N0=.1:.1:64;
thermal=.1:0.1:14;
W0=[];
MemN0=[];
Energy=[];
s=size(N0,2);
tic
y=[];
b=0.9;
for i=1:size(thermal,2)
  for j=1:s
    y(i,j)=abc2(thermal(i),N0(j),b);
  end
  num=1;
    for j=1:size(y,2)-1
         if y(i,j)*y(i,j+1)<0
             MemN0(i,num)=(N0(j)+N0(j+1))/2;
             num=num+1;
         end
    end
  i
end
toc


for i=1:size(y,1)
   plot(y(i,:))
   axis([0 320 -0.1 0.1])
   grid on
   pause(0.2)
end
for i=1:size(thermal,2)
    num=1;
    for j=1:size(y,2)-1
```

```
        if y(i,j)*y(i,j+1)<0
            MemN0(i,num)=(N0(j)+N0(j+1))/2;
            num=num+1;
        end
    end
end
s2=size(MemN0,2);
parfor i=1:size(thermal,2)
  for j=1:s2
    [Ener-
gy(i,j),W0(i,j),totalF(i,j),H6(i,j)]=WB02(thermal(i),MemN0(i,j));
  end
   i
 end
for i=1:size(thermal,2)
  for j=1:s2
     if abs(H6(i,j))<1e-2
        indexi=i;
        indexj=j;
        criticaltemperature=thermal(i);
        criticalmembrane=MemN0(i,j);
     end
  end
 end
totalF=double(totalF);
for i=1:size(thermal,2)
    for j=1:size(MemN0,2)
        if totalF(i,j)>0
            figure(1)
            plot(thermal(i),MemN0(i,j),'o')
            hold on
        elseif totalF(i,j)<0
            plot(thermal(i),MemN0(i,j),'.')
            hold on
        end
    end
end
ylabel('Membrane force')
xlabel('Thermal Loading')
h=gcf;
saveas(h,'membrane.fig')
for i=1:size(thermal,2)
    for j=1:size(MemN0,2)
        if totalF(i,j)>0
            figure(2)
            plot(W0(i,j),thermal(i),'o')
            hold on
        elseif totalF(i,j)<0
            plot(W0(i,j),thermal(i),'.')
            hold on
        end
    end
end
xlabel('centerspan displacement')
ylabel('Thermal Loading')
h=gcf;
saveas(h,'centerspandisplacement.fig')
```

```
for i=1:size(thermal,2)
    for j=1:size(MemN0,2)
        if totalF(i,j)>0
            figure(3)
            plot(thermal(i),Energy(i,j),'o')
            hold on
        elseif totalF(i,j)<0
            plot(thermal(i),Energy(i,j),'.')
            hold on
        end
    end
end
ylabel('total energy')
xlabel('Thermal Loading')
h=gcf;
saveas(h,'totalenergy.fig')
for i=1:size(thermal,2)
    for j=1:size(MemN0,2)
        if totalF(i,j)>0
            figure(4)
            plot(thermal(i),totalF(i,j),'o')
            hold on
        elseif totalF(i,j)<0
            plot(thermal(i),totalF(i,j),'.')
            hold on
        end
    end
end
ylabel('stability analysis')
xlabel('Thermal Loading')
h=gcf;
saveas(h,'stability.fig')
savefile = 'pqfile.mat';

function y1=abc2(thermal,N0,b)
format long
HB=0.05;HP=0.05; a=0.8;  alpha11=.002; alpha22=.5;  Lp=.9;
syms x
Thermal=thermal*alpha11;
Cb=12/HB^2;
Cp=12*(HP/HB)/(HB^2);
Ct=Cb+Cp;  Bt=(1/2)*HP*Cp-(1/2)*HB*Cb;
roh=Bt/Ct;
DB=1;
DP=(HP/HB)^3;
D1=DB+DP+Cb*((1/2)*HB)^2+Cp*(HP/2)^2-roh*Bt;
DC=DB+DP;
miu=-(HB/2)*Cb+alpha22*(HP/2)*Cp;
nstar=Cb+alpha22*Cp;
mstar=miu-roh*nstar;
kb= .9;
ratio=1/2.6;
ratio1=1/2.5;
LamdaB= kb*ratio*Cb;
LamdaP= kb*ratio1*Cp;
aa=1-a;
bb=1-b;
```

```
m1=D1*(1-N0/(LamdaB+LamdaP));
m2=DC*(1-N0/(LamdaB+LamdaP));
m3=DB*(1-N0/LamdaB);
Kb=sqrt(N0/m1);
Kb3=sqrt(N0/m3);
bb1=-(DB+DP-N0*(DB/LamdaB+DP/LamdaP));
aa1=DB*DP/LamdaB/LamdaP*(LamdaB+LamdaP-N0);
delta=bb1^2+4*aa1*N0;
alpha1=sqrt((-bb1+sqrt(delta))/aa1/2);
beta1=sqrt((+bb1+sqrt(delta))/aa1/2);
P1=(1-DB*alpha1^2/LamdaB)/(1-DP*alpha1^2/LamdaP);
P2=(1+DB*beta1^2/LamdaB)/(1+DP*beta1^2/LamdaP);
%% equations for displacement of base and patch
Mlamda=mstar*Thermal+(roh+.5*HB)*N0;
Com1=cosh(alpha1*(b-a));
H_11=((1-P2)*(sin(beta1*a)*cosh(alpha1*b))/(P1-
1)+P2*beta1*(sinh(alpha1*a)*cos(beta1*b))/P1/alpha1)/Com1;
H_12=((1-P2)*(cos(beta1*a)*cosh(alpha1*b))/(P1-1)-
P2*beta1*(sinh(alpha1*a)*sin(beta1*b))/P1/alpha1)/Com1;
H_21=-((1-P2)*(sinh(alpha1*b)*sin(beta1*a))/(P1-
1)+P2*beta1*(cosh(alpha1*a)*cos(beta1*b))/P1/alpha1)/Com1;
H_22=-((1-P2)*(sinh(alpha1*b)*cos(beta1*a))/(P1-1)-
P2*beta1*(cosh(alpha1*a)*sin(beta1*b))/P1/alpha1)/Com1;
jj1=(1-DB*alpha1^2/LamdaB);
jj2=(1+DB*beta1^2/LamdaB);
PR1=jj1*(1-P2)/(P1-1)-jj2;
PR2=H_11*sinh(alpha1*b)+H_21*cosh(alpha1*b);
PR3=H_11*cosh(alpha1*b)+H_21*sinh(alpha1*b);
PR4=(sinh(alpha1*b)*H_12+cosh(alpha1*b)*H_22);
PR5=(cosh(alpha1*b)*H_12+sinh(alpha1*b)*H_22);
H1=PR1*sin(beta1*a)-
(alpha1*PR2+beta1*cos(beta1*b))*m3*Kb3*sin(Kb3*bb)+(jj1*PR3-
jj2*sin(beta1*b))*cos(Kb3*bb);
H2=-PR1*cos(beta1*a)+(alpha1*PR4-
beta1*sin(beta1*b))*m3*Kb3*sin(Kb3*bb)+(jj1*PR5-
jj2*cos(beta1*b))*cos(Kb3*bb);
PR0=H2/H1;
PR6=sin(beta1*a)*PR0+cos(beta1*a);
PR7=-sin(beta1*b)+PR0*cos(beta1*b);
PR8=cos(beta1*b)+PR0*sin(beta1*b);
C21=H_22+PR0*H_21;
C20=H_12+PR0*H_11;
PR9=-sin(beta1*a)+PR0*cos(beta1*a);
PR10=alpha1*(C20*sinh(alpha1*b)+C21*cosh(alpha1*a))+beta1*PR7;
PR11=jj1*(C20*cosh(alpha1*b)+C21*sinh(alpha1*b))-jj2*PR8;


H3=(-(P1-P2)/(P1-1)-PR1/N0)*PR6;
H4=-(m3*Kb3*sin(Kb3*b)*PR10+cos(Kb3*b)*PR11)/N0;
H5=-PR1*PR6/N0/sin(Kb*a);
H6=D1*Kb*cos(Kb*a)*H5-
(DB+DP*P1)*alpha1*(C20*sinh(alpha1*a)+C21*cosh(alpha1*a))-
(DB+DP*P2)*beta1*PR9;
H9=(m3*Kb3*cos(Kb3*b)*PR10-sin(Kb3*b)*PR11)/N0;
H8=-H4*cos(Kb3)-H9*sin(Kb3);
MM=Mlamda/H6;
```

```
phi1=H5*sin(Kb*x)*MM;
wb2prime=MM*((1-
DB*alpha1^2/LamdaB)*(cosh(alpha1*x)*C20+sinh(alpha1*x)*C21)+(1+DB*beta1
^2/LamdaB)*(sin(beta1*x)*PR0+cos(beta1*x))+H3);
intW2square=MM^2*(.5*(b-a)*(jj1^2*(C20^2-
C21^2)+jj2^2*(1+PR0^2)+2*H3^2)+jj1^2*(1/4/alpha1)*((C20^2+C21^2)*(sinh(
2*alpha1*b)-sinh(2*alpha1*a))+2*C20*C21*(cosh(2*alpha1*b)-
cosh(2*alpha1*a)))...
                   +jj2^2*(1/4/beta1)*((1-PR0^2)*(sin(2*beta1*b)-
sin(2*beta1*a))+2*PR0*(cos(2*beta1*b)-cos(2*beta1*a)))...

+2*jj1*jj2/(alpha1^2+beta1^2)*(alpha1*(C20*sinh(alpha1*b)+C21*cosh(alph
a1*b))*(cos(beta1*b)-PR0*sin(beta1*b))...
                   -
alpha1*(C20*sinh(alpha1*a)+C21*cosh(alpha1*a))*(cos(beta1*a)-
PR0*sin(beta1*a))...

+beta1*(C20*cosh(alpha1*b)+C21*sinh(alpha1*b))*(sin(beta1*b)+PR0*cos(be
ta1*b))...
                   -
be-
ta1*(C20*cosh(alpha1*a)+C21*sinh(alpha1*a))*(sin(beta1*a)+PR0*cos(beta1
*a)))...
                   +2*H3*jj1/alpha1*(C20*(sinh(alpha1*b)-
sinh(alpha1*a))+C21*(cosh(alpha1*b)-cosh(alpha1*a)))...
                   +2*H3*jj2/beta1*(PR0*(cos(beta1*b)-
cos(beta1*a))+sin(beta1*b)-sin(beta1*a)));
%
intW1square=MM^2*((LamdaB+LamdaP)*H5/(LamdaB+LamdaP-N0))^2*(0.5*a-
sin(2*Kb*a)/4/Kb);
intW3square=MM^2*((H8^2*bb+0.5*(LamdaB/(LamdaB-N0))^2*(H4^2+H9^2))*bb...
    +2*H8*(LamdaB/(LamdaB-N0))*(H4*(sin(Kb3)-sin(Kb3*b))-H9*(cos(Kb3)-
cos(Kb3*b)))/Kb3...
    -(LamdaB/(LamdaB-N0))^2*H4*H9*(cos(2*Kb3)-cos(2*Kb3*b))/Kb3/2+...
    (LamdaB/(LamdaB-N0))^2*(H4^2-H9^2)*(sin(2*Kb3)-sin(2*Kb3*b))/Kb3/4);
ff=-N0*(aa/Cb+a/Ct)-(1/2)*intW1square-(1/2)*intW2square-
(1/2)*intW3square-(.5*HB+roh)*(subs(phi1, a))+(aa+a*nstar/Ct)*Thermal;
y1=ff;

function [Eng,W0,totalF,H6]=WB02(thermal,N0)
format long
 HB=0.05;HP=0.05; a=0.8;  alpha11=.002; alpha22=.5; b=0.9; Lp=0.9;
syms x
Thermal=thermal*alpha11;
Cb=12/HB^2;
Cp=12*(HP/HB)/(HB^2);
Ct=Cb+Cp;  Bt=(1/2)*HP*Cp-(1/2)*HB*Cb;  roh=Bt/Ct;
DB=1;
DP=(HP/HB)^3;
D1=DB+DP+Cb*((1/2)*HB)^2+Cp*(HP/2)^2-roh*Bt;
DC=DB+DP;
miu=-(HB/2)*Cb+alpha22*(HP/2)*Cp;
nstar=Cb+alpha22*Cp;
mstar=miu-roh*nstar;
kb= .9;
```

```
ratio=1/2.6;
ratio1=1/2.5;
LamdaB= kb*ratio*Cb;
LamdaP= kb*ratio1*Cp; aa=1-a;
bb=1-b;
%% define some parameters
m1=D1*(1-N0/(LamdaB+LamdaP));
m2=DC*(1-N0/(LamdaB+LamdaP));
m3=DB*(1-N0/LamdaB);
m4=DP*(1-N0/LamdaP);
LAMDA=sqrt(1+LamdaP/LamdaB)*sqrt(1-LamdaP/(LamdaB+LamdaP-N0));

Kb=sqrt(N0/m1);
Kb2=sqrt(N0/m2);
Kb3=sqrt(N0/m3);
bb1=-(DB+DP-N0*(DB/LamdaB+DP/LamdaP));
aa1=DB*DP/LamdaB/LamdaP*(LamdaB+LamdaP-N0);
delta=bb1^2+4*aa1*N0;
alpha1=sqrt((-bb1+sqrt(delta))/aa1/2);
beta1=sqrt((+bb1+sqrt(delta))/aa1/2);
P1=(1-DB*alpha1^2/LamdaB)/(1-DP*alpha1^2/LamdaP);
P2=(1+DB*beta1^2/LamdaB)/(1+DP*beta1^2/LamdaP);
Mlamda=mstar*Thermal+(roh+.5*HB)*N0;
Com1=cosh(alpha1*(b-a));
H_11=((1-P2)*(sin(beta1*a)*cosh(alpha1*b))/(P1-
1)+P2*beta1*(sinh(alpha1*a)*cos(beta1*b))/P1/alpha1)/Com1;
H_12=((1-P2)*(cos(beta1*a)*cosh(alpha1*b))/(P1-1)-
P2*beta1*(sinh(alpha1*a)*sin(beta1*b))/P1/alpha1)/Com1;
H_21=-((1-P2)*(sinh(alpha1*b)*sin(beta1*a))/(P1-
1)+P2*beta1*(cosh(alpha1*a)*cos(beta1*b))/P1/alpha1)/Com1;
H_22=-((1-P2)*(sinh(alpha1*b)*cos(beta1*a))/(P1-1)-
P2*beta1*(cosh(alpha1*a)*sin(beta1*b))/P1/alpha1)/Com1;
jj1=(1-DB*alpha1^2/LamdaB);
jj2=(1+DB*beta1^2/LamdaB);
PR1=jj1*(1-P2)/(P1-1)-jj2;
PR2=H_11*sinh(alpha1*b)+H_21*cosh(alpha1*b);
PR3=H_11*cosh(alpha1*b)+H_21*sinh(alpha1*b);
PR4=(sinh(alpha1*b)*H_12+cosh(alpha1*b)*H_22);
PR5=(cosh(alpha1*b)*H_12+sinh(alpha1*b)*H_22);
H1=PR1*sin(beta1*a)-
(alpha1*PR2+beta1*cos(beta1*b))*m3*Kb3*sin(Kb3*bb)+(jj1*PR3-
jj2*sin(beta1*b))*cos(Kb3*bb);
H2=-PR1*cos(beta1*a)+(alpha1*PR4-
beta1*sin(beta1*b))*m3*Kb3*sin(Kb3*bb)+(jj1*PR5-
jj2*cos(beta1*b))*cos(Kb3*bb);
PR0=H2/H1;
PR6=sin(beta1*a)*PR0+cos(beta1*a);
PR7=-sin(beta1*b)+PR0*cos(beta1*b);
PR8=cos(beta1*b)+PR0*sin(beta1*b);
C21=H_22+PR0*H_21;
C20=H_12+PR0*H_11;
PR9=-sin(beta1*a)+PR0*cos(beta1*a);
PR10=alpha1*(C20*sinh(alpha1*b)+C21*cosh(alpha1*a))+beta1*PR7;
PR11=jj1*(C20*cosh(alpha1*b)+C21*sinh(alpha1*b))-jj2*PR8;
H3=(-(P1-P2)/(P1-1)-PR1/N0)*PR6;
H4=-(m3*Kb3*sin(Kb3*b)*PR10+cos(Kb3*b)*PR11)/N0;
H5=-PR1*PR6/N0/sin(Kb*a);
```

```
H6=D1*Kb*cos(Kb*a)*H5-
(DB+DP*P1)*alpha1*(C20*sinh(alpha1*a)+C21*cosh(alpha1*a))-
(DB+DP*P2)*beta1*PR9;
H9=(m3*Kb3*cos(Kb3*b)*PR10-sin(Kb3*b)*PR11)/N0;
H8=-H4*cos(Kb3)-H9*sin(Kb3);
MM=Mlamda/H6;

C13=(Mlamda/H6)*((1-DB*alpha1^2/LamdaB)*(PR7-PR13)/alpha1-
(1+DB*beta1^2/LamdaB)*(PR6-PR10)/beta1-H3*(b-a)+...
    (LamdaB+LamdaP)*H5*cos(Kb*a)/Kb/(LamdaB+LamdaP-N0)-
LamdaB*(H4*(sin(Kb3*b)-sin(Kb3))-H9*(cos(Kb3*b)-cos(Kb3)))/Kb3/(LamdaB-
N0)-H8*bb);
phi1=H5*sin(Kb*x)*(Mlamda/H6);
phib2=(cosh(alpha1*x)*H_12+sinh(alpha1*x)*H_22+PR0*(cosh(alpha1*x)*H_11
+sinh(alpha1*x)*H_21)+cos(beta1*x)+PR0*sin(beta1*x)+H3)*(Mlamda/H6);
phip2=(P1*(cosh(alpha1*x)*H_12+sinh(alpha1*x)*H_22+PR0*(cosh(alpha1*x)*
H_11+sinh(alpha1*x)*H_21))+P2*(cos(beta1*x)+PR0*sin(beta1*x))+H3)*(Mlam
da/H6);
phib3=(H8+H4*cos(Kb3*x)+H9*sin(Kb3*x))*(Mlamda/H6);
phi1prime=diff(phi1,x);
phib2prime=diff(phib2,x);
phip2prime=diff(phip2,x);
phib3prime=diff(phib3,x);

phi1doubleprime=diff(phi1,x,2);
phib2doubleprime=diff(phib2,x,2);
phip2doubleprime=diff(phip2,x,2);
phib3doubleprime=diff(phib3,x,2);

a1=0.5*(DB+DP)+Cb*Cp*(HB+HP)^2/Ct/8;
a2=0.5*Cb*Cp*(HB+HP)*(1-alpha22)*Thermal/Ct;

Eng=a1*(int(phi1prime^2,x,0,
a))+.5*D1^2/(LamdaB+LamdaP)*(int(phi1doubleprime^2,x,0, a))...
    +a2*(subs(phi1,a))+0.5*((N0^2+Cb*Cp*(1-
alpha22)^2*Thermal^2)/Ct)*a...

+0.5*DB*(int(phib2prime^2,x,a,Lp))+.5*DB^2/(LamdaB)*(int(phib2doublepri
me^2,x,a, Lp))...

+0.5*DP*(int(phip2prime^2,x,a,Lp))+.5*DP^2/(LamdaP)*(int(phip2doublepri
me^2,x,a, Lp))...

+0.5*DB*(int(phib3prime^2,x,Lp,1))+.5*DB^2/(LamdaB)*(int(phib3doublepri
me^2,x,Lp, 1))+0.5*(N0^2/Cb)*aa;
F1=(LamdaB+LamdaP-N0)*(D1/(LamdaB+LamdaP))^2*phi1doubleprime^2-
N0*phi1^2+D1*phi1prime^2+2*(D1/(LamdaB+LamdaP))*N0*phi1*phi1doubleprime;
F3=(LamdaB-N0)*(DB/LamdaB)^2*phib3doubleprime^2-
N0*phib3^2+DB*phib3prime^2+2*(DB/LamdaB)*N0*phib3*phib3doubleprime;
F2=(LamdaB+LamdaP-N0)*(DB/LamdaB)^2*phib2doubleprime^2-
2*(DB/LamdaB)*(LamdaP-
N0)*phib2*phib2doubleprime+2*DP*phip2*phip2doubleprime+(LamdaP-
N0)*phib2^2-LamdaP*phip2^2+DB*phib2prime^2+DP*phip2prime^2;

totalF=(int(F1,x,0,a)+int(F2,x,a,b)+int(F3,x,b,1))/Mlamda^2;
W0=-(Mlamda/H6)*(LamdaB+LamdaP)*H5/Kb/(LamdaB+LamdaP-N0)+C13;
```

```
% Profiles for edge contact configuration with different shear stiff-
ness
clear
N0=.1:.01:40;
thermal=.1:0.1:14;
W0=[];
MemN0=[];
Energy=[];
s=size(N0,2);
matlabpool(2)
tic
y=[];
parfor i=1:size(thermal,2)
  for j=1:s
    y(i,j)=abc4(thermal(i),N0(j));
  end
  i
end
toc
matlabpool close
for i=1:size(y,1)
   plot(y(i,:))
   axis([0 320 -0.1 0.1])
   grid on
   pause(0.2)
end
for i=1:size(thermal,2)
  num=1;
for j=1:size(y,2)-1
         if y(i,j)*y(i,j+1)<0
             MemN0(i,num)=(N0(j)+N0(j+1))/2;
             num=num+1;
         end
end
end
 s2=size(MemN0,2);
for i=1:size(thermal,2)
  for j=1:s2
      if MemN0(i,j)~=0
    [Ener-
gy(i,j),W0(i,j),totalF(i,j),H6(i,j)]=WB04(thermal(i),MemN0(i,j));
      end
%     y2=[thermal(i),y(i,j)];
  end
   i
end
for i=1:size(thermal,2)
  for j=1:s2
     if abs(H6(i,j))<1e-2
        indexi=i;
        indexj=j;
        criticaltemperature=thermal(i);
        criticalmembrane=MemN0(i,j);
     end
  end
```

```
end
totalF=double(totalF);
for i=1:size(thermal,2)
    for j=1:size(MemN0,2)
        if totalF(i,j)>0
            figure(1)
            plot(thermal(i),MemN0(i,j),'o')
            hold on
        elseif totalF(i,j)<0
            plot(thermal(i),MemN0(i,j),'.')
            hold on
        end
    end
end
ylabel('Membrane force')
xlabel('Thermal Loading')
h=gcf;
saveas(h,'membrane.fig')
for i=1:size(thermal,2)
    for j=1:size(MemN0,2)
        if totalF(i,j)>0
            figure(2)
            plot(W0(i,j),thermal(i),'o')
            hold on
        elseif totalF(i,j)<0
            plot(W0(i,j),thermal(i),'.')
            hold on
        end
    end
end
xlabel('centerspan displacement')
ylabel('Thermal Loading')
h=gcf;
saveas(h,'centerspandisplacement.fig')

for i=1:size(thermal,2)
    for j=1:size(MemN0,2)
        if totalF(i,j)>0
            figure(3)
            plot(thermal(i),Energy(i,j),'o')
            hold on
        elseif totalF(i,j)<0
            plot(thermal(i),Energy(i,j),'.')
            hold on
        end
    end
end
ylabel('total energy')
xlabel('Thermal Loading')
h=gcf;
saveas(h,'totalenergy.fig')

for i=1:size(thermal,2)
    for j=1:size(MemN0,2)
        if totalF(i,j)>0
            figure(4)
```

```
            plot(thermal(i),totalF(i,j),'o')
            hold on
        elseif totalF(i,j)<0
            plot(thermal(i),totalF(i,j),'.')
            hold on
        end
    end
end
ylabel('stability analysis')
xlabel('Thermal Loading')
h=gcf;
saveas(h,'stability.fig')
savefile = 'pqfile08.mat';
save(savefile)



function y1=abc4(thermal,N0)
format long
HB=0.05;HP=0.05; a=0.8;  alpha11=.002; alpha22=.5; b=0.9; Lp=0.9;
syms x
Thermal=thermal*alpha11;
Cb=12/HB^2;
Cp=12*(HP/HB)/(HB^2);
Ct=Cb+Cp;  Bt=(1/2)*HP*Cp-(1/2)*HB*Cb;
roh=Bt/Ct;
DB=1;
DP=(HP/HB)^3;
D1=DB+DP+Cb*((1/2)*HB)^2+Cp*(HP/2)^2-roh*Bt;
DC=DB+DP;
miu=-(HB/2)*Cb+alpha22*(HP/2)*Cp;
nstar=Cb+alpha22*Cp;
mstar=miu-roh*nstar;
kb= .9;
ratio=1/2.2;
ratio1=1/2.6;
LamdaB= kb*ratio*Cb;
LamdaP= kb*ratio1*Cp;
aa=1-a;
bb=1-b;
m1=D1*(1-N0/(LamdaB+LamdaP));
m2=DC*(1-N0/(LamdaB+LamdaP));
m3=DB*(1-N0/LamdaB);
Kb=sqrt(N0/m1);
Kb3=sqrt(N0/m3);
Mlamda=mstar*Thermal+(roh+.5*HB)*N0;
m5=(1+DB/LamdaB*Kb3^2)/Kb3;
m6=(1+D1/(LamdaB+LamdaP)*Kb^2)/Kb;

f1=N0*(1/3*(Lp^3-a^3)/DP+(Lp-a)/LamdaP-a/DP*(Lp-.5*a)*(Lp-a));
f2=m5*(sin(Kb3*Lp)-sin(Kb3*a))-cos(Kb3*a)*(Lp-a);
f3=m5*(cos(Kb3*Lp)-cos(Kb3*a))-sin(Kb3*a)*(Lp-a);

H1=f1-f3*cos(Kb3*(1-Lp))/sin(Kb3);
H2=f2*cos(Kb3*Lp)-f3*sin(Kb3*Lp)+f1;
H3=-f2*cos(Kb3*(1-Lp))/sin(Kb3)-f1*cos(Kb3)/sin(Kb3);
```

```
H4=H2;
H5=(H1*f2-H3*f3)/f1/H2;

H6=(H5+H1*cos(Kb3*a)/H2+H3*sin(Kb3*a)/H4)/sin(Kb*a);
H7=-m5/sin(Kb3);
H8=H7-H5*Lp;
H9=H6*sin(Kb*a)-N0*a*(Lp-0.5*a)*H5/DP;
H11=D1*Kb*cos(Kb*a)*H6+DB*Kb3*(H1*sin(Kb3*a)-H3*cos(Kb3*a))/H2+N0*(a-
Lp)*H5;

MM=Mlamda/H11;
jj1=cos(Kb3)/sin(Kb3);
jj2=LamdaB/(LamdaB-N0);
jj3=sin(2*Kb3*Lp)-sin(2*Kb3*a);
jj4=cos(2*Kb3*Lp)-cos(2*Kb3*a);
jj5=sin(Kb3*Lp)-sin(Kb3*a);
jj6=cos(Kb3*Lp)-cos(Kb3*a);
phi1=H6*sin(Kb*x)*MM;
intW2square=MM^2*(jj2^2/H2^2*(.5*(Lp-a)*(H1^2+H3^2)-(H3^2-
H1^2)/4/Kb3*jj3-H1*H3*jj4/2/Kb3)+H5^2*(Lp-a)+jj2*2*H5/H2*(H1*jj5-
H3*jj6)/Kb3);
intW1square=MM^2*((LamdaB+LamdaP)*H6/(LamdaB+LamdaP-N0))^2*(0.5*a-
sin(2*Kb*a)/4/Kb);
intW3square=MM^2*(.5*(1-Lp)*(1+jj1)-(jj1-1)*jj3/4/Kb3+jj1*jj4/2/Kb3);
ff=-N0*(aa/Cb+a/Ct)-(1/2)*intW1square-(1/2)*intW2square-
(1/2)*intW3square-(.5*HB+roh)*(subs(phi1,  a))+(aa+a*nstar/Ct)*Thermal;  %
subs(C1,N0,1)
y1=ff;

function [Eng,W0,totalF,H6]=WB04(thermal,N0)
format long
HB=0.05;HP=0.05; a=0.8;  alpha11=.002; alpha22=.5; b=0.9; Lp=0.9;
syms x
Thermal=thermal*alpha11;
Cb=12/HB^2;
Cp=12*(HP/HB)/(HB^2);
Ct=Cb+Cp;
Bt=(1/2)*HP*Cp-(1/2)*HB*Cb;
roh=Bt/Ct;
DB=1;
DP=(HP/HB)^3;
D1=DB+DP+Cb*((1/2)*HB)^2+Cp*(HP/2)^2-roh*Bt; %D*
DC=DB+DP;
miu=-(HB/2)*Cb+alpha22*(HP/2)*Cp;
nstar=Cb+alpha22*Cp;
mstar=miu-roh*nstar;
kb= .9;
ratio=1/2.2;
ratio1=1/2.6;
LamdaB= kb*ratio*Cb;
LamdaP= kb*ratio1*Cp;
aa=1-a;
bb=1-b;
m1=D1*(1-N0/(LamdaB+LamdaP));
m2=DC*(1-N0/(LamdaB+LamdaP));
m3=DB*(1-N0/LamdaB);
```

```
m4=DP*(1-N0/LamdaP);
LAMDA=sqrt(1+LamdaP/LamdaB)*sqrt(1-LamdaP/(LamdaB+LamdaP-N0));

Kb=sqrt(N0/m1);
Kb2=sqrt(N0/m2);
Kb3=sqrt(N0/m3);
Mlamda=mstar*Thermal+(roh+.5*HB)*N0;
m5=(1+DB/LamdaB*Kb3^2)/Kb3;
m6=(1+D1/(LamdaB+LamdaP)*Kb^2)/Kb;

f1=N0*(1/3*(Lp^3-a^3)/DP+(Lp-a)/LamdaP-a/DP*(Lp-.5*a)*(Lp-a));
f2=m5*(sin(Kb3*Lp)-sin(Kb3*a))-cos(Kb3*a)*(Lp-a);
f3=m5*(cos(Kb3*Lp)-cos(Kb3*a))-sin(Kb3*a)*(Lp-a);

H1=f1-f3*cos(Kb3*(1-Lp))/sin(Kb3);
H2=f2*cos(Kb3*Lp)-f3*sin(Kb3*Lp)+f1;
H3=-f2*cos(Kb3*(1-Lp))/sin(Kb3)-f1*cos(Kb3)/sin(Kb3);
H4=H2;
H5=(H1*f2-H3*f3)/f1/H2;

H6=(H5+H1*cos(Kb3*a)/H2+H3*sin(Kb3*a)/H4)/sin(Kb*a);
H7=-m5/sin(Kb3);
H8=H7-H5*Lp;
H9=H6*sin(Kb*a)-N0*a*(Lp-0.5*a)*H5/DP;
H10=(m5*(cos(Kb3*(1-Lp)-1))/sin(Kb3)-N0*(Lp^3/DP/3+Lp/LamdaP)*H5-H9*Lp);
H11=D1*Kb*cos(Kb*a)*H6+DB*Kb3*(H1*sin(Kb3*a)-H3*cos(Kb3*a))/H2+N0*(a-
Lp)*H5;

MM=Mlamda/H11;
jj1=cos(Kb3)/sin(Kb3);

C18=(Mlamda/H11)*(m6*cos(Kb*a)*H6+N0*(a^3/DP/3+a/LamdaP)*H5+H9*a+H10);

phi1=H6*sin(Kb*x)*MM;
phib2=(H5+H1/H2*cos(Kb3*x)+H3/H4*sin(Kb3*x))*MM;
phip2=(-.5*N0/DP*H5*x^2+N0/DP*H5*Lp*x+H9)*MM;
phib3=(cos(Kb3*x)-jj1*sin(Kb3*x))*MM;
phi1prime=diff(phi1,x);
phib2prime=diff(phib2,x);
phip2prime=diff(phip2,x);
phib3prime=diff(phib3,x);

phi1doubleprime=diff(phi1,x,2);
phib2doubleprime=diff(phib2,x,2);
phip2doubleprime=diff(phip2,x,2);
phib3doubleprime=diff(phib3,x,2);

a1=0.5*(DB+DP)+Cb*Cp*(HB+HP)^2/Ct/8;
a2=0.5*Cb*Cp*(HB+HP)*(1-alpha22)*Thermal/Ct;
Eng=a1*(int(phi1prime^2,x,0,
a))+.5*D1^2/(LamdaB+LamdaP)*(int(phi1doubleprime^2,x,0, a))...
    +a2*(subs(phi1,a))+0.5*((N0^2+Cb*Cp*(1-
alpha22)^2*Thermal^2)/Ct)*a...
```

```
+0.5*DB*(int(phib2prime^2,x,a,Lp))+.5*DB^2/(LamdaB)*(int(phib2doublepri
me^2,x,a, Lp))...

+0.5*DP*(int(phip2prime^2,x,a,Lp))+.5*DP^2/(LamdaP)*(int(phip2doublepri
me^2,x,a, Lp))...

+0.5*DB*(int(phib3prime^2,x,Lp,1))+.5*DB^2/(LamdaB)*(int(phib3doublepri
me^2,x,Lp, 1))+0.5*(N0^2/Cb)*aa;
F1=(LamdaB+LamdaP-N0)*(D1/(LamdaB+LamdaP))^2*phi1doubleprime^2-
N0*phi1^2+D1*phi1prime^2+2*(D1/(LamdaB+LamdaP))*N0*phi1*phi1doubleprime;
F2=(LamdaB-N0)*(DB/LamdaB)^2*phib2doubleprime^2-
N0*phib2^2+DB*phib2prime^2+2*(DB/LamdaB)*N0*phib2*phib2doubleprime;
F3=(LamdaB-N0)*(DB/LamdaB)^2*phib3doubleprime^2-
N0*phib3^2+DB*phib3prime^2+2*(DB/LamdaB)*N0*phib3*phib3doubleprime;
G1=DP*phip2prime+DP^2*phip2doubleprime/LamdaP;
totalF=(int(F1,x,0,a)+int(F2,x,a,Lp)+int(F3,x,Lp,1)+int(G1,x,a,Lp))/Mla
mda^2;
W0=-(Mlamda/H11)*(LamdaB+LamdaP)*H6/Kb/(LamdaB+LamdaP-N0)+C18;
```

E – MATLAB code (Eye without retina)

```
clear
clc
t=4;R=12;ha=0.8; hb=2;Eb=2.4e6; Ea=2.8e6; niub=0.49; niua=0.49
[x1105,phi1105,WR1105,UR1105]=alldisplacement(t,R,10.5,ha,hb,Eb,Ea,niub
,niua)
[x11,phi111,WR111,UR111]=alldisplacement(t,R,11,ha,hb,Eb,Ea,niub,niua)
[x115,phi1115,WR1115,UR1115]=alldisplacement(t,R,11.5,ha,hb,Eb,Ea,niub,
niua)
p=[2666 3066 5333 8000 10132];  %% 20 23 40 60 76 mmHg
p1=[20 23 40 60 76]
i=size(p,2);
figure(1)
for j=1:i
  plot(x1105,WR1105(j,:),'k',x11,WR111(j,:),'k--',x115,WR1115(j,:),'k.')
   hold on
end
set(gca, 'XLim', [0 1.4])
title('\it R=12,R_{1}=10.5,11,11.5,t=4')
set(gca,'FontSize',18);
set(gca,'linewidth',1.5);
xlabel('\it \phi')
ylabel('$\bar {W}_{1}$','interpreter','latex')
box on
print -dtiff w -r600
figure(2)
for j=1:i
  plot(x1105,UR1105(j,:),'k',x11,UR111(j,:),'k--',x115,UR1115(j,:),'k.')
hold on
end
set(gca, 'XLim', [0 1.4])
 title('\it R=12,R_{1}=10.5,11,11.5,t=4')
set(gca,'FontSize',18);
set(gca,'linewidth',1.5);
xlabel('\it \phi')
ylabel('$\bar {u}$','interpreter','latex')
box on
print -dtiff u -r600
figure(3)
for j=1:i
  plot(x1105,WR1105(j,:),x1105,UR1105(j,:),'r')
  hold on
end
set(0,'DefaultFigureWindowStyle','docked');
figure(4)
figHandler = figure;
hold on
drawsameradius(x11,phi111,WR111,UR111)
hold on
circleplot(0,0,1)
xlabel(' ')
ylabel(' ')
magnify
axis equal
box on
```

```
print -dtiff samer -r600



function circleplot(x0,y0,r)
xCenter = x0;
yCenter = y0;
theta = 0 : 0.05 : 2*pi;
radius = r;
x = radius * cos(theta) + xCenter;
y = radius * sin(theta) + yCenter;
plot(x, y,'k*','MarkerSize',5);

function
drawsamepressure(x,phi1,x2,phi2,x3,phi3,WW1,UU1,WW2,UU2,WW3,UU3,i)
[x1,y1]=xycoordinates(x,phi1,WW1,UU1,i)
h1=plot([x1, fliplr(x1),-x1, fliplr(-x1)],[y1, fliplr(-y1),-y1,
fliplr(y1)],'k--')
hold on
[x1,y1]=xycoordinates(x2,phi2,WW2,UU2,i)
h2=plot([x1, fliplr(x1),-x1, fliplr(-x1)],[y1, fliplr(-y1),-y1,
fliplr(y1)],'k:')
hold on
[x1,y1]=xycoordinates(x3,phi3,WW3,UU3,i)
h3=plot([x1, fliplr(x1),-x1, fliplr(-x1)],[y1, fliplr(-y1),-y1,
fliplr(y1)],'k-.')
xlabel('\phi')
function drawsameradius(x,phi1,WW,UU)
[x1,y1]=xycoordinates(x,phi1,WW,UU,1)
h1=plot([x1, fliplr(x1),-x1, fliplr(-x1)],[y1, fliplr(-y1),-y1,
fliplr(y1)],'k','MarkerSize',2.5)
hold on
[x1,y1]=xycoordinates(x,phi1,WW,UU,2)
h2=plot([x1, fliplr(x1),-x1, fliplr(-x1)],[y1, fliplr(-y1),-y1,
fliplr(y1)],'k--')
hold on
[x1,y1]=xycoordinates(x,phi1,WW,UU,3)
h3=plot([x1, fliplr(x1),-x1, fliplr(-x1)],[y1, fliplr(-y1),-y1,
fliplr(y1)],'k:','MarkerSize',1.5)
hold on
[x1,y1]=xycoordinates(x,phi1,WW,UU,5)
h5=plot([x1, fliplr(x1),-x1, fliplr(-x1)],[y1, fliplr(-y1),-y1,
fliplr(y1)],'--','MarkerSize',5)
set(h5,'Color',[.7 .7 .7]);
legend('20','23','40','76')


function drawsamewidth(x,phi1,WW,UU)
[x1,y1]=xycoordinates(x,phi1,WW,UU,1)
h1=plot([x1, fliplr(x1),-x1, fliplr(-x1)],[y1, fliplr(-y1),-y1,
fliplr(y1)],'k','MarkerSize',2.5)
hold on
[x1,y1]=xycoordinates(x,phi1,WW,UU,2)
h2=plot([x1, fliplr(x1),-x1, fliplr(-x1)],[y1, fliplr(-y1),-y1,
fliplr(y1)],'k--')
 hold on
```

```
[x1,y1]=xycoordinates(x,phi1,WW,UU,3)
h3=plot([x1, fliplr(x1),-x1, fliplr(-x1)],[y1, fliplr(-y1),-y1,
fliplr(y1)],'k:','MarkerSize',1.5)
hold on
[x1,y1]=xycoordinates(x,phi1,WW,UU,5)
h5=plot([x1, fliplr(x1),-x1, fliplr(-x1)],[y1, fliplr(-y1),-y1,
fliplr(y1)],'--','MarkerSize',5)
set(h5,'Color',[.7 .7 .7]);
legend('20','23','40','76')


function [x1,y1]=xycoordinates(x,phi1,W,U,i)
newx=[x,phi1+0.01:0.01:pi/2];
 newterm=ones(1,size(newx,2)-size(x,2));
 xx=[real(W(i,:)),real(W(i,size(x,2)))*newterm];
 yy=[real(U(i,:)),real(U(i,size(x,2)))*newterm];
 a=pi/2-newx;
 x1=-xx.*cos(a)-yy.*sin(a)+cos(a);
 y1=-xx.*sin(a)+yy.*cos(a)+sin(a);


function deltaV=volumedifference(x,t,R,WW,UU)
for j=1:size(WW,1)
 xx=real(WW(j,:));
 yy=real(UU(j,:));
 a=pi/2-x;
 x1=-xx.*cos(a)-yy.*sin(a)+cos(a);
 y1=-xx.*sin(a)+yy.*cos(a)+sin(a);
 V=0;
 l=sqrt(x1.^2+y1.^2);
 phi=x;
 for i=2:size(l,2)-1
 l1=l(i);
 l2=l(i+1);
 phi1=phi(i);
 phi2=phi(i+1);
 r1=sin(phi1)*l1;
 r2=sin(phi2)*l2;
 deltah=cos(phi1)*l1-cos(phi2)*l2;
 V=V+1/3*pi*deltah*(r2^2+r1*r2+r1^2);
 end
tbar=t/R/2;
r2=1-real(xx(1,size(x1,2)));
r1=r2*cos(tbar);
h=real(y1(1,size(x1,2)));
deltaV(j)=2/3*pi-(V+pi/6*(3*r1^2+3*r2^2+h^2)*h);
end
```

Eye with retina

```
clear
clc

t=4;R=12;R1=10.5;ha=0.8; hb=2;Eb=2.4e6; Ea=2.8e6; niub=0.49; niua=0.49;
p=2670; p1=3170;
```

```
phi1=pi/10;  %(20-40 degree, pi/6)
phi2=pi/2-0.5*t/R;
Ca=12/(ha/R)^2;
A1=Ca*(1-niua^2)-niua^2;
Z=4*sqrt(A1);
P=-p*R^3/(Ea*ha^3/12/(1-niua^2));
P1=-p1*R^3/(Ea*ha^3/12/(1-niua^2));

Cb=12*Eb/Ea*(hb/ha)/(ha/R)^2*(t/R1)/(1-niua^2);
Db=Eb/Ea*(hb/ha)^3*(t/R1)*(R/R1)^2*(1-niub^2)/(1-niua^2);
w0=-P*cos(phi2)/(Ca*(1+niua)*2*cos(phi2)+Cb+Db);
w01=w0+1-R1/R;

apha11=(3+sqrt(5+i*Z))/4;apha12=(3+sqrt(5-i*Z))/4;
beta11=(3-sqrt(5+i*Z))/4;beta12=(3-sqrt(5-i*Z))/4;

F11=hypergeom([apha11,beta11],2,sin(phi1)^2);F12=hypergeom([apha12,beta
12],2,sin(phi1)^2);
F21=hypergeom([apha11+1,beta11+1],3,sin(phi1)^2);F22=hypergeom([apha12+
1,beta12+1],3,sin(phi1)^2);
F31=hypergeom([apha11+2,beta11+2],4,sin(phi1)^2);F32=hypergeom([apha12+
2,beta12+2],4,sin(phi1)^2);
F41=hypergeom([apha11+3,beta11+3],5,sin(phi1)^2);F42=hypergeom([apha12+
3,beta12+3],5,sin(phi1)^2);

M11=sin(phi1)*F11;M12=sin(phi1)*F12;
M21=cos(phi1)*F11+sin(phi1)^2*cos(phi1)*apha11*beta11*F21;M22=cos(phi1)
*F12+sin(phi1)^2*cos(phi1)*apha12*beta12*F22;
M31=-sin(phi1)*F11+(3*sin(phi1)*cos(phi1)^2-
sin(phi1)^3)*apha11*beta11*F21+2/3*sin(phi1)^3*cos(phi1)^2*apha11*(apha
11+1)*beta11*(beta11+1)*F31;
M32=-sin(phi1)*F12+(3*sin(phi1)*cos(phi1)^2-
sin(phi1)^3)*apha12*beta12*F22+2/3*sin(phi1)^3*cos(phi1)^2*apha12*(apha
12+1)*beta12*(beta12+1)*F32;
M41=-cos(phi1)*F11+(3*cos(phi1)^3-
10*sin(phi1)^2*cos(phi1))*apha11*beta11*F21+(4*sin(phi1)^2*cos(phi1)^3-
2*sin(phi1)^4*cos(phi1))*apha11*(apha11+1)*beta11*(beta11+1)*F31...

+1/3*sin(phi1)^4*cos(phi1)^3*apha11*(apha11+1)*(apha11+2)*beta11*(beta1
1+1)*(beta11+2)*F41;
M42=-cos(phi1)*F12+(3*cos(phi1)^3-
10*sin(phi1)^2*cos(phi1))*apha12*beta12*F22+(4*sin(phi1)^2*cos(phi1)^3-
2*sin(phi1)^4*cos(phi1))*apha12*(apha12+1)*beta12*(beta12+1)*F32...

+1/3*sin(phi1)^4*cos(phi1)^3*apha12*(apha12+1)*(apha12+2)*beta12*(beta1
2+1)*(beta12+2)*F42;

f11=hypergeom([apha11,beta11],2,sin(phi2)^2);f12=hypergeom([apha12,beta
12],2,sin(phi2)^2);
f21=hypergeom([apha11+1,beta11+1],3,sin(phi2)^2);f22=hypergeom([apha12+
1,beta12+1],3,sin(phi2)^2);
f31=hypergeom([apha11+2,beta11+2],4,sin(phi2)^2);f32=hypergeom([apha12+
2,beta12+2],4,sin(phi2)^2);
f41=hypergeom([apha11+3,beta11+3],5,sin(phi2)^2);f42=hypergeom([apha12+
3,beta12+3],5,sin(phi2)^2);
```

```
m11=sin(phi2)*f11;m12=sin(phi2)*f12;
m21=cos(phi2)*f11+sin(phi2)^2*cos(phi2)*apha11*beta11*f21;m22=cos(phi2)
*f12+sin(phi2)^2*cos(phi2)*apha12*beta12*f22;
m31=-sin(phi2)*f11+(3*sin(phi2)*cos(phi2)^2-
sin(phi2)^3)*apha11*beta11*f21+2/3*sin(phi2)^3*cos(phi2)^2*apha11*(apha
11+1)*beta11*(beta11+1)*f31;
m32=-sin(phi2)*f12+(3*sin(phi2)*cos(phi2)^2-
sin(phi2)^3)*apha12*beta12*f22+2/3*sin(phi2)^3*cos(phi2)^2*apha12*(apha
12+1)*beta12*(beta12+1)*f32;
m41=-cos(phi2)*f11+(3*cos(phi2)^3-
10*sin(phi2)^2*cos(phi2))*apha11*beta11*f21+(4*sin(phi2)^2*cos(phi2)^3-
2*sin(phi2)^4*cos(phi2))*apha11*(apha11+1)*beta11*(beta11+1)*f31...

+1/3*sin(phi2)^4*cos(phi2)^3*apha11*(apha11+1)*(apha11+2)*beta11*(beta1
1+1)*(beta11+2)*f41;
m42=-cos(phi2)*f12+(3*cos(phi2)^3-
10*sin(phi2)^2*cos(phi2))*apha12*beta12*f22+(4*sin(phi2)^2*cos(phi2)^3-
2*sin(phi2)^4*cos(phi2))*apha12*(apha12+1)*beta12*(beta12+1)*f32...

+1/3*sin(phi2)^4*cos(phi2)^3*apha12*(apha12+1)*(apha12+2)*beta12*(beta1
2+1)*(beta12+2)*f42;

a11=apha11-1/2; a12=apha12-1/2;
b11=beta11-1/2;  b12=beta12-1/2;
A11=[a11,b11,a11-1,a11-2]; A12=[a12,b12,a12-1,a12-2];
B11=[b11,a11-1,b11-1,b11-1]; B12=[b12,a12-1,b12-1,b12-1];

r1=evalin(symengine, sprintf('meijerG([[],[A11,B11]],[[0,-
1],[]],%f)',sin(phi1)^2));
GG=subs(r1);
r2=evalin(symengine, sprintf('meijerG([[],[A12,B12]],[[0,-
1],[]],%f)',sin(phi1)^2));
gg=subs(r2);
N11=sin(phi1)*GG(1); N12=sin(phi1)*gg(1);
N21=(cos(phi1)+2*cos(phi1)*(a11-1))*GG(1)-2*cos(phi1)*GG(2);
N22=(cos(phi1)+2*cos(phi1)*(a12-1))*gg(1)-2*cos(phi1)*gg(2);
N31=(sin(phi1)*2*(a11-1)*(cot(phi1)^2*(2*a11-3)-
1)+2*cos(phi1)*2*cot(phi1)*(a11-1)-
sin(phi1))*GG(1)+(sin(phi1)*(2*cot(phi1)^2*(5-2*a11-
2*b11)+2)+2*cos(phi1)*(-2*cot(phi1)))*GG(2)...
    +sin(phi1)*4*cot(phi1)^2*GG(3);
N32=(sin(phi1)*2*(a12-1)*(cot(phi1)^2*(2*a12-3)-
1)+2*cos(phi1)*2*cot(phi1)*(a12-1)-
sin(phi1))*gg(1)+(sin(phi1)*(2*cot(phi1)^2*(5-2*a12-
2*b12)+2)+2*cos(phi1)*(-2*cot(phi1)))*gg(2)...
    +sin(phi1)*4*cot(phi1)^2*gg(3);
N41=GG(1)*(3*cos(phi1)*2*(a11-1)*(cot(phi1)^2*(2*a11-3)-
1)+sin(phi1)*(4*cot(phi1)^3*(a11-1)*(a11-2)*(2*a11-3)-
4*cot(phi1)*a11*(a11-1))-cos(phi1)-3*sin(phi1)*2*cot(phi1)*(a11-1))...
    +GG(2)*(3*cos(phi1)*(2*cot(phi1)^2*(5-2*a11-
2*b11)+2)+sin(phi1)*(4*cot(phi1)^3*(3*b11+3*a11-7-2*(a11-1)^2-2*(b11-
1)^2-2*(a11-1)*(b11-1))+4*cot(phi1)*(3*b11+a11-3))-3*sin(phi1)*(-
2*cot(phi1)))...
    +GG(3)*(3*cos(phi1)*4*cot(phi1)^2+sin(phi1)*(4*cot(phi1)^3*(2*b11-
3)-12*cot(phi1)))...
    +GG(4)*sin(phi1)*(-8*cot(phi1)^3);
```

```
N42=gg(1)*(3*cos(phi1)*2*(a12-1)*(cot(phi1)^2*(2*a12-3)-
1)+sin(phi1)*(4*cot(phi1)^3*(a12-1)*(a12-2)*(2*a12-3)-
4*cot(phi1)*a12*(a12-1))-cos(phi1)-3*sin(phi1)*2*cot(phi1)*(a12-1))...
    +gg(2)*(3*cos(phi1)*(2*cot(phi1)^2*(5-2*a12-
2*b12)+2)+sin(phi1)*(4*cot(phi1)^3*(3*b12+3*a12-7-2*(a12-1)^2-2*(b12-
1)^2-2*(a12-1)*(b12-1))+4*cot(phi1)*(3*b12+a12-3))-3*sin(phi1)*(-
2*cot(phi1)))...
    +gg(3)*(3*cos(phi1)*4*cot(phi1)^2+sin(phi1)*(4*cot(phi1)^3*(2*b12-
3)-12*cot(phi1)))...
    +gg(4)*sin(phi1)*(-8*cot(phi1)^3);
r1=evalin(symengine, sprintf('meijerG([[],[A11,B11]],[[0,-
1],[]],%f)',sin(phi2)^2));
LL=subs(r1);
r2=evalin(symengine, sprintf('meijerG([[],[A12,B12]],[[0,-
1],[]],%f)',sin(phi2)^2));
ll=subs(r2);
n11=sin(phi2)*LL(1); n12=sin(phi2)*ll(1);
n21=(cos(phi2)+2*cos(phi2)*(a11-1))*LL(1)-2*cos(phi2)*LL(2);
n22=(cos(phi2)+2*cos(phi2)*(a12-1))*ll(1)-2*cos(phi2)*ll(2);
n31=(sin(phi2)*2*(a11-1)*(cot(phi2)^2*(2*a11-3)-
1)+2*cos(phi2)*2*cot(phi2)*(a11-1)-
sin(phi2))*LL(1)+(sin(phi2)*(2*cot(phi2)^2*(5-2*a11-
2*b11)+2)+2*cos(phi2)*(-2*cot(phi2)))*LL(2)...
    +sin(phi2)*4*cot(phi2)^2*LL(3);
n32=(sin(phi2)*2*(a12-1)*(cot(phi2)^2*(2*a12-3)-
1)+2*cos(phi2)*2*cot(phi2)*(a12-1)-
sin(phi2))*ll(1)+(sin(phi2)*(2*cot(phi2)^2*(5-2*a12-
2*b12)+2)+2*cos(phi2)*(-2*cot(phi2)))*ll(2)...
    +sin(phi2)*4*cot(phi2)^2*ll(3);
n41=LL(1)*(3*cos(phi2)*2*(a11-1)*(cot(phi2)^2*(2*a11-3)-
1)+sin(phi2)*(4*cot(phi2)^3*(a11-1)*(a11-2)*(2*a11-3)-
4*cot(phi2)*a11*(a11-1))-cos(phi2)-3*sin(phi2)*2*cot(phi2)*(a11-1))...
    +LL(2)*(3*cos(phi2)*(2*cot(phi2)^2*(5-2*a11-
2*b11)+2)+sin(phi2)*(4*cot(phi2)^3*(3*b11+3*a11-7-2*(a11-1)^2-2*(b11-
1)^2-2*(a11-1)*(b11-1))+4*cot(phi2)*(3*b11+a11-3))-3*sin(phi2)*(-
2*cot(phi2)))...
    +LL(3)*(3*cos(phi2)*4*cot(phi2)^2+sin(phi2)*(4*cot(phi2)^3*(2*b11-
3)-12*cot(phi2)))...
    +LL(4)*sin(phi2)*(-8*cot(phi2)^3);
n42=ll(1)*(3*cos(phi2)*2*(a12-1)*(cot(phi2)^2*(2*a12-3)-
1)+sin(phi2)*(4*cot(phi2)^3*(a12-1)*(a12-2)*(2*a12-3)-
4*cot(phi2)*a12*(a12-1))-cos(phi2)-3*sin(phi2)*2*cot(phi2)*(a12-1))...
    +ll(2)*(3*cos(phi2)*(2*cot(phi2)^2*(5-2*a12-
2*b12)+2)+sin(phi2)*(4*cot(phi2)^3*(3*b12+3*a12-7-2*(a12-1)^2-2*(b12-
1)^2-2*(a12-1)*(b12-1))+4*cot(phi2)*(3*b12+a12-3))-3*sin(phi2)*(-
2*cot(phi2)))...
    +ll(3)*(3*cos(phi2)*4*cot(phi2)^2+sin(phi2)*(4*cot(phi2)^3*(2*b12-
3)-12*cot(phi2)))...
    +ll(4)*sin(phi2)*(-8*cot(phi2)^3);

l1=1/Ca/(1-niua);l2=1/Ca/(1+niua);l3=1/Ca/(1-niua^2);

%%%%%%%%%%%%%%%%%%%%%%%%%%%%%%%%%%%%%%%%%%
g=log(cot(phi1/2));
g1=g*sin(phi1)+cot(phi1);g2=g*cos(phi1)-1-csc(phi1)^2;
```

```
K11=M11; K12=M12; K13=-1/l1*sin(phi1); K14=-K11; K15=-K12;K16=-
N11;K17=-N12;K18=-g1; K19=-K13;
K21=M21; K22=M22; K23=-1/l1*cos(phi1); K24=-K21; K25=-K22; K26=-N21;
K27=-N22; K28=-g2; K29=-K23;
K31=M21+M11*cot(phi1); K32=M22+M12*cot(phi1); K33=-1/l3*cos(phi1);
K34=-K31; K35=-K32; K36=-(N21+N11*cot(phi1));
K37=-(N22+N12*cot(phi1)); K38=l1/l3*(1-g*cos(phi1)); K39=1/l3*cos(phi1);
K41=M31+M21*cot(phi1)-M11*csc(phi1)^2; K42=M32+M22*cot(phi1)-
M12*csc(phi1)^2; K43=sin(phi1)/l3;
K44=-K41; K45=-K42; K46=-(N31+N21*cot(phi1)-N11*csc(phi1)^2); K47=-
(N32+N22*cot(phi1)-N12*csc(phi1)^2);
K48=l1/l3*g1; K49=-K43;
K51=M41+M31*cot(phi1)-2*csc(phi1)^2*M21+M11*2*cot(phi1)*csc(phi1)^2;
K52=M42+M32*cot(phi1)-2*csc(phi1)^2*M22+M12*2*cot(phi1)*csc(phi1)^2;
K53=K39; K54=-K51; K55=-K52;
K56=-(N41+N31*cot(phi1)-2*csc(phi1)^2*N21+N11*2*cot(phi1)*csc(phi1)^2);
K57=-(N42+N32*cot(phi1)-2*csc(phi1)^2*N22+N12*2*cot(phi1)*csc(phi1)^2);
K58=l1/l3*g2; K59=-K53;
K61=M11; K62=M12; K63=0; K64=-K61; K65=-K62; K66=-N11; K67=-N12; K68=0;
K69=0;
P11=0.5*P*g1; P21=0.5*P*g2;P31=0.5*P1*l2/l3-P*(1-
0.5*(1+niua)*g*cos(phi1));P41=-0.5*P*l1/l3*g1;P51=-0.5*P*l1/l3*g2;
P61=0;

g=log(cot(phi2/2));
g1=g*sin(phi2)+cot(phi2);g2=g*cos(phi2)-1-csc(phi2)^2;

K71=0;K72=0;K73=0;K74=m11; K75=m12; K76=n11; K77=n12; K78=g1;    K79=-
sin(phi2)/l1;
K81=0; K82=0; K83=0; K84=m21+m11*cot(phi2); K85=m22+m12*cot(phi2);
K86=n21+n11*cot(phi2);K87=n22+n12*cot(phi2);  K88=-l1/l3*(1-g*cos(phi2));
K89=-cos(phi2)/l3;

K91=0; K92=0; K93=0; K94=m31+m21*cot(phi2)-
m11*csc(phi2)^2;K95=m32+m22*cot(phi2)-m12*csc(phi2)^2;
K96=n31+n21*cot(phi2)-n11*csc(phi2)^2;K97=n32+n22*cot(phi2)-
n12*csc(phi2)^2; K98=-l1/l3*g1; K99=sin(phi2)/l3;
P71=-0.5*P*g1; P81=P*(1-0.5*(1+niua)*g*cos(phi2))-w01/l3;
P91=0.5*P*l1/l3*g1;

K=[K11 K12 K13 K14 K15 K16 K17 K18 K19;
    K21 K22 K23 K24 K25 K26 K27 K28 K29;
    K31 K32 K33 K34 K35 K36 K37 K38 K39;
    K41 K42 K43 K44 K45 K46 K47 K48 K49;
    K51 K52 K53 K54 K55 K56 K57 K58 K59;
    K61 K62 K63 K64 K65 K66 K67 K68 K69;
    K71 K72 K73 K74 K75 K76 K77 K78 K79;
    K81 K82 K83 K84 K85 K86 K87 K88 K89;
    K91 K92 K93 K94 K95 K96 K97 K98 K99];
F=[P11 P21 P31 P41 P51 P61 P71 P81 P91]';
COE=inv(K)*F

A1=COE(1); A2=COE(2);A6=COE(3);
B1=COE(4);B2=COE(5);B3=COE(6);B4=COE(7);B5=COE(8);B6=COE(9);
phi=0.00235:0.01:phi1;
```

```
Gphi=log(cos(phi./2))-log(sin(phi./2));
Q=A1*sin(phi).*hypergeom([apha11,beta11],2,sin(phi).^2)+A2.*sin(phi).*h
ypergeom([apha12,beta12],2,sin(phi).^2);
Qprime=A1.*(cos(phi).*hypergeom([apha11,beta11],2,sin(phi).^2)+sin(phi)
.^2.*cos(phi)*apha11*beta11.*hypergeom([apha11+1,beta11+1],3,sin(phi).^
2))+...

A2.*(cos(phi).*hypergeom([apha12,beta12],2,sin(phi).^2)+sin(phi).^2.*co
s(phi)*apha12*beta12.*hypergeom([apha12+1,beta12+1],3,sin(phi).^2));


w1=A6*cos(phi)-l3*(Qprime+Q.*cot(phi))+l2*P1*0.5 ;
u1=A6*sin(phi)-l1*Q;
w1primephi1=A6*K43*(-l3)+A1*K41*(-l3)+A2*K42*(-l3);
plot(phi,w1)
x=phi1:0.01:phi2;
for i=1:size(x,2)
    GGG1(i)=subs(evalin(symengine,
sprintf('meijerG([[],[a11,b11]],[[0,-1],[]],%f)',sin(x(i))^2)));
    GGG2(i)=subs(evalin(symengine,
sprintf('meijerG([[],[a12,b12]],[[0,-1],[]],%f)',sin(x(i))^2)));
    GGG3(i)=subs(evalin(symengine, sprintf('meijerG([[],[b11,a11-
1]],[[0,-1],[]],%f)',sin(x(i))^2)));
    GGG4(i)=subs(evalin(symengine, sprintf('meijerG([[],[b12,a12-
1]],[[0,-1],[]],%f)',sin(x(i))^2)));
end
Q2=B1.*sin(x).*hypergeom([apha11,beta11],2,sin(x).^2)+B2.*sin(x).*hyper
geom([apha12,beta12],2,sin(x).^2)+...
    B3.*sin(x).*GGG1+B4.*sin(x).*GGG2;
Q2prime=B1.*(cos(x).*hypergeom([apha11,beta11],2,sin(x).^2)+sin(x).^2.*
cos(x)*apha11*beta11.*hypergeom([apha11+1,beta11+1],3,sin(x).^2))+...
B2.*(cos(x).*hypergeom([apha12,beta12],2,sin(x).^2)+sin(x).^2.*cos(x)*a
pha12*      beta12.*hypergeom([apha12+1,beta12+1],3,sin(x).^2))...
+B3.*{(cos(x)+2*cos(x).*(a11-1)).*GGG1-2*cos(x).*GGG3}...
+B4.*{(cos(x)+2*cos(x).*(a12-1)).*GGG2-2*cos(x).*GGG4};

lo=log(cot(x/2));
w2=B6*cos(x)-l3.*(Q2prime+Q2.*cot(x))+l3*P.*(1-
0.5*(1+niua)*lo.*cos(x))+l1*B5.*(1-lo.*cos(x));
u2=B6*sin(x)-l1*(Q2+(0.5*P+B5).*(cot(x)+lo.*sin(x)));

plot(x,w2)
figure(1)
plot(phi,w1,x,w2)
figure(2)
plot(phi,u1,x,u2)
w1=double(w1); u1=double(u1);
w2=double(w2); u2=double(u2);
[x1,y1]=xycoordinates(phi,x,phi2,w1,u1,w2,u2,1);

plot(x1,y1)
h1=plot([x1, fliplr(x1),-x1, fliplr(-x1)],[y1, fliplr(-y1),-y1,
fliplr(y1)],'b');
hold on
syms c d
h=ezplot('c^2+d^2=1');
```

```
set(h, 'Color', 'm','LineStyle',':');
axis([-1.5,1.5,-1.5,1.5],'square')
xlabel(' ')
ylabel(' ')

Include the retina

Er=0.03e6;
hr=0.2;
niur=0.49; Rr=11.5; pr=p1-p;
wr0=w2(1);
Cr=12*Er/Ea*(hr/ha)*(R/ha)^2/(1-niua^2);
Dr=Er/Ea*(hr/ha)^3*(R/Rr)^2*(1-niur^2)/(1-niua^2);
Br=Cr/Dr*(1-niur^2)-niur^2;
Zr=4*sqrt(Br);
Pr=pr*Rr^3/(Ea*ha^3/12/(1-niua^2));
[v1,v2]=aa(Zr)
rapha11=(3+v1)/4;rapha12=(3+v2)/4;
rbeta11=(3-v1)/4;rbeta12=(3-v2)/4;

F11r=hypergeom([rapha11,rbeta11],2,sin(phi1)^2);F12r=hypergeom([rapha12
,rbeta12],2,sin(phi1)^2);
F21r=hypergeom([rapha11+1,rbeta11+1],3,sin(phi1)^2);F22r=hypergeom([rap
ha12+1,rbeta12+1],3,sin(phi1)^2);
F31r=hypergeom([rapha11+2,rbeta11+2],4,sin(phi1)^2);F32r=hypergeom([rap
ha12+2,rbeta12+2],4,sin(phi1)^2);

M11r=sin(phi1)*F11r;M12r=sin(phi1)*F12r;
M21r=cos(phi1)*F11r+sin(phi1)^2*cos(phi1)*rapha11*rbeta11*F21r;M22r=cos
(phi1)*F12r+sin(phi1)^2*cos(phi1)*rapha12*rbeta12*F22r;
M31r=-sin(phi1)*F11r+(3*sin(phi1)*cos(phi1)^2-
sin(phi1)^3)*rapha11*rbeta11*F21r+2/3*sin(phi1)^3*cos(phi1)^2*rapha11*(
rapha11+1)*rbeta11*(rbeta11+1)*F31r;
M32r=-sin(phi1)*F12r+(3*sin(phi1)*cos(phi1)^2-
sin(phi1)^3)*rapha12*rbeta12*F22r+2/3*sin(phi1)^3*cos(phi1)^2*rapha12*(
rapha12+1)*rbeta12*(rbeta12+1)*F32r;

l1r=Dr/Cr/(1-niur);l2r=1/Cr/(1+niur);l3r=Dr/Cr/(1-niur^2);
KK11r=M11r*l1r; KK12r=M12r*l1r; KK13r=-sin(phi1);
KK21r=(M21r+M11r*cot(phi1))*l3r; KK22r=(M22r+M12r*cot(phi1))*l3r;
KK23r=-cos(phi1);
KK31r=(M31r+M21r*cot(phi1)-M11r*csc(phi1)^2)*l3r;
KK32r=(M32r+M22r*cot(phi1)-M12r*csc(phi1)^2)*l3r;
KK33r=sin(phi1);

F1r=-u2(1)+0.5*(ha+hr)/R*w1primephi1;
F2r=0.5*l2r*Pr-wr0;
F3r=w1primephi1;

KKr=[KK11r KK12r KK13r;
    KK21r KK22r KK23r;
    KK31r KK32r KK33r];
Fr=[F1r;F2r;F3r];
COEr=inv(KKr)*Fr
A1r=COEr(1); A2r=COEr(2);A6r=COEr(3);
phi=0.00235:0.01:phi1;
```

```
Qr=A1r*sin(phi).*hypergeom([rapha11,rbeta11],2,sin(phi).^2)+A2r.*sin(ph
i).*hypergeom([rapha12,rbeta12],2,sin(phi).^2);
Qrprime=A1r.*(cos(phi).*hypergeom([rapha11,rbeta11],2,sin(phi).^2)+sin(
phi).^2.*cos(phi)*rapha11*rbeta11.*hypergeom([rapha11+1,rbeta11+1],3,si
n(phi).^2))+...

A2r.*(cos(phi).*hypergeom([rapha12,rbeta12],2,sin(phi).^2)+sin(phi).^2.
*cos(phi)*rapha12*rbeta12.*hypergeom([rapha12+1,rbeta12+1],3,sin(phi).^
2));

wr=A6r*cos(phi)-l3r*(Qrprime+Qr.*cot(phi))+l2r*Pr*0.5+1-Rr/R ;
ur=A6r*sin(phi)-l1r*Qr;
figure(3)
plot(phi,wr,'k.',phi,w1,'k.',x,w2,'k.','MarkerSize',3)
hold on
plot(phi,w1+ha/2/R,'k-.',phi,w1-ha/2/R,'k-.',x,w2+ha/2/R,'k--',x,w2-
ha/2/R,'k--')
hold on
plot(phi,wr+hr/2/R,'k',phi,wr-hr/2/R,'k')
xlabel('\phi')
ylabel('w')

figure(5)
plot(phi(1:size(phi,2)-1),ur(1:size(phi,2)-1),'k',phi,u1,'k-.',x,u2,'k-
-')
xlabel('\phi')
ylabel('u')
a=pi/2-phi; ro=0.9;
xx=real(wr);yy=real(ur);
xr=-xx.*cos(a)-yy.*sin(a)+cos(a);
yr=-xx.*sin(a)+yy.*cos(a)+sin(a);
yrfinal=(cos(phi1)-ro).*xr/sin(phi1)+yr;
figure(6)
plot(xr,yr,x1,y1)
xx=real(wr+hr/2/R);yy=real(ur);
xr1=xr+(hr/2)/R*cos(a);
yr1=yr+(hr/2)/R*sin(a);
yrfinal=(cos(phi1)-ro).*xr/sin(phi1)+yr;
xx=real(wr-hr/2/R);yy=real(ur);
xr2=xr+(-hr/2)/R*cos(a);
yr2=yr+(-hr/2)/R*sin(a);
bb=0.00235:0.01:pi/2;
bb=pi/2-bb;
figure(7)
plot(xr,yr,'k:',x1,y1,'k:','MarkerSize',3)
hold on
plot(x1-(ha/2)/R*cos(bb),y1-(ha/2)/R*sin(bb),'k--
',x1+(ha/2)/R*cos(bb),y1+(ha/2)/R*sin(bb),'k--')
hold on
plot(xr1,yr1,'k',xr2,yr2,'k')
axis([0,1.2,0,1.2])
figure(8)
plot([x1, fliplr(x1),-x1, fliplr(-x1)],[y1, fliplr(-y1),-y1,
fliplr(y1)],'k--')
```

F – MATLAB code (Eye with retina)

```
clear
clc

t=4;R=12;R1=11;ha=0.8; hb=2;Eb=2.4e6; Ea=.03e6; niub=0.3; niua=0.3;
p=3000; p1=3100;
phi1=pi/10;  %(20-40 degree, pi/6)
phi2=pi/2-0.5*t/R;
Ca=12/(ha/R)^2;
Cb=12*(R1/ha)^2*(hb/ha)*(Eb/Ea)*(1-niua^2)/(1-niub^2);
A1=Ca*(1-niua^2)-niua^2;
Z=4*sqrt(A1);
P=p*R^3/(Ea*ha^3/12/(1-niua^2));
P1=p1*R^3/(Ea*ha^3/12/(1-niua^2));

Cr=12*Eb/Ea*(hb/ha)/(ha/R)^2*(t/R1);
Dr=Eb/Ea*(hb/ha)^3*(t/R1)*(R/R1)^2;
w0=-P*cos(phi2)/(Ca*(1+niua)*2*cos(phi2)+Cr+Dr);
w01=w0+1-R1/R;

apha11=(3+sqrt(5+i*Z))/4;apha12=(3+sqrt(5-i*Z))/4;
beta11=(3-sqrt(5+i*Z))/4;beta12=(3-sqrt(5-i*Z))/4;

F11=hypergeom([apha11,beta11],2,sin(phi1)^2);F12=hypergeom([apha12,beta
12],2,sin(phi1)^2);
F21=hypergeom([apha11+1,beta11+1],3,sin(phi1)^2);F22=hypergeom([apha12+
1,beta12+1],3,sin(phi1)^2);
F31=hypergeom([apha11+2,beta11+2],4,sin(phi1)^2);F32=hypergeom([apha12+
2,beta12+2],4,sin(phi1)^2);
F41=hypergeom([apha11+3,beta11+3],5,sin(phi1)^2);F42=hypergeom([apha12+
3,beta12+3],5,sin(phi1)^2);

M11=sin(phi1)*F11;M12=sin(phi1)*F12;
M21=cos(phi1)*F11+sin(phi1)^2*cos(phi1)*apha11*beta11*F21;M22=cos(phi1)
*F12+sin(phi1)^2*cos(phi1)*apha12*beta12*F22;
M31=-sin(phi1)*F11+(3*sin(phi1)*cos(phi1)^2-
sin(phi1)^3)*apha11*beta11*F21+2/3*sin(phi1)^3*cos(phi1)^2*apha11*(apha
11+1)*beta11*(beta11+1)*F31;
M32=-sin(phi1)*F12+(3*sin(phi1)*cos(phi1)^2-
sin(phi1)^3)*apha12*beta12*F22+2/3*sin(phi1)^3*cos(phi1)^2*apha12*(apha
12+1)*beta12*(beta12+1)*F32;
M41=-cos(phi1)*F11+(3*cos(phi1)^3-
10*sin(phi1)^2*cos(phi1))*apha11*beta11*F21+(4*sin(phi1)^2*cos(phi1)^3-
2*sin(phi1)^4*cos(phi1))*apha11*(apha11+1)*beta11*(beta11+1)*F31...

+1/3*sin(phi1)^4*cos(phi1)^3*apha11*(apha11+1)*(apha11+2)*beta11*(beta1
1+1)*(beta11+2)*F41;
M42=-cos(phi1)*F12+(3*cos(phi1)^3-
10*sin(phi1)^2*cos(phi1))*apha12*beta12*F22+(4*sin(phi1)^2*cos(phi1)^3-
2*sin(phi1)^4*cos(phi1))*apha12*(apha12+1)*beta12*(beta12+1)*F32...

+1/3*sin(phi1)^4*cos(phi1)^3*apha12*(apha12+1)*(apha12+2)*beta12*(beta1
2+1)*(beta12+2)*F42;
```

```
f11=hypergeom([apha11,beta11],2,sin(phi2)^2);f12=hypergeom([apha12,beta
12],2,sin(phi2)^2);
f21=hypergeom([apha11+1,beta11+1],3,sin(phi2)^2);f22=hypergeom([apha12+
1,beta12+1],3,sin(phi2)^2);
f31=hypergeom([apha11+2,beta11+2],4,sin(phi2)^2);f32=hypergeom([apha12+
2,beta12+2],4,sin(phi2)^2);
f41=hypergeom([apha11+3,beta11+3],5,sin(phi2)^2);f42=hypergeom([apha12+
3,beta12+3],5,sin(phi2)^2);

m11=sin(phi2)*f11;m12=sin(phi2)*f12;
m21=cos(phi2)*f11+sin(phi2)^2*cos(phi2)*apha11*beta11*f21;m22=cos(phi2)
*f12+sin(phi2)^2*cos(phi2)*apha12*beta12*f22;
m31=-sin(phi2)*f11+(3*sin(phi2)*cos(phi2)^2-
sin(phi2)^3)*apha11*beta11*f21+2/3*sin(phi2)^3*cos(phi2)^2*apha11*(apha
11+1)*beta11*(beta11+1)*f31;
m32=-sin(phi2)*f12+(3*sin(phi2)*cos(phi2)^2-
sin(phi2)^3)*apha12*beta12*f22+2/3*sin(phi2)^3*cos(phi2)^2*apha12*(apha
12+1)*beta12*(beta12+1)*f32;
m41=-cos(phi2)*f11+(3*cos(phi2)^3-
10*sin(phi2)^2*cos(phi2))*apha11*beta11*f21+(4*sin(phi2)^2*cos(phi2)^3-
2*sin(phi2)^4*cos(phi2))*apha11*(apha11+1)*beta11*(beta11+1)*f31...

+1/3*sin(phi2)^4*cos(phi2)^3*apha11*(apha11+1)*(apha11+2)*beta11*(beta1
1+1)*(beta11+2)*f41;
m42=-cos(phi2)*f12+(3*cos(phi2)^3-
10*sin(phi2)^2*cos(phi2))*apha12*beta12*f22+(4*sin(phi2)^2*cos(phi2)^3-
2*sin(phi2)^4*cos(phi2))*apha12*(apha12+1)*beta12*(beta12+1)*f32...

+1/3*sin(phi2)^4*cos(phi2)^3*apha12*(apha12+1)*(apha12+2)*beta12*(beta1
2+1)*(beta12+2)*f42;

a11=apha11-1/2; a12=apha12-1/2;
b11=beta11-1/2;  b12=beta12-1/2;
A11=[a11,b11,a11-1,a11-2]; A12=[a12,b12,a12-1,a12-2];
B11=[b11,a11-1,b11-1,b11-1]; B12=[b12,a12-1,b12-1,b12-1];

r1=evalin(symengine, sprintf('meijerG([[],[A11,B11]],[[0,-
1],[]],%f)',sin(phi1)^2));
%sin()^2 is equavalent to z
GG=subs(r1);
r2=evalin(symengine, sprintf('meijerG([[],[A12,B12]],[[0,-
1],[]],%f)',sin(phi1)^2));
gg=subs(r2);
N11=sin(phi1)*GG(1); N12=sin(phi1)*gg(1);
N21=(cos(phi1)+2*cos(phi1)*(a11-1))*GG(1)-2*cos(phi1)*GG(2);
N22=(cos(phi1)+2*cos(phi1)*(a12-1))*gg(1)-2*cos(phi1)*gg(2);
N31=(sin(phi1)*2*(a11-1)*(cot(phi1)^2*(2*a11-3)-
1)+2*cos(phi1)*2*cot(phi1)*(a11-1)-
sin(phi1))*GG(1)+(sin(phi1)*(2*cot(phi1)^2*(5-2*a11-
2*b11)+2)+2*cos(phi1)*(-2*cot(phi1)))*GG(2)...
    +sin(phi1)*4*cot(phi1)^2*GG(3);
N32=(sin(phi1)*2*(a12-1)*(cot(phi1)^2*(2*a12-3)-
1)+2*cos(phi1)*2*cot(phi1)*(a12-1)-
sin(phi1))*gg(1)+(sin(phi1)*(2*cot(phi1)^2*(5-2*a12-
2*b12)+2)+2*cos(phi1)*(-2*cot(phi1)))*gg(2)...
    +sin(phi1)*4*cot(phi1)^2*gg(3);
```

```
N41=GG(1)*(3*cos(phi1)*2*(a11-1)*(cot(phi1)^2*(2*a11-3)-
1)+sin(phi1)*(4*cot(phi1)^3*(a11-1)*(a11-2)*(2*a11-3)-
4*cot(phi1)*a11*(a11-1))-cos(phi1)-3*sin(phi1)*2*cot(phi1)*(a11-1))...
    +GG(2)*(3*cos(phi1)*(2*cot(phi1)^2*(5-2*a11-
2*b11)+2)+sin(phi1)*(4*cot(phi1)^3*(3*b11+3*a11-7-2*(a11-1)^2-2*(b11-
1)^2-2*(a11-1)*(b11-1))+4*cot(phi1)*(3*b11+a11-3))-3*sin(phi1)*(-
2*cot(phi1)))...
    +GG(3)*(3*cos(phi1)*4*cot(phi1)^2+sin(phi1)*(4*cot(phi1)^3*(2*b11-
3)-12*cot(phi1)))...
    +GG(4)*sin(phi1)*(-8*cot(phi1)^3);
N42=gg(1)*(3*cos(phi1)*2*(a12-1)*(cot(phi1)^2*(2*a12-3)-
1)+sin(phi1)*(4*cot(phi1)^3*(a12-1)*(a12-2)*(2*a12-3)-
4*cot(phi1)*a12*(a12-1))-cos(phi1)-3*sin(phi1)*2*cot(phi1)*(a12-1))...
    +gg(2)*(3*cos(phi1)*(2*cot(phi1)^2*(5-2*a12-
2*b12)+2)+sin(phi1)*(4*cot(phi1)^3*(3*b12+3*a12-7-2*(a12-1)^2-2*(b12-
1)^2-2*(a12-1)*(b12-1))+4*cot(phi1)*(3*b12+a12-3))-3*sin(phi1)*(-
2*cot(phi1)))...
    +gg(3)*(3*cos(phi1)*4*cot(phi1)^2+sin(phi1)*(4*cot(phi1)^3*(2*b12-
3)-12*cot(phi1)))...
    +gg(4)*sin(phi1)*(-8*cot(phi1)^3);
r1=evalin(symengine, sprintf('meijerG([[],[A11,B11]],[[0,-
1],[]],%f)',sin(phi2)^2));
LL=subs(r1);
r2=evalin(symengine, sprintf('meijerG([[],[A12,B12]],[[0,-
1],[]],%f)',sin(phi2)^2));
ll=subs(r2);
n11=sin(phi2)*LL(1); n12=sin(phi2)*ll(1);
n21=(cos(phi2)+2*cos(phi2)*(a11-1))*LL(1)-2*cos(phi2)*LL(2);
n22=(cos(phi2)+2*cos(phi2)*(a12-1))*ll(1)-2*cos(phi2)*ll(2);
n31=(sin(phi2)*2*(a11-1)*(cot(phi2)^2*(2*a11-3)-
1)+2*cos(phi2)*2*cot(phi2)*(a11-1)-
sin(phi2))*LL(1)+(sin(phi2)*(2*cot(phi2)^2*(5-2*a11-
2*b11)+2)+2*cos(phi2)*(-2*cot(phi2)))*LL(2)...
    +sin(phi2)*4*cot(phi2)^2*LL(3);
n32=(sin(phi2)*2*(a12-1)*(cot(phi2)^2*(2*a12-3)-
1)+2*cos(phi2)*2*cot(phi2)*(a12-1)-
sin(phi2))*ll(1)+(sin(phi2)*(2*cot(phi2)^2*(5-2*a12-
2*b12)+2)+2*cos(phi2)*(-2*cot(phi2)))*ll(2)...
    +sin(phi2)*4*cot(phi2)^2*ll(3);
n41=LL(1)*(3*cos(phi2)*2*(a11-1)*(cot(phi2)^2*(2*a11-3)-
1)+sin(phi2)*(4*cot(phi2)^3*(a11-1)*(a11-2)*(2*a11-3)-
4*cot(phi2)*a11*(a11-1))-cos(phi2)-3*sin(phi2)*2*cot(phi2)*(a11-1))...
    +LL(2)*(3*cos(phi2)*(2*cot(phi2)^2*(5-2*a11-
2*b11)+2)+sin(phi2)*(4*cot(phi2)^3*(3*b11+3*a11-7-2*(a11-1)^2-2*(b11-
1)^2-2*(a11-1)*(b11-1))+4*cot(phi2)*(3*b11+a11-3))-3*sin(phi2)*(-
2*cot(phi2)))...
    +LL(3)*(3*cos(phi2)*4*cot(phi2)^2+sin(phi2)*(4*cot(phi2)^3*(2*b11-
3)-12*cot(phi2)))...
    +LL(4)*sin(phi2)*(-8*cot(phi2)^3);
n42=ll(1)*(3*cos(phi2)*2*(a12-1)*(cot(phi2)^2*(2*a12-3)-
1)+sin(phi2)*(4*cot(phi2)^3*(a12-1)*(a12-2)*(2*a12-3)-
4*cot(phi2)*a12*(a12-1))-cos(phi2)-3*sin(phi2)*2*cot(phi2)*(a12-1))...
    +ll(2)*(3*cos(phi2)*(2*cot(phi2)^2*(5-2*a12-
2*b12)+2)+sin(phi2)*(4*cot(phi2)^3*(3*b12+3*a12-7-2*(a12-1)^2-2*(b12-
1)^2-2*(a12-1)*(b12-1))+4*cot(phi2)*(3*b12+a12-3))-3*sin(phi2)*(-
2*cot(phi2)))...
```

```
    +ll(3)*(3*cos(phi2)*4*cot(phi2)^2+sin(phi2)*(4*cot(phi2)^3*(2*b12-
3)-12*cot(phi2)))...
    +ll(4)*sin(phi2)*(-8*cot(phi2)^3);

l1=1/Ca/(1-niua);l2=1/Ca/(1+niua);l3=1/Ca/(1-niua^2);

%%%%%%%%%%%%%%%%%%%%%%%%%%%%%%%%%%%%%%%%%%%%%%%%%%%%%%%%%%%%%%%%%%%%%%%%%%%%
g=log(cot(phi1/2));
g1=g*sin(phi1)+cot(phi1);g2=g*cos(phi1)-1-csc(phi1)^2;
K11=M11; K12=M12; K13=-1/l1*sin(phi1); K14=-K11; K15=-K12;K16=-
N11;K17=-N12;K18=-g1; K19=-K13;
K21=M21; K22=M22; K23=-1/l1*cos(phi1); K24=-K21; K25=-K22; K26=-N21;
K27=-N22; K28=-g2; K29=-K23;
K31=M21+M11*cot(phi1); K32=M22+M12*cot(phi1); K33=-1/l3*cos(phi1);
K34=-K31; K35=-K32; K36=-(N21+N11*cot(phi1));
K37=-(N22+N12*cot(phi1)); K38=l1/l3*(1-g*cos(phi1)); K39=1/l3*cos(phi1);
K41=M31+M21*cot(phi1)-M11*csc(phi1)^2; K42=M32+M22*cot(phi1)-
M12*csc(phi1)^2; K43=sin(phi1)/l3;
K44=-K41; K45=-K42; K46=-(N31+N21*cot(phi1)-N11*csc(phi1)^2); K47=-
(N32+N22*cot(phi1)-N12*csc(phi1)^2);
K48=l1/l3*g1; K49=-K43;
K51=M41+M31*cot(phi1)-2*csc(phi1)^2*M21+M11*2*cot(phi1)*csc(phi1)^2;
K52=M42+M32*cot(phi1)-2*csc(phi1)^2*M22+M12*2*cot(phi1)*csc(phi1)^2;
K53=K39; K54=-K51; K55=-K52;
K56=-(N41+N31*cot(phi1)-2*csc(phi1)^2*N21+N11*2*cot(phi1)*csc(phi1)^2);
K57=-(N42+N32*cot(phi1)-2*csc(phi1)^2*N22+N12*2*cot(phi1)*csc(phi1)^2);
K58=l1/l3*g2; K59=-K53;
K61=M11; K62=M12; K63=0; K64=-K61; K65=-K62; K66=-N11; K67=-N12; K68=0;
K69=0;
P11=0.5*P*g1; P21=0.5*P*g2;P31=0.5*P1*l2/l3-P*(1-
0.5*(1+niua)*g*cos(phi1));P41=-0.5*P*l1/l3*g1;P51=-0.5*P*l1/l3*g2;
P61=0;

g=log(cot(phi2/2));
g1=g*sin(phi2)+cot(phi2);g2=g*cos(phi2)-1-csc(phi2)^2;

K71=0;K72=0;K73=0;K74=m11; K75=m12; K76=n11; K77=n12; K78=g1;    K79=-
sin(phi2)/l1;
K81=0; K82=0; K83=0; K84=m21+m11*cot(phi2); K85=m22+m12*cot(phi2);
K86=n21+n11*cot(phi2);K87=n22+n12*cot(phi2);  K88=-l1/l3*(1-g*cos(phi2));
K89=-cos(phi2)/l3;

K91=0; K92=0; K93=0; K94=m31+m21*cot(phi2)-
m11*csc(phi2)^2;K95=m32+m22*cot(phi2)-m12*csc(phi2)^2;
K96=n31+n21*cot(phi2)-n11*csc(phi2)^2;K97=n32+n22*cot(phi2)-
n12*csc(phi2)^2; K98=-l1/l3*g1; K99=sin(phi2)/l3;
P71=-0.5*P*g1; P81=P*(1-0.5*(1+niua)*g*cos(phi2))-w01/l3;
P91=0.5*P*l1/l3*g1;

K=[K11 K12 K13 K14 K15 K16 K17 K18 K19;
    K21 K22 K23 K24 K25 K26 K27 K28 K29;
    K31 K32 K33 K34 K35 K36 K37 K38 K39;
    K41 K42 K43 K44 K45 K46 K47 K48 K49;
    K51 K52 K53 K54 K55 K56 K57 K58 K59;
    K61 K62 K63 K64 K65 K66 K67 K68 K69;
    K71 K72 K73 K74 K75 K76 K77 K78 K79;
```

```
    K81 K82 K83 K84 K85 K86 K87 K88 K89;
    K91 K92 K93 K94 K95 K96 K97 K98 K99];
F=[P11 P21 P31 P41 P51 P61 P71 P81 P91]';
COE=inv(K)*F

A1=COE(1); A2=COE(2);A6=COE(3);
B1=COE(4);B2=COE(5);B3=COE(6);B4=COE(7);B5=COE(8);B6=COE(9);
phi=0.0235:0.01:phi1;

Gphi=log(cos(phi./2))-log(sin(phi./2));
Q=A1*sin(phi).*hypergeom([apha11,beta11],2,sin(phi).^2)+A2.*sin(phi).*h
ypergeom([apha12,beta12],2,sin(phi).^2);
Qprime=A1.*(cos(phi).*hypergeom([apha11,beta11],2,sin(phi).^2)+sin(phi)
.^2.*cos(phi)*apha11*beta11.*hypergeom([apha11+1,beta11+1],3,sin(phi).^
2))+...

A2.*(cos(phi).*hypergeom([apha12,beta12],2,sin(phi).^2)+sin(phi).^2.*co
s(phi)*apha12*beta12.*hypergeom([apha12+1,beta12+1],3,sin(phi).^2));


w1=A6*cos(phi)-l3*(Qprime+Q.*cot(phi))+l2*P1*0.5 ;
u1=A6*sin(phi)-l1*Q;
w1primephi1=-A6*sin(phi1)+A1*K41*(-1/Ca/(1-niua^2))+A2*K42*(-1/Ca/(1-
niua^2));
plot(phi,w1)
x=phi1:0.01:phi2;
for i=1:size(x,2)
    GGG1(i)=subs(evalin(symengine,
sprintf('meijerG([[],[a11,b11]],[[0,-1],[]],%f)',sin(x(i))^2)));
    GGG2(i)=subs(evalin(symengine,
sprintf('meijerG([[],[a12,b12]],[[0,-1],[]],%f)',sin(x(i))^2)));
    GGG3(i)=subs(evalin(symengine, sprintf('meijerG([[],[b11,a11-
1]],[[0,-1],[]],%f)',sin(x(i))^2)));
    GGG4(i)=subs(evalin(symengine, sprintf('meijerG([[],[b12,a12-
1]],[[0,-1],[]],%f)',sin(x(i))^2)));
end
Q2=B1.*sin(x).*hypergeom([apha11,beta11],2,sin(x).^2)+B2.*sin(x).*hyper
geom([apha12,beta12],2,sin(x).^2)+...
    B3.*sin(x).*GGG1+B4.*sin(x).*GGG2;
Q2prime=B1.*(cos(x).*hypergeom([apha11,beta11],2,sin(x).^2)+sin(x).^2.*
cos(x)*apha11*beta11.*hypergeom([apha11+1,beta11+1],3,sin(x).^2))+...

B2.*(cos(x).*hypergeom([apha12,beta12],2,sin(x).^2)+sin(x).^2.*cos(x)*a
pha12*beta12.*hypergeom([apha12+1,beta12+1],3,sin(x).^2))...
    +B3.*{(cos(x)+2*cos(x).*(a11-1)).*GGG1-2*cos(x).*GGG3}...
        +B4.*{(cos(x)+2*cos(x).*(a12-1)).*GGG2-2*cos(x).*GGG4};

lo=log(cot(x/2));
w2=B6*cos(x)-l3.*(Q2prime+Q2.*cot(x))+l3*P.*(1-
0.5*(1+niua)*lo.*cos(x))+l1*B5.*(1-lo.*cos(x));
u2=B6*sin(x)-l1*(Q2+(0.5*P+B5).*(cot(x)+lo.*sin(x)));
plot(x,w2)
figure(1)
plot(phi,w1,x,w2)
figure(2)
plot(phi,u1,x,u2)
```

```
 w1=double(w1); u1=double(u1);
 w2=double(w2); u2=double(u2);
 [x1,y1]=xycoordinates(phi,x,phi2,w1,u1,w2,u2,1);

 plot(x1,y1)
 h1=plot([x1, fliplr(x1),-x1, fliplr(-x1)],[y1, fliplr(-y1),-y1,
fliplr(y1)],'b');
 hold on
syms c d
h=ezplot('c^2+d^2=1');
set(h, 'Color', 'm','LineStyle',':');
axis([-1.3,1.3,-1.3,1.3])
xlabel(' ')
ylabel(' ')

%%%%%%%%%%%%%%%%%%%%%%%%%%%%%%%%%%%%%%%%%
Er=.03e6; hr=0.2; niur=0.49; R2=11.5; pr=p-p1;
w02=w2(1)-1+R2/R;



Cr=12*(R2/ha)^2*(hr/ha)*(Er/Ea)*(1-niua^2)/(1-niur^2);
Ar=Cr*(1-niur^2)-niur^2;
Zr=4*sqrt(Ar);
Pr=pr*R^3/(Ea*ha^3/12/(1-niua^2));
z=5+i*Zr;
 r = roots([1 0 z]);
  p = imag(r);
   v = r(p<0);
rapha11=(3+v)/4;rapha12=(3+sqrt(5-i*Zr))/4;
rbeta11=(3-v)/4;rbeta12=(3-sqrt(5-i*Zr))/4;

F11r=hypergeom([apha11r,beta11r],2,sin(phi1)^2);F12r=hypergeom([apha12r
,beta12r],2,sin(phi1)^2);
F21r=hypergeom([apha11r+1,beta11r+1],3,sin(phi1)^2);F22r=hypergeom([aph
a12r+1,beta12r+1],3,sin(phi1)^2);
F31r=hypergeom([apha11r+2,beta11r+2],4,sin(phi1)^2);F32r=hypergeom([aph
a12r+2,beta12r+2],4,sin(phi1)^2);

M11r=sin(phi1)*F11r;M12r=sin(phi1)*F12r;
M21r=cos(phi1)*F11r+sin(phi1)^2*cos(phi1)*apha11r*beta11r*F21r;M22r=cos
(phi1)*F12r+sin(phi1)^2*cos(phi1)*apha12r*beta12r*F22r;
M31r=-sin(phi1)*F11r+(3*sin(phi1)*cos(phi1)^2-
sin(phi1)^3)*apha11r*beta11r*F21r+2/3*sin(phi1)^3*cos(phi1)^2*apha11r*(
apha11r+1)*beta11r*(beta11r+1)*F31r;
M32r=-sin(phi1)*F12r+(3*sin(phi1)*cos(phi1)^2-
sin(phi1)^3)*apha12r*beta12r*F22r+2/3*sin(phi1)^3*cos(phi1)^2*apha12r*(
apha12r+1)*beta12r*(beta12r+1)*F32r;


l1r=1/Cr/(1-niur);l2r=1/Cr/(1+niur);l3r=1/Cr/(1-niur^2);

KK11r=M11r*l1r; KK12r=M12r*l1r; KK13r=-sin(phi1);
KK21r=(M21r+M11r*cot(phi1))*l3r; KK22r=(M22r+M12r*cot(phi1))*l3r;
KK23r=-cos(phi1);
```

```
KK31r= (M31r+M21r*cot(phi1)-M11r*csc(phi1)^2)*l3r;
KK32r=(M32r+M22r*cot(phi1)-M12r*csc(phi1)^2)*l3r;
KK33r=sin(phi1);
F1r=-u2(1)+0.5*(ha+hr)*w1primephi1/R;
 F2r=0.5*l2r*Pr-w02;
 F3r=-w1primephi1;

KKr=[KK11r KK12r KK13r;
    KK21r KK22r KK23r;
    KK31r KK32r KK33r];
Fr=[F1r;F2r;F3r];
COEr=inv(KKr)*Fr
A1r=COEr(1); A2r=COEr(2);A6r=COEr(3);
phi=0.0235:0.01:phi1;

Qr=A1r*sin(phi).*hypergeom([apha11r,beta11r],2,sin(phi).^2)+A2r.*sin(ph
i).*hypergeom([apha12r,beta12r],2,sin(phi).^2);
Qrprime=A1r.*(cos(phi).*hypergeom([apha11r,beta11r],2,sin(phi).^2)+sin(
phi).^2.*cos(phi)*apha11r*beta11r.*hypergeom([apha11r+1,beta11r+1],3,si
n(phi).^2))+...

A2r.*(cos(phi).*hypergeom([apha12r,beta12r],2,sin(phi).^2)+sin(phi).^2.
*cos(phi)*apha12r*beta12r.*hypergeom([apha12r+1,beta12r+1],3,sin(phi).^
2));


wr=A6r*cos(phi)-l3r*(Qrprime+Qr.*cot(phi))+l2r*Pr*0.5 ;
ur=A6r*sin(phi)-l1r*Qr;
figure(3)
plot(phi,wr,phi,w1,'r')
a=pi/2-phi; ro=0.9;
xx=real(wr);yy=real(ur);
xr=-xx.*cos(a)-yy.*sin(a)+Rr/R*cos(a);
yr=-xx.*sin(a)+yy.*cos(a)+Rr/R*sin(a);
yrfinal=(cos(phi1)-ro).*xr/sin(phi1)+yr;
figure(4)
plot(xr,yr)



clear
clc


t=4;R=12;R1=10.5;ha=0.8; hb=2;Eb=2.4e6; Ea=2.8e6; niub=0.49; niua=0.49;
p=2670; p1=2670;
phi1=pi/10;  %(20-40 degree, pi/6)
phi2=pi/2-0.5*t/R;
Ca=12/(ha/R)^2;
A1=Ca*(1-niua^2)-niua^2;
Z=4*sqrt(A1);
P=-p*R^3/(Ea*ha^3/12/(1-niua^2));
P1=-p1*R^3/(Ea*ha^3/12/(1-niua^2));

Cb=12*Eb/Ea*(hb/ha)/(ha/R)^2*(t/R1)/(1-niua^2);
```

```
Db=Eb/Ea*(hb/ha)^3*(t/R1)*(R/R1)^2*(1-niub^2)/(1-niua^2);
w0=-P*cos(phi2)/(Ca*(1+niua)*2*cos(phi2)+Cb+Db);
w01=w0+1-R1/R;

apha11=(3+sqrt(5+i*Z))/4;apha12=(3+sqrt(5-i*Z))/4;
beta11=(3-sqrt(5+i*Z))/4;beta12=(3-sqrt(5-i*Z))/4;

F11=hypergeom([apha11,beta11],2,sin(phi1)^2);F12=hypergeom([apha12,beta
12],2,sin(phi1)^2);
F21=hypergeom([apha11+1,beta11+1],3,sin(phi1)^2);F22=hypergeom([apha12+
1,beta12+1],3,sin(phi1)^2);
F31=hypergeom([apha11+2,beta11+2],4,sin(phi1)^2);F32=hypergeom([apha12+
2,beta12+2],4,sin(phi1)^2);
F41=hypergeom([apha11+3,beta11+3],5,sin(phi1)^2);F42=hypergeom([apha12+
3,beta12+3],5,sin(phi1)^2);

M11=sin(phi1)*F11;M12=sin(phi1)*F12;
M21=cos(phi1)*F11+sin(phi1)^2*cos(phi1)*apha11*beta11*F21;M22=cos(phi1)
*F12+sin(phi1)^2*cos(phi1)*apha12*beta12*F22;
M31=-sin(phi1)*F11+(3*sin(phi1)*cos(phi1)^2-
sin(phi1)^3)*apha11*beta11*F21+2/3*sin(phi1)^3*cos(phi1)^2*apha11*(apha
11+1)*beta11*(beta11+1)*F31;
M32=-sin(phi1)*F12+(3*sin(phi1)*cos(phi1)^2-
sin(phi1)^3)*apha12*beta12*F22+2/3*sin(phi1)^3*cos(phi1)^2*apha12*(apha
12+1)*beta12*(beta12+1)*F32;
M41=-cos(phi1)*F11+(3*cos(phi1)^3-
10*sin(phi1)^2*cos(phi1))*apha11*beta11*F21+(4*sin(phi1)^2*cos(phi1)^3-
2*sin(phi1)^4*cos(phi1))*apha11*(apha11+1)*beta11*(beta11+1)*F31...

+1/3*sin(phi1)^4*cos(phi1)^3*apha11*(apha11+1)*(apha11+2)*beta11*(beta1
1+1)*(beta11+2)*F41;
M42=-cos(phi1)*F12+(3*cos(phi1)^3-
10*sin(phi1)^2*cos(phi1))*apha12*beta12*F22+(4*sin(phi1)^2*cos(phi1)^3-
2*sin(phi1)^4*cos(phi1))*apha12*(apha12+1)*beta12*(beta12+1)*F32...

+1/3*sin(phi1)^4*cos(phi1)^3*apha12*(apha12+1)*(apha12+2)*beta12*(beta1
2+1)*(beta12+2)*F42;

f11=hypergeom([apha11,beta11],2,sin(phi2)^2);f12=hypergeom([apha12,beta
12],2,sin(phi2)^2);
f21=hypergeom([apha11+1,beta11+1],3,sin(phi2)^2);f22=hypergeom([apha12+
1,beta12+1],3,sin(phi2)^2);
f31=hypergeom([apha11+2,beta11+2],4,sin(phi2)^2);f32=hypergeom([apha12+
2,beta12+2],4,sin(phi2)^2);
f41=hypergeom([apha11+3,beta11+3],5,sin(phi2)^2);f42=hypergeom([apha12+
3,beta12+3],5,sin(phi2)^2);

m11=sin(phi2)*f11;m12=sin(phi2)*f12;
m21=cos(phi2)*f11+sin(phi2)^2*cos(phi2)*apha11*beta11*f21;m22=cos(phi2)
*f12+sin(phi2)^2*cos(phi2)*apha12*beta12*f22;
m31=-sin(phi2)*f11+(3*sin(phi2)*cos(phi2)^2-
sin(phi2)^3)*apha11*beta11*f21+2/3*sin(phi2)^3*cos(phi2)^2*apha11*(apha
11+1)*beta11*(beta11+1)*f31;
m32=-sin(phi2)*f12+(3*sin(phi2)*cos(phi2)^2-
sin(phi2)^3)*apha12*beta12*f22+2/3*sin(phi2)^3*cos(phi2)^2*apha12*(apha
12+1)*beta12*(beta12+1)*f32;
```

```
m41=-cos(phi2)*f11+(3*cos(phi2)^3-
10*sin(phi2)^2*cos(phi2))*apha11*beta11*f21+(4*sin(phi2)^2*cos(phi2)^3-
2*sin(phi2)^4*cos(phi2))*apha11*(apha11+1)*beta11*(beta11+1)*f31...

+1/3*sin(phi2)^4*cos(phi2)^3*apha11*(apha11+1)*(apha11+2)*beta11*(beta1
1+1)*(beta11+2)*f41;
m42=-cos(phi2)*f12+(3*cos(phi2)^3-
10*sin(phi2)^2*cos(phi2))*apha12*beta12*f22+(4*sin(phi2)^2*cos(phi2)^3-
2*sin(phi2)^4*cos(phi2))*apha12*(apha12+1)*beta12*(beta12+1)*f32...

+1/3*sin(phi2)^4*cos(phi2)^3*apha12*(apha12+1)*(apha12+2)*beta12*(beta1
2+1)*(beta12+2)*f42;

a11=apha11-1/2; a12=apha12-1/2;
b11=beta11-1/2;  b12=beta12-1/2;
A11=[a11,b11,a11-1,a11-2]; A12=[a12,b12,a12-1,a12-2];
B11=[b11,a11-1,b11-1,b11-1]; B12=[b12,a12-1,b12-1,b12-1];

r1=evalin(symengine, sprintf('meijerG([[],[A11,B11]],[[0,-
1],[]],%f)',sin(phi1)^2));
GG=subs(r1);
r2=evalin(symengine, sprintf('meijerG([[],[A12,B12]],[[0,-
1],[]],%f)',sin(phi1)^2));
gg=subs(r2);
N11=sin(phi1)*GG(1); N12=sin(phi1)*gg(1);
N21=(cos(phi1)+2*cos(phi1)*(a11-1))*GG(1)-2*cos(phi1)*GG(2);
N22=(cos(phi1)+2*cos(phi1)*(a12-1))*gg(1)-2*cos(phi1)*gg(2);
N31=(sin(phi1)*2*(a11-1)*(cot(phi1)^2*(2*a11-3)-
1)+2*cos(phi1)*2*cot(phi1)*(a11-1)-
sin(phi1))*GG(1)+(sin(phi1)*(2*cot(phi1)^2*(5-2*a11-
2*b11)+2)+2*cos(phi1)*(-2*cot(phi1)))*GG(2)...
    +sin(phi1)*4*cot(phi1)^2*GG(3);
N32=(sin(phi1)*2*(a12-1)*(cot(phi1)^2*(2*a12-3)-
1)+2*cos(phi1)*2*cot(phi1)*(a12-1)-
sin(phi1))*gg(1)+(sin(phi1)*(2*cot(phi1)^2*(5-2*a12-
2*b12)+2)+2*cos(phi1)*(-2*cot(phi1)))*gg(2)...
    +sin(phi1)*4*cot(phi1)^2*gg(3);
N41=GG(1)*(3*cos(phi1)*2*(a11-1)*(cot(phi1)^2*(2*a11-3)-
1)+sin(phi1)*(4*cot(phi1)^3*(a11-1)*(a11-2)*(2*a11-3)-
4*cot(phi1)*a11*(a11-1))-cos(phi1)-3*sin(phi1)*2*cot(phi1)*(a11-1))...
    +GG(2)*(3*cos(phi1)*(2*cot(phi1)^2*(5-2*a11-
2*b11)+2)+sin(phi1)*(4*cot(phi1)^3*(3*b11+3*a11-7-2*(a11-1)^2-2*(b11-
1)^2-2*(a11-1)*(b11-1))+4*cot(phi1)*(3*b11+a11-3))-3*sin(phi1)*(-
2*cot(phi1)))...
    +GG(3)*(3*cos(phi1)*4*cot(phi1)^2+sin(phi1)*(4*cot(phi1)^3*(2*b11-
3)-12*cot(phi1)))...
    +GG(4)*sin(phi1)*(-8*cot(phi1)^3);
N42=gg(1)*(3*cos(phi1)*2*(a12-1)*(cot(phi1)^2*(2*a12-3)-
1)+sin(phi1)*(4*cot(phi1)^3*(a12-1)*(a12-2)*(2*a12-3)-
4*cot(phi1)*a12*(a12-1))-cos(phi1)-3*sin(phi1)*2*cot(phi1)*(a12-1))...
    +gg(2)*(3*cos(phi1)*(2*cot(phi1)^2*(5-2*a12-
2*b12)+2)+sin(phi1)*(4*cot(phi1)^3*(3*b12+3*a12-7-2*(a12-1)^2-2*(b12-
1)^2-2*(a12-1)*(b12-1))+4*cot(phi1)*(3*b12+a12-3))-3*sin(phi1)*(-
2*cot(phi1)))...
    +gg(3)*(3*cos(phi1)*4*cot(phi1)^2+sin(phi1)*(4*cot(phi1)^3*(2*b12-
3)-12*cot(phi1)))...
```

```
    +gg(4)*sin(phi1)*(-8*cot(phi1)^3);
r1=evalin(symengine, sprintf('meijerG([[],[A11,B11]],[[0,-
1],[]],%f)',sin(phi2)^2));
LL=subs(r1);
r2=evalin(symengine, sprintf('meijerG([[],[A12,B12]],[[0,-
1],[]],%f)',sin(phi2)^2));
ll=subs(r2);
n11=sin(phi2)*LL(1); n12=sin(phi2)*ll(1);
n21=(cos(phi2)+2*cos(phi2)*(a11-1))*LL(1)-2*cos(phi2)*LL(2);
n22=(cos(phi2)+2*cos(phi2)*(a12-1))*ll(1)-2*cos(phi2)*ll(2);
n31=(sin(phi2)*2*(a11-1)*(cot(phi2)^2*(2*a11-3)-
1)+2*cos(phi2)*2*cot(phi2)*(a11-1)-
sin(phi2))*LL(1)+(sin(phi2)*(2*cot(phi2)^2*(5-2*a11-
2*b11)+2)+2*cos(phi2)*(-2*cot(phi2)))*LL(2)...
    +sin(phi2)*4*cot(phi2)^2*LL(3);
n32=(sin(phi2)*2*(a12-1)*(cot(phi2)^2*(2*a12-3)-
1)+2*cos(phi2)*2*cot(phi2)*(a12-1)-
sin(phi2))*ll(1)+(sin(phi2)*(2*cot(phi2)^2*(5-2*a12-
2*b12)+2)+2*cos(phi2)*(-2*cot(phi2)))*ll(2)...
    +sin(phi2)*4*cot(phi2)^2*ll(3);
n41=LL(1)*(3*cos(phi2)*2*(a11-1)*(cot(phi2)^2*(2*a11-3)-
1)+sin(phi2)*(4*cot(phi2)^3*(a11-1)*(a11-2)*(2*a11-3)-
4*cot(phi2)*a11*(a11-1))-cos(phi2)-3*sin(phi2)*2*cot(phi2)*(a11-1))...
    +LL(2)*(3*cos(phi2)*(2*cot(phi2)^2*(5-2*a11-
2*b11)+2)+sin(phi2)*(4*cot(phi2)^3*(3*b11+3*a11-7-2*(a11-1)^2-2*(b11-
1)^2-2*(a11-1)*(b11-1))+4*cot(phi2)*(3*b11+a11-3))-3*sin(phi2)*(-
2*cot(phi2)))...
    +LL(3)*(3*cos(phi2)*4*cot(phi2)^2+sin(phi2)*(4*cot(phi2)^3*(2*b11-
3)-12*cot(phi2)))...
    +LL(4)*sin(phi2)*(-8*cot(phi2)^3);
n42=ll(1)*(3*cos(phi2)*2*(a12-1)*(cot(phi2)^2*(2*a12-3)-
1)+sin(phi2)*(4*cot(phi2)^3*(a12-1)*(a12-2)*(2*a12-3)-
4*cot(phi2)*a12*(a12-1))-cos(phi2)-3*sin(phi2)*2*cot(phi2)*(a12-1))...
    +ll(2)*(3*cos(phi2)*(2*cot(phi2)^2*(5-2*a12-
2*b12)+2)+sin(phi2)*(4*cot(phi2)^3*(3*b12+3*a12-7-2*(a12-1)^2-2*(b12-
1)^2-2*(a12-1)*(b12-1))+4*cot(phi2)*(3*b12+a12-3))-3*sin(phi2)*(-
2*cot(phi2)))...
    +ll(3)*(3*cos(phi2)*4*cot(phi2)^2+sin(phi2)*(4*cot(phi2)^3*(2*b12-
3)-12*cot(phi2)))...
    +ll(4)*sin(phi2)*(-8*cot(phi2)^3);

l1=1/Ca/(1-niua);l2=1/Ca/(1+niua);l3=1/Ca/(1-niua^2);

%%%%%%%%%%%%%%%%%%%%%%%%%%%%%%%%%%%%%%%%%%%%%%%%%%%%%%%%%%%%%%%%%%%%%%%%%%%%
g=log(cot(phi1/2));
g1=g*sin(phi1)+cot(phi1);g2=g*cos(phi1)-1-csc(phi1)^2;
K11=M11; K12=M12; K13=-1/l1*sin(phi1); K14=-K11; K15=-K12;K16=-
N11;K17=-N12;K18=-g1; K19=-K13;
K21=M21; K22=M22; K23=-1/l1*cos(phi1); K24=-K21; K25=-K22; K26=-N21;
K27=-N22; K28=-g2; K29=-K23;
K31=M21+M11*cot(phi1); K32=M22+M12*cot(phi1); K33=-1/l3*cos(phi1);
K34=-K31; K35=-K32; K36=-(N21+N11*cot(phi1));
K37=-(N22+N12*cot(phi1)); K38=l1/l3*(1-g*cos(phi1)); K39=1/l3*cos(phi1);
K41=M31+M21*cot(phi1)-M11*csc(phi1)^2; K42=M32+M22*cot(phi1)-
M12*csc(phi1)^2; K43=sin(phi1)/l3;
```

```
K44=-K41; K45=-K42; K46=-(N31+N21*cot(phi1)-N11*csc(phi1)^2); K47=-
(N32+N22*cot(phi1)-N12*csc(phi1)^2);
K48=l1/l3*g1; K49=-K43;
K51=M41+M31*cot(phi1)-2*csc(phi1)^2*M21+M11*2*cot(phi1)*csc(phi1)^2;
K52=M42+M32*cot(phi1)-2*csc(phi1)^2*M22+M12*2*cot(phi1)*csc(phi1)^2;
K53=K39; K54=-K51; K55=-K52;
K56=-(N41+N31*cot(phi1)-2*csc(phi1)^2*N21+N11*2*cot(phi1)*csc(phi1)^2);
K57=-(N42+N32*cot(phi1)-2*csc(phi1)^2*N22+N12*2*cot(phi1)*csc(phi1)^2);
K58=l1/l3*g2; K59=-K53;
K61=M11; K62=M12; K63=0; K64=-K61; K65=-K62; K66=-N11; K67=-N12; K68=0;
K69=0;
P11=0.5*P*g1; P21=0.5*P*g2;P31=0.5*P1*l2/l3-P*(1-
0.5*(1+niua)*g*cos(phi1));P41=-0.5*P*l1/l3*g1;P51=-0.5*P*l1/l3*g2;
P61=0;

g=log(cot(phi2/2));
g1=g*sin(phi2)+cot(phi2);g2=g*cos(phi2)-1-csc(phi2)^2;

K71=0;K72=0;K73=0;K74=m11; K75=m12; K76=n11; K77=n12; K78=g1;    K79=-
sin(phi2)/l1;
K81=0; K82=0; K83=0; K84=m21+m11*cot(phi2); K85=m22+m12*cot(phi2);
K86=n21+n11*cot(phi2);K87=n22+n12*cot(phi2);  K88=-l1/l3*(1-g*cos(phi2));
K89=-cos(phi2)/l3;

K91=0; K92=0; K93=0; K94=m31+m21*cot(phi2)-
m11*csc(phi2)^2;K95=m32+m22*cot(phi2)-m12*csc(phi2)^2;
K96=n31+n21*cot(phi2)-n11*csc(phi2)^2;K97=n32+n22*cot(phi2)-
n12*csc(phi2)^2; K98=-l1/l3*g1; K99=sin(phi2)/l3;
P71=-0.5*P*g1; P81=P*(1-0.5*(1+niua)*g*cos(phi2))-w01/l3;
P91=0.5*P*l1/l3*g1;

K=[K11 K12 K13 K14 K15 K16 K17 K18 K19;
    K21 K22 K23 K24 K25 K26 K27 K28 K29;
    K31 K32 K33 K34 K35 K36 K37 K38 K39;
    K41 K42 K43 K44 K45 K46 K47 K48 K49;
    K51 K52 K53 K54 K55 K56 K57 K58 K59;
    K61 K62 K63 K64 K65 K66 K67 K68 K69;
    K71 K72 K73 K74 K75 K76 K77 K78 K79;
    K81 K82 K83 K84 K85 K86 K87 K88 K89;
    K91 K92 K93 K94 K95 K96 K97 K98 K99];
F=[P11 P21 P31 P41 P51 P61 P71 P81 P91]';
COE=inv(K)*F

A1=COE(1); A2=COE(2);A6=COE(3);
B1=COE(4);B2=COE(5);B3=COE(6);B4=COE(7);B5=COE(8);B6=COE(9);
phi=0.00235:0.01:phi1;

Gphi=log(cos(phi./2))-log(sin(phi./2));
Q=A1*sin(phi).*hypergeom([apha11,beta11],2,sin(phi).^2)+A2.*sin(phi).*h
ypergeom([apha12,beta12],2,sin(phi).^2);
Qprime=A1.*(cos(phi).*hypergeom([apha11,beta11],2,sin(phi).^2)+sin(phi)
.^2.*cos(phi)*apha11*beta11.*hypergeom([apha11+1,beta11+1],3,sin(phi).^
2))+...

A2.*(cos(phi).*hypergeom([apha12,beta12],2,sin(phi).^2)+sin(phi).^2.*co
s(phi)*apha12*beta12.*hypergeom([apha12+1,beta12+1],3,sin(phi).^2));
```

```
w1=A6*cos(phi)-l3*(Qprime+Q.*cot(phi))+l2*P1*0.5 ;
u1=A6*sin(phi)-l1*Q;
w1primephi1=A6*K43*(-l3)+A1*K41*(-l3)+A2*K42*(-l3);
plot(phi,w1)
x=phi1:0.01:phi2;
for i=1:size(x,2)
    GGG1(i)=subs(evalin(symengine,
sprintf('meijerG([[],[a11,b11]],[[0,-1],[]],%f)',sin(x(i))^2)));
    GGG2(i)=subs(evalin(symengine,
sprintf('meijerG([[],[a12,b12]],[[0,-1],[]],%f)',sin(x(i))^2)));
    GGG3(i)=subs(evalin(symengine, sprintf('meijerG([[],[b11,a11-
1]],[[0,-1],[]],%f)',sin(x(i))^2)));
    GGG4(i)=subs(evalin(symengine, sprintf('meijerG([[],[b12,a12-
1]],[[0,-1],[]],%f)',sin(x(i))^2)));
end
Q2=B1.*sin(x).*hypergeom([apha11,beta11],2,sin(x).^2)+B2.*sin(x).*hyper
geom([apha12,beta12],2,sin(x).^2)+...
    B3.*sin(x).*GGG1+B4.*sin(x).*GGG2;
Q2prime=B1.*(cos(x).*hypergeom([apha11,beta11],2,sin(x).^2)+sin(x).^2.*
cos(x)*apha11*beta11.*hypergeom([apha11+1,beta11+1],3,sin(x).^2))+...

B2.*(cos(x).*hypergeom([apha12,beta12],2,sin(x).^2)+sin(x).^2.*cos(x)*a
pha12*beta12.*hypergeom([apha12+1,beta12+1],3,sin(x).^2))...
    +B3.*{(cos(x)+2*cos(x).*(a11-1)).*GGG1-2*cos(x).*GGG3}...
        +B4.*{(cos(x)+2*cos(x).*(a12-1)).*GGG2-2*cos(x).*GGG4};



lo=log(cot(x/2));
w2=B6*cos(x)-l3.*(Q2prime+Q2.*cot(x))+l3*P.*(1-
0.5*(1+niua)*lo.*cos(x))+l1*B5.*(1-lo.*cos(x));
u2=B6*sin(x)-l1*(Q2+(0.5*P+B5).*(cot(x)+lo.*sin(x)));
plot(x,w2)
figure(1)
plot(phi,w1,x,w2)
figure(2)
plot(phi,u1,x,u2)
 w1=double(w1); u1=double(u1);
 w2=double(w2); u2=double(u2);
 [x1,y1]=xycoordinates(phi,x,phi2,w1,u1,w2,u2,1);

 plot(x1,y1)
 h1=plot([x1, fliplr(x1),-x1, fliplr(-x1)],[y1, fliplr(-y1),-y1,
fliplr(y1)],'b');
 hold on
syms c d
h=ezplot('c^2+d^2=1');
set(h, 'Color', 'm','LineStyle',':');
axis([-1.5,1.5,-1.5,1.5],'square')
xlabel(' ')
ylabel(' ')

%%%%%%%%%%%%%%%%%%%%%%%%%%%%%%%%%%%%%%%%%%%
```

```
Er=0.03e6;
hr=0.2;
niur=0.49; Rr=11.5; pr=p1-p;
wr0=w2(1);
Cr=12*Er/Ea*(hr/ha)*(R/ha)^2/(1-niua^2);
Dr=Er/Ea*(hr/ha)^3*(R/Rr)^2*(1-niur^2)/(1-niua^2);
Br=Cr/Dr*(1-niur^2)-niur^2;
% A22=.5*(Cb+Ca)*(1-0.5*(niua^2+niub^2))-0.25*(niua+niub)^2;
Zr=4*sqrt(Br);
Pr=pr*Rr^3/(Ea*ha^3/12/(1-niua^2));
[v1,v2]=aa(Zr)
rapha11=(3+v1)/4;rapha12=(3+v2)/4;
rbeta11=(3-v1)/4;rbeta12=(3-v2)/4;

F11r=hypergeom([rapha11,rbeta11],2,sin(phi1)^2);F12r=hypergeom([rapha12
,rbeta12],2,sin(phi1)^2);
F21r=hypergeom([rapha11+1,rbeta11+1],3,sin(phi1)^2);F22r=hypergeom([rap
ha12+1,rbeta12+1],3,sin(phi1)^2);
F31r=hypergeom([rapha11+2,rbeta11+2],4,sin(phi1)^2);F32r=hypergeom([rap
ha12+2,rbeta12+2],4,sin(phi1)^2);

M11r=sin(phi1)*F11r;M12r=sin(phi1)*F12r;
M21r=cos(phi1)*F11r+sin(phi1)^2*cos(phi1)*rapha11*rbeta11*F21r;M22r=cos
(phi1)*F12r+sin(phi1)^2*cos(phi1)*rapha12*rbeta12*F22r;
M31r=-sin(phi1)*F11r+(3*sin(phi1)*cos(phi1)^2-
sin(phi1)^3)*rapha11*rbeta11*F21r+2/3*sin(phi1)^3*cos(phi1)^2*rapha11*(
rapha11+1)*rbeta11*(rbeta11+1)*F31r;
M32r=-sin(phi1)*F12r+(3*sin(phi1)*cos(phi1)^2-
sin(phi1)^3)*rapha12*rbeta12*F22r+2/3*sin(phi1)^3*cos(phi1)^2*rapha12*(
rapha12+1)*rbeta12*(rbeta12+1)*F32r;


l1r=Dr/Cr/(1-niur);l2r=1/Cr/(1+niur);l3r=Dr/Cr/(1-niur^2);

KK11r=M11r*l1r; KK12r=M12r*l1r; KK13r=-sin(phi1);
KK21r=(M21r+M11r*cot(phi1))*l3r; KK22r=(M22r+M12r*cot(phi1))*l3r;
KK23r=-cos(phi1);
KK31r=(M31r+M21r*cot(phi1)-M11r*csc(phi1)^2)*l3r;
KK32r=(M32r+M22r*cot(phi1)-M12r*csc(phi1)^2)*l3r;
KK33r=sin(phi1);

F1r=-u2(1)+0.5*(ha+hr)/R*w1primephi1;
 F2r=0.5*l2r*Pr-wr0;
 F3r=w1primephi1;
KKr=[KK11r KK12r KK13r;
    KK21r KK22r KK23r;
    KK31r KK32r KK33r];
Fr=[F1r;F2r;F3r];
COEr=inv(KKr)*Fr
A1r=COEr(1); A2r=COEr(2);A6r=COEr(3);
phi=0.00235:0.01:phi1;

Qr=A1r*sin(phi).*hypergeom([rapha11,rbeta11],2,sin(phi).^2)+A2r.*sin(ph
i).*hypergeom([rapha12,rbeta12],2,sin(phi).^2);
```

```
Qrprime=A1r.*(cos(phi).*hypergeom([rapha11,rbeta11],2,sin(phi).^2)+sin(
phi).^2.*cos(phi)*rapha11*rbeta11.*hypergeom([rapha11+1,rbeta11+1],3,si
n(phi).^2))+...

A2r.*(cos(phi).*hypergeom([rapha12,rbeta12],2,sin(phi).^2)+sin(phi).^2.
*cos(phi)*rapha12*rbeta12.*hypergeom([rapha12+1,rbeta12+1],3,sin(phi).^
2));


wr=A6r*cos(phi)-l3r*(Qrprime+Qr.*cot(phi))+l2r*Pr*0.5+1-Rr/R ;
ur=A6r*sin(phi)-l1r*Qr;
figure(3)
plot(phi,wr,'k.',phi,w1,'k.',x,w2,'k.','MarkerSize',3)
hold on
plot(phi,w1+ha/2/R,'k-.',phi,w1-ha/2/R,'k-.',x,w2+ha/2/R,'k--',x,w2-
ha/2/R,'k--')
hold on
plot(phi,wr+hr/2/R,'k',phi,wr-hr/2/R,'k')
xlabel('\phi')
ylabel('w')
figure(5)
plot(phi(1:size(phi,2)-1),ur(1:size(phi,2)-1),'k',phi,u1,'k-.',x,u2,'k-
-')
xlabel('\phi')
ylabel('u')
a=pi/2-phi; ro=0.9;
xx=real(wr);yy=real(ur);
xr=-xx.*cos(a)-yy.*sin(a)+cos(a);
yr=-xx.*sin(a)+yy.*cos(a)+sin(a);
yrfinal=(cos(phi1)-ro).*xr/sin(phi1)+yr;
figure(6)
plot(xr,yr,x1,y1)
xx=real(wr+hr/2/R);yy=real(ur);
xr1=xr+(hr/2)/R*cos(a);
yr1=yr+(hr/2)/R*sin(a);
yrfinal=(cos(phi1)-ro).*xr/sin(phi1)+yr;
xx=real(wr-hr/2/R);yy=real(ur);
xr2=xr+(-hr/2)/R*cos(a);
yr2=yr+(-hr/2)/R*sin(a);
bb=0.00235:0.01:pi/2;
bb=pi/2-bb;
figure(7)
plot(xr,yr,'k:',x1,y1,'k:','MarkerSize',3)
hold on
plot(x1-(ha/2)/R*cos(bb),y1-(ha/2)/R*sin(bb),'k--
',x1+(ha/2)/R*cos(bb),y1+(ha/2)/R*sin(bb),'k--')
hold on
plot(xr1,yr1,'k',xr2,yr2,'k')
axis([0,1.2,0,1.2])

figure(8)
plot([x1, fliplr(x1),-x1, fliplr(-x1)],[y1, fliplr(-y1),-y1,
fliplr(y1)],'k--')
```